WATER BALANCE STUDY OF A STORAGE TANK IN DROUGHT PRONE AREA

A THESIS

Submitted in partial fulfilment of the requirements for the award of the degree of

DOCTOR OF PHILOSOPHY

in

WATER RESOURCES DEVELOPMENT AND MANAGEMENT

by

DILLIP KUMAR BARIK

DEPARTMENT OF WATER RESOURCES DEVELOPMENT & MANAGEMENT
INDIAN INSTITUTE OF TECHNOLOGY ROORKEE
ROORKEE - 247 667 (INDIA)

APRIL, 2009

INDIAN INSTITUTE OF TECHNOLOGY ROORKEE
ROORKEE

CANDIDATE'S DECLARATION

I hereby certify that the work which is being presented in the thesis entitled **WATER BALANCE STUDY OF A STORAGE TANK IN DROUGT PRONE AREA** in partial fulfilment of the requirement for the award of the degree of ***Doctor of Philosophy*** and submitted in the Department of **WATER RESOURCES DEVELOPMENT AND MANAGEMENT** of Indian Institute of Technology Roorkee, Roorkee is an authentic record of my own work carried out during a period from July 2003 to April 2009 under the supervision of Dr. U.C. Chaube, Professor, and Dr. G.C. Mishra, Emeritus Fellow Department of Water Resources Development and Management, Indian Institute of Technology Roorkee, Roorkee.

The matter presented in this thesis has not been submitted by me for the award of any other degree in this institute or any other Institute.

(DILLIP KUMAR BARIK)

This is to certify that the above statement made by the candidate is correct to the best of our knowledge.

(G. C. MISHRA)
Supervisor

(U.C. CHAUBE)
Supervisor

Date: 23/04/2009

The Ph.D. Viva-Voce examination of **Mr. Dillip Kumar Barik**, Research Scholar, has been held on .....

Signature of Supervisors

Signature of External Examiner

ABSTRACT

Water scarcity problems in a drought prone area can be mitigated by conservation and management of water available in the area. Water balance study is a pre-requisite for planning of an efficient water management practice. In water scarcity areas, run off originating from rainfall is conserved in storage tanks. These storage tanks are shallow reservoirs formed by constructing earthen embankments across seasonal streams. In some places water from the seasonal streams is diverted to natural depressions. These storage tanks support supplementary irrigation, function as important water source for people, livestock, pisciculture and are places of recreation and worship. In India, tank irrigation is about 20% of the total area irrigated. Storage tanks also facilitate ground water recharge. A water balance study in a storage tank reveals whether the prevailing water source meets the water demand in its command area. The component processes involved in water balance in a storage tank are: (i) evaporation from the water body, (ii) run off from contributing catchment of the tank, (iii) direct rainfall (iv) infiltration from the tank bed and (v) outflow from the storage tank. These process level models have been integrated in this thesis to quantify the depth of water available in the storage tank during a water year.

Penman's method and heat balance method are used for computation of evaporation from a water body. In this thesis it is found that the Penman's method computes an average evaporation rate as compared to heat balance method. The heat balance method is more accurate as the method computes zero evaporation on the day, the water temperature in the tank coincides with the dew point temperature of the atmosphere. In shallow storage tank (less than 3m), the variation in depth of water due to evaporation has nominal effect on evaporation rate from the water body.

SCS (Soil Conservation Service) method is widely used for computation of runoff from a catchment. Since, the storage parameter changes during a water year owing to several rainfall events, it is pertinent that the curve number should be updated. In the present study the curve number is updated by taking account of change in soil moisture due to evaporation and drainage from the soil profile.

The depth of water in a storage tank is primarily governed by infiltration. The infiltration rate has been computed using Green and Ampt infiltration theory. The assumption of Green and Ampt infiltration theory, that the soil is saturated behind a moving front, is valid for a two layered soil system, if the upper layer has higher hydraulic conductivity than that of lower layer. Incase, the upper layer in two layered soil system has lower hydraulic conductivity than that of the underlying layer, the soil moisture behind the moving front in the first layer is equal to the saturation moisture content of the upper layer. When the moving front surpasses the upper layer, the moisture content behind the moving front in the lower layer is less than the saturated moisture content of the underlying layer. Green and Ampt infiltration theory is inapplicable for computing infiltration from a storage tank, underlain by a layered soil system if the upper soil layer is less permeable than that of the lower layer, as the simulated infiltration rate does not follow the decreasing trend of infiltration given by Horton's equation. With a postulation that water front moves in unsaturated state in the lower layer at a moisture content corresponding to which the unsaturated hydraulic conductivity of the lower layer is same as the saturated hydraulic conductivity of the upper layer, the simulated infiltration rate follows the decreasing trend as given by Horton's infiltration equation.

The temporal variation in depth of water in a storage tank has been presented for four soil groups. The soil moisture characteristics for these four groups of soil have been taken from published data. The variation of the drying time of a storage tank in a

homogeneous soil layer has been computed for different initial depth. It is found that the variation of drying time with initial depth of water is quasi-linear in nature. The drying time is very closely inversely proportional to the hydraulic conductivity of the sub soil. But, in case of a two layered soil system, where the bottom soil layer has lower hydraulic conductivity, the variation of drying time with initial depth of filling is very much non-linear in nature.

Water availability in a storage tank has been predicted as a case study. The tank is situated in a drought prone area. The present height of the spillway crest needs to be raised from 1.525m to 3.155m to maintain a minimum depth of 1.0m in the Asha Sagar storage tank at the end of the water year. Otherwise, the tank would remain dry during the later half of the water year. If the crest level will be raised to a height of 6.8m, all the potential runoff from the contributing catchment will get stored and water can be supplied for irrigation during post monsoon period to a command area of 121 ha, besides supporting for pisciculture in the storage tank.

ACKNOWLEDGEMENTS

I wish to express my sincere thanks to my Ph. D. supervisors, Dr. G. C. Mishra, Emeritus Fellow, Department of Water Resources Development and Management, I.I.T. Roorkee, and Dr. U. C. Chaube, Professor, Department of Water Resources Development and Management, I.I.T. Roorkee, for their guidance and encouragement throughout this thesis work. I am greatly indebted to Dr. G. C. Mishra for his invaluable supervision, pragmatic advice, good teaching, and in-depth knowledge with innovative ideas without whom this thesis would not have been completed. I wish my heartfelt gratitude to him for his constant motivation and to keep my morale high during difficult times.

I am grateful to Dr. R. P. Singh, Professor and Head, Department of Water Resources Development and Management, I.I.T. Roorkee, for his generous help in providing the infrastructure during my Ph.D. programme.

I am also thankful to Ministry of Human Resources Development and Ministry of Water Resources, Govt. of India for providing me financial support during my study period.

My sincere thanks are due to Dr. M. L. Kansal, Professor Department of Water Resources Development and Management and Dr. Ranveer Singh, Professor Department of Hydrology, for their constructive remarks and suggestions. I am also thankful to all the faculty members of the Department of Water Resources Development and Management, I.I.T. Roorkee.

I wish to thank Dr. R. K. Tripathy, Professor, College of Agriculture, O.U.A.T. Bhubaneswar, for providing the meteorological data. I am also thankful to IMD Pune

for providing the some meteorological data. Thanks are due to Department of Irrigation, Bhawanipatna for providing the catchment and pond data.

Special thanks are due to Mrs. Geetanjali Mishra for her good wishes and encouragement during my stay at I.I.T. Roorkee.

My sincere thanks are due to my late parents for providing me divine power throughout the period of the study at IIT Roorkee.

I am grateful to my parents-in-laws Mr. Manik Chndra Pramanik and Mrs. Pratima Pramanik who treated me as one of their family members and provided me constant moral support and encouragement during my study.

My special thanks are due to my wife Mrs. Mukul who is always a constant source of inspiration and encouragement and mental and moral support to me and to her sacrifice made for me. Thanks are also due to my elder brother Mr. Ashok Kumar Barik and sister-in-law Mrs. Namita Barik, and my sisters' Mrs. Hemanti Barik, and Mrs. Arati Barik and my brother-in-laws, Mr. Nandalal Barik and Mr. Chandra Mohan Barik, and other family members for their encouragement, support, and belief in me.

Last but not the least, I want to thank my friends and colleagues, Dr.B.Sahoo, Dr. M. R. Ramesh, Dr. K. Gopi Krishna, Mr. Venkateswara Rao Komma, Mr. Ravindra V. Kale, Mrs. K.P. Samal, Mr. K.K. Mohanta, Ms. Sailaza Verma, Dr. D. Deshmukh, Dr. P.K. Singh, Mr. S. Singh Rawat, Mr.Pradeep Kumar, Mr. Gaikuad, Mr. A. Saha, Mr. B. Nikama and others for helping me directly or indirectly in my work and making my stay happy and memorable at I.I.T. Roorkee. Thanks are due to my brother-in-laws Mr.Swapan Kumar and Mr. Tapan Kumar for their directly or indirectly help and good wishes during my stay in Roorkee.

(Dillip Kumar Barik)

TABLE OF CONTENTS

LIST OF TABLES

LIST OF FIGURES

NOTATIONS

The following notations are used in this thesis. In chapter-II, which deals with review of literature, original notations have been used.

a_1, a_2 = mean atmospheric transmissive coefficient (-);

a_t = atmospheric transmissive coefficient (-);

a = coefficient that depends on cloud (-);

A_a = area of the agricultural land use (m^2);

A_f = Area of the forest land use (m^2);

A_{tank} = surface area of the storage tank (m^2);

b = coefficient that depends on cloud (-);

B = constant in equation A.13.1(-);

c_p = specific heat of water (J/kg ^{0}C);

c = fraction of sky covered by cloud (-);

C = locus of the sun (m);

C_B = coefficient in Bowen ratio (mb^0C^{-1})

C_1, C_2 Plank's 1st and 2nd constant (Wm^2) and (m^0K);

CN = curve number (-);

$\overline{CN}$ = weighted curve number (-);

c_a = fraction of solar radiation not absorbed by the cloud (-);

c_d = dust coefficient (-);

D_0 = initial depth of water in the storage tank (m);

d_w = depth of water table from the tank bed (m);

e = eccentricity of the earth orbit (m);

e_s = saturation vapor pressure (mb);

e_a = vapor pressure at air temperature (mb)

E evaporation rate (mm/day);

E_a = correction factor for equation of time (-);

E_t = equation of time (minute);

$E_{b\lambda}$ = energy emitted by the blackbody $\left(W/m^2\mu m\right)$;

G_{sc} = solar constant (W/m^2);

h = hydraulic head (m);

h_1, h_2, h_3, h_4 = hydraulic head at point 1,2,3 and 4 respectively in Fig. 5.1(m);

h_v = soil capillary pressure (m);

H_N = net radiation reaching to the surface per unit area (W/m^2);

H_L = long wave radiation per unit area (W/m^2);

H_B = back radiation from water surface per unit area (W/m^2);

H_E = heat loss due to evaporation per unit area (W/m^2);

H_S = sensible heat per unit area (W/m^2);

H_{SW} = sort wave radiation per unit area (W/m^2);

H_H = extraterrestrial radiation per unit area (W/m^2);

H_{OH} = extraterrestrial radiation on the horizontal surface (W/m^2);

H_{nB} = net back radiation from the water surface (W/m^2);

H_{nL} = net long wave radiation per unit area (W/m^2);

H = hour angle during sunrise to noon or from noon to sunset (degree);

H_1 = incoming heat per unit area (W/m^2);

H_2 = out going heat per unit area (W/m^2);

h_s = seepage head (m);

h_{sh} = hour angle (degree);

h_{f1} = suction head of the fine sediment layer (m);

h_{f2} = suction head of the sub soil layer (m);

h_{s1} = hour angle at time t_1 (degree);

h_{s2} = hour angle at time t_2 (degree);

$k(\theta)$ = unsaturated hydraulic conductivity (m/day);

$\tilde{k}_1$ = saturated hydraulic conductivity in the fine sediment layer (m/day);

$\tilde{k}_2$ = saturated hydraulic conductivity in the subsoil (m/day);

k_h = harmonic mean of the saturation hydraulic conductivity (m/day);

l = pore connectivity parameter (-);

L_w = latent heat of vaporization (J/kg);

L_{st} = standard meridian for local time zone (degree);

L_{loc} = longitude of the location in question (degree);

m_v = empirical parameters depends on soil type (-);

n_v = empirical parameters depends on soil type [-];

p = reference pressure at mean sea level (mb);

p_a = atmospheric pressure (mb);

p_w = pore water pressure (m);

P_1 = location of the earth at equator[-];

P_{Wc} = mean daily perceptible atmospheric water content (-);

q = seepage rate (m/day);

r = distance from earth to sun at nth day (m);

r_0 = mean earth distance from the earth to sun (m);

R_s = albedo (-);

rad = radian (-);

R_g = reflectivity of the ground (-);

S = potential storage parameter (mm);

ST = local standard time (time);

t_{d_s} = time taken to the saturation front to surpass the fine sediment layer (day);

t_{ss} = solar time at sunset (hour);

t_{ssi} = standard time for sunset (hour);

t_{sri} = standard time for sunrise (hour);

T = temperature of the black body surface (^{0}C);

T_a = average air temperature (^{0}C);

T_d = dew point temperature(^{0}C);

T_w = average water temperature (^{0}C);

t_w = time required to reach water table to the saturation wetting front (day);

t_{dry} = time required to the tank to get dry (day);

V_w = volume of water in the storage tank (m^3);

$W(t_d)$ = cumulative infiltration at the time of the saturation wetting front surpass the fine sediment layer (m);

$W(t_w)$ = cumulative infiltration at the time of the saturation wetting front the water table (m);

$W(n^*)$ = quantity that has infiltrated at the n^* day when the saturation front is just behind the interface (m);

x = semi-major axis of the ellipse (m);

y = Semi-minor axis of the ellipse (m);

Z elevation of the site (m);

z_f = saturation water front depth (m);

α = Empirical parameter, depends on soil type (cm^{-1});

α_s = solar altitude angle (degree);

α_0 = proportionality constant (-);

ρ = density of water (kg/m^3);

σ = Stefan Boltzman constant $\left(W/m^2K^4\right)$;

λ = wave length (m);

ϕ = latitude of the location (degree);

θ_{i1} = initial soil moisture content in the fine sediment layer (cm^3/cm^3);

θ_{i2} = initial soil moisture content in the sub soil layer (cm^3/cm^3) ;

θ_{s1}		saturation soil moisture content in the fine sediment layer (cm^3/cm^3) ;
θ_{s2}		saturation soil moisture content in the sub soil layer(cm^3/cm^3);
θ_r	=	residual moisture content (cm^3/cm^3) ;
θ_s	=	Saturated soil moisture content (cm^3/cm^3);
θ_z	=	solar zenith angle (degree);
θ_{z1}	=	cosine of solar zenith angle (degree);
θ_{am}	=	optical mass (-);
υ	=	The anomaly of the earth at a given time and which is equal to $\frac{2\pi n}{365}$
υ_z	=	solar zenith angle at pole (degree);
Δt	=	time step ;
Δs	=	change in soil moisture due to evaporation and drainage;
ε	=	ratio between $\frac{\tilde{k}_1}{\tilde{k}_2}$
ε_a	=	emissivity of air (-);
ε_w	=	emissivity of water (-);
τ	=	correction factor (-)

ABBREVIATIONS

The following abbreviations are used in this thesis:

Fig.	=	Figure;
eg.	=	For example;
i.e.	=	That is;
Exp	=	Expontial;
ASCE	=	American Society of Civil Engineers;
USA	=	United States of America;
SCS	=	Soil Conservation Service;
Res.	=	Research;
Jr.	=	Journal;
Wat.	=	Water;
D.S.T	=	Dead Storage Level

CHAPTER-1

INTRODUCTION

1.1 GENERAL

Water balance study is a pre-requisite for planning of efficient water management practice. In semi-arid regions, run off originating from rainfall is conserved in storage tanks. These storage tanks are shallow reservoirs formed by constructing earthen embankments across seasonal streams. In some places water from seasonal streams is diverted to natural depressions. Such storage tanks are common in the dry zone of Sri Lanka (Jayatilaka *et al.*, 2003) and in southern and central part of India (Anbumozhi *et al.*, 2001). The storage tanks support supplementary irrigation, function as an important water source for people, livestock, pisciculture and are places of recreation and worship. In India, tank irrigation is about 20% of the total area irrigated. In Tamil Nadu state of India, there are more than 39, 000 tanks (Palanisami and Meinzen-Dick, 2001). Storage tanks are used as surface water harvesting structures, and act as sources of ground water recharge. Water balance studies are used to assess whether a potential or existing source will meet the projected water demand. Silting of tank reduces loss due to infiltration, decreases the storage facilities, increases the water temperature during summer, and enhances evaporation loss. However the water infiltrated is conserved in groundwater storage. A rigorous water balance of the tank would enable to determine the depth of water that should be maintained in the tank, the amount of water that gets recharged to underground storage and the extent of removing the fine sediments deposited on the bed of tank surface to increase the storage capacity.

The component processes involved in water balance in a storage tank are: (1) run off from contributing catchment of the tank, (2) evaporation loss from the storage tank, (3) infiltration from the tank bed. These process level models are integrated in a water balance study. A typical medium size storage tank is shown in Fig. 1.1

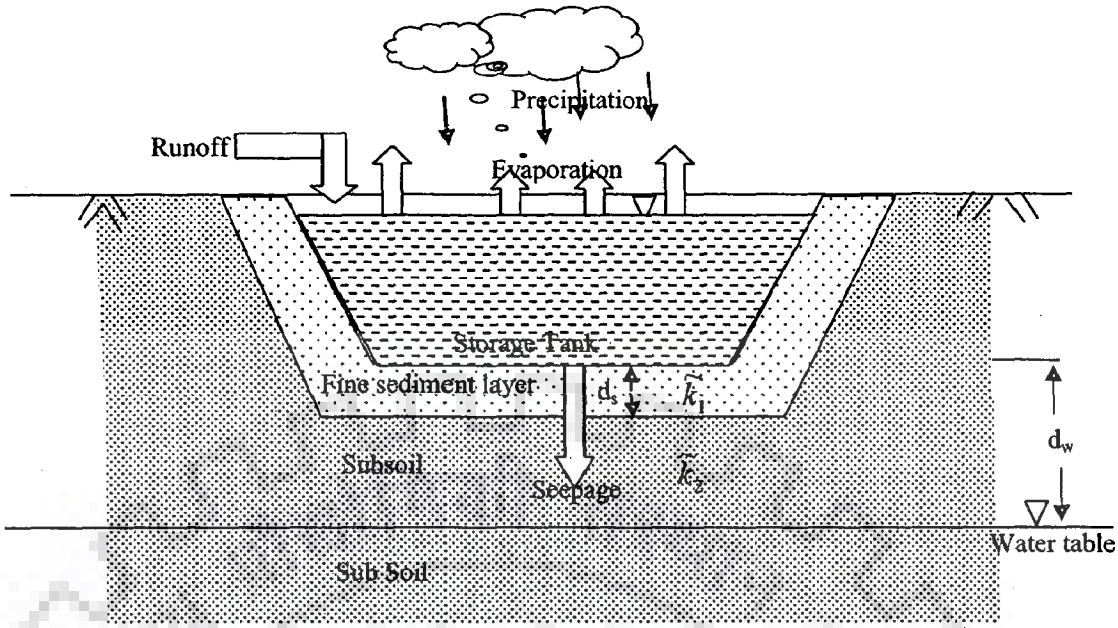

Fig.1.1 Schematic diagram of different components of a water balance model in the storage tank

The process level models have been studied by many hydrologists. Soil Conservation Service (SCS) method has been widely used for computation of surface runoff from a single rainfall event for three different antecedent soil moisture conditions. A rigorous quantification of storage, S has been made by Hawkins (1978). Several investigators have contributed for prediction of the curve number (Hjelmfelt, 1991; Ponce and Hawkins, 1996). Ponce and Hawkins (1996) have provided a critical review of the SCS method and its limitations and usefulness. Despite widespread use of SCS-CN methodology, the accurate estimation of parameter CN has been a topic of discussion among hydrologists and water resources community (McCuen, 2002; Simonton et al., 1996; Bonta, 1997; Sahu et al., 2007; and Mishra and Singh, 2006).

A sensitivity analysis shows that the errors in CN have more serious consequences on runoff estimates than the errors of similar magnitude in initial abstraction or rainfall (Deshmukh, 2008). Soil moisture in the top soil layer of the catchment changes during inter-storm period because of evapotranspiration and drainage of the top surface layer. Hence the storage, S and the curve number are required to be updated for accurate estimation of the runoff for subsequent rainfall events. Literature review shows that

continuous updating of curve number considering evaporation and drainage have not been approached.

In comparison to evaporation, significant amount of water is lost from a storage tank due to infiltration depending upon the hydro-geological condition at the tank site. The evaporation loss depends upon in coming solar radiation which in tern varies with solar hour angle. Therefore, considering change in solar hour angle with time, evaporation can be estimated accurately.

A well known equation to predict infiltration into underlying unsaturated homogeneous soils is the Green and Ampt equation. If the difference between the values of seepage coefficients (hydraulic conductivities) of the fine sediments layer deposited on the tank bed and underlying soil is significant, then, water may percolate from the fine sediment layer in isolated jets (Polubarinova-Kochina, 1962) and may not fill all the soil pores in the underlying layer. The Green and Ampt approach has been effectively applied to layered soils of decreasing permeability (Childs and Bybordi, 1969; vide. Pachepsky and Timlin 1996). In a two-layered soil system, where the underlying soil layer has higher conductivity and porosity than the overlying soil, several investigators have found that, the underlying coarse soil layer will not be saturated and water moves into the coarser soil through narrow flow channels (finger). The concept of a saturation piston flow in Green and Ampt infiltration equation is inapplicable in such layered soil system.

Thus, a commonly used Green and Ampt model, in which a sharply-defined wetting front and piston flow are assumed, cannot be used for the case in which underlying soil is coarser than the top soil layer (Pachepsky and Timlin 1996).Where the upper layer is coarser one having higher porosity and higher conductivity, Green and Ampt assumption of sharply defined wetting front is applicable. Sonu (1986) computed vertical infiltration by using Green and Ampt infiltration equation into stratified soil for groundwater accretion by assuming top layer has higher hydraulic conductivity. Chu and

Mariño (2005) determined ponding condition and infiltration into layered soils under unsteady rainfall by using Green and Ampt infiltration equation by assuming upper soil layer having more hydraulic conductivity.

1.2 OBJECTIVES OF PRESENT RESEARCH

The objective of the present study is to carry out a rigorous water balance in a storage tank and apply to a case study in a drought prone area.

1.2 ORGANIZATION OF THESIS

The presentation of the work in this thesis has been organized in eight chapters as follows:

Chapter-I: Introduction

This chapter consists of a general introduction to research objectives. The objectives of the study have also been identified here.

Chapter-II: Literature of Review

This chapter covers the critical review of the previous investigations pertaining to evaporation, SCS method for runoff computation, and application of Green and Ampt infiltration theory for layered soil system.

Chapter-III: Computation of Evaporation from a Storage Tank by Using Heat Balance Equation

This chapter deals with estimation of evaporation. Hourly evaporation has been estimated from a storage tank using heat balance equation. Variation in the depth of water in the storage tank due to evaporation has been taken into consideration.

Chapter-IV: Computation of Runoff by SCS Method by Updating Curve Number

In this chapter considering evaporation and drainage from the upper soil layer, the storage parameter has been continuously updated for estimation of curve number. Runoff from the contributing catchment has been obtained using SCS method.

Chapter-V: Computation of Seepage from a Storage Tank using Green and Ampt Infiltration Theory

In this chapter infiltration from a storage tank in a two layered soil system has been analyzed using Green and Ampt infiltration theory. The variation in depth of water due to infiltration has been taken into account. Analytical expression for infiltration has been derived. Application of Green and Ampt theory to layered system has been investigated.

Chapter-VI: Computation of Seepage from a Storage Tank using Green and Ampt Infiltration Theory Considering Evaporation, Rainfall, Runoff and Seepage

In this chapter applying a numerical method considering all components contributing to variation in depth of water in the storage tank, infiltration rate has been estimated and water balance study has been done by using rainfall, infiltration, evaporation (obtained by Panmen's method) and runoff (obtained by SCS method) to know the depth of availability in the storage tank.

Chapter-VII: Water Availability in Asha Sagar Storage Tank –A Case Study

In this chapter a case study has been presented to check the water availability in the Asha Sagar storage tank which is located in a drought prone area. The water balance has been done by using rainfall, infiltration, evaporation (obtained by heat balance equation), runoff (obtained by SCS method by updating curve number), and outflow from the storage tank.

Chapter-VIII: Conclusions

Finally in this chapter the important conclusions based on the present study have been drawn. Also it briefs the specific contributions of the present study and the scope of future work.

CHAPTER-2

LITERATURE REVIEW

2.1 INTRODUCTION

The demand for improved and sustainable agricultural production is increasing day-by-day in developing countries because of population growth. Water availability for supplementary irrigation is one of the prime factors for adequate food production. In semi arid region, the surface runoff is stored in storage tanks which are generally of small to medium size. It is widely recognized that the productivity of the limited water resources needs to be maximized. Quantification of the water availability in storage tank in the dry zones accounting for all the components of dry-land hydrology is the pre-requisite for efficient water use.

The hydrology of tank water balance deals with the component processes of evaporation from water bodies and soil moisture zone, infiltration, surface runoff generation and seepage from storage tank. Over the years, several researchers have studied on the water balance of tank irrigation system using physically based deterministic approaches. Recently, for the dry zones of Sri Lanka, Jayatilaka et al. (2003) presented a small-scale model for cascades of the order of 10 interconnected reservoirs. The model is designed to estimate tank water availability on a daily basis accounting for generation of runoff, and seepage. There had been several studies carried out to understand the key hydrologic parameters of tank cascades and quantifying water balance components (e.g., Dharmasena, 1989, 1991; Kitamura, 1984, 1990; Itakura, 1995; Usgodaarachi et al., 1996; Shinogi et al., 1998; Tasumi et al., 1999). Similarly, Nath and Bolte (1998) developed a water budget simulation model for forecasting water requirement in an aquaculture pond at Asian Institute of Technology

(AIT). In this model, water gain by precipitation, regulated inflow and runoff, and water loss by evaporation and seepage are quantified.

A brief review of the significant contributions, made by various researchers in tank water balance study that, integrates various component process, is presented in the literature review.

2.2 EVAPORATION

Evaporation is a complex phenomenon and it is the subject of scientific inquiry since the early 19th century. The earliest attempts to explain the evaporation process is the involvement of the principles of vapor pressure which was proposed by Dalton in 1802. An authentic description and observations of different philosophers and thinkers about evaporation is given by Brutsaert (1982).

Evaporation is primarily governed by meteorological parameters such as: temperature, wind speed, relative humidity, and solar radiation. The other minor influences include surface roughness and vegetation on the upwind and downwind side of the pond/lake. Usually, evaporation increases with increases in wind speed and water surface temperature. Similarly, an increase in the dew point temperature tends to decrease the differential vapor pressure and consequently decreases evaporation. According to Knapp et al. (1984) evaporation is sensitive to water temperature.

Significant amounts of water can be lost from ponds and storage tanks because of evaporation (Szumiec, 1979). This evaporative water loss from the irrigation tanks, E, is primarily a function of ambient air temperature, relative humidity and wind velocity which can be estimated as (Gray, 1970):

$$E = \frac{A\phi_e}{\rho_w L} \tag{2.1}$$

where ϕ_e is evaporative heat loss (kJ m^{-2} day^{-1}), ρ_w is water density (kg m^{-3}), L is latent heat of vaporization of water (kJ kg^{-1}), and A is the constant for unit conversion.

Nath (1996) and Henderson-Sellers (1984) suggest that more accurate evaporative heat loss estimates can be obtained using the approach of Ryan et al. (1974):

$$\phi_e = (e_s - e_a)\left[\lambda(T_{wv} - T_{av})^{\frac{1}{3}} + b_0 u_2\right] \tag{2.2a}$$

where

$$T_{wv} = \left\{\frac{T_{wk}}{[1.0 - (0.378 \times e_s / P)]}\right\}, \tag{2.2b}$$

$$T_{av} = \left\{\frac{T_{ak}}{[1.0 - (0.378 \times e_a / P)]}\right\}, \tag{2.2c}$$

e_s is saturated vapor pressure at the current water temperature (mm Hg), e_a is water vapor pressure immediately above the pond or tank surface (mmHg), T_{wv} and T_{av} are the virtual water and air temperatures, respectively (^{0}K), T_{wk} and T_{ak} are the absolute water and air temperature (^{0}K), P is the barometric pressure (mm Hg), which is equivalent to atmospheric pressure, λ and b_0 are constants with values of 311.02 kJ m^{-2} day^{-1} mmHg^{-1} K$^{-1/3}$ and 368.61 kJ m^{-2} day^{-1} mmHg^{-1} (m s^{-1}) $^{-1}$, respectively, and u_2 is wind velocity (m s^{-1}) at a reference height of 2 m. The conductive heat removal component of Eq. (2.2a) is valid only when T_{wv} is greater than T_{av} (Ryan et al., 1974)

Many methods exist for either measuring or estimating evaporative losses from free water surfaces. There are number of methods proposed by various researchers to explain the theory of evaporation and the influence of various factors to the evaporation. The widely accepted methods are discussed below.

2.2.1 Combination Methods

The concepts of combination methods are relatively new. Penman has given the first basic method for estimating evaporation from natural surfaces (Penman, 1948). In the combination methods both the aerodynamic terms and the radiation terms appear

explicitly in the same equation and hence, these are called "combination methods". These methods are convenient because they require meteorological information from one level only. Hence, the combination methods are widely used in hydrology (Thom and Oliver, 1977). Most of the combination equations assume two conditions: (1) vertical divergence of the heat fluxes between the surface and the point of measurement is negligible and (2) that the turbulent heat transfer coefficients for water vapor and sensible heat are substantially equal. It means that the conditions can be met by taking measurements as close to the evaporating surface as possible (van Bavel, 1966). According to van Bavel (1966) in spite of accurate estimates made by combination methods, there are many literatures sighted with contradictions regarding the efficiency of the method. van Bavel stated this could be for the following reasons:

(a) Unavailability of short term accurate data on evaporation;

(b) Net radiation is estimated rather than measured;

(c) Empirical formulations of the wind function calibrated for one location cannot be used for other locations.

Accurate estimation of evaporation can be obtained by using daily totals of net radiation, a simple wind function that accounts for the roughness of the surface, and daily values of standard meteorological data. Many investigators have suggested improvements to the original Penman method. However, all of them retain the same form, i.e., the aerodynamic and radiation terms. Some of the accepted modified methods were the FAO-24 Penman method, the Penman- Montieth method, the Kohler-Nordenson-Fox method, and the Kohler-Parmele method.

2.2.2 The FAO-24 Penman Method

The FAO-24 Penman method to calculate evapotranspiration is like the Penman method (1948). This equation was first calibrated with grass as a reference crop and crop coefficients for different crops were used to find the amount of water lost due to

evapotranspiration (Doorenbos and Pruitt, 1977). A coefficient has also been assigned for water surface that would predict the amount of water lost due to evaporation. These coefficients relate crop evapotranspiration to reference crop evapotranspiration and are assigned values depending on the aridity of the region, crop characteristics, time of planting and sowing, and general climatic conditions (Doorenbos and Pruitt, 1977). Coefficients for open water were in the range of 1.1 - 1.2 depending on the atmospheric conditions (humid or arid).

Some modifications are made to the original Penman method in order to use the equation with more accuracy. The improvements included a revised wind term and a modified adjustment factor "c" to account for the differences in day and night time climatic conditions. The "c" was used even by Penman when he originally proposed the combination method (Penman, 1948). The equation, as proposed by Doorenbos and Pruitt (1977) for the FAO, is as follows:

$$ET_0 = c[W R_n + (1-W) f(u)(e_a - e_d)] \quad (2.3)$$

where ET_o is the reference crop evapotranspiration (mm/day), W is the temperature related weighing factor, R_n is the net radiation (mm/day), $f(u)$ is the wind related function (km/ day), (e_a-e_d) is the difference between saturated vapor pressure (mb) at mean air temperature, and mean actual vapor pressure of the air (mb). The wind function is given as:

$$f(u) = 0.27\left(1 + \frac{U}{100}\right) \quad (2.4)$$

where U is wind speed (km/ day) measured at 2 m height from ground surface.

2.2.3 The Penman-Montieth Method

Another variation of the original Penman method is given by Montieth (1965). This variation introduced new terms that would explain the resistance offered by plants with and without the stomata to the water. These were the aerodynamic resistance to water

vapor (r_a) and bulk stomatal resistance (r_s). Aerodynamic resistance is the time for a unit volume of air to exchange with a unit area of surface. This partly depends on the speed of the air stream and partly on the roughness of the surface. The bulk stomatal resistance is the internal resistance offered by the leaf. In the case of leaves bloated with water, the latter is zero since there is no resistance offered by the stomata (Montieth, 1965). The equation presented below is a variation of the Montieth equation (1965), used by the Soil Conservation Service (1993).

$$E = \left\{ \left(\frac{\Delta}{\Delta + \gamma_s} \right) (R_n - G) + \left(\frac{\gamma}{\gamma + \Delta} \right) (1710 - 6.85T) \left(\frac{1}{r_a} \right) (eoz - ez) \right\} \frac{1}{\lambda} \qquad (2.5)$$

where Δ is the slope of saturation - vapor pressure curve (kPa/ °C), γ is the psychrometric constant (kPa/ °C), R_n is net radiation (MJ/ m^2/day), T is the mean temperature (°C), r_a is the resistance offered by air (s/ m), γ_s is the ratio of the resistance offered by air to the resistance offered by stomatal pores (r_c), eoz is the vapor pressure, kPa, at height z (m), and ez is the saturation vapor pressure at dew point temperature (kPa), λ is the latent heat of vaporization (MJ/ m^2/day), and E is the evaporation (mm/ day).

The above equation shows that the rate of evaporation depends on heat from external sources, temperature, humidity, wind speed, surface roughness, and crop resistance. When the leaf resistance is constant, evaporation increases linearly with radiation, wet-bulb depression and with air temperature, when radiation and wet-bulb depression are held constant. Evaporation is independent of wind speed when the wet-bulb depression is the same at the leaf surface and the surrounding air (Montieth, 1965). Due to the presence of the various resistance terms, this equation was widely used to predict loss of water due to evapotranspiration from crops. With slight modification to the equation proposed by Montieth to account for the surface parameters based on

surface roughness and vegetation type, Allen (1986) investigated that, evapotranspiration can be estimated accurately with this equation.

2.2.4 The Kohler-Parmele Method

Kohler and Parmele have given their version of the Penman equation (Kohler and Parmele, 1967). Though the investigators felt that the equations proposed by other researchers are adequate, but there are certain drawbacks that need to be overcome. For example, in the original Penman equation, it was assumed that the net radiation term (Q_n) is representative of the heat exchange at the water surface and Δ can be calculated at air temperature, T_a. If observations are to be made directly over the water surface, the net radiation term in Penman's method would be accurate. But unfortunately, that is rarely so. Penman's method does not take into account of any difference between the air and surface water temperatures and hence, the calculation of the net radiation term is treated as a function of air temperature only. In order to accommodate the difference, the net radiation can be expressed as follows:

$$Q_n = Q_{ir} - Q_b \tag{2.6a}$$

$$Q_n = Q_{ir} - \varepsilon \sigma T_0^4 \tag{2.6b}$$

where Q_{ir} is the difference between incident and reflected radiation (inches/ day), Q_b is emitted radiation (inches/ day), Q_n is the net radiation (inches/ day), ε is emissivity of water surface, σ is Stefan-Boltzmann's constant (cal. / cm^2 / K^4 / day), and T_o is the water surface temperature (°K). Taking only the first two terms of the binomial expansion of Q_b and substituting into the Penman's method, the following equation is obtained (Kohler and Parmele, 1967). In the above equation heat energy is converted into depth of water by dividing with density of water and latent heat of vaporization.

$$E = \frac{\left(Q_{ir} - \varepsilon \sigma T_0^4\right)\Delta + E_a\left[\gamma + 4\varepsilon T_a^3 / f(u)\right]}{\Delta + \left[\gamma + 4\varepsilon T_a^3 / f(u)\right]} \tag{2.7}$$

where E_a is the evaporation calculated using only the aerodynamic term, Δ is the slope of the vapor pressure curve (mb/ °C), γ is the psychrometric constant (mb/ °F), and *f(u)* is the associated wind term (miles/day). The term that appears in parentheses with the γ, has to be corrected for accounting long wave radiation at temperature T_0 rather than at T_a.

A wind function was proposed, which is similar to the wind function originally proposed by Penman. The proposed wind function is as follows:

$$f(u) = (0.181 + 0.00236U_4) \tag{2.8}$$

where U_4 is the wind speed (miles/ day) measured at height 4 m above the surface. Usually, wind speed is measured at a height of 2 meters. In order to find the wind speed at any other height, correction needs to be applied. The velocity varies exponentially and was first developed by Prandtl (Streeter et al., 1988).

$$u = u_0 \left(\frac{z}{z_0} \right)^{\frac{1}{7}} \tag{2.9}$$

where u_o is the velocity, typically in m/s, measured at z_o, in m, and u is the velocity (m/s) computed for any height of z (m). The exponent (1/7) is replaced by 0.2 as recommended by the SCS (1993).

2.2.5 The Kohler-Nordenson-Fox Method

Efforts had been made to estimate evaporation at Lake Hefner, Oklahoma, which had produced another prediction equation by Kohler et al. (1955). Though some of their attention was directed at verifying pan evaporation data, they questioned the practice of applying the pan evaporation data to a large lake. The main objection was that the complex dynamics of lake evaporation cannot be substituted by pan evaporation. There is a marked difference between the two.

Observations demonstrated that the annual exchange of sensible heat at the pan-air interface is large depending on the meteorological and radiation factors. However, the annual heat transfer through the bottom of the lake is zero. Hence, pan data should be adjusted before applying the coefficient. Kohler et al. (1955) had proposed the following equation for estimating lake evaporation:

$$E_a = \left(\frac{ez_0 - ez}{33.364}\right)^{0.88} (0.37 + 0.0041U) \tag{2.10}$$

where U is the wind velocity measured, in miles/ day, ez_o and ez are the vapor pressures, measured in inches of mercury, at the water surface and the over lying air respectively, and E_a is the estimated evaporation in inches/day. The 0.88 as a power term is relevant to the sensible heat transfer from the water surface of the pan, but does not make any difference whether the 0.88 or unity is used for lake evaporation (Kohler et al., 1955). The authors admit that due to lack of good data, the data from Lake Hefner was used and the equation was found to give good results when compared to mass transfer techniques.

2.2.6 The Borrelli-Sharif Method

Researchers at Texas Tech. University have proposed an equation that is another variation of the Penman equation. The major difference from the other method is that, there are no empirical coefficients in the model. The presence of each of the terms in the equation was explained by widely accepted theory as:

$$L_e E = \left[\frac{\Delta Q_n}{\left[\Delta\left(1 + \frac{1.45\, C_p T}{L_e}\right) + \gamma\, Le_t\right]}\right] + \left[\frac{\gamma\, \mathrm{Pr}_t^{-1}}{\left[\Delta\left(1 + \frac{1.45\, C_p T}{L_e}\right)\right]}\right] \tag{2.11}$$

$$\left[\frac{\varepsilon\, \rho\, k_0^{\,2} L_e}{P \ln\left[\frac{z-d}{z_0}\right]^2}\right] u_s \left(e_z^* - e_z\right)$$

where L_e is the latent heat of vaporization (cal/cm^3), E is estimated evaporation (cm/ day), Δ is the slope of the saturation pressure - temperature curve (mb/ °C), Q_n is the net radiation (langleys/ day), C_p is the specific heat of air at constant pressure (cal./ gm/ K), T is mean temperature (K), γ is psychrometric constant (mb/ °C), Pr_t, is the turbulent Prandtl's number, Le_t is dimensionless Lewis number, ε is the emissivity of water surface. ρ is density of the atmosphere (gm/cm^3), k_o is the von Karman's constant, P is the atmospheric pressure (mb), u_z is wind speed, (km/ day), e_z* is the vapor pressure at mean air temperature (mb), and e_z is the vapor pressure at dew point temperature (mb).

Some of the drawbacks of the existing models addressed by this model are the influence of air density variations in the atmosphere that result from temperature and humidity differences, the fallacious assumption that eddy coefficients for momentum (K_m), for heat (K_h), for water vapor (K_e) are equal. Another drawback of other methods is that they assume there is the linear relationship of the wind velocity with evaporation (Sharif, 1989). Improvements are made in this model that takes into consideration the above drawbacks and recommendations are made as to how to overcome these shortcomings in other methods. It is accepted that there is an upper limit to the effect of wind velocity on the magnitude of evaporation. According to the wet-bulb theory, when equilibrium exists, the heat needed to evaporate water is drawn from the air. The temperature drops down to its lowest limit called the "wet-bulb" temperature. The temperature cannot drop down any further even if there is an increase in the velocity of the air. This also implies that there is a finite upper limit to the effect of wind velocity on evaporation. Further research is needed to exactly quantify the wind speed upper limit (Sharif, 1989). Very accurate estimates were expected from this method since there are no empirical coefficients or constants.

2.2.7 Miscellaneous Methods

Some of the other prominent methods used for estimating evaporation are the Utah State University method, the Morton's method, and the Stewart-Rouse method. Investigators at Utah State University have modified the Penman method by adopting an albedo value of 0.06 for free water surface and by adjusting the wind function (USU Report, 1994). The proposed equation is as follows:

$$E_{lake} = \frac{0.7}{\lambda}\left[\frac{\Delta}{\Delta+\gamma}R_{nl} + \frac{\gamma}{\Delta+\gamma}15.36(1.0+0.01U_2)(es_a - es_d)\right] \quad (2.12)$$

where E_{lake} is the evaporation of lake (cal/cm^2/d), λ is the latent heat of water (cal/cm^3), Δ is the slope of the saturation vapor pressure - temperature (mb/ °C), γ is the psychometric constant (mb/ °C), R_{ni} is net radiation (cal/ cm^2 / d), U_2 is the wind speed (miles/ day), es_a is the saturation vapor pressure {mb) and es_d is the actual vapor pressure (mb). According to the USU report, the evaporation estimates do not account for the water surface temperature. Effects of water inflow and outflow, subterranean thermal springs are not included. This could lead to erroneous evaporation estimates during the winter months. Better estimates can be expected from the equation if water surface temperatures were used (USU Report, 1994). Stewart et al. (1976) have proposed a simple method to estimate evaporation from temperature and radiation measurements. The equation is as follows:

$$LE_i = \left[\frac{S}{S/\gamma}\right](1.624 + 0.9265K) \quad (2.13)$$

where LE_i is the evaporative heat flux, S is the slope of the saturation vapor pressure - temperature curve at mean air temperature (kPa/ °C), K is the incoming solar radiation (MJ/m^2). One of the limitations of the method is that its accuracy is confined to shallow lakes and ponds. Morton (1979) modified an equation proposed by him earlier in 1975. This modification was done in order to make the equation less sensitive to differences

in land and lake based environments. One of the advantages of the model is that it has no local optimization coefficients. Changes to albedo and emissivity terms modify the model in such a way that it can provide estimates of monthly evaporation from shallow lakes and estimates of annual evaporation from any lake. Due to the above reasons, this model can be used to estimate evaporation in any part of the world. The equation proposed by Morton (1979) is as follows:

$$E_w = \psi(R_w + M) \tag{2.14a}$$

where

$$\psi = 0.26\left[1 + \frac{\lambda}{\Delta}\left(\frac{0.5 + 0.5r + \lambda/\Delta}{r + \lambda/\Delta}\right)\right]^{-1} \tag{2.14b}$$

$$M = 0.66B - 0.44R_w \tag{2.14c}$$

where E_w is the lake evaporation (W/ m^2), λ is the heat transfer coefficient (mb/ °C), Δ is the slope of the saturation vapor pressure - temperature (mb/ °C), r is the relative humidity, a dimensionless ratio, M is the advection energy (W/m^2), B is the net longwave radiation loss if the surface were at air temperature (W/ m^2), and R_w is the net radiation if the surface were at air temperature (W/ m^2).

Researchers have provided mathematical representations to the theory of evaporation in the form of equations and those are used to estimate the magnitude of evaporation.

There are several other methods for estimating evaporation. Methods have been classified into five major groups as: (i) combination group, (ii) solar radiation, temperature group, (iii) Dalton group, (iv) temperature, day length group, and (v) temperature group and the brief description of these methods are presented in Table 2.1 (Rosenberry et. al.2007).

Table 2.1 Methods for calculation of evaporation (E) in mmd^{-1}

1. **Combination Group**

Method	Equation	Developed for	Reference
Priestley-Taylor	$E = \alpha \frac{s}{s+\gamma} \frac{Q_n - Q_x}{L\rho} \times 86.4$	Periods of 10 day or greater	Stewart and Rouse ,1976
deBruin-Keijman	$E = \frac{s}{0.85s + 0.63\gamma} \frac{Q_n - Q_x}{L\rho} \times 86.4$	Daily	deBruin and Keijman, 1979
Penman	$E = \frac{s}{s+\gamma} \frac{Q_n - Q_x}{L\rho} \times 86.4 + \frac{\gamma}{s+\gamma} \{0.26(0.5 + 0.54U_2)(e_s - e_a)\}$	Period greater than 10 day	Brutsaert, 1982
Brutsaert-Stricker	$E = (2\alpha - 1)\left(\frac{s}{s+\gamma}\right)\left(\frac{Q_n - Q_x}{L\rho}\right) \times 86.4 + \frac{\gamma}{s+\gamma} \times \{0.26(0.5 + 0.54U_2)(e_s - e_a)\}$	Daily	Brutsaert and Stricker, 1979

Method	Equation	Developed for	Reference
deBruin	$E = 1.192\left(\frac{\alpha}{\alpha - 1}\right)\left(\frac{\gamma}{s+\gamma}\right)$ $\frac{(2.9 + 2.1U_2)(e_s - e_a)}{L\rho} \times 86.4$	Period greater than 10 day	deBruin, 1978

2. Solar Radiation, Temperature Group

Jensen-Haise	$E = (0.014T_a - 0.37)$ $(Q_s \times 3.523 \times 10^{-2})$	Periods greater than 5 days	McGuinness and Bordne, 1972
Makkink	$E = \left(\left(52.6\frac{sQ_s}{s+\gamma L\rho}\right) - 0.12\right)$	Monthly (Holland)	McGuinness and Bordne, 1972
Stephens-Stewart	$E = (0.0082T_a - 0.19)$ $(Q_s \times 3.495 \times 10^{-2})$	Monthly (Florida)	McGuinness and Bordne, 1972

3.Dalton Group

Mass transfer	$E = (NU_2(e_0 - e_a)) \times 10$	Depends on calibration of N	Harbeck et al., 1958

Method	Equation	Developed for	Reference
Ryan-Harleman	$E=\frac{(2.7(T_0-T_a)^{0333}+3.1U_2)(e_0-e_a)}{L\rho}\times 864$	Daily	Rasmussen et al.,1995

4. Temperature, Day Length Group

Blaney-Criddle	$E=(0.0173T_a-0.314)\times T_a\times (D\div D_{TA})\times 25.4$	Monthly	McGuinness and Bordne,1972
Hamon	$E=0.55\left(\frac{D}{12}\right)^2\frac{SVD}{100}(25.4)$	Daily	Hamon,1961

5.Temperature Group

Papadakis	$E=0.5625(e_s\ \max-(e_s\ \min-2))\left(\frac{10}{d}\right)$	Monthly	McGuinness and Bordne, 1972
Thornthwaite	$E=\left(1.6\left(\frac{10T_a}{I}\right)^{6.75\times10^{-7}I^3-7.71\times10^{-5}I^2+1.79\times10^{-2}I+0.49}\right)\left(\frac{10}{d}\right)$	Monthly	Mather, 1978

The notations and symbols used in Table 2.1 are as follow:

$\alpha = 1.26$ = Priestley-Taylor empirically derived constant, dimensionless,

s = slope of the saturated vapor pressure- temperature curve at mean air temperature $\left(P_a {}^0C^{-1}\right)$,

γ = psychrometric constant (depends on temperature and atmospheric pressure) $\left(P_a {}^0C^{-1}\right)$,

Q_n = net radiation $\left(Q_s - Q_r + Q_{ar} - Q_{ds}\right)\left(W m^{-2}\right)$,

Q_s = solar radiation $\left(W m^{-2}\right)$,

Q_x = change in heat stored in the water body $\left(W m^{-2}\right)$,

L = latent heat of vaporization $\left(MJ\, kg^{-1}\right)$,

ρ = density of water $\left(998 kg\, m^{-3} at\, 20^0C\right)$,

N=mass-transfer coefficient (used 0.01644 for Mirror Lake),

I=annual heat index $\left(I = \sum i, i = \left(T_a / 5\right)^{1.514}\right)$,

U_2 = wind speed at 2m above surface $\left(m s^{-1}\right)$,

e_0 = saturated vapor pressure at temperature of the water surface (mb),

e_s = saturated vapor pressure at temperature of the air (mb),

e_a = vapor pressure at temperature and relative humidity of the air (mb),

SVD = saturated vapor density at mean air temperature $\left(g m^{-3}\right)$,

T_a = air temperature, ${}^0F$ for the Blaney- Criddle, Jensen-Haise and Stephens-Stewart equation and ${}^0C$ for the Thornthwaite equation,

D=hours of daylight,

D_{TA} = total annual hours of daylight for specific latitude; for Mirror Lake, at $44^0 N$, $D_{TA} = 4470$,

d=number of days in month,

$e_s$max and $e_s$min=saturated vapor pressures at daily maximum and minimum air temperatures (Pa).

The multipliers 10, 25.4, or 86.4 that appear in several equations are to convert output to

$mm\, d^{-1}$.

Evaporation rates are to a great extent dependent upon the characteristics of the water body. Evaporation from small shallow ponds is usually considered to be quite different from that in large lakes mainly due to differences in the rates of heating and cooling of the water bodies, which because of the size and depth of water in the storage tank and small ponds are different from those in lakes. Additionally, in semi-arid regions, hot dry air moving from a land surface over a small water body like a storage tank or pond results in higher evaporation rates.

In mountainous regions, determination of the spatial and temporal distribution of hydrological parameters such as evaporation and precipitation is difficult. In these regions, hydrological data requirements are usually much greater than in non-mountainous regions. The applications of many of the empirical equations, which are based on climatological data for estimating evaporation, have not been thoroughly tested for high altitude conditions. Particularly, the ability of these equations for defining the variability of evaporation is basically unknown. Historically, pan data are the most common means for defining free water evaporation. Pan evaporation is considered as an indication of the atmospheric evaporative power. Evaporation from a free surface is estimated by multiplying a coefficient to pan evaporation, which is known as pan coefficient. Most of the evaporation pans in India are Class A pans which are made of unpainted galvanized iron or stainless steel of about 122 cm in diameter and 25.4 cm deep. The pans are supported on low wooden frames and are filled with about 20 cm of water. However, the density of evaporation pan stations is much less than that of weather stations. Data input requirements for the different models vary, ranging in complexity from those that use only temperature data to those that require temperature, wind, humidity, and radiation data. The equations using all the four parameters are usually considered the most responsive to climatic variations. The availability of climatic data is a major consideration in selecting a model for calculating

evaporation. Although daily temperature for different location in India can be made available easily, the availability of wind speed, relative humidity, and radiation data is very limited as well as quite short-term in some cases.

As stated by Jensen (1973), "lake evaporation is frequently used as a measure of potential evapotranspiration." This statement is supported by an ongoing study in the Green River Basin of Wyoming for which the preliminary results indicate that the magnitudes of pan evaporation and evapotranspiration from well-watered mountain meadow vegetation are very similar (Burman et al., 1984). Thus, for high soil moisture conditions, evaporation rates calculated for the water surface should be applicable to the surrounding area. Further, Idso (1981) stated that healthy and robust vegetation will decrease evaporation for extensive surfaces area, but less effect for smaller surface areas. Thus, the effect of the presence of vegetation appears to range from being a water conservation mechanism to that of increasing evaporation.

Evaporation pans provide one of the simplest, inexpensive, and most widely used methods of estimating evaporative losses. The use of pan data involves the application of a coefficient to measured pan readings to estimate evaporation from a larger water body. Among many of these existing equations, most of them are based directly upon the equation derived by Penman (1948), the method originally intended for open water surfaces. Penman's method is now commonly applied to estimate the vegetative water use. Although various versions of the Penman equation have been developed, the method developed by Kohler et al. (1955) is the most widely used.

It is not possible to use pan data directly to define the temporal variability of net evaporation. Thus, in many cases, it is decided to use the limited pan data as a source of evaporation data against which evaporation estimates using the climatological models could be compared. Because of a number of models which exist for calculating evaporation estimates, the selection of the most appropriate method for a given

situation is difficult. Selection of a method generally depends upon the availability of data and the ability of the method to estimate both the magnitude and variation of evaporative losses. Unfortunately, for a given situation, no definite guidelines have been given for selecting the method to use.

There have been several validation studies on evaporation (Ventura et al., 1999; Hussein, 1999; Al-Ghobari, 2000; Kashyap and Panda, 2001; George et al., 2002) that have confirmed that the Penman–Monteith (PM) equation generally performs well than all other empirically derived equations. There is a new trend in using data mining techniques such as artificial neural networks (ANN) to estimate evaporation. Some typical studies have been done (Kumar, et al. 2002) in modelling daily evapotranspiration by using ANN. Ambast, et al. (2002) developed a remote sensing based simplified operational procedure to estimate sensible heat flux incorporating the local meteorological conditions to estimate evapotranspiration. The model utilizes the surface reflectance in visible, infrared and thermal bands to generate surface albedo, surface temperature and leaf area index and thus surface energy fluxes to determine regional evapotranspiration. They investigated that their proposed procedure is computationally simple with reasonable accuracy of results.

2.3 RUNOFF ESTIMATION METHODS

A multitude of methods/models are available in hydrologic literature to simulate the complex process of rainfall-runoff in a watershed.

2.3.1 SCS Method for Runoff

In year 1954, the United States Department of Agriculture, Soil Conservation Service (now called the Natural Resources Conservation Service (NRCS)) developed a unique procedure known as Soil Conservation Service Curve Number (SCS-CN) method. Although a complete account of the development of the curve number is unavailable (Hjelmfelt, 1991; Ponce and Hawkins, 1996), Rallison and Cronshey (1979) have

provided some historical insight into its development, and Ponce and Hawkins (1996) have provided a critical review of the method and its limitations and usefulness. Mishra et al. (2005) have carried out an extensive review of the method and various improvements suggested by different researchers. This method, which is basically empirical, was developed to provide a rational basis for estimating the effects of land treatment/land use changes upon runoff resulting from storm rainfall. According to Garen and Moore (2005) "... the reason for the wide application of curve number method includes its simplicity, ease of use, widespread acceptance, and the significant infrastructure and institutional momentum for this procedure within NRCS. To the date, there has been no alternative that possesses so many advantages, which is why it has been and continues to be commonly used, whether or not it is, in a strict scientific sense, appropriate ..."

2.3.2 Theoretical Background

The SCS-CN method is based on the water balance equation and two fundamental hypotheses. The first hypothesis equates the ratio of actual amount of direct surface runoff Q to the total rainfall P (or maximum potential surface runoff) to the ratio of actual infiltration (F) to the amount of the potential maximum retention S. The second hypothesis relates the initial abstraction (I_a) to the potential maximum retention (S), also described as the potential post initial abstraction retention (McCuen, 2002), expressed mathematically as:

(a) Water balance equation

$$P = I_a + F + Q \tag{2.15}$$

(b) Hypothesis of proportional equality

$$\frac{Q}{P - I_a} = \frac{F}{S} \tag{2.16}$$

(c) Hypothesis of relation between initial abstraction and potential maximum retention

$$I_a = \lambda S \tag{2.17}$$

The values of P, Q, and S are given in depth dimensions, while the initial abstraction coefficient λ is dimensionless. The first (or fundamental) hypothesis (Eq. 2.15) is primarily a proportionality concept (Mishra and Singh, 2003a). Apparently, as $Q \rightarrow (P\text{-}I_a)$, $F \rightarrow S$. The parameter S of the SCS-CN method depends on soil type, land use, hydrologic condition, and antecedent moisture condition (AMC). The initial abstraction coefficient λ is frequently viewed as a regional parameter depending on geologic and climatic factors (Boszany, 1989). The existing SCS-CN method assumes λ to be equal to 0.2 for practical applications. Many other studies carried out in the United States and other countries report λ to vary in the range of (0, 0.3). A study by Hawkins et al. (2001) suggested that value of $\lambda = 0.05$ gives a better fit to the data and would be more appropriate for use in runoff calculations.

The second hypothesis (2.17) is a linear relationship between initial abstraction I_a and potential maximum retention S. Combining Eqs. (2.15) and (2.16), the expression for Q has been written as:

$$Q = \frac{(P - I_a)^2}{P - I_a + S} \tag{2.18}$$

Equation (2.18) is the general form of the popular SCS-CN method and is valid for $P \geq I_a$. For $\lambda = 0.2$, combining Eqs. (2.17) and (2.18) results in

$$Q = \frac{(P - 0.2S)^2}{P + 0.8S} \tag{2.19}$$

Equation (2.19) is the popular form of existing SCS-CN method. Thus, the existing SCS-CN method with $\lambda = 0.2$ is a one-parameter model for computing surface runoff from daily storm rainfall.

Since the parameter S can vary in the range of $0 \leq S \leq \infty$, it is mapped onto a dimensionless curve number CN, varying in a more appealing range $0 \leq CN \leq 100$, as:

$$S = \frac{25400}{CN} - 254 \tag{2.20}$$

where S is in mm. The difference between S and CN is that the former is a dimensional quantity [L] whereas the later is non-dimensional. $CN = 100$ represents a condition of zero potential maximum retention ($S = 0$), that is, an impermeable watershed. Conversely, $CN = 0$ represents a theoretical upper bound to potential maximum retention ($S = \infty$), that is, an infinitely abstracting watershed. However, the practical design values validated by experience lie in the range (40, 98) (Van and Mullem, 1989). CN has no intrinsic meaning; it is only a convenient transformation of S to establish a 0–100 scale (Hawkins, 1978).

2.3.3 Curve Number

Despite the widespread use of SCS-CN methodology, the accurate estimation of parameter CN has been a topic of discussion among hydrologists and water resources community (McCuen, 2002; Springer et al., 1980; Hjelmfelt, 1980; Simanton et al., 1996; Steenhuis et al., 1995; Bonta, 1997; Ponce and Hawkins, 1996; Sahu et al., 2007; Mishra and Singh, 2006). Originally CNs were developed using daily rainfall-runoff records corresponding to the maximum annual flows from gauged watersheds for which information on their soils, cover, and hydrologic condition was available (SCS, 1972).

The CN corresponding to the curve that separated half of the plotted data from the other half is taken as the median curve number for the watershed. Thus the developed curve numbers represent the averages or median site values for soil groups, cover, and hydrologic condition and corresponds to AMC II (CN_{II}) condition. The upper enveloping curve was taken to correspond to AMC III (CN_{III}) and the lower

curve to AMC I (CN_I). The average condition is taken to mean average response, which is later extended to imply average soil moisture condition (Miller and Cronshey, 1989). Depending on 5-day antecedent rainfall, CN_{II} is convertible to CN_I and CN_{III} using the relationships given by various researchers.

However, to estimate the average *CN* values (CN_{II}) mathematically from the rainfall (*P*)-runoff (*Q*) data of a gauged watershed, Hawkins (1993) suggested *S* (or *CN*) computation using the expression

$$S = 5\left[P + 2Q - \sqrt{Q(4Q+5P)}\right] \tag{2.21}$$

Note that Eq. (2.21) can be easily derived from Eq. (2.19).

In a subsequent study, Bonta (1997) evaluated the potential of derived distributions to determine curve numbers from measured *P-Q* data, treating them as separate distributions. The derived distribution method resulted in fewer variable estimates of *CN* for a wide range of sample sizes than the rank order method of Hawkins (1993). The derived-distribution method has potential even when data availability is limited. Schneider and McCuen (2005) developed a new Log-normal frequency method to estimate curve numbers from measured *P-Q* data. The developed method was found to be more accurate than the rank-order method. Recently, Mishra and Singh (2006) investigated the variation of *CN* with AMC and developed a new power relationship between the *S* (or *CN*) and the 5-day antecedent rainfall. The developed *CN*-AMC relationship is applicable to gauged as well as ungauged watersheds and eliminates the problem of sudden jump from one AMC level to other.

2.3.4 Applications

Since its inception, the SCS-CN method has witnessed myriad and variety of applications to the fields not originally intended, due to the reason of its simplicity, stability and accountability for most runoff producing watershed characteristics, viz., soil type, land use treatment, surface condition, and antecedent moisture condition. A

considerable amount of literature on the method has been published and the method has undergone through various stages of critical reviews several times (Rallison, 1980; Chen, 1982; Ponce and Hawkins, 1996; Mishra and Singh, 2003a). Rallison (1980) provided detailed information about the origin and evaluation of the SCS-CN methodology and highlighted major concerns to its application to the hydrology and water resources problems and suggested for future research areas. Chen (1982) evaluated the mathematical and physical significance of this methodology for estimating the runoff volume. A sensitivity analysis shows that the errors in *CN* have more serious consequences on runoff estimates than the errors of similar magnitude in initial abstraction or rainfall. The values of curve number in the SCS method have been optimized for the conventional and conservation bench terrace systems using the observed rainfall–runoff data to better predict the runoff instead of using the standard values (Sharda, et al. 2002).

Though primarily intended for event-based rainfall-runoff modeling of the ungauged watersheds, the SCS-CN method has been applied successfully in the realm of hydrology and watershed management and environmental engineering, such as long-term hydrologic simulation (Knisel, 1980; Woodward and Gburek, 1992; Pandit and Gopalakrishnan, 1996; Choi et al., 2002; Mishra and Singh, 2004a; Geetha et al., 2007); prediction of infiltration and rainfall-excess rates (Aron et al., 1977; Mishra and Singh, 2002a, 2004b); sediment yield modeling (Mishra and Singh, 2003a; Mishra et al., 2006a); and determination of sub-surface flow (Yuan et al., 2001). The method has also been successfully applied to distributed watershed modeling (White, 1988; Moglen, 2000; Mishra and Singh, 2003a).

Many researchers (Ragan and Jackson, 1980; Slack and Welch, 1980; Tiwari et al., 1991, Pandey and Sahu, 2002) have utilized the satellite data in a GIS environment to estimate the USDA soil conservation Services (SCS) Runoff Curve Number (CN).

GIS, which has been designed to restore, manipulate, retrieve and display spatial and non-spatial data, is an important tool in analysis of parameters such as land use/ land cover, soils, topographical and hydrological conditions. To carry out resource monitoring and assessment of area of interest, information derived through remote sensing data has to be merged or integrated with database in GIS. Thus the remote sensing along with GIS application aid to collect, analyze and interpret the data rapidly on large scale intermittently and is very much helpful for watershed planning. For ungauged watersheds accurate prediction of the quantity of runoff from land surface into rivers and streams requires much effort and time. But this information is essential in dealing with watershed development and management problems. Conventional methods of runoff measurements are not easy for inaccessible terrain and not economical for a large number of small watersheds. Remote sensing technology can augment the conventional method to a great extent in rainfall-runoff studies.

Advances in computational power and the growing availability of spatial data have made it possible to accurately describe watershed characteristics for modeling of watershed hydrology. Recent studies (Sharda et al., 1993, Schumann et al., 2000, Saxena et al., 2000) illustrate that Remote Sensing (RS) and Geographic Information System (GIS) techniques are of great use in characterization and prioritization of watershed areas. The degree of various categories of agricultural, forest and other land covers can be determined accurately through RS (Garbrecht et al., 2001). The large amount of spatially detailed information derived from digital images, ground surveys, and digital terrain models and handled within a GIS, offers new opportunities for watershed parameterization. One of the options for use of RS and GIS is to improve the estimation of watershed parameters like Curve Number for a drainage watershed with widely used SCS model from its land use data and digitized soil map (Pandey et al., 2002). In general, land use/land cover accuracy is directly related to the spatial

resolution of the sensors. Satellite data help in deriving *CN*s for large drainage watersheds (Still and Shih, 1985; Kumar, 1997).

2.4 GREEN AND AMPT INFILTRATION THEORY

Even though Green and Ampt infiltration theory originally developed for idealized conditions (*i.e.*, homogeneous soil and constant surface ponding depth), the Green-Ampt model has been extended to take into account more realistic features. Ravi and William, 1998, have focused on the use of Green and Ampt model for estimating water flux by various authors as given in Table 2.2.

Table 2.2 Models of soil water movement based on the Green-Ampt concept

Model Author(s)	Important Features / Limitations
Green and Ampt (1911)	Developed an infiltration model, where the infiltration rate and cumulative infiltration are implicit in time. Assumptions and limitations for the model are (i) sharp wetting front; (ii) constant ponding depth; (iii) homogeneous soil; and (iv) uniform antecedent water content.
Bouwer (1969)	Developed an infiltration model for layered soils. Assumptions and limitations for the models are (i) non-uniform antecedent water content; and (ii) constant ponding depth.
Childs and Bybordi (1969)	Developed an implicit equation for cumulative infiltration in layered soils. Assumptions and limitations for the model

Model Author(s)	Important Features / Limitations
	are (i) constant ponding depth; and (ii) uniform antecedent water content.
Mein and Larson (1973)	Developed pre-ponding and ponded infiltration model. Assumptions and limitations for the model are (i) constant rainfall rate which is greater than saturated hydraulic conductivity; (ii) homogeneous soil; and (iii) uniform antecedent water content.
Swartzendruber (1974)	Developed infiltration equation for pre-ponding and ponding where, cumulative infiltration is implicitly in time after ponding. Assumptions and limitations for the model are (i) constant surface water flux which is greater than saturated hydraulic conductivity; (ii) homogeneous soil; and (iii) uniform antecedent water content.
Morel-Seytoux and Khanji (1974)	Developed a rigorous infiltration equation under the two-phase flow of air and water for the wetting front suction, h_f, and a viscous correction factor β, in terms of initial water content. Assumptions and limitations for the model are (i) homogeneous soil; and (ii) uniform

Model Author(s)	Important Features / Limitations
	antecedent water content.
James and Larson (1976)	Developed infiltration and redistribution equation for an intermittent rainfall. Assumptions and limitations for the model are (i) homogeneous soil; and (ii) uniform antecedent water content.
Li et al. (1976)	Developed a model which is the explicit approximation to the Green-Ampt model for calculating the cumulative infiltration and infiltration rate as the functions of time. Assumptions and limitations for the model are (i) homogeneous soil; (ii) constant head ponding at the surface; and (iii) uniform antecedent water content.
Eagleson (1978)	Developed an infiltration/exfiltration model to estimate the water infiltration during a wetting season and exfiltration during a drying season. Assumptions and limitations for the model are: (i) the water table depth is much greater than the larger of the penetration depth and the root depth; (ii) soil water content throughout the surface boundary layer is spatially uniform at the start of each storm period and at the start of

Model Author(s)	Important Features / Limitations
	each inter-storm period (iii) vegetation is distributed uniformly and roots extend through the entire volume of soil; and (iv) homogeneous soil system.
Smith and Parlange (1978)	Developed two-parameter models for ponding time and infiltration rate. Assumptions and limitations for the model are (i) arbitrary transient rainfall; (ii) homogeneous soil; and (iii) uniform antecedent water content.
Chu (1978)	Developed pre-ponding and ponded infiltration model for transient rainfall. Assumptions and limitations for the model are (i) homogeneous soil; and (ii) uniform antecedent water content.
Flerchinger *et al.* (1988)	Developed an explicit equation for cumulative infiltration for layered soils, which is an extension of Li et al. (1976) approach for layered soils. Assumption and limitation for the model is (i) constant head at the surface.

Model Author(s)	Important Features / Limitations
Philip (1992)	Gave a solution for falling head ponded infiltration. The solution form is the same as that for constant head infiltration; only the values of the constants are changed.
Philip (1993)	Developed variable-head ponded infiltration model due to constant or arbitrarily transient rainfall. Assumptions and limitations for the model are (i) homogeneous soil; and (ii) uniform antecedent water content
Salvucci and Entekhabi (1994)	Developed an infiltration model which is the explicit approximations for Green-Ampt infiltration rate and cumulative infiltration as a function of time. Assumptions and limitations for the model are (i) homogeneous soil; and (ii) uniform antecedent water content.

A well known equation to predict infiltration into underlying unsaturated homogeneous soils is the Green and Ampt equation. If the difference between the values of seepage coefficients (hydraulic conductivities) of the fine sediments layer deposited on the tank bed and underlying soil is significant, then, water may percolate from the fine sediment layer in isolated jets (Polubarinova-Kochina, 1962) and may not fill all the soil pores. The Green and Ampt approach has been effectively applied to

layered soils of decreasing permeability (Childs and Bybordi, 1969; vide. Pachepsky and Timlin 1996). In a two-layered soil system, where the underlying soil layer has higher conductivity and porosity than the overlying soil, several investigators have found that, the underlying coarse soil layer will not be saturated and water moves into the coarser soil through narrow flow channels (finger). The concept of a saturation piston flow in Green and Ampt infiltration equation is inapplicable in such layered soil system.

Thus, a commonly used Green and Ampt model, in which a sharply-defined wetting front and piston flow are assumed, cannot be used for the case in which underlying soil is coarser than the top soil layer (Pachepsky and Timlin 1996).Where the upper layer is coarser one having higher porosity and higher conductivity Green and Ampt assumption of sharply defined wetting front is applicable. Sonu (1986) computed vertical infiltration by using Green and Ampt infiltration equation into stratified soil for groundwater accretion by assuming top layer has higher hydraulic conductivity. Chu and Mari$\tilde{n}$o (2005) determined ponding condition and infiltration into layered soils under unsteady rainfall by using Green and Ampt infiltration equation by assuming upper soil layer having more hydraulic conductivity.

The major loss of water in the tank is due to seepage and percolation. Seepage and percolation losses in the tank are often inseparable and so both are considered as a single component. Panigrahi & Panda, 2001 investigated in rice the field that, seepage and percolation is an extremely variable factor, depending on soil texture, drainage conditions, head variation, soil hydraulic conductivity, cultural and water management in the field. The same is applicable to the tank water balance study also.

2.5 TANK WATER BALANCE STUDIES

The most common water harvesting structures are of two types: a) embankment type ponds for hilly and rugged area, and b) excavated or dugout type farm ponds for flat topography (Sharda and Juayl, 2008). The quantitative behaviour of water in a system can be studied by mass balance of water i.e. inflow, outflow and change in storage (Yadav, and Keshari, 2006).

Nath and Bolte (1998) developed water balance model at AIT wherein evaporation is computed by using measured water temperature value in heat balance equation.

Andreas et al. (2004) developed a simple deterministic water balance model within a cascade-type approach. In their approach, evaporation is calculated using the Penman method.

Water balance studies (Verma & Sarma, 1990; Jensen et al., 1993; Srivastava, 2000, Panigrahi & Panda, 2003) have reported on the feasibility of a system to meet the irrigation demand of the crops. However, the general methodology has not been synthesized in the form of a model. Pandey et al. 2006 developed a water balance model to study the availability of storage rain water for irrigation and picsiculture.

Agrawal, et al. 2004 developed a computer program in Visual Basic 6.0 to simulate various water-balance parameters such as actual evapotranspiration, percolation, seepage, supplemental irrigation, surface runoff, and ponding depth in the field on a daily basis. Physically based saturated and unsaturated flow processes are incorporated into the model to simulate the aforesaid model parameters that occur during wet and dry periods.

In the water balance of tank, evaporation plays a crucial role particularly for the smaller size tank located in the semi-arid or arid regions (Kenabatho and Parida 2005). Due to differences in the heating and cooling of water bodies, evaporation from small shallow

tank is usually considered to be quite different from that of large and deep tanks (Subramanya 2006). In many cases, seepage losses from tank also contribute significantly (Harboe et al. 1994; Wegner 1999). Lack of proper consideration may lead to error on the water balance, as reported by Hugo (2002). Most of the studies reported in the literature do not explicitly model the tank losses. For example, Harboe et al. (1994) adopted mean monthly evaporation rate and a pre-defined relationship of seepage as a function of reservoir storage level in the tank water balance equation. Shiau and Lee (2005) assumed the tank losses to be negligible in their water balance equation, however, they included the tank spill. Ganji et al. (2008) used only the evaporation loss term in the water balance equation. Sun et al. (1996), in their work have used a generalized network formulation to incorporate the non-linear evaporation loss function of a reservoir in their water supply optimization model.

Sivaprgasam, et al. 2009 have conducted water balance in a reservoir by using genetic Programming technique and they observed that in water balance study, the losses from the reservoir in the form of evaporation and seepage are the vital components. Mishra, et al. 2005 have conducted the water balance study of Jalmahal Lake for recreation purpose. They have studied all processes separately and then integrated to check the availability of the water in the lake in a year.

It is important to establish the purposes (i.e. irrigation, animal watering, pisciculture, or a combination) for which water will be used once collected. To determine the temporal availability of the quantity of water needed (Husenappa et al., 1981) a water balance study is very much necessary.

2.5 CONCLUSIONS

From the literature review the following conclusions can be derived:

1. Evaporation from storage tank and pond can be estimated accurately by using water temperature. Hourly water temperature can be estimated from heat

balance equation by taking care of hourly variation in solar hour angle in case of non availability of the measured water temperature data.

2. There is a scope to update SCS curve number by accounting change in soil moisture in the unsaturated soil layer due to infiltration during a rainfall event, drainage and evaporation from soil moisture zone during post rainfall period, instead of presuming an antecedent soil moisture condition for calculating runoff from subsequent rainfall events.
3. The loss of water stored in a storage tank is mainly due to seepage losses from the tank bed and evaporation from the tank water. The seepage losses can be quantified without any difficulty by using Green and Ampt. infiltration equation, in which the variation in the depth of water can be incorporated easily.
4. Individual process level models of water balance study have been investigated by several investigators. These process level models can be integrated effectively in a water balance study.

CHAPTER-3

COMPUTATION OF EVAPORATION FROM A STORAGE TANK BY HEAT BALANCE METHOD

3.1 INTRODUCTION

Storage tanks provide water for irrigation, fishing, recreation, drinking water supply, and support aquatic ecosystems. Water stored in tanks gets depleted due to seepage and evaporation. Tank evaporation is governed by climate of the region besides depth of water in the tank, and water spread area. Evaporation plays an important role not only in the water budget of a tank, but also in the energy budget. Evaporation from the tank water varies with water temperature. Measuring evaporation accurately is difficult task without significant investment in instrumentation and data processing (Winter et al., 2003; Winter, 1981). These practical and theoretical considerations impose significant challenges to estimate tank evaporation in more accurate and scientific way (both observational and modeling). Besides these challenges, it is difficult to maintain an accurate and long-term studies of tank evaporation in order to better understand the variation in evaporation. Observational studies of tank evaporation have used a variety of different methods to measure evaporation rates. These include the mass transfer, water balance, and energy budget methods (Winter, 1981; Winter et al., 1995). The mass transfer method has been used in numerous studies (Yu and Knapp, 1985; Ikebuchi et al., 1988; Laird and Kristovich, 2002) due to its suitability for modeling (Hostetler and Bartlein, 1990; Blodgett et al., 1997). On the other hand, water balance studies can potentially provide a more reliable estimate of evaporation (Myrup et al., 1979), so long as each water budget component is accurately measured which is often a difficult task, especially to ascertain the groundwater and surface water interaction component. In general, the energy balance is the best method for computing evaporation (Rosenberry et al. 1993; Winter et al. 1995). An accurate method for

computing evaporation is by using water temperature. Water temperature has been modeled by various researchers (Krant *et al.,* 1982; de Jager and Walmsley, 1984; Klemetson and Rogers, 1985; Catchcart and Wheaton, 1987; Losodo, 1988).The quantification of different components of heat balance (either by empirical formulae or by analytical method) have been made by several investigators. These have been used for computation of the different components of heat balance in this study. In this chapter, using heat balance equation, water temperature and the evaporation from the storage tank are quantified considering the variation in water temperature and depth of water in the tank.

3.2 STATEMENT OF THE PROBLEM

A storage tank, whose water spread area does not change with change in the depth of water in the tank, is considered for heat balance and computation of evaporation. The incoming and outgoing heat flux components for heat balance are shown in Figure 3.1.The heat loss to the soil from tank bed is neglected. Extraterrestrial solar radiation reaching a horizontal plane i.e. a plane normal to the solar radiation, is calculated based on longitude and latitude of the location. Incoming heat fluxes to the water body are: daily direct shortwave radiation from the sun, long wave back radiation from atmosphere. The intermittent heat fluxes contained in the rain water and runoff from the contributing catchment is neglected in this study. Shortwave solar radiation as well as long wave back radiation from atmosphere is time variant. The heat losses from water body are in the form of evaporation, sensible heat, and back radiation from water body and these vary with water temperature and time. There will be intermittent heat loss from the storage tank during over flow which is neglected during heat balance. In this study, air temperature, and relative humidity have been taken constant in a day, as hourly variation data are difficult to get. Incoming solar radiation varies with hour angle. It is required to estimate the water temperature hourly from heat balance

equation and to quantify tank water evaporation considering the variation in the depth of water and water temperature.

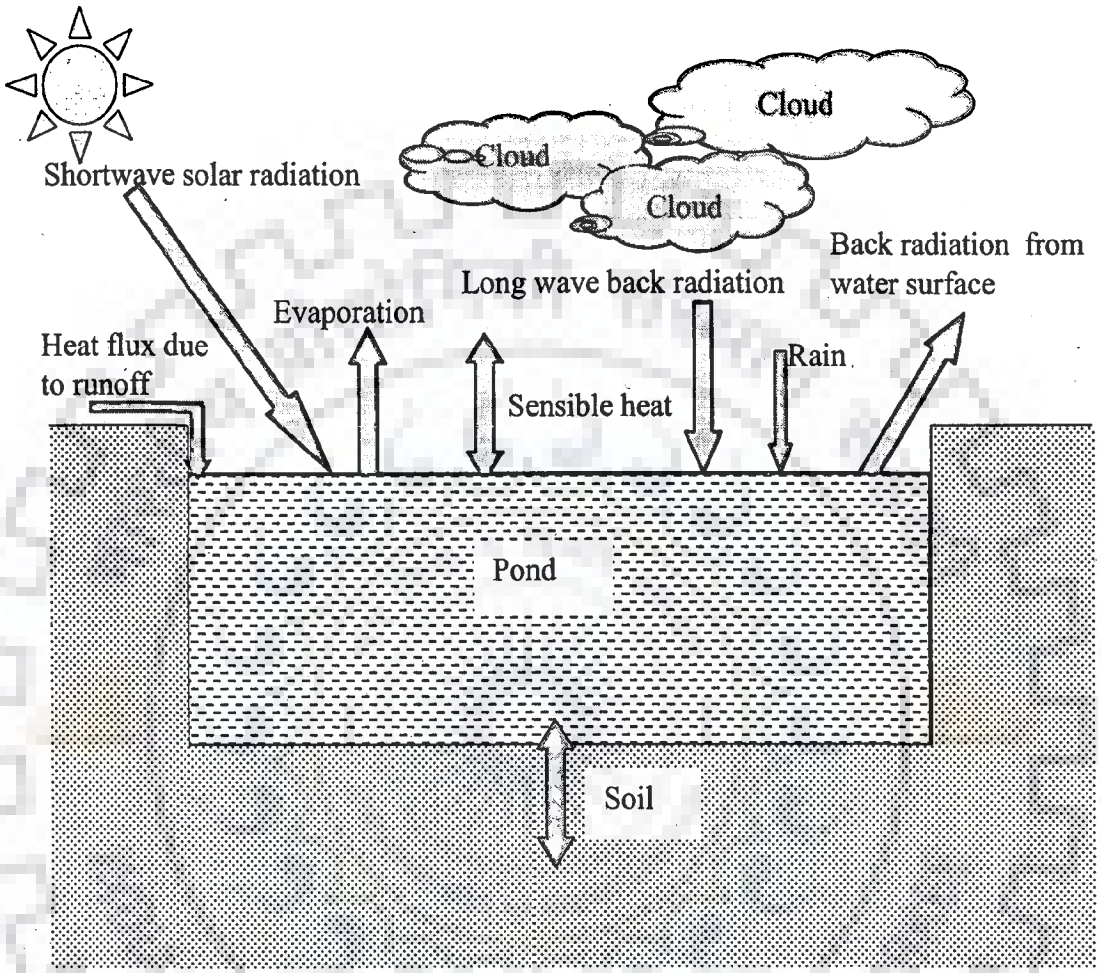

Fig. 3.1 A storage tank and components of heat balance model

3.3 ANALYSIS

Let H_1 (W/m^2) and H_2 (W/m^2) be the incoming radiation reaching to the surface of the storage tank and out going radiation from the tank per unit area respectively. Net energy flux H_N (W/m^2) in the tank water during a non rainy day is given by the following heat balance equation:

$$H_N = H_{SW} + H_L - H_B - H_E - H_S \tag{3.1}$$

where

H_N = net radiation on the tank surface (W/m^2),

H_{SW} = shortwave radiation reaching to the earth surface (W/m^2),

H_L = long wave back radiation from atmospheric constituents (W/m^2),

H_B= back radiation from the water surface (W/m^2),

H_E= heat loss due to evaporation (W/m^2),

H_S= heat flux due to conduction or sensible heat transfer (W/m^2).

Designating $H_1 = H_{SW} + H_L$ *and* $H_2 = H_B + H_E + H_S$, the net radiation can be written in the form of H_1 and H_2 as:

$$H_N = H_1 - H_2 \tag{3.2}$$

3.3.1 Incoming Solar Radiation

Shortwave radiation originates from sun. The solar radiation while passing through the earth's atmosphere is subjected to the mechanisms of atmospheric absorption and scattering. A fraction of the radiation reaching to the earth's surface is reflected back into atmosphere and subjected to the same atmospheric phenomena such as absorption and scattering and the remainder is absorbed by the earth's surface. The magnitude of absorbed radiation by the earth surface varies with the altitude of the sun. The altitude of sun varies daily and seasonally for a fixed location on the earth. Hence, the shortwave radiation reaching to the earth surface varies daily and seasonally for a particular location. Shortwave radiation can be measured directly by using radiometer. But it is not available every where easily as radiometers are very much expensive. Hence, practically it is not possible to get measured shortwave radiation data in many places. In that condition shortwave radiation can be estimated reliably from the radiation striking the earth's atmosphere and the atmospheric conditions that affect its reflection and absorption. The atmospheric conditions affecting the absorption of the short wave radiation are complex processes and those are described with empirical relationships. These empirical relationships are widely used to estimate shortwave

radiation. The fraction of radiation reaching to the water surface after reduced by scattering and absorption is estimated from the following expression (Water Resources Engineers, Inc-1967):

$$H_{SW} = H_H a_t (1 - R_s) c_a \tag{3.3}$$

where

H_H = hourly extraterrestrial solar radiation on a horizontal plane (W/m^2),

a_t = atmospheric transmission coefficient,

R_s = albedo or the reflection coefficient, and

c_a = fraction of solar radiation not absorbed by the clouds.

Hourly extraterrestrial solar radiation H_H, during h_1 to h_2 hour, on a horizontal plane is estimated from the following expression:

$$H_H = G_{SC}\left(1 + 0.034\cos\frac{2\pi n}{365}\right)\frac{12}{\pi}\times \left[\cos\phi\cos\delta(\sin h_{h2} - \sin h_{h1}) + \frac{\pi}{180}(h_{h2} - h_{h1})\sin\phi\sin\delta\right]\times\tau \tag{3.4}$$

ϕ = latitude of the location in degree,

δ = solar declination angle in degree,

h_{h1}= hour angle in degree at time h_1 hour,

h_{h2}= hour angle in degree at time h_2 hour,

τ = a correction factor, and

G_{sc} = solar constant (W/m^2).

n = 1 for the 1st day of January and 365 for the 31st of December.

The detail derivation of H_H is given in Appendix-A.

Atmospheric transmission coefficient (a_t) is estimated by:

$$a_t = \frac{a_2 + 0.5(1 - a_1 - c_d)}{1 - 0.5R_g(1 - a_1 - c_d)} \tag{3.5}$$

where

a_1 and a_2 are mean atmospheric transmission coefficients and they vary with the atmospheric moisture content and optical mass.

c_d = dust coefficient which varies from 0.0 to 0.13 (Water Resources Engineers Inc, 1967) and the average value has been taken for this analysis is equal to 0.065.

R_g = reflectivity of the ground, which varies with the type of ground cover. For water surface R_g is used as R_s (albedo of water surface, Brown and Barnwell 1987):

$$R_s = a\left(\frac{180}{\pi}\alpha_s\right)^b \tag{3.6}$$

where

α_s is the solar altitude in radian, and a and b are coefficients which depend on cloud cover. In this analysis, the average values of a and b have been taken to prevail throughout the year as data about cloud cover were not available. Typical values of the coefficients are provided in Table-3.1

Solar altitude (α_s) is estimated from the following equation (Martin and McCutcheon, 1999):

Table 3.1 Coefficients a and b based on cloud cover

Description	Fraction cloud cover (c)	*a*	*b*
Overcast	c > 0.9	0.33	-0.45
Broken	0.5 < c <0.9	0.95	-0.75
Scattered	0.1 < c < 0.5	2.20	-0.97
Clear	c < 0.1	1.18	-0.77

Solar altitude (α_s) is estimated from the following equation (Martin and McCutcheon , 1999):

$$\alpha_s = \left\{ \tan^{-1}\left(\frac{\theta_{z1}}{\sqrt{1-\theta_{z1}^2}} \right) \right\} \frac{\pi}{180} \tag{3.7}$$

where

$$\theta_{z1} = \sin\phi \sin\delta + \cos\phi \cos\delta \cosh_{h1} \tag{3.8}$$

θ_{z1} is the cosine of solar zenith angle θ_z and it is in radian. The detail derivation is given in Appendix-A

The mean atmospheric coefficient is estimated by using this following expression:

$$a_1 = Exp[-(0.465 + 0.134P_{wc})(0.129 + 0.171Exp(-0.88\theta_{am}))\theta_{am}] \tag{3.9}$$

The mean atmospheric transmission coefficient after scattering and absorption is estimated by (Eiker, 1972):

$$a_2 = Exp[-(0.465 + 0.134P_{wc})(0.179 + 0.421Exp(-0.721\theta_{am}))\theta_{am}] \tag{3.10}$$

where

θ_{am} is the dimensionless optical mass and P_{wc} is the mean daily precipitatable atmospheric water content which is estimated from the following equation:

$$p_{wc} = 0.85Exp(0.11 + 0.0614T_d) \tag{3.11}$$

where

T_d = the dew point temperature in ^0C

The optical air mass can be computed from the elevation of the site and the sun's altitudes as follow:

$$\theta_{am} = \frac{\left(\frac{288 - 0.0065Z}{288} \right)^{5.256}}{\sin\alpha_s + 0.15(\alpha_s + 3.855)^{-1.253}} \tag{3.12}$$

where

Z = is the elevation of the site in (m) above mean sea level, the solar altitude α_s is in degree

By substituting the expression for R_s, a_1, a_2, from (3.6), (3.9), and (3.10) in (3.5), the value of a_t is obtained. Hence, after evaluating all terms appearing in (3.3), the shortwave radiation reaching to the water surface is estimated.

3.3.2 Long Wave Radiation

The fraction of absorbed short wave radiation by the clouds and atmosphere generates heat in the atmosphere, which is known as atmospheric heat. This atmospheric heat is in turn reflected at longer wave lengths and it is known as long wave solar radiation. The long wave radiation is computed using the Stefan-Boltzman law and is obtained by integrating radiation emitted by the black-body at all wave lengths. The long wave radiation is given by:

$$H_L = \alpha_0(1+0.17C_1)\sigma(T_a+273.16)^6 \tag{3.13}$$

Net long wave radiation (H_{nL}) is the incoming radiation minus the amount of radiation reflected back to the atmosphere. Reflectance on the water surface is generally assumed to be 3% cited by (Martin and McCutcheon, 1999) based on studies by Wunderlich (1972). Hence net long wave radiation reaching to the water surface can be written as:

$$H_{nL} = \alpha_0(0.97)\sigma(1+0.17C_1)(T_a+273.16)^6 \tag{3.14}$$

It is difficult to get hourly air temperature for this study. Hence, air temperature is assumed to be constant through out the day. The average of maximum and minimum temperature has been taken in this analysis.

3.3.3 Back Radiation from Tank Water Body

Water also emits long-wave radiation which represents a loss of heat. The amount of heat loss is generally computed by assuming the back radiation from water surface as the black-body radiation. The radiation of the black-body is estimated by using the

Stefan -Boltzman law. Hence, radiation from water body is a function of wave length and temperature and can be governed by Plank's law of radiation and it is estimated as:

$$H_B = \sigma T^4 \tag{3.15}$$

The water surface back radiation is impacted by the emissivity of water. The net back radiation from water surface is:

$$H_{nB} = \varepsilon_w \sigma (T_w + 273.16)^4 \tag{3.16}$$

where

H_{nB} = net back radiation from water surface or heat loss (W/ m^2),

T_w = water surface temperature (^{0} C),

ε_w = emissivity of the water surface, approximated as equal to 0.97,

σ = Stefans-Boltzman constant $\frac{W}{m^2 K^4}$.

3.3.4 Heat Loss Due to Evaporation

The evaporation of water from water body leads to loss of heat energy. The heat loss is estimated from the density of the water evaporated, latent heat of evaporation and the rate of evaporation as given by the following expression:

$$H_E = \rho L_w E \tag{3.17}$$

where

H_E = heat loss from water body due to evaporation (W/m^2),

ρ = density of water (Kg/m^3),

E =rate of evaporation (m/s),

L_w = latent heat of evaporation (J/Kg).

Latent heat of evaporation is normally expressed as a function of water temperature as (Martin and McCutcheon, 1999):

$$L_w \approx 1000(2499 - 2.36 T_w) \tag{3.18}$$

The rate of evaporation (E) is proportional to the water vapor pressure gradient between the water and atmosphere. In case of evaporation from water body, the gradient is between the saturated vapor pressure at the temperature of water surface and the actual vapor pressure at the temperature of the air. Due to the movement of wind over the surface of water, turbulence will generate in air and water. Hence it is difficult to understand the evaporation process fully. However, the extensive observation indicates that the evaporation rate can be approximated as:

$$E = f(U_w)(e_s - e_a) \tag{3.19}$$

where

U_w = wind speed (m/s),

e_s = the saturated vapor pressure at the water surface temperature (mb).

There is a widely used formulation for saturation vapor pressure of air over water by the U.S. Army Corps of Engineers (Environmental Laboratory, 1985) is given by:

$$e_s = 2.171 \times 10^8 \, Exp\left\{\frac{-4157}{T_w + 239.09}\right\} \tag{3.20}$$

e_a = the vapor pressure at the air temperature in mb can be expressed same as above

$$e_a = 2.171 \times 10^8 \, Exp\left\{\frac{-4157}{T_d + 239.09}\right\} \tag{3.21}$$

$f(U_w)$ = Wind speed function and it can be expressed in an empirical equation as:

$$f(U_w) = a_w + b_w U_w \tag{3.22}$$

where

a_w and b_w are the coefficients. A general value can be taken as a_w= 4.18 x10^{-9} $mb^{-1}m/s$, b_w = 0.95 x 10^{-9} mb^{-1} (Meyer, 1928)

Incorporating the expression for wind function from (3.19) to (3.22):

$$E = (a_w + b_w U_w)(e_s - e_a) \tag{3.23}$$

Hence, heat loss from evaporation is estimated from (3.17)

3.3.5 Sensible Heat Transfer

Sensible heat transfer is the transport of the heat due to convection and conduction and it is neglected by many researchers during heat balance study. But to compute the evaporation more accurately from heat balance, sensible heat is considered one of the components of heat balance in this study. The sensible heat is calculated by the approach based on the Bowen Ratio as:

$$Bowen\,Ratio = \frac{H_S}{H_E} = C_B \frac{p_a}{p}\left(\frac{T_w - T_a}{e_s - e_a}\right) \tag{3.24}$$

where

C_B = a coefficient equal to 0.61 (mb^0C^{-1}),

p_a = atmospheric pressure (mb),

p= reference pressure at mean sea level (mb).

e_s and e_a are saturation vapor pressure and vapor pressure at the air temperature respectively (mb) and can be expressed as:

Hence, sensible heat from the water body is estimated from:

$$H_S = C_B \frac{p_a}{p}\left(\frac{T_w - T_a}{e_s - e_a}\right) \times H_E \tag{3.25}$$

3.3.6 Water Temperature and Evaporation

The basic heat balance equation in the storage tank is: the change in heat content in the storage tank is equal to the incoming heat minus the outgoing heat. Mathematically it is written as (Martin and McCutcheon, 1999):

$$\rho c_p \left\{\frac{d(V_w T_w)}{dt}\right\} = A_{\tan k}\{H_1(t,T_a) - H_2(t,T_w)\} \tag{3.26}$$

where

V_w = volume of water (m^3),

ρ = density of water (Kg/m^3),

C_p= specific heat of water at constant pressure (J/Kg^0C),

A_{tank} = surface area of water body (m^2).

Substituting the expression for $H_1(t,T_a)$ and $H_2(t,T_w)$ in (3.26) from (3.2):

$$\rho c_p\left\{\frac{d(V_w T_w)}{dt}\right\} = A_{\tan k}\{H_{SW} + H_L - H_B - H_E - H_S\} \tag{3.27}$$

or

$$A_{\tan k}\left[H_{SW} + H_L - H_B - H_E\left\{1 + C_B\frac{p_a}{p}\left(\frac{T_w - T_a}{e_s - e_a}\right)\right\}\right] = \rho c_p\left\{\frac{d(V_w T_w)}{dt}\right\} \tag{3.28}$$

$$A_{\tan k}\left[H_{SW} + H_L - H_B - H_E\left\{1 + C_B\frac{p_a}{p}\left(\frac{T_w - T_a}{e_s - e_a}\right)\right\}\right] = \rho c_p\left\{V_w\frac{dT_w}{dt} + T_w\frac{dV_w}{dt}\right\} \tag{3.29}$$

Substituting $V_w = A_{\tan k}D_w$ in (3.29), the following expression is obtained:

$$A_{\tan k}\left[H_{SW} + H_L - H_B - H_E\left\{1 + C_B\frac{p_a}{p}\left(\frac{T_w - T_a}{e_s - e_a}\right)\right\}\right] = A_{\tan k}\rho c_p\left\{D_w\frac{dT_w}{dt} + T_w\frac{dD_w}{dt}\right\} \tag{3.30}$$

The finite difference form of (3.30) is:

$$\begin{aligned}&\rho c_p\left\{D_w(i)\frac{T_w(i+1) - T_w(i)}{\Delta t} + T_w(i)\frac{D_w(i+1) - D_w(i)}{\Delta t}\right\}\\ &= \left[H_{SW}(i) + H_L(i) - H_B(i) - H_E(i)\left\{1 + C_B\frac{p_a}{p}\left(\frac{T_w(i) - T_a}{e_s - e_a}\right)\right\}\right]\end{aligned} \tag{3.31}$$

or

$$\begin{aligned}&D_w(i)\frac{T_w(i+1) - T_w(i)}{\Delta t} + T_w(i)\frac{D_w(i+1) - D_w(i)}{\Delta t}\\ &= \frac{1}{\rho c_p}\left[H_{SW}(i) + H_L(i) - H_B(i) - H_E(i)\left\{1 + C_B\frac{p_a}{p}\left(\frac{T_w(i) - T_a}{e_s - e_a}\right)\right\}\right]\end{aligned}$$

or

$$D_w(i)\frac{T_w(i+1)-T_w(i)}{\Delta t}=\frac{1}{\rho c_p}\left[H_{SW}(i)+H_L(i)-H_B(i)-H_E(i)\left\{1+C_B\frac{p_a}{p}\left(\frac{T_w(i)-T_a}{e_s-e_a}\right)\right\}\right]$$
$$-T_w(i)\frac{D_w(i+1)-D_w(i)}{\Delta t}$$

or

$$T_w(i+1)=\frac{\Delta t}{\rho c_p D_w(i)}\left[H_{SW}(i)+H_L(i)-H_B(i)-H_E(i)\left\{1+C_B\frac{p_a}{p}\left(\frac{T_w(i)-T_a}{e_s-e_a}\right)\right\}\right]$$
$$-T_w(i)\frac{D_w(i+1)-D_w(i)}{\Delta t}\frac{\Delta t}{D_w(i)}+T_w(i)$$

or

$$T_w(i+1)=\frac{\Delta t}{\rho c_p D_w(i)}\left[H_{SW}(i)+H_L(i)-H_B(i)-H_E(i)\left\{1+C_B\frac{p_a}{p}\left(\frac{T_w(i)-T_a}{e_s-e_a}\right)\right\}\right]$$
$$-T_w(i)\frac{\{D_w(i+1)-D_w(i)\}}{D_w(i)}+T_w(i)$$

(3.32)

Since $D_w(i+1)$ is not known, for small time step, the term $\frac{\{D_w(i+1)-D_w(i)\}}{D_w(i)}$ is approximated as $\frac{\{D_w(i)-D_w(i-1)\}}{D_w(i)}$. $T_w(i+1)$ is computed starting from $i=0$ making use of the initial condition i.e. at i=0, $T_w(0)$ and $D_w(0)$ are known. $D_w(0)=D_0$, the initial filling depth of the tank. The evaporation rate *E (i+1)* is computed from (3.23). The depth of water at the end of $(i+1)^{th}$ time step is obtained from the relation $D_w(i+1)=D_w(i)-E(i+1)$,

Equations (3.32) and (3.23) have been used for estimating water temperature and rate of evaporation in hourly basis.

3.3.7 Daily Evaporation and Water Temperature

The daily evaporation has been estimated integrating the hourly evaporation for 24 hour. The average daily water temperature has been estimated by taking average of the

changes in water temperature for 24 hours and the adding to the initial water temperature on the same day.

3.4 RESULTS AND DISCUSSION

The meteorological data, for which evaporation from a storage tank is computed, are given in Table- A.1 (Appendix- A).

Considering variation in solar hour angle and time invariant meteorological parameters ($T_a(t)$ = 30 ^{0}C, RH (t) =90%, U_w (t) =5km/hour, $T_w(0)$ = 30 ^{0}C) (for a hypothetical case), hourly water temperature and evaporation are computed and presented in Figs. 3.2 and 3.3 respectively for initial depth D_0 =2.0 m and 3.0m. The time origin starts at 12 .0AM. As shown in figure, water temperature is a minimum at about 7.0 AM after which it rises during the day time and reaches a maximum value at about 5.0PM. Then, the temperature decreases and the cycle is repeated. Corresponding to D_0 =3.00 m the maximum temperature of water is about 30.6 ^{0}C which occurs at 5.00 PM. For D_0 =2.0m, the maximum temperature is about 30.9 ^{0}C. Thus for 1.0m less in depth of water, the temperature would be higher by about 0.3 ^{0}C after a lapse of about 17 hours. . There is a rising trend in the minimum as well maximum temperature. Minimum temperature occurs during morning hours 8.00 AM to 9.00 AM and maximum occurs at about 5.00PM. It could be seen that for the hypothetical case there is no difference in the minimum temperatures whether the depth is 3.00m or 2.00m after a lapse of 18 hours. The trend in the variation of hourly evaporation is very much similar to the trend in the variation of water temperature since the meteorological parameters are assumed as time invariant.

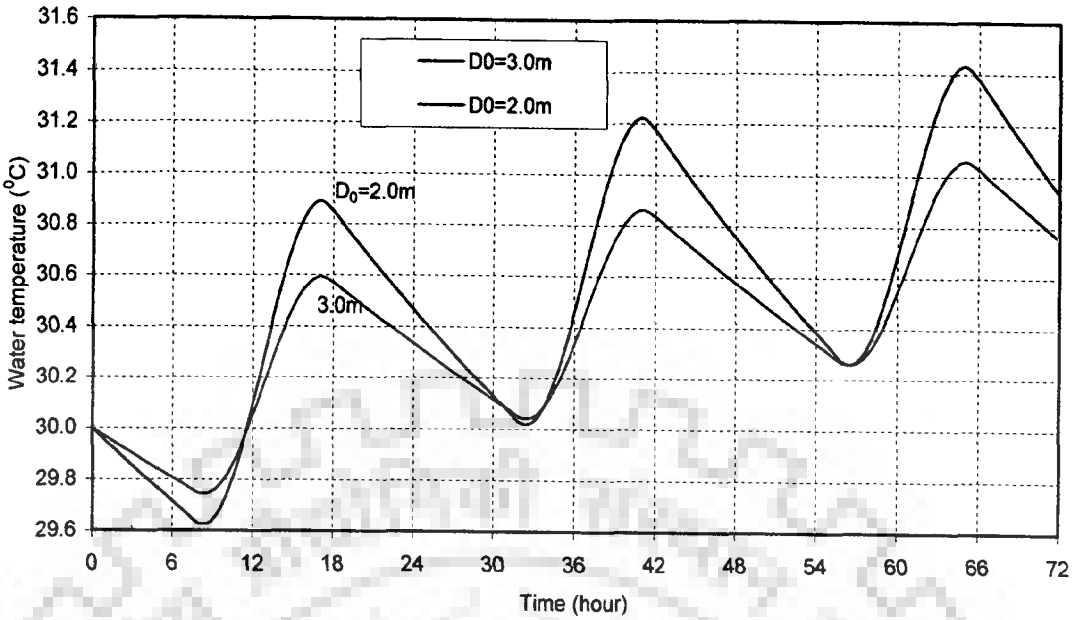

Fig. 3.2 Variation of water temperature (T_w) with time (hour) corresponding to constant meteorological parameters (T_a, RH, U_w) and hourly variation in solar radiation (H_{sw})

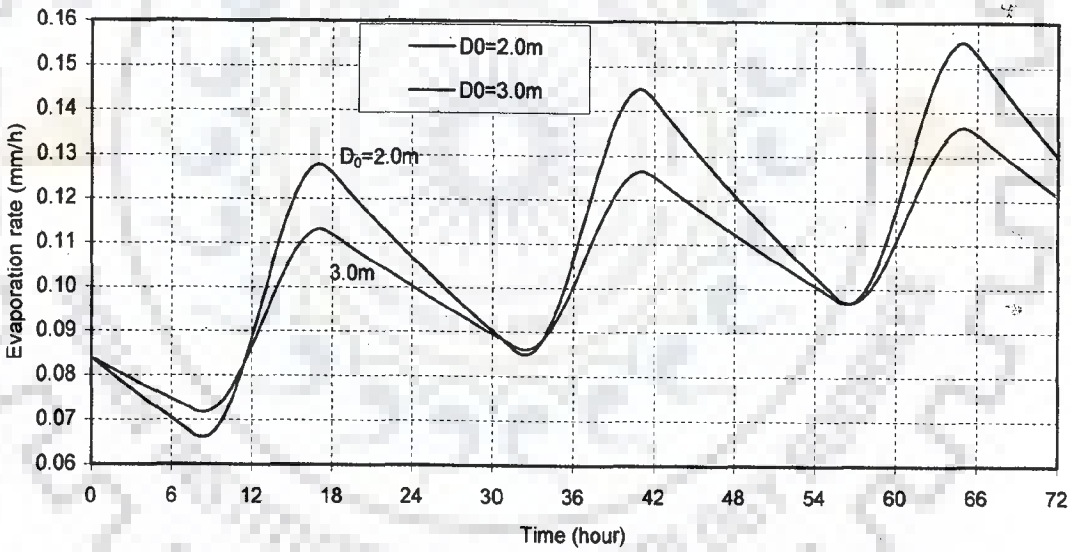

Fig. 3.3 Variation of evaporation (E) with time (hour) corresponding to constant meteorological parameters (T_a, RH, U_w) and hourly variation in solar radiation (H_{sw})

Considering the observed set of meteorological parameters {T_a(t), RH(t), U_w (t)}, given in Appendix A.9, and hourly variation in solar hour angle, and assuming no change in depth of water in the tank, the hourly water temperature and evaporation are computed. The variations in water temperatures for D_0=2.0m and 3.0m are presented in Fig. 3.4.

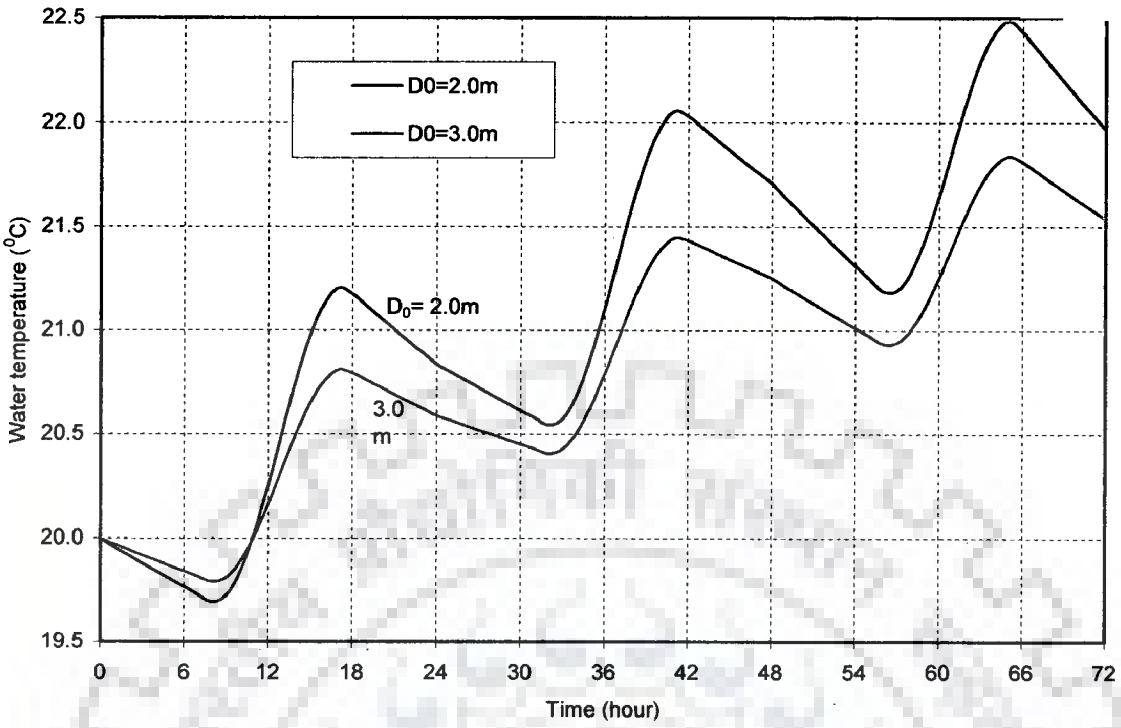

Fig. 3.4 Variation of water temperature (T_w) with time (hour), for different depths of water (D_0), in the tank, corresponding to the measured meteorological parameters.

As seen from the figure, the temperature rises during a day and attains a maximum at about 5.0 PM, then it reaches a minimum at a time between 7 .0 AM to 8.0 AM after which the cycle is repeated. The tank having higher initial depth has lower water temperature after a lapse of 12 hours. For the two tanks, having a difference of 1.0m in initial depth D_0, differences in their daily maximum water temperatures, and daily minimum water temperatures increase with time. There is increasing trend in the daily maximum and the daily minimum temperatures. The graphs are characterized by a periodicity and a trend. The temperature prediction would facilitate to find required water depth to maintain temperature in a storage tank for aquaculture.

The hourly variation of evaporation for D_0=2.0m and 3.0m are presented in Fig. 3.5. The effect of wind speed on evaporation can be clearly seen in the figure. At 24 hours due to sharp decrease in wind speed there is a drop in the evaporation rate. On next day due to increase in the wind speed there a sharp rise in the evaporation rate.

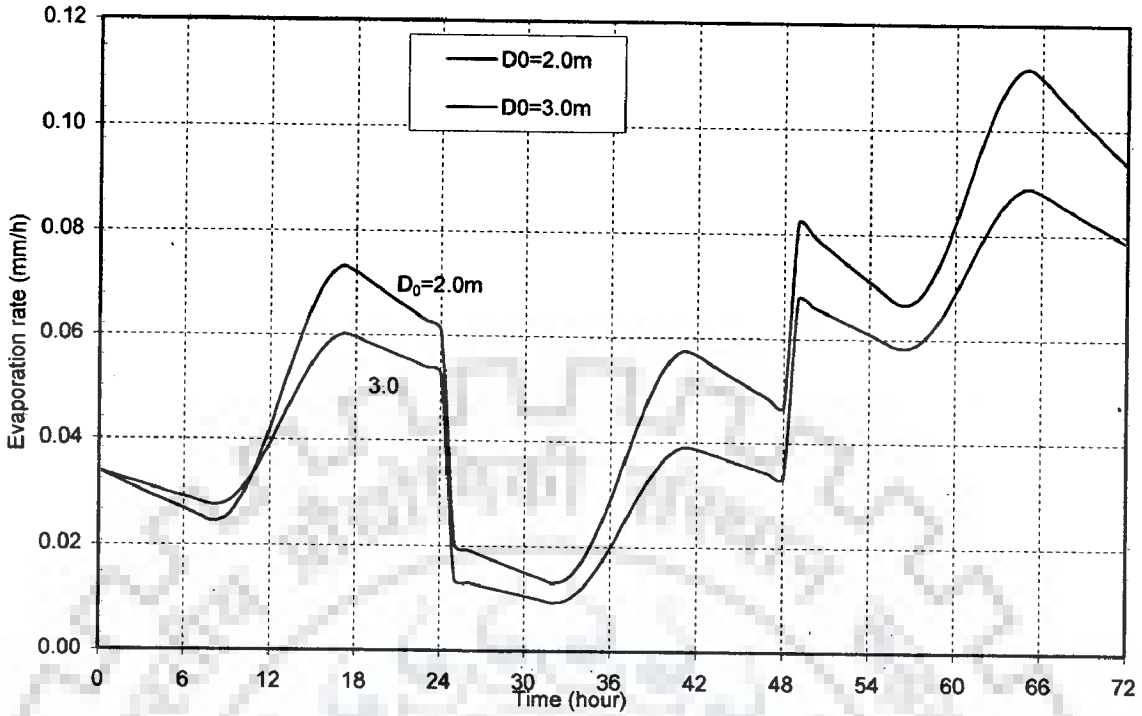

Fig. 3.5 Variation of evaporation rate (E) with time (hour), for different depth of water (D_0), in the storage tank, corresponding to measured meteorological parameters (T_a, RH, U_w)

Mostly evaporation in the storage tank with less depth is always higher than that from the tank with larger depth.

Considering the variation in depth of water in the tank owing to evaporation, the hourly variation in water temperature and evaporation are computed and presented Figs. 3.6 and 3.7. The difference in the variation in water temperature is nominal when variation in the depth of water due to evaporation is considered. Similar is the effect on evaporation rate.

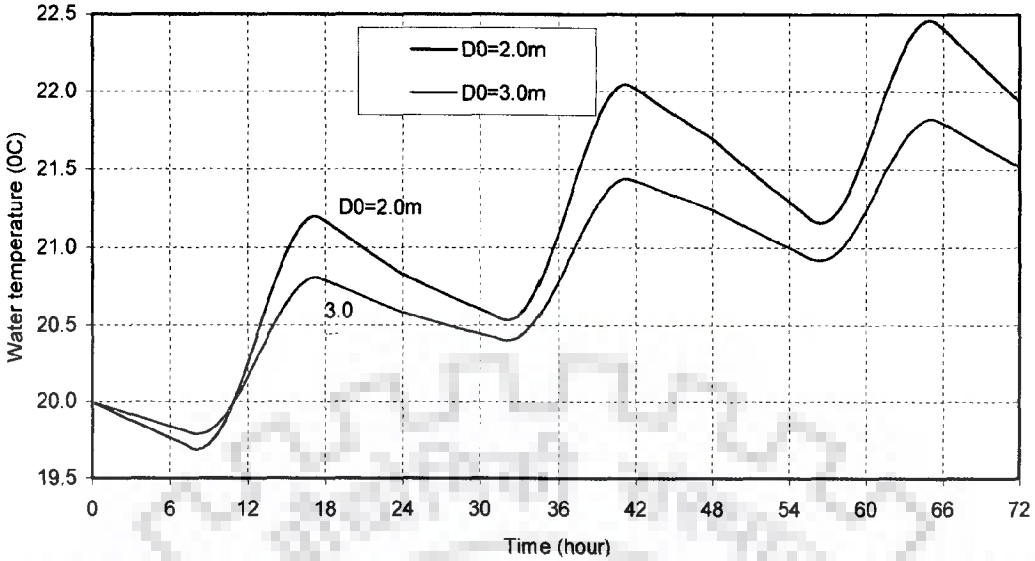

Fig.3.6 Variation of water temperature (T_w) with time (hour), considering variation in the depth of water (D_0) in the storage tank due to evaporation alone, for D_0=2.0m and 3.0m

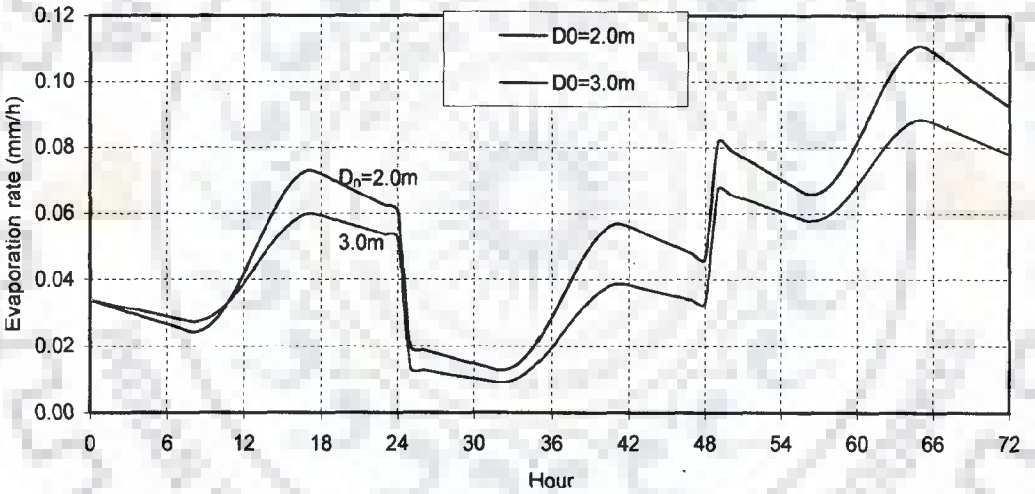

Fig. 3.7 Variation of evaporation (E) with time (hour), considering variation in the depth of water, in the storage tank, due to evaporation alone, for D_0=2.0m and 3.0m

Corresponding to the meteorological data average daily (12.0 AM to next 12.0 AM) water temperature is presented in Figs. 3.8 (a) and 3.8 (b), for D_0=2.0m and 3.0m. The dew point temperature corresponding to the prevailing average daily air temperature is also presented in Figs. 3.8 (a) and 3.8 (b) .It may be seen that on 14th day for D_0=2.0m the T_w and T_d are nearly same, which means the daily evaporation on the day of 14th should be nearer to zero. The variations in daily evaporation for D_0=2.0m and 3.0m are

presented in Figs. 3.9 (a) and 3.9 (b). As seen from the figure on the day of 14^{th} the evaporation is very nominal. There is very marginal decrease in the daily evaporation rate on some days for the tank with higher initial depth D_0=3.0m.

Considering variation in depth of water due to evaporation, the daily water temperature and daily evaporation rates are computed and presented in Figs. 3.10(a) and (b), 3.11(a) and (b) respectively. There are marginal differences in water temperatures and evaporation rates whether change in water depth due to evaporation is considered or not.

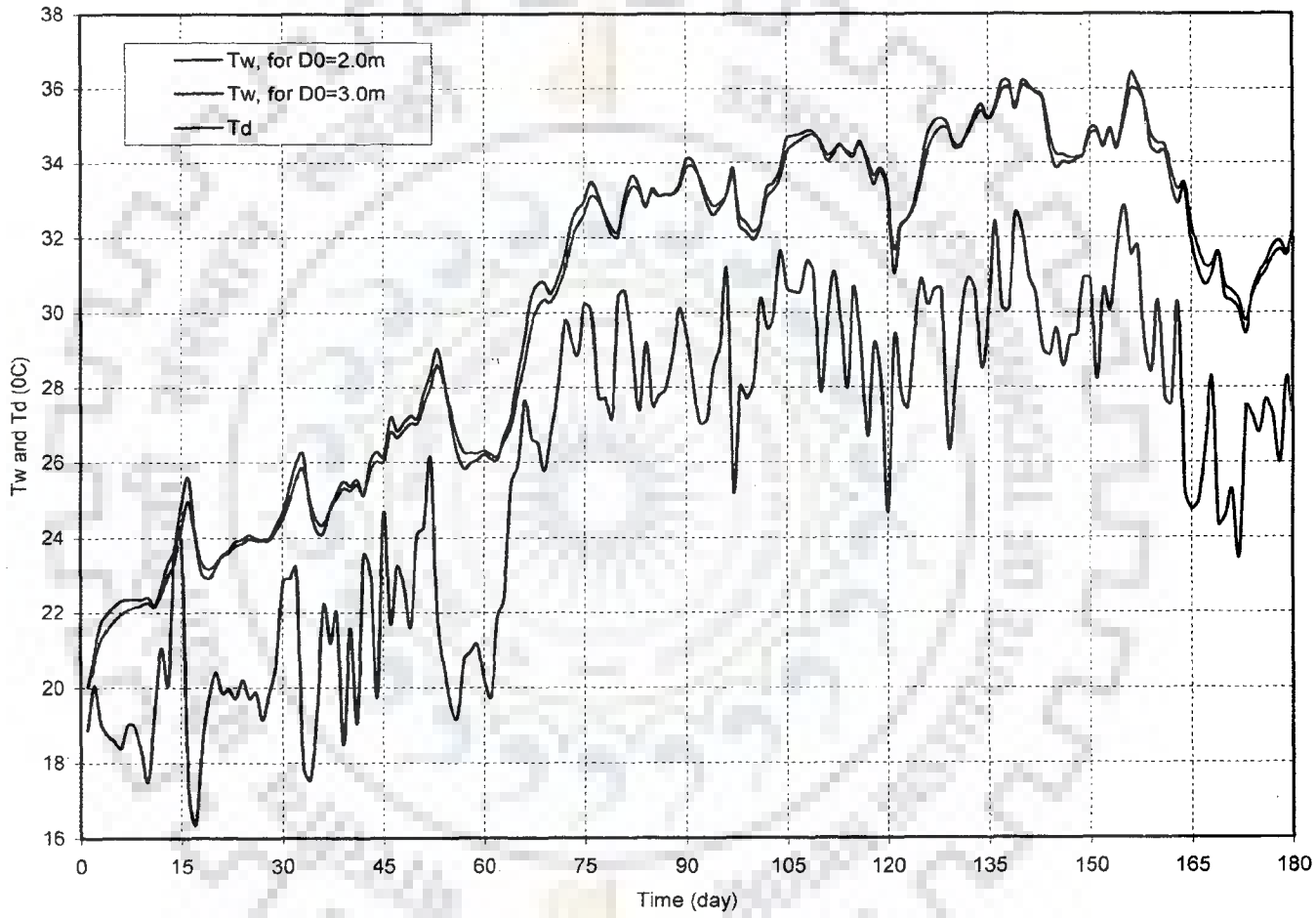

Fig. 3.8 (a) Variation of water temperature and dew point temperature (^{0}C) with time for D_0=2.0m and 3.0m, variation in the depth of water due to evaporation neglected

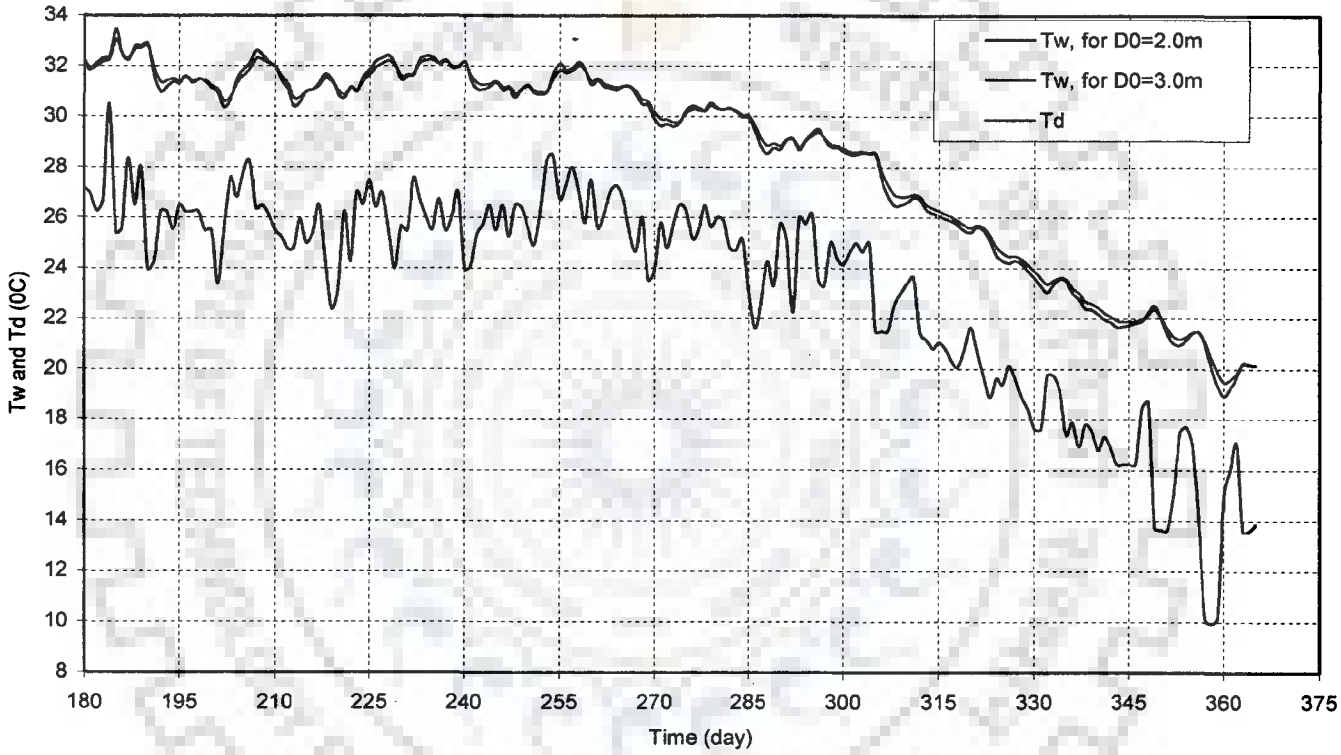

Fig. 3.8 (b) Variation of water temperature and dew point temperature (^{0}C) with time for D_0=2.0m and 3.0m, variation in the depth of water due to evaporation neglected

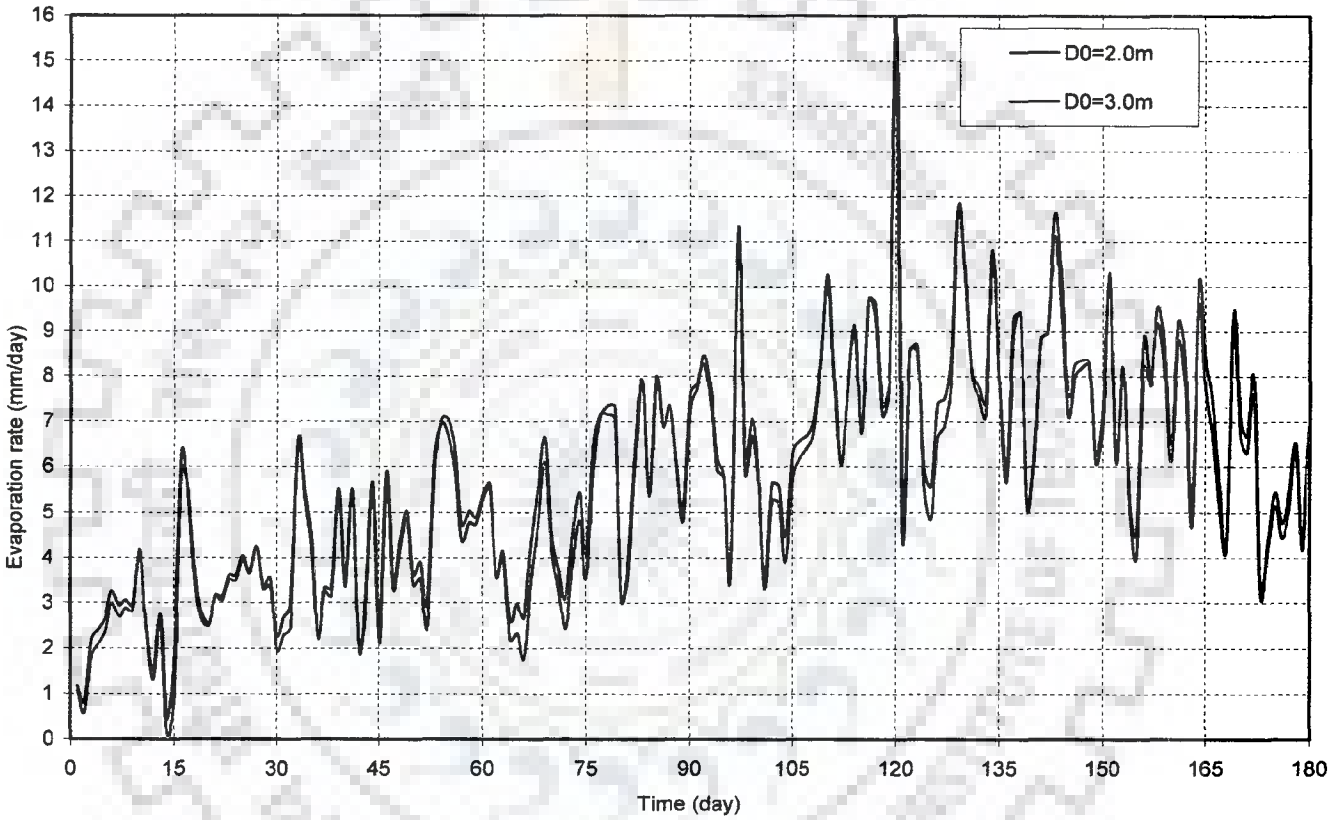

Fig. 3.9 (a) Variation of evaporation rate (E) with time (day) for D_0=2.0m and 3.0m

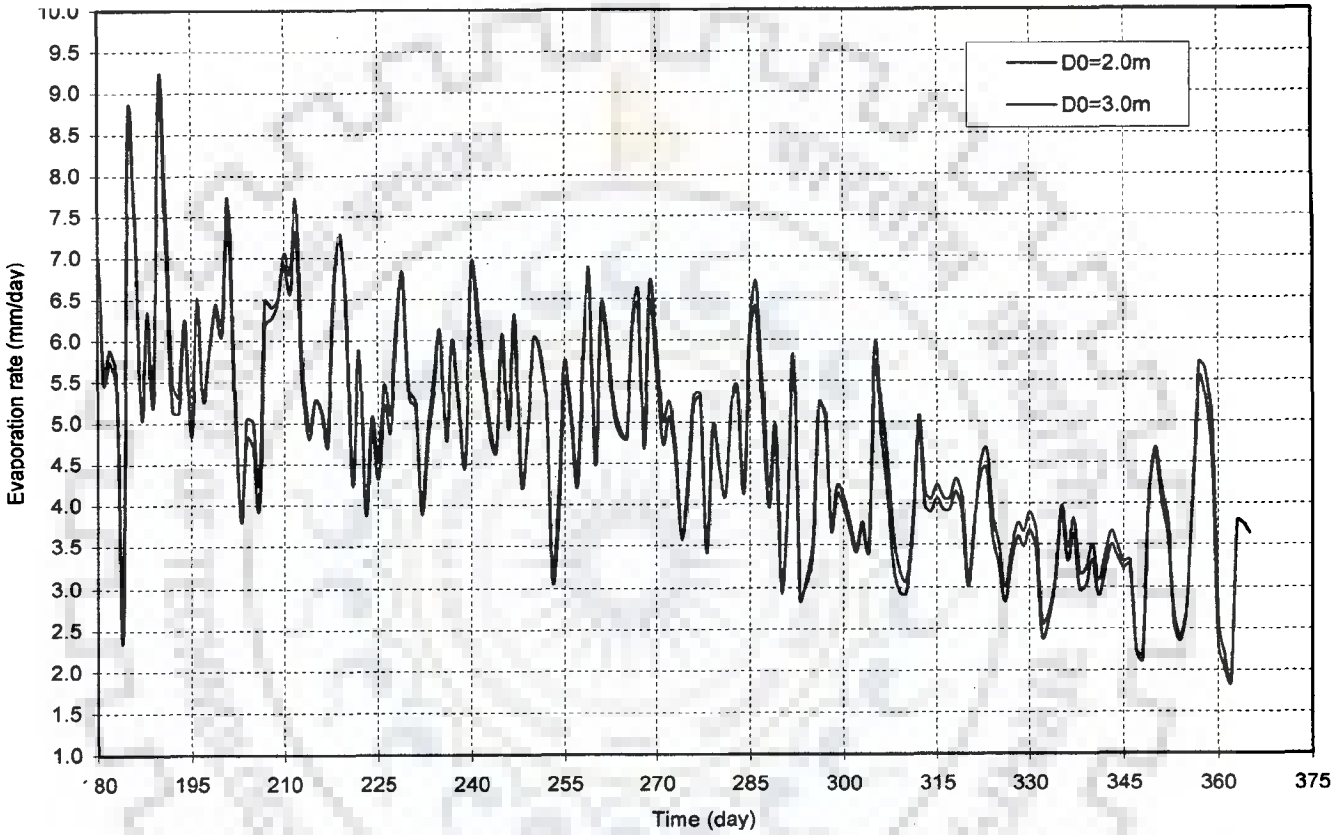

Fig. 3.9 (b) Variation of evaporation rate (E) with time (day) for D0=2.0m and 3.0m

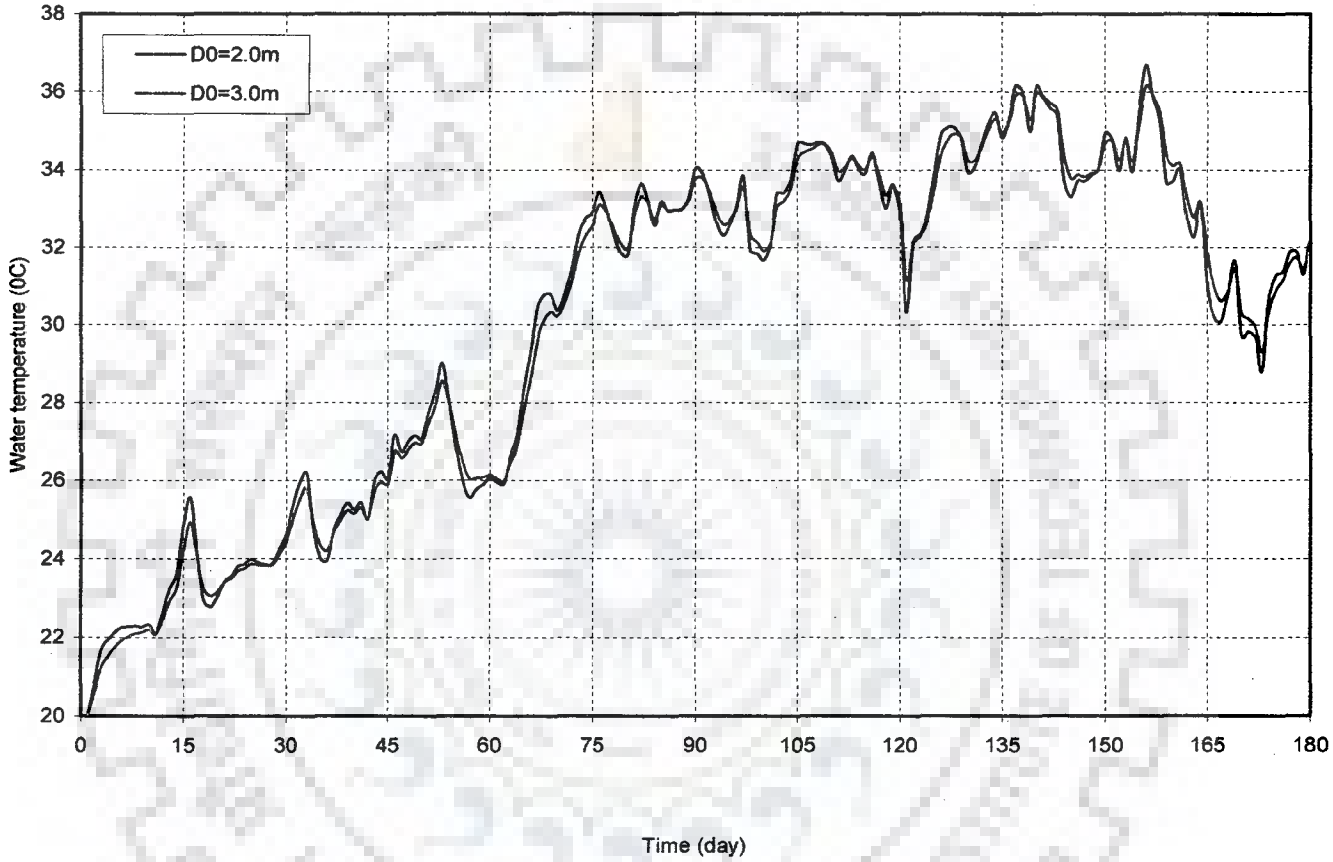

Fig. 3.10 (a) Variation of water temperature (^{0}C) with time, considering variation in the depth of water due to evaporation, for D_0=2.0m and 3.0m

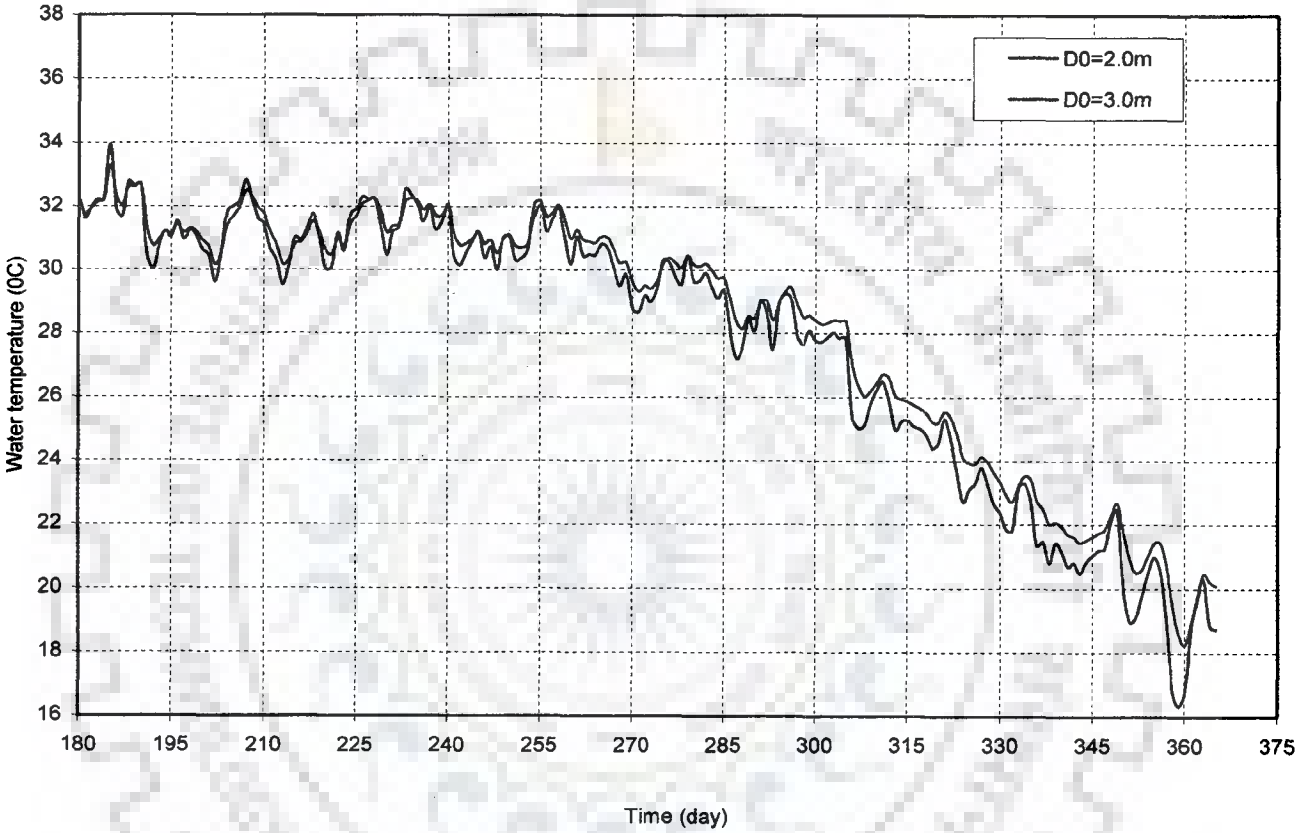

Fig. 3.10 (b) Variation of water temperature (^{0}C) with time considering variation in the depth of water due to evaporation, for D_0=2.0m and 3.0m

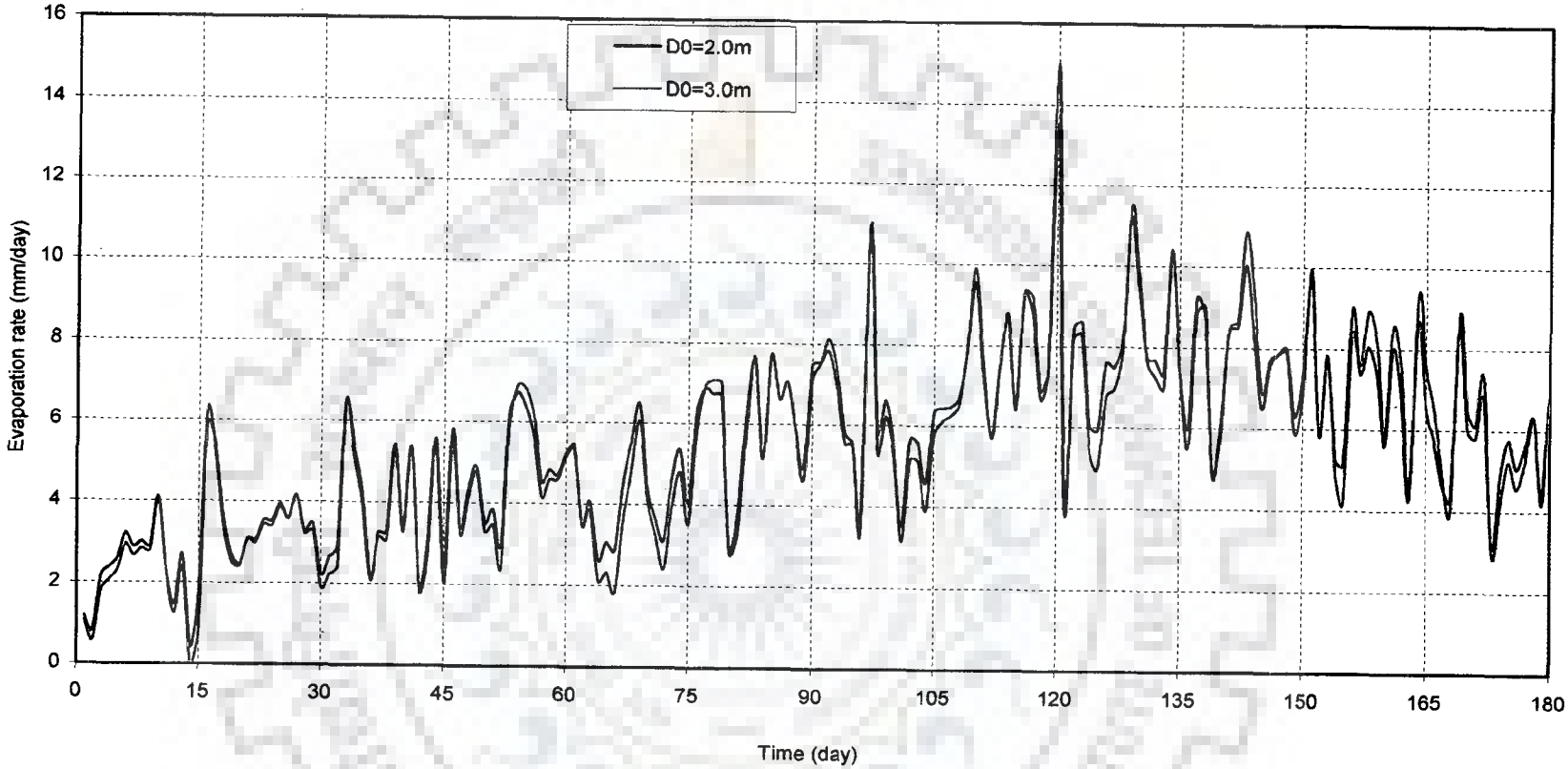

Fig. 3.11 (a) Variation of evaporation (mm/day) with time considering variation in the depth of water due to evaporation, for D_0=2.0m and 3.0m

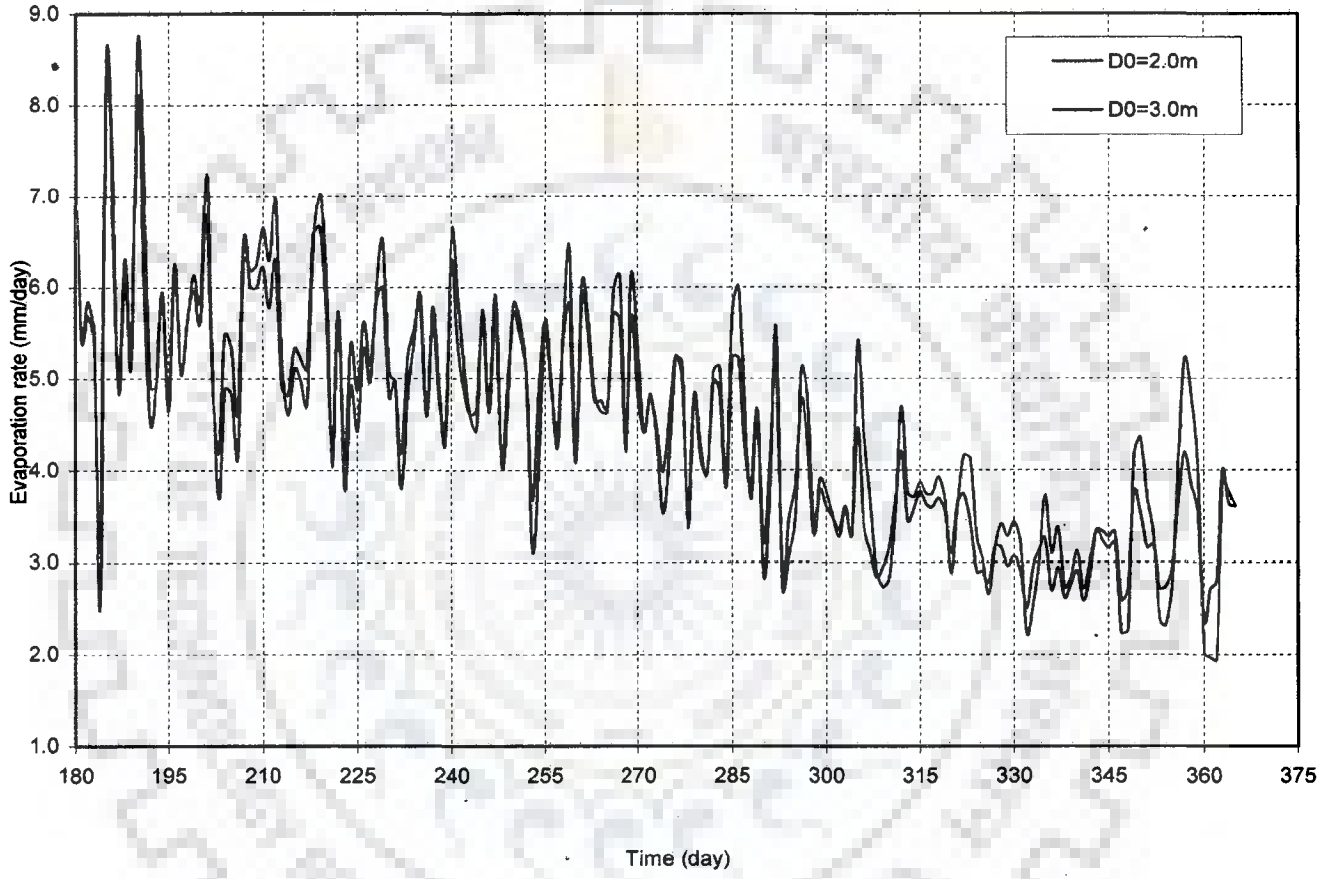

Fig. 3.11 (b) Variation of evaporation (mm/day) with time considering variation in the depth of water due to evaporation, for D_0=2.0m and 3.0m

A comparison of the observed pan evaporation and computed evaporation from heat balance are presented in Figs. 3.12 (a) and (b). As seen from the figures, the pan evaporation rates are higher than those computed from heat balance as usual.

A comparison between evaporation rates computed using Penman's method and heat balance method is made in Figs. 3.13 (a) and (b). As seen from the figures, in Penman's method, the evaporation rates computed using heat balance gets averaged.

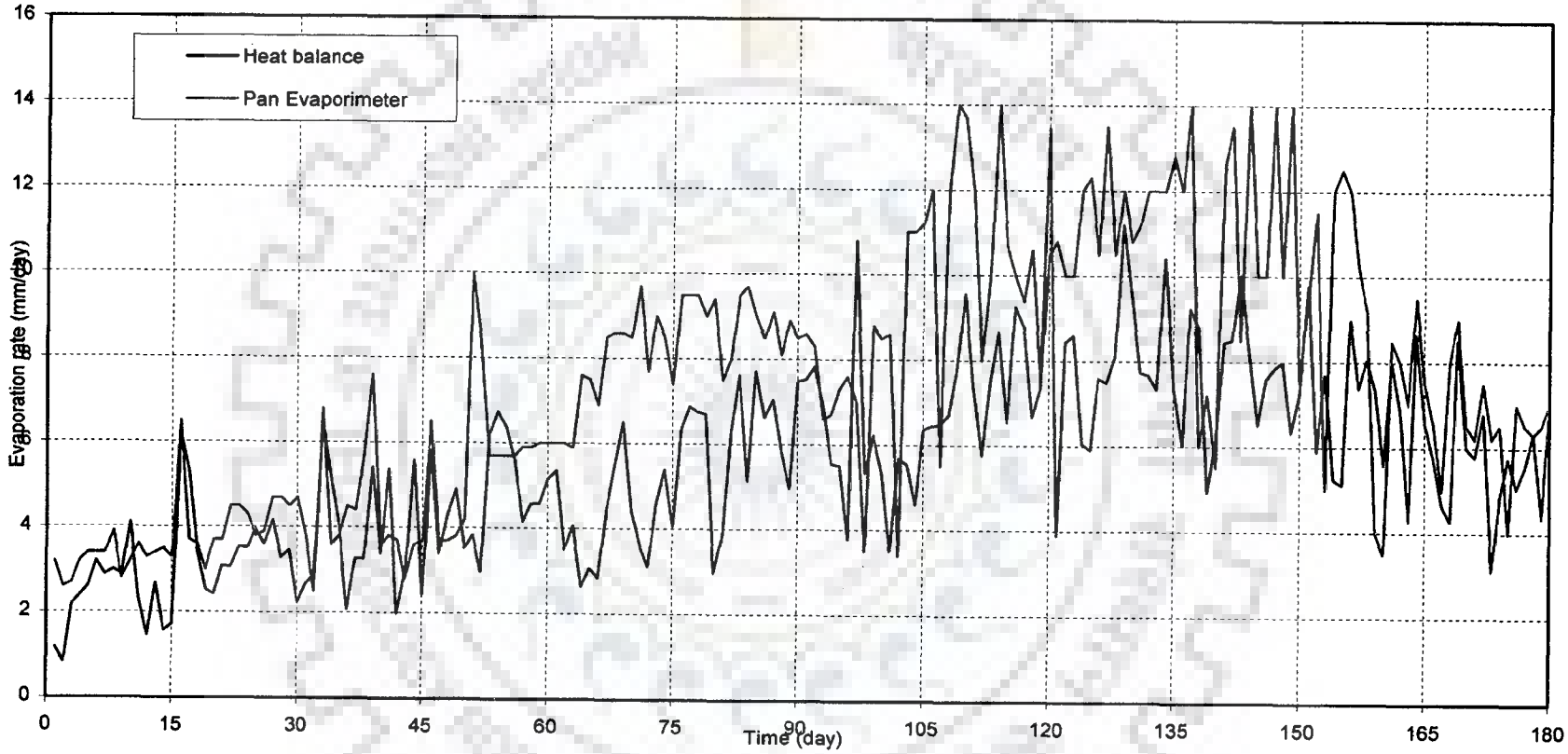

Fig. 3.12 (a) Comparisons of variation of evaporation rate measured by Pan Evaporimeter and estimated by modeled water temperature

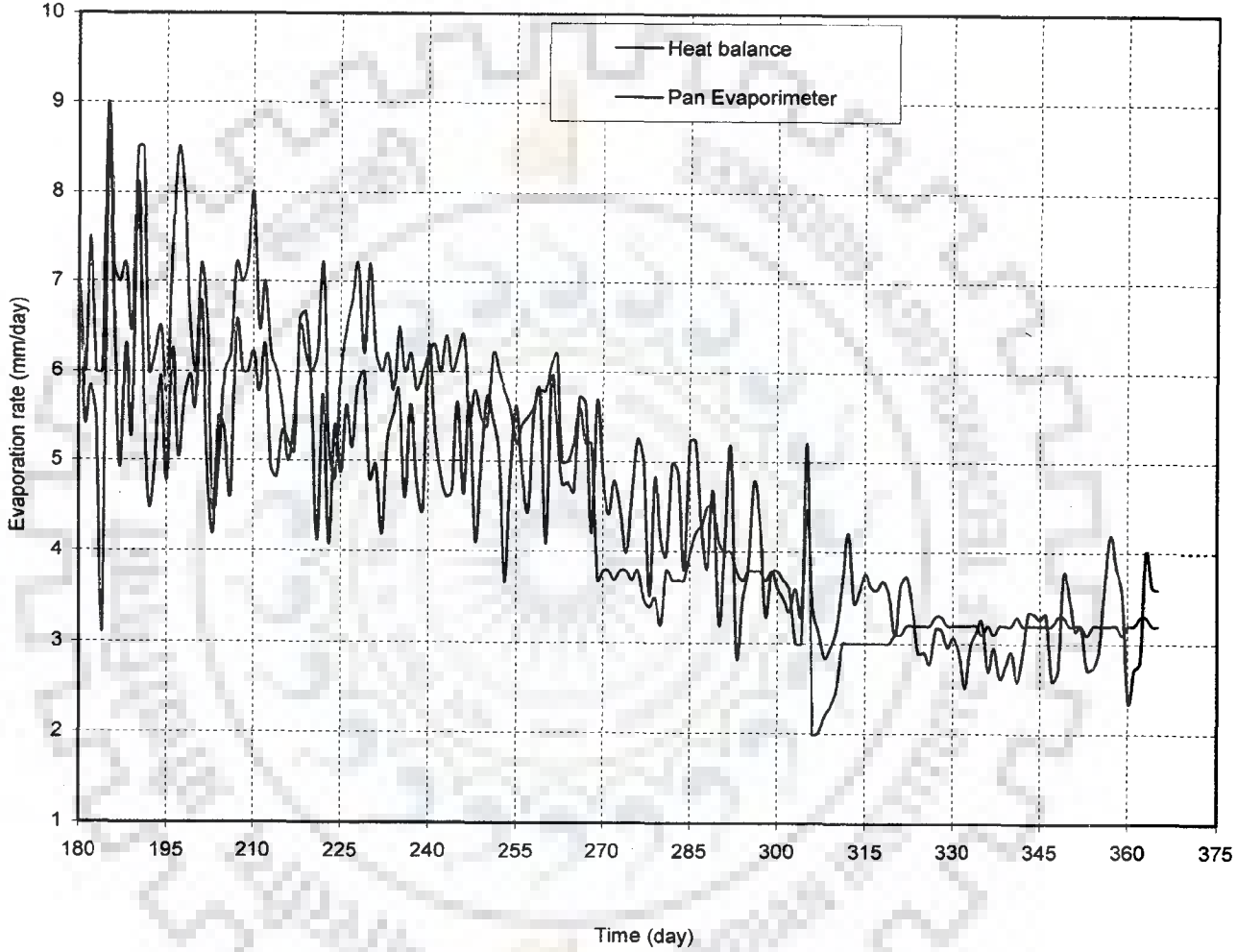

Fig. 3.12 (b) Comparisons of variation of evaporation rate measured by Pan Evaporimeter and estimated by modeled water temperature

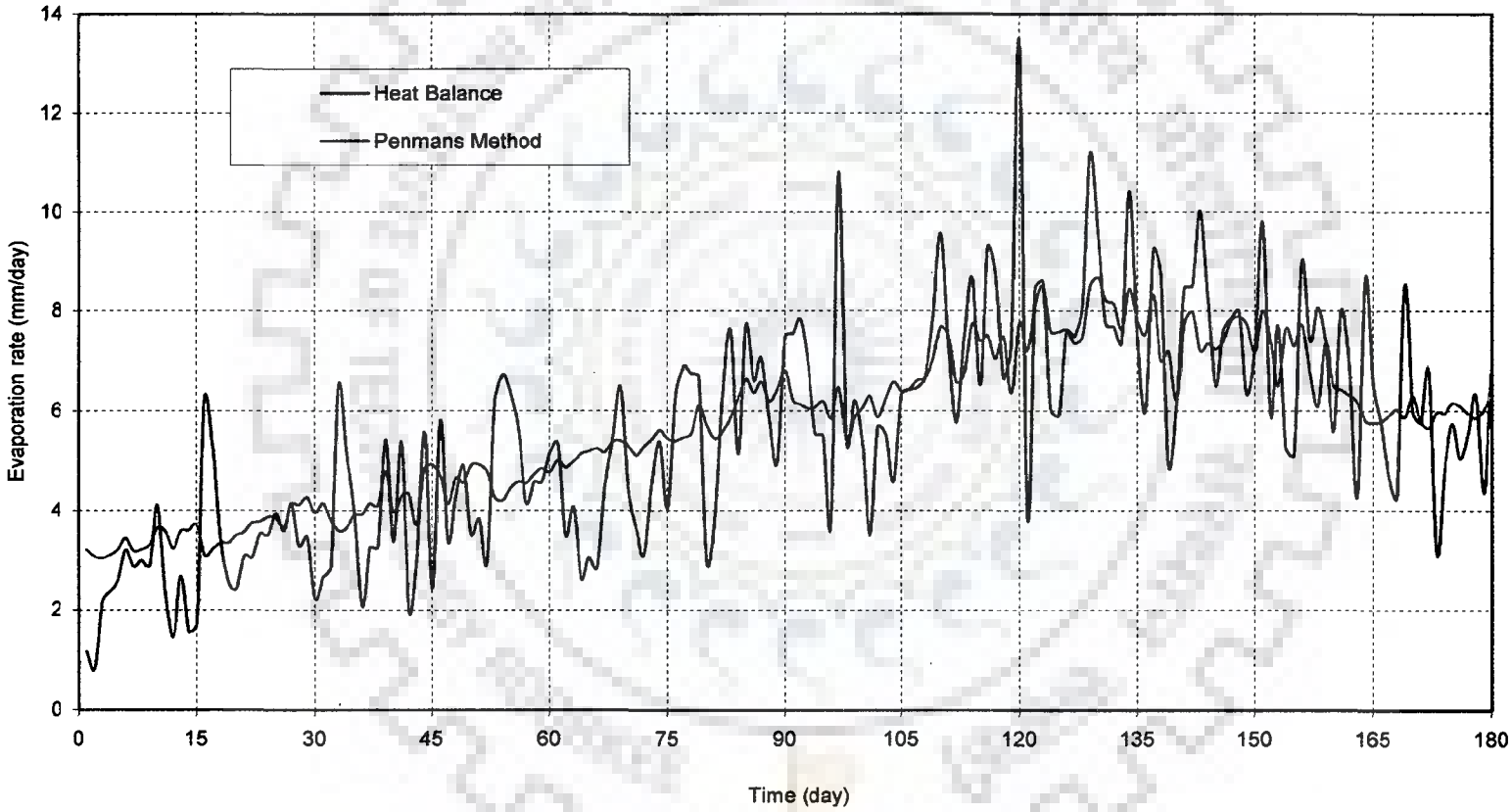

Fig. 3.13 (a) Comparisons of variation of evaporation rate estimated by Penman's method and by modeled water temperature

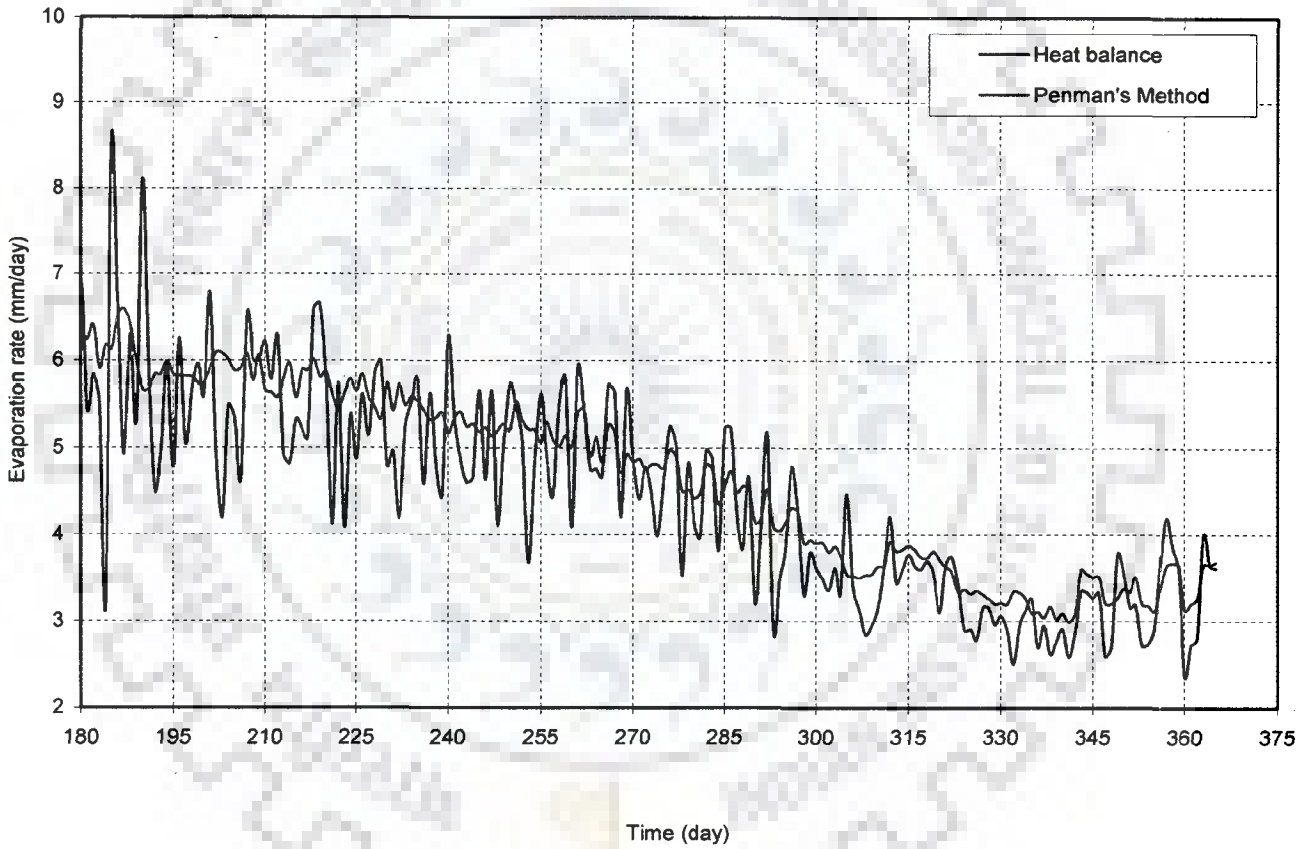

Fig. 3.13 (b) Comparisons of variation of evaporation rate estimated by Penman's method and by modeled water temperature

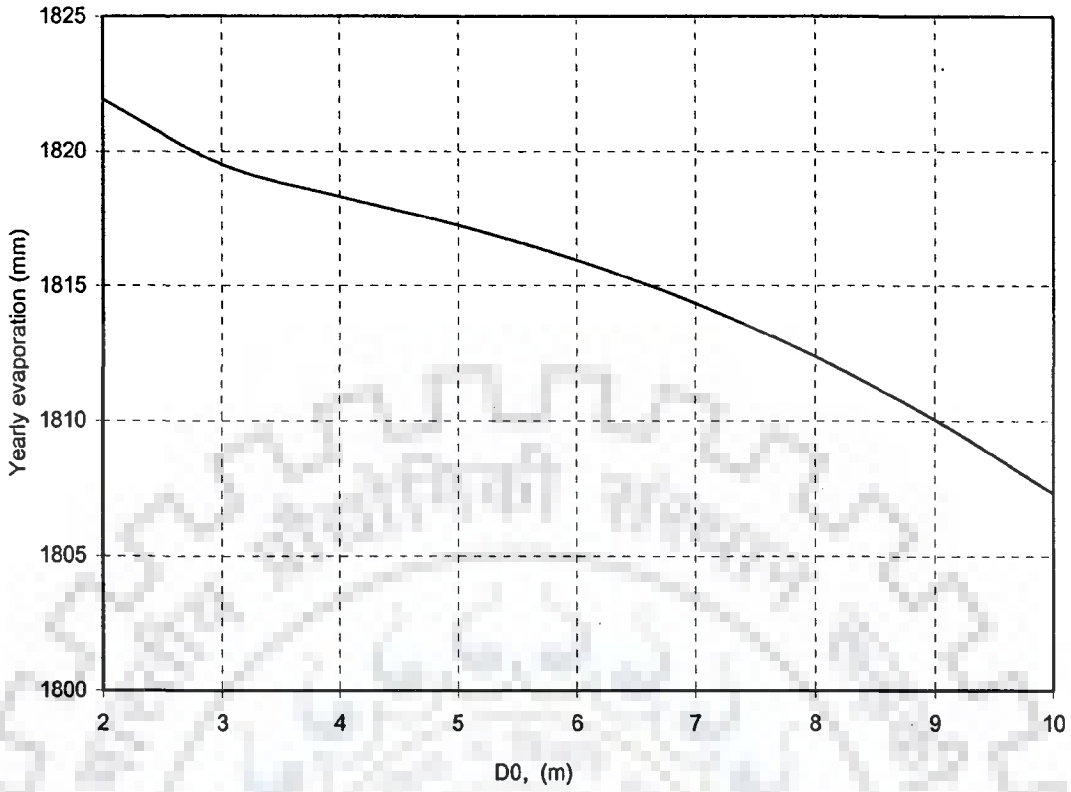

Fig.3.14 Variation of yearly evaporation with different initial depth of water (D_0) in the storage tank, variation in the depth of water due to evaporation considered

Variation of the yearly evaporation with initial depth of water in the tank is presented in Fig 3.14. It could be seen that, when the initial depth of water in the tank is increased from 2 to 10m, the yearly evaporation rate decreases from 1820mm to 1800mm. Thus there is marginal decrease in the evaporation rate by maintaining more depth of water in the storage tank.

3.5 CONCLUSIONS

Based on the above analysis the following conclusions are drawn.

1. The heat balance method is accurate as it computes zero evaporation the day, the water temperature in the tank coincide with the dew point temperature of the atmosphere.
2. In Penman's method, the evaporation rates computed using heat balance gets averaged.

3. The wind speed has significant influence on evaporation rates.
4. There are marginal differences in water temperatures and evaporation rates whether change in water depth due to evaporation is considered or not.
5. The yearly evaporation rate is less for higher depth of water in a storage tank. However the gain is of the order of 20mm when the initial depth of water in the tank is increased from 2 m to 10m.

CHAPTER- 4

UPDATING SCS CURVE NUMBER AND COMPUTATION OF RUNOFF

4.1 INTRODUCTION

Hydrologic studies to determine runoff and peak discharge should ideally be based on long-term stream flow records for the area. However, accurate information on runoff is still scarce (Gupta, 1989; Yurekli et al., 2004). Obtaining actual runoff at various catchment conditions is not an easy task and it requires large number of experimental catchments or plots. Furthermore, this approach is expensive, time consuming and thus uneconomic. Therefore, it is necessary to estimate runoff by using hydrological model based on measurable and available watershed characteristics. The rainfall-runoff models vary in complexity, functionality and applicability to a given region or storm type. Selection of the model depends upon the available information, the required accuracy, the resolution of the output and the time available for the modeling exercise (Audu, 1999). Rainfall-runoff models those being widely used are: MIKE SHE/11, RSM, HMS-RAS, and SWMM. The SCS curve number method is currently the most appropriate and authentic numerical model used by soil scientists (Roberson et al., 1988). It is used to estimate direct runoff from storm rainfall and it is well established in hydrologic engineering for environmental impact analyses (Ponce and Hawkins, 1996). The curve number method is well-known for its simplicity, predictability, stability, reliance on only one parameter and its responsiveness to major runoff-producing watershed properties (Ponce and Hawkins, 1996). The SCS-CN method was originally developed by the Soil Conservation Service (Soil Conservation Service 1964; 1972) for conditions prevailing in the United States. Since then, it has been adapted to conditions in other parts of the world. The curve numbers are related to rainfall and watershed data such as soil and vegetation, and can be estimated from look-up tables

(Garen and Moore, 2005). The combinations of hydrological soil groups, land uses, and treatment classes are hydrologic soil-cover complex (Sorrell and P.E., 2003). For each combination a number is assigned which is known as curve number, which is an index to its runoff potential on soil. These curve numbers are based on soil moisture conditions which are referred to as Antecedent Moisture Conditions (AMC). There are three types of AMC i.e. AMC-I, AMC-II and AMC-III. AMC-I has the lowest runoff potential and the watershed soils are dry. AMC-III has the highest runoff potential as the watershed is practically saturated from antecedent rainfall and AMC-II is an average soil moisture condition.

Sharma (1987) estimated actual curve number (CN) values by analyzing 7 years data of rainfall and runoff in bare crust-forming sandy soils in the Indian Arid Zone and he observed that SCS curve number is less than the actual one estimated from the response of the experimental watersheds. Although the SCS-CN method is the most popular method for performing ungauged watershed analysis, there has been extensive criticism of the method because it does not lead to accurate reproduction of runoff hydrographs; the predicted infiltration rates are not in accordance with classical unsaturated flow theory; the method is applied to watersheds for which it was not calibrated, and the original calibration results are not available (U.S. Army Corps, 1994).

Springer et al. (1980) stated that one of the major weaknesses of the SCS-CN method is the absence of local calibration using experimental watershed data. Smith (1997) and Willeke (1997) believe that there is a desperate need to advance the SCS method. There is strong resistance from some practicing engineers and regulatory agencies to eliminate the method altogether, and thus a suitable interim solution is to develop a reliable modification to the method wherein the storage parameter, *S*, is more constrained and is based on the concept of saturation excess. One problem often

encountered when using the curve number method is that the spatial and temporal variability of a storm, the quality of measured data, and the effect of antecedent soil moisture conditions result in a set of curve numbers for the same watershed instead of a single CN (Ponce and Hawkins 1996). This demonstrates that lumping all of the many properties of a storm and a watershed into a single parameter, S, to produce a runoff value is not physically based.

4.2 STATEMENT OF THE PROBLEM

There is a need to estimate the storage parameter using hydrological processes, which governed the storage parameter. In this study, curve number is updated by considering the soil moisture depletion due to evaporation and drainage during inter storm periods. Soil moisture movement is predicted using Richards' equation and applying the boundary condition at the surface. Soil moisture evaporation and drainage during inter storm periods are computed from soil moisture balance and the curve number is updated.

4.3 ANALYSIS

As derived by Hawkins (1978) (given in Appendix B), the modified storage parameter, $V(t)$, at time t is related to storage $S(t)$ at time t by the following relation:

$$V(t)=1.2S(t)=1.2\left\{\frac{25400}{CN(t)}-254\right\} \tag{4.1}$$

V (t) would increase with time due to soil moisture depletion consequent to evaporation and drainage and would decrease due to the part of rainfall not appearing as runoff.

4.3.1Mass Balance and Storage Balance on a Rainy Day, $P(j+1)>0.2S(j)$

Performing the mass balance on $(j+1)^{th}$ day during which the rainfall amount is $P(j+1)$

$$P(j+1)=I_a(j+1)+F(j+1)+R(j+1) \tag{4.2a}$$

or

$$F(j+1)=P(j+1)-I_a(j+1)-R(j+1) \tag{4.2b}$$

Performing the storage balance over the time period $(j)to(j+1)$

$$V(j+1)=V(j)-I_a(j+1)-F(j+1)-\Delta S_{sm}(j+1)+E_c(j+1) \tag{4.3a}$$

$V(j+1)$ is the storage at the end of $(j+1)^{th}$ day

$\Delta S_{sm}(j+1)=S_{sm}(j+1)-S_{sm}(j)$

= changes in soil moisture due to drainage and evaporation from soil moisture zone.

Incorporating (4.2b) in (4.3a)

$$V(j+1)=V(j)-\{P(j+1)-R(j+1)\}-\Delta S_{sm}(j+1)+E_c(j+1) \tag{4.3b}$$

The canopy evaporation is evaluated as follows:

The upper limit of canopy evaporation, $E_c(j+1)$ is the potential evaporation on $(j+1)^{th}$ day, $E_p(j+1)$. The lower limit of canopy evaporation is the amount intercepted by canopy equal to 0.2S (j). Hence,

$$\text{If } E_p(j+1)<0.2S(j); E_c(j+1)=E_p(j+1)$$

$$\text{If } E_p(j+1)>0.2S(j);\ E_c(j+1)=0.2S(j)$$

Ascertaining, $E_c(j+1)$ compute $S(j+1)$ using the relation

$$S(j+1)=V(j+1)/1.2 \tag{4.3c}$$

If $E_p(j+1)<0.2S(j)$, then $0.2S(j)$ - $E_p(j+1)$ will be equal to $E_c(j+2)$ subjected to evaporative demand on $(j+2)^{th}$ day and this process will continue.

4.3.2Mass Balance and Storage Balance on a Rainy Day When $P(j+1)<0.2S(j)$

During $P(j+1)<0.2S(j)$ there is no runoff, hence, the mass balance equation is as:

$$P(j+1)=I_a(j+1)+F(j+1) \tag{4.4a}$$

Performing the storage balance over the time period $(j)to(j+1)$ similar to as rainy day

$$V(j+1) = V(j) - P(j+1) - \Delta S_{sm}(j+1) + E_c(j+1) \quad (4.4b)$$

If $E_p(j+1) < P(j+1); E_c(j+1) = E_p(j+1)$

If $E_p(j+1) > P(j+1); E_c(j+1) = P(j+1)$

Ascertaining, $E_c(j+1)$ as above $S(j+1)$ is computed using the relation (4.3c)

4.3.3Mass Balance during a Non Rainy Day $P(j+1) = 0.0$

During non rainy day, $E_c(j+1)$ is assumed to be zero in this analysis, hence storage balance over a period $(j)to(j+1)$ is as:

$$V(j+1) = V(j) - \Delta S_{sm}(j+1) \quad (4.5)$$

During the rainy days, $\Delta S_{sm}(j+1)$ is computed from Richards' equation applying a boundary condition, $\theta(0,t) = \theta_s$. During non rainy days $\Delta S_{sm}(j+1)$ is computed applying a boundary condition $\theta(0,t) = \theta_u$ as given in Appendix B .The curve number is updated using (4.3b, 4.4b and 4.5)

4.4 RESULTS AND DISCUSSION

A method of estimation of runoff from contributing catchment to a storage tank during the monsoon period is described in the following paragraph.

4.4.1 Initial Curve Number for the Study Area

The total catchment area of the storage pond is 9.0 km^2. The land use characteristics of the catchment area are categorized as follows:

1. Agricultural land, A(1)= 5.3 km^2
2. Forest area, A(2)=2.5 km^2
3. Settlement area A(3)= 1.2km^2

For computation of surface runoff by SCS-CN method, the following curve numbers from table (presented in Appendix-B) have been assigned to the above areas based on AMC-II condition which generally prevails during pre-monsoon period.

The curve number for the agricultural area: 81

The curve number for the forest area: 55

The curve number for the settlement area: 92

Based on the basic infiltration rate 6.0 cm /hr (Srivastava et al., 2004), the soils in the study area are classified as 'Hydrological soil group A' (presented in Appendix-B). The composite curve number is

$$\overline{CN} = \frac{\sum_{i=1}^{3} CN(i) \times A(i)}{\sum_{i=1}^{3} A(i)} = 75.25 \approx 75 \qquad (4.6)$$

4.4.2 Updating Storage Parameter and Curve Number

The soil moisture at the ground surface during a non rainy day is governed by the prevailing relative humidity in atmosphere. During a rainy day, boundary soil moisture has been taken as saturated moisture content. The variation of boundary soil moisture content with time is given in Appendix-B. The method of computation of change in volumetric soil moisture content in the root zone (120cm) due to evaporation and drainage is presented in Appendix-B. The variation of soil moisture in the root zone during the year is presented in Figures 4.1(a) and 4.1(b).

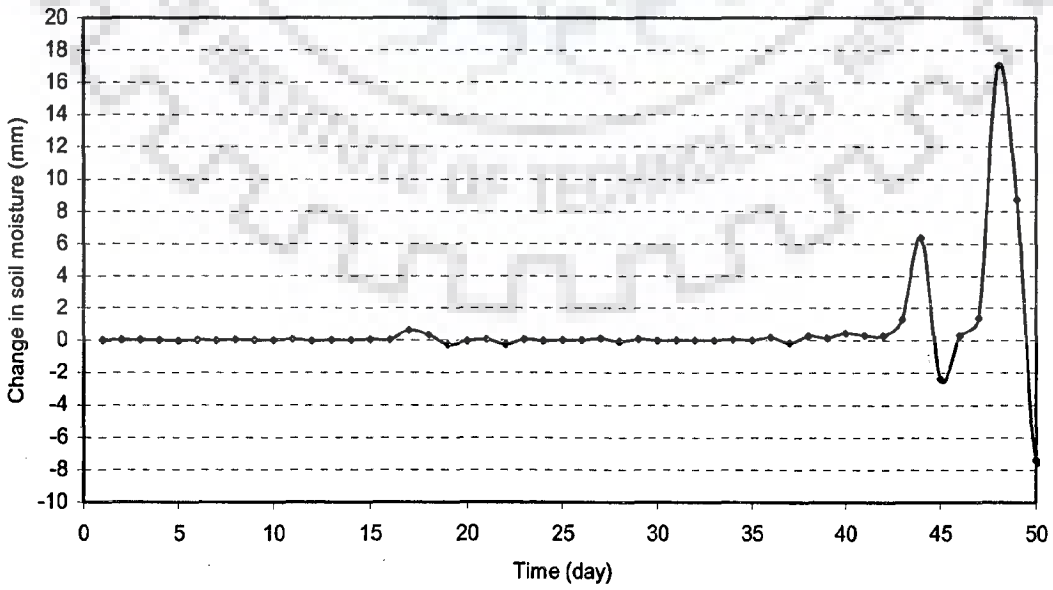

Fig. 4.1a Change in soil moisture content with time due to infiltration, soil evaporation and drainage in the root zone (for 50 days from 1st

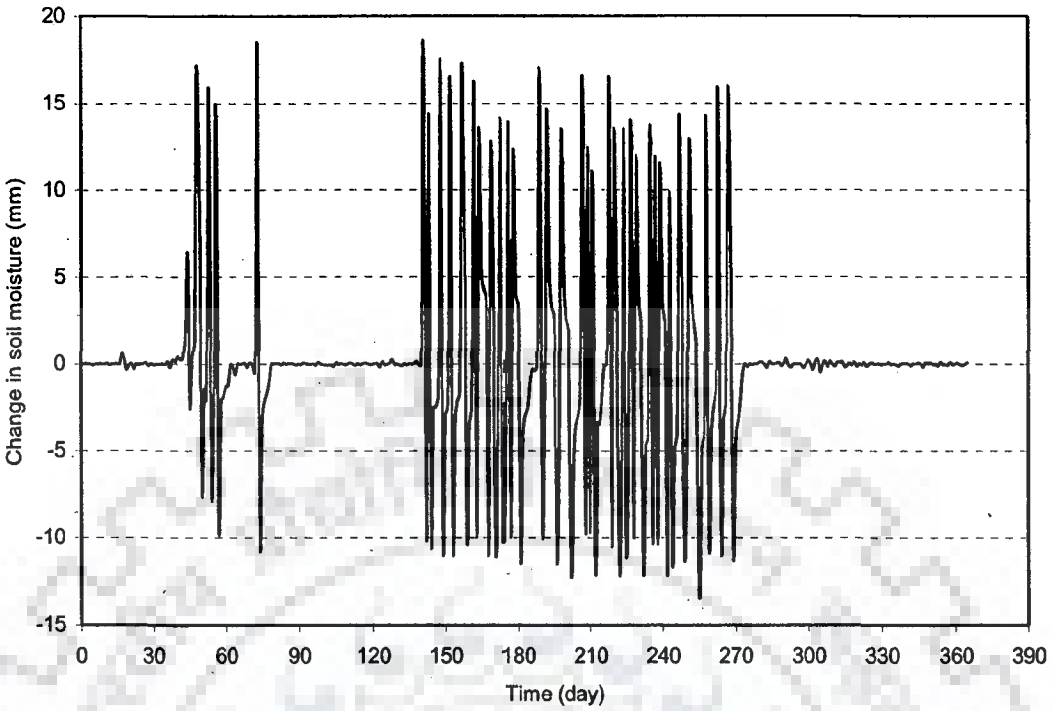

Fig 4.1b Change in soil moisture content with time due to infiltration, soil evaporation and drainage in the root zone for a

It is seen from the figures, that the change in soil moisture owing to infiltration and drainage are significant during rainfall and immediate post rainfall period. Since transpiration has not been considered the change in soil moisture during post rainfall period, after drainage has ceased is very nominal. If the change in soil moisture is positive, it is due to infiltration and if it is negative, it is due to drainage and soil evaporation.

The storage S, for different initial soil moisture conditions AMC-II (CN (0) =75), AMC-III (CN (0) = 89) and AMC-I (CN (0) =57) are updated, considering change in soil moisture in the soil moisture zone and canopy evaporation are presented in the Figure 4.2. The corresponding curve numbers are presented in Figure 4.3.

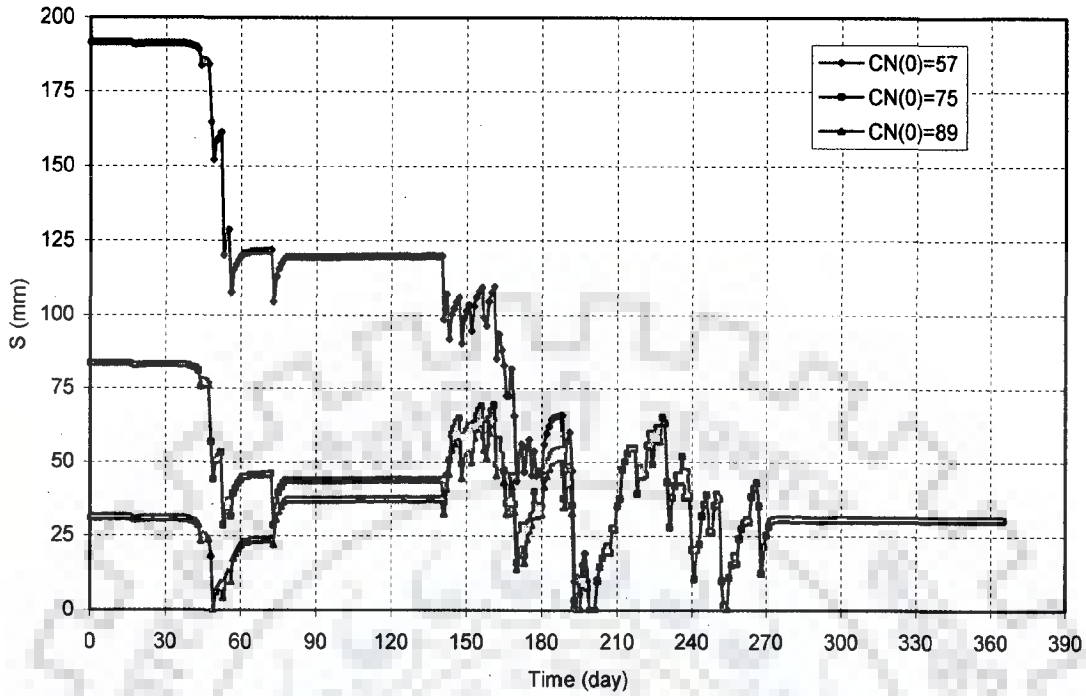

Fig. 4.2 Variation of storage parameter with time for CN (0) =57, 75 and 89

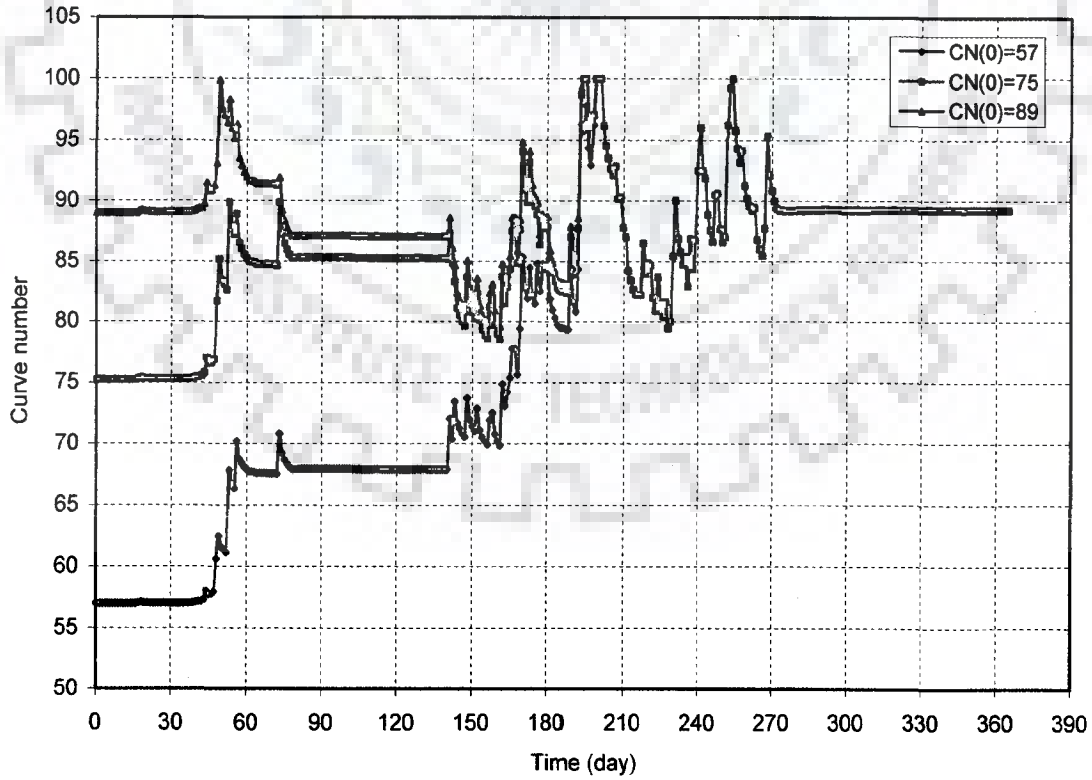

Fig. 4.3 Variation of curve number with time for CN (0) =57, 75 and 89

It is seen from figures that, in the beginning, till the occurrence of the first rainfall, the storage parameter as well as curve number remains nearly constant. With occurrence of rainfall events the storage parameters decreases and almost attains a zero value (saturated condition). Accordingly the curve number increases and attains the maximum value (100) indicating that maximum runoff potential condition has been attained. During immediate post rainfall period owing to drainage and soil evaporation, the storage parameters increases and curve number decreases. As seen from the figures during later part of inter storm and during post monsoon period, the curve number does not change as the soil moisture extraction by plant has not been considered. During the monsoon period because of several rainfall events, there is variation in the storage parameter and curve number.

It is seen from the figures that, AMC-III condition prevails at the end of the monsoon period irrespective of the initial curve number (whether it was for AMC-I or AMC-II or AMC-III). If at particular time, the curve numbers corresponding to all the three initial conditions are identical, then the remaining variations are identical. As expected the soil moisture condition at the end of monsoon period is AMC-III condition irrespective of the initial AMC conditions.

A comparison among runoff depths computed with the three initial AMC conditions are presented in Figures 4.4 to 4.6. As seen from the figures AMC conditions have significant control on runoff from a catchment. For the particular catchment considered, the total volume of runoff depth produced during the monsoon period are 286.56mm, 348.07mm and 389.22mm for AMC conditions I, II and III respectively. If throughout the monsoon period a constant curve number (AMC-II) is assumed the runoff is very much underestimated and it is 126.54mm and is presented in Figure 4.7. Therefore, for a realistic computation of runoff depth continuous updating of curve number is preferable.

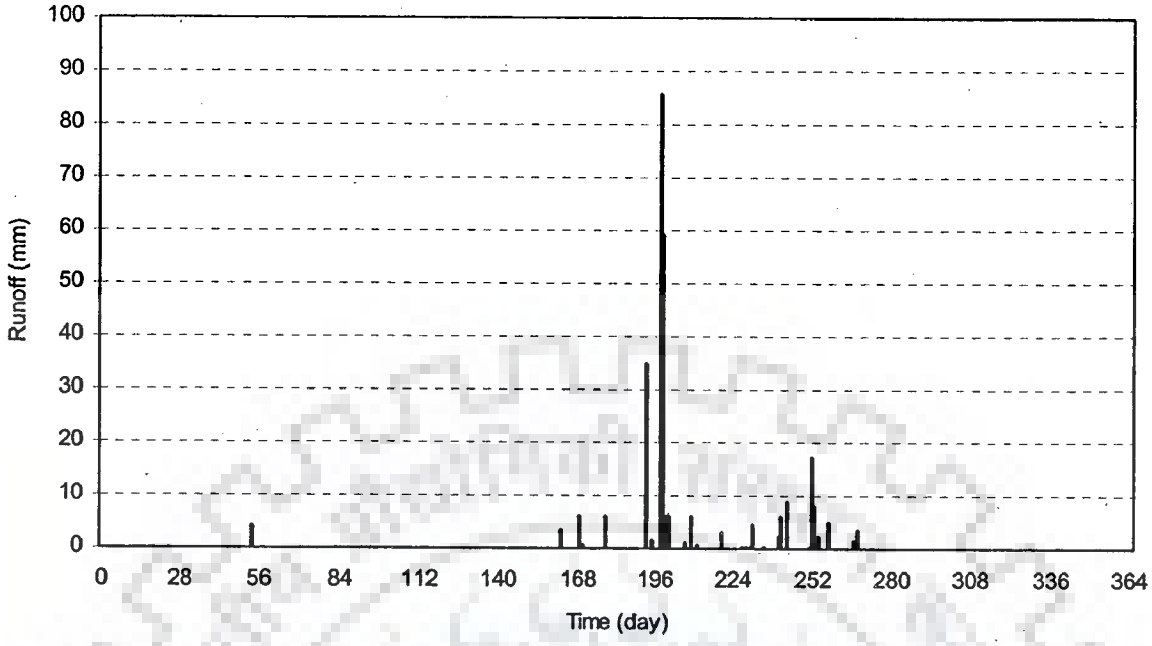

Fig.4.4 Runoff generated for initial guess of AMC-I condition

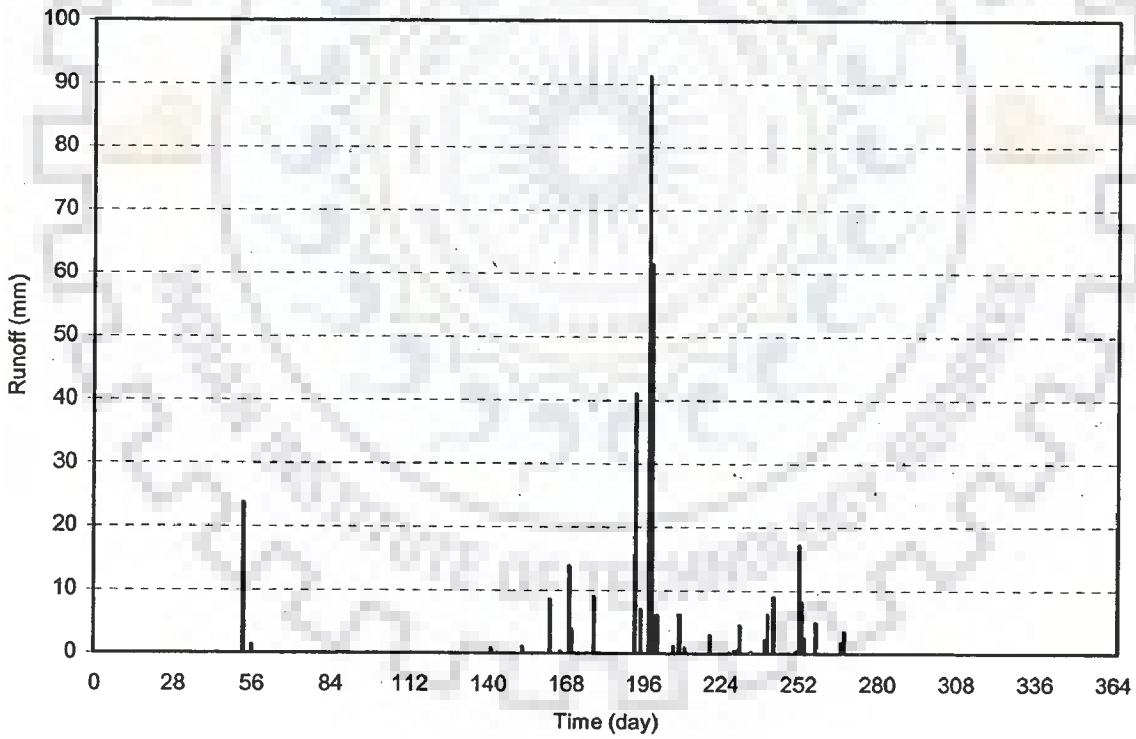

Fig.4.5 Runoff generated for initial guess of AMC-II condition

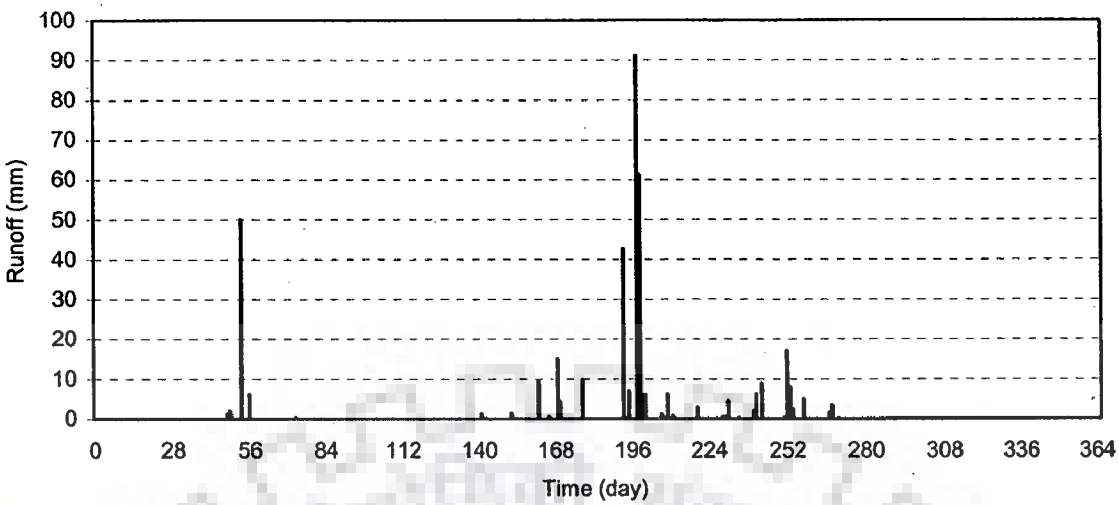

Fig.4.6 Runoff generated for initial guess of AMC-III condition

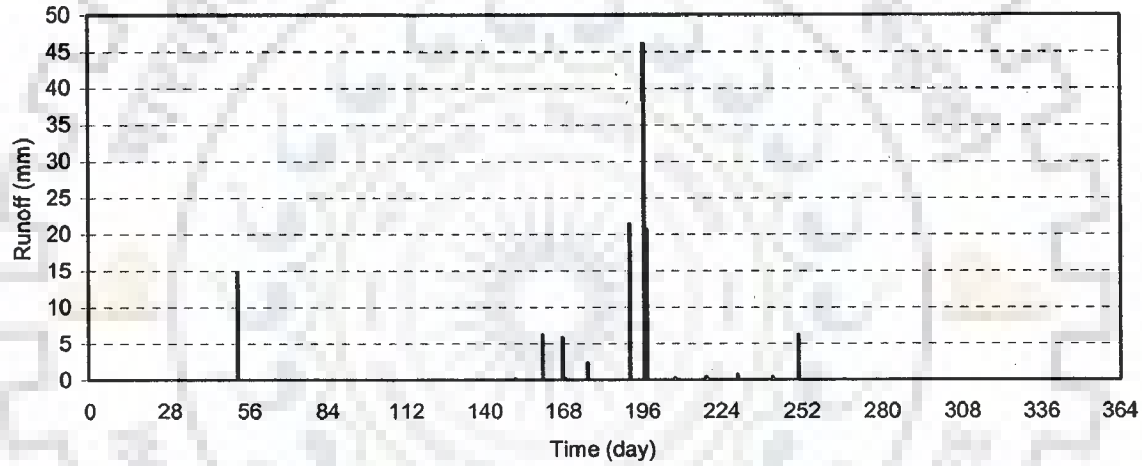

Fig.4.7 Runoff generated for constant AMC-II condition

4.5 CONCLUSIONS

Based on the study the following conclusions can be drawn:

1. For a realistic computation of runoff depth continuous updating of curve number is preferable.
2. A constant curve number throughout the monsoon period very much under-predict the runoff depth from a catchment.
3. For more accurate estimation of surface runoff transpiration from soil moisture zone in forest and agricultural lands should be considered, where the rainfall is evenly distributed throughout the year.

CHAPTER-5

INFILTRATION FROM A STORAGE TANK IN A TWO LAYERED SOIL SYSTEM USING GREEN AND AMPTTHEORY

5.1 INTRODUCTION

In general, the water stored in a storage tanks, originates from surface runoff. Therefore, in due course of time, fine sediments carried by the inflow get deposited on the bed of the tank. Consequently, the sedimentation reduces the storage capacity of the tank. Also shallow depth of water in the tank leads to enhanced rate of evaporation from tank storage. On the other hand, fine sediments on tank bed reduce seepage loss through bed surface and restrict recharge to underlying aquifer. If the difference between the values of seepage coefficients (hydraulic conductivities) of the fine sediments layer deposited on the tank bed and underlying soil is significant, and water table is lying at large depth below the tank bed, in that case, water may percolate from the fine sediment layer in isolated jets (Polubarinova-Kochina, 1962, p143) and may not fill all the soil pores. In that case, a condition of flow through unsaturated soil medium would prevail. In this chapter, the seepage losses from an irrigation tank are quantified using Green and Ampt infiltration theory assuming that water percolates through the tank bed.

5.2 STATEMENT OF THE PROBLEM

Let a storage tank having a flat bed surface overlie a homogeneous soil layer of large depth. Let the initially dry storage tank, get filled for the first time up to a depth D_0 at time $t = 0$. The infiltration through the tank bed can be conveniently assumed as one dimensional and taking place in vertical downward direction. Let d_s be thickness of the fine sediments at the bottom of the tank, $\tilde{k}_1$ be its saturated hydraulic conductivity, and θ_{s1} be the moisture content at saturation and $\tilde{k}_2$ be the saturated hydraulic conductivity and θ_{s2} be the moisture content at saturation of the underlying subsoil.

Prior to the onset of filling of the tank, the moisture content of the soil in the fine sediment layer and subsoil are θ_{i1} and θ_{i2} respectively which can be taken as the field capacity of the respective soil medium. Depth of water in the tank varies because of infiltration from the tank. Let $D_w(t)$ be the depth of water in the tank at time t after onset of filling. In the beginning, the upper fine sediment layer gets saturated. The influence of the subsoil becomes effective once the saturation front surpasses the upper sediment layer. Let prior to the saturation front surpassing the interface, h_{1f} be the average suction head acting at the moving front in the fine sediment layer and z_f be the position of saturation front at time *t*. Once the saturation front surpasses the interface, let h_3(t) be the hydraulic head at the interface of the fine sediment layer and subsoil, and h_{2f} be the average suction head at the moving front. It is required to find the infiltration rate from the tank.

5.3 ANALYSIS

5.3.1 Stage 1: Movement of Saturation Front in the Upper Fine Sediment Layer

A vertical section through the tank is shown in Fig.5.1. The hydraulic head, *h*, at a point in the flow medium is defined as:

$$h = \frac{p_w}{\gamma_w} - z \tag{5.1}$$

where p_w =pore water pressure; γ_w = unit weight of water, *z*= ordinate of the point.

Choosing an origin at point 1 (Fig.5.1), the hydraulic head at point 1 is: $h_1 = D_w(t)$. Let at time t, the saturation front is at a depth z_f. Accordingly, the hydraulic head at the saturation front is: $h_2 = -h_{f1} - z_f$.

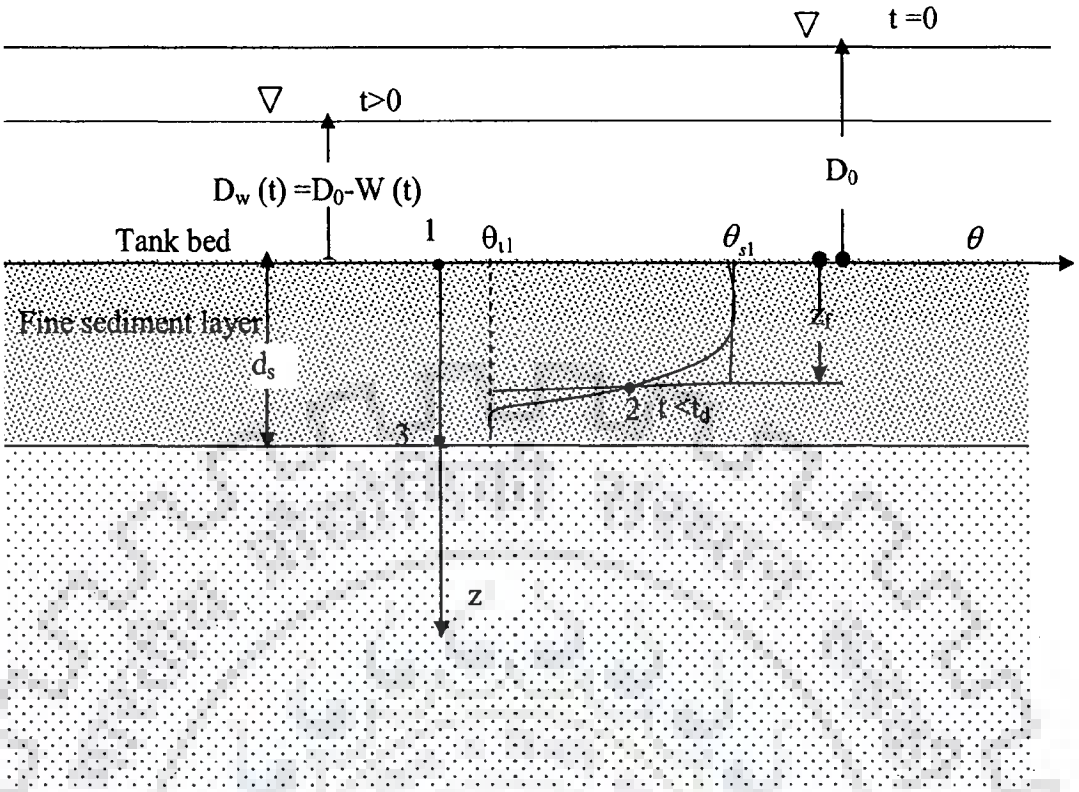

Fig.5.1 Unsaturated flow through the fine sediment layer

Applying Green and Ampt infiltration theory

$$I = \tilde{k}_1 \frac{h_{f1} + z_f + D_w(t)}{z_f} \tag{5.2}$$

Multiplying $(\theta_{s1} - \theta_{i1})$ with the denominator and numerator, and incorporating

$$I = \frac{dW}{dt}; \quad W(t) = (\theta_{s1} - \theta_{i1})z_f; \; D_w(t) = D_0 - W(t) \text{ in (5.2)}$$

$$\frac{dW}{dt} = \tilde{k}_1 \frac{(\theta_{s1} - \theta_{i1})(h_{f1} + D_0) + \{1 - (\theta_{s1} - \theta_{i1})\}W(t)}{W(t)} \tag{5.3}$$

or

$$\tilde{k}_1 dt = \frac{W(t)}{(\theta_{s1} - \theta_{i1})(h_{f1} + D_0) + \{1 - (\theta_{s1} - \theta_{i1})\}W(t)} dW \tag{5.4}$$

or

$$\tilde{k}_1 \{1 - (\theta_{s1} - \theta_{i1})\} dt = \frac{\{1 - (\theta_{s1} - \theta_{i1})\}W(t)}{(\theta_{s1} - \theta_{i1})(h_{f1} + D_0) + \{1 - (\theta_{s1} - \theta_{i1})\}W(t)} dW \tag{5.5}$$

or

$$\tilde{k}_1\{1-(\theta_{s1}-\theta_{i1})\}dt = \frac{\{1-(\theta_{s1}-\theta_{i1})\}W(t)+(\theta_{s1}-\theta_{i1})(h_{f1}+D_0)-(\theta_{s1}-\theta_{i1})(h_{f1}+D_0)}{\{1-(\theta_{s1}-\theta_{i1})\}W(t)+(\theta_{s1}-\theta_{i1})(h_{f1}+D_0)}dW$$

$$= dW - \frac{(\theta_{s1}-\theta_{i1})(h_{f1}+D_0)dW}{\{1-(\theta_{s1}-\theta_{i1})\}W(t)+(\theta_{s1}-\theta_{i1})(h_{f1}+D_0)} \tag{5.6}$$

Integrating and applying the condition $W(0)=0$ at $t=0$,

$$\{1-(\theta_{s1}-\theta_{i1})\}\tilde{k}_1 t = W(t) - \frac{(\theta_{s1}-\theta_{i1})(h_{f1}+D_0)}{\{1-(\theta_{s1}-\theta_{i1})\}}\ln\frac{(\theta_{s1}-\theta_{i1})(h_{f1}+D_0)+\{1-(\theta_{s1}-\theta_{i1})\}W(t)}{(\theta_{s1}-\theta_{i1})(h_{f1}+D_0)} \tag{5.7}$$

Time t_{ds} required for the saturation front to surpass the distance d_s is obtained substituting $W(t)=(\theta_{s1}-\theta_{i1})d_s$ in (5.7). The relation is

$$t_{ds} = \frac{(\theta_{s1}-\theta_{i1})}{\{1-(\theta_{s1}-\theta_{i1})\}\tilde{k}_1}\left[d_s - \frac{(h_{f1}+D_0)}{\{1-(\theta_{s1}-\theta_{i1})\}}\ln\left\{1+\frac{\{1-(\theta_{s1}-\theta_{i1})\}d_s}{(h_{f1}+D_0)}\right\}\right] \tag{5.8}$$

5.3.2 Stage 2: Movement of Saturation Front Beyond the Fine Sediment Layer

The saturation front for $t > t_{ds}$ is shown in Fig 5.2. Let at time $t > t_{ds}$, the hydraulic heads at locations 1 and 4 be respectively

$$h_1(t) = D_0 - W(t) \tag{5.9}$$

$$h_4(t) = -h_{f2} - z_f(t) \tag{5.10}$$

The hydraulic head $h_3(t)$ at location 3 is unknown a priori $h_1(t), h_3(t), h_4(t)$, and $z_f(t)$ vary with time. According to Green and Ampt infiltration theory, at a particular time, velocity within the saturation front from location 1 to 4 is same but the velocity varies with time. Darcy velocity through fine sediment upper layer is equal to the Darcy velocity in the under lying soil layer.

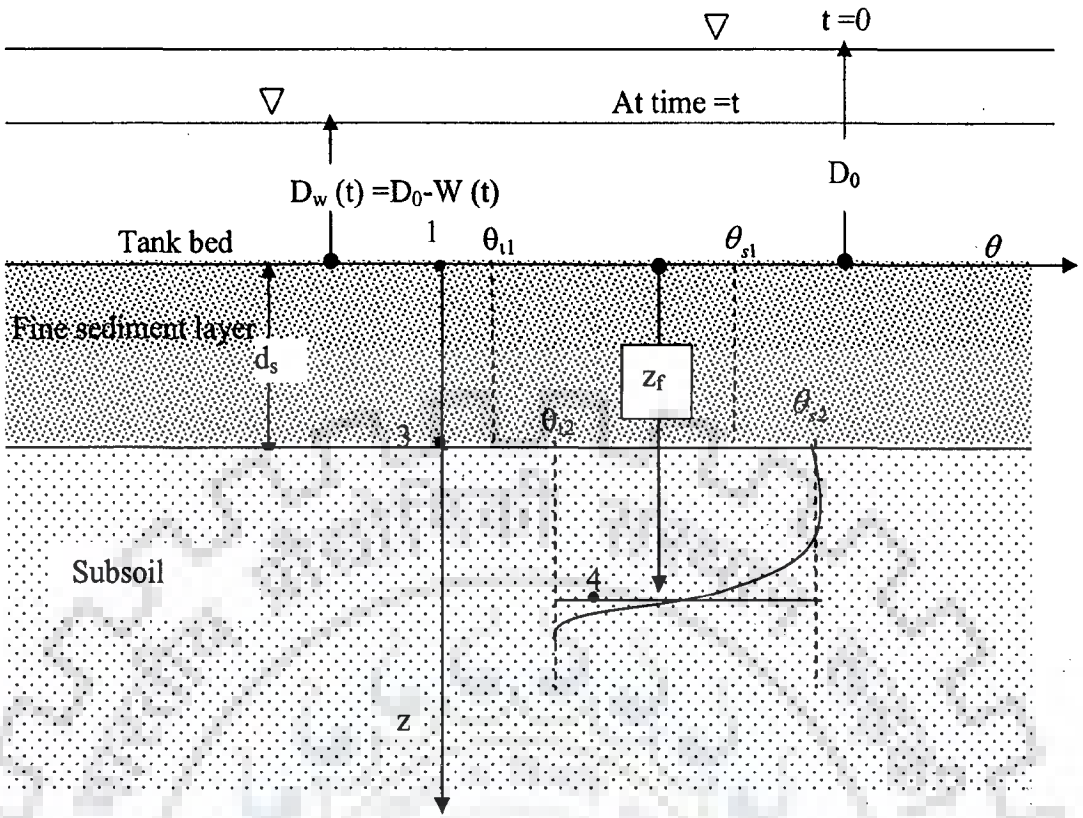

Fig.5.2 Unsaturated flow beyond the fine sediment layer

Applying Darcy's law

$$-\tilde{k}_1 \frac{[h_3(t)-h_1(t)]}{d_s} = -\tilde{k}_2 \frac{[h_4(t)-h_3(t)]}{z_f(t)-d_s} \tag{5.11}$$

Solving for $h_3(t)$

$$h_3(t) = \frac{\varepsilon\{z_f(t)-d_s\}h_1(t)+d_s\,h_4(t)}{\varepsilon\{z_f(t)-d_s\}+d_s} \quad , \qquad \varepsilon = \frac{\tilde{k}_1}{\tilde{k}_2} \tag{5.12}$$

From (5.11)

$$I(t) = \frac{\tilde{k}_2\{h_3(t)-h_4(t)\}}{z_f(t)-d_s} = \frac{\tilde{k}_2}{z_f(t)-d_s}\left[\left\{\frac{\varepsilon\{z_f(t)-d_s\}h_1(t)+d_s\,h_4(t)}{\varepsilon\{z_f(t)-d_s\}+d_s}\right\}-h_4(t)\right]$$

$$= \frac{\tilde{k}_2}{z_f(t)-d_s}\left[\frac{\varepsilon\{z_f(t)-d_s\}h_1(t)-\varepsilon\{z_f(t)-d_s\}h_4(t)}{\varepsilon\{z_f(t)-d_s\}+d_s}\right] = \frac{\tilde{k}_2[h_1(t)-h_4(t)]}{\{z_f(t)-d_s\}+\frac{d_s}{\varepsilon}} \tag{5.13}$$

Incorporating (5.9) and (5.10) in (5.13)

$$I(t) = \frac{\tilde{k}_2[D_0-W(t)+h_{f2}+z_f(t)]}{\{z_f(t)-d_s\}+\frac{d_s}{\varepsilon}}$$

$$= \frac{\tilde{k}_2\left[D_0 - W(t) + h_{f2} + d_s + z_f(t) - d_s\right]}{\left\{z_f(t) - d_s\right\} + \frac{d_s}{\varepsilon}} \tag{5.14}$$

Multiplying the numerator and the denominator by $(\theta_{s2} - \theta_{i2})$ on right hand side and simplifying

$$I(t) = \frac{\tilde{k}_2\left[\left(D_0 + h_{f2} + d_s\right)(\theta_{s2} - \theta_{i2}) - W(t)(\theta_{s2} - \theta_{i2}) + \left\{z_f(t) - d_s\right\}(\theta_{s2} - \theta_{i2})\right]}{(\theta_{s2} - \theta_{i2})\left\{z_f(t) - d_s\right\} + (\theta_{s2} - \theta_{i2})\frac{d_s}{\varepsilon}} \tag{5.15}$$

Since, $W(t) - W(t_{ds}) = (\theta_{s2} - \theta_{i2})\left\{z_f(t) - d_s\right\}$

$$I(t) = \frac{dW(t)}{dt} = \tilde{k}_2 \frac{\left[\left(D_0 + h_{f2} + d_s\right)(\theta_{s2} - \theta_{i2}) - W(t)(\theta_{s2} - \theta_{i2}) + W(t) - W(t_{ds})\right]}{(\theta_{s2} - \theta_{i2})\frac{d_s}{\varepsilon} + W(t) - W(t_{ds})} \tag{5.16}$$

or

$$\tilde{k}_2 dt = \frac{(\theta_{s2} - \theta_{i2})\frac{d_s}{\varepsilon} + W(t) - W(t_{ds})}{\left[\left(D_0 + h_{f2} + d_s\right)(\theta_{s2} - \theta_{i2}) - W(t)(\theta_{s2} - \theta_{i2}) + W(t) - W(t_{ds})\right]} dW(t) \tag{5.17}$$

Integrating

$$\tilde{k}_2 t\Big|_{t_d}^{t} = \int_{W(t_{ds})}^{W(t)} \frac{(\theta_{s2} - \theta_{i2})\frac{d_s}{\varepsilon} + W(t) - W(t_{ds})}{\left(D_0 + h_{f2} + d_s\right)(\theta_{s2} - \theta_{i2}) - W(t_{ds}) + \left[1 - (\theta_{s2} - \theta_{i2})\right]W(t)} dW \tag{5.18}$$

Defining,

$$A = (\theta_{s2} - \theta_{i2})\frac{d_s}{\varepsilon} - W(t_{ds}); \quad B = \left(D_0 + h_{f2} + d_s\right)(\theta_{s2} - \theta_{i2}) - W(t_{ds}); \quad C = \left[1 - (\theta_{s2} - \theta_{i2})\right]$$

and integrating,

$$\tilde{k}_2(t - t_{ds}) = \int_{W(t_{ds})}^{W(t)} \frac{A + W(t)}{B + CW(t)} dW$$

$$= \frac{1}{C}\int_{W(t_{ds})}^{W(t)} \frac{A + W(t)}{\frac{B}{C} + W(t)} dW = \frac{1}{C}\int_{W(t_{ds})}^{W(t)} \frac{A + \frac{B}{C} - \frac{B}{C} + W(t)}{\frac{B}{C} + W(t)} dW \tag{5.19}$$

or

$$C\,\tilde{k}_2(t-t_{ds}) = \int_{W(t_{ds})}^{W(t)} \frac{\left(A-\frac{B}{C}\right)+\frac{B}{C}+W(t)}{\frac{B}{C}+W(t)}\,dW$$

$$= \left(A-\frac{B}{C}\right)\ln\left[\frac{B}{C}+W(t)\right]_{W(t_{ds})}^{W(t)} + W(t)-W(t_{ds})$$

$$= W(t)-W(t_{ds})+\left(A-\frac{B}{C}\right)\ln\left[\frac{\frac{B}{C}+W(t)}{\frac{B}{C}+W(t_{ds})}\right] \qquad (5.20)$$

Substituting the value of constants A, B, C in the above expression

$$\{1-(\theta_{s2}-\theta_{i2})\}\,\tilde{k}_2(t-t_{ds})+W(t_{ds})$$
$$= W(t)+\left[(\theta_{s2}-\theta_{i2})\frac{d_s}{\varepsilon}-W(t_{ds})-\frac{(D_0+h_{f2}+d_s)(\theta_{s2}-\theta_{i2})-W(t_{ds})}{\{1-(\theta_{s2}-\theta_{i2})\}}\right]\times \qquad (5.21)$$
$$\ln\left[\frac{\frac{(D_0+h_{f2}+d_s)(\theta_{s2}-\theta_{i2})-W(t_{ds})}{\{1-(\theta_{s2}-\theta_{i2})\}}+W(t)}{\frac{(D_0+h_{f2}+d_s)(\theta_{s2}-\theta_{i2})-W(t_{ds})}{\{1-(\theta_{s2}-\theta_{i2})\}}+W(t_{ds})}\right]$$

The cumulative infiltration $W(t)$ at any time $t\,(>t_{ds})$ is estimated from the above relation. Let the water table exist at a finite depth d_w below the bed of the tank. The time t_w, the saturation front would take to reach the water table, is determined substituting $W(t)=W(t_w)=(\theta_{s1}-\theta_{i1})d_s+(\theta_{s2}-\theta_{i2})(d_w-d_s)$ in equation (5.21). Incorporating $W(t_w)-W(t_{ds})=(\theta_{s2}-\theta_{i2})(d_w-d_s)$ in (5.21) and simplifying

$$\left[\{1-(\theta_{s2}-\theta_{i2})\}\tilde{k}_2(t_w-t_{ds})-(\theta_{s2}-\theta_{i2})(d_w-d_s)\right]$$

$$= \left[(\theta_{s2}-\theta_{i2})\frac{d_s}{\varepsilon}-W(t_{ds})-\frac{(D_0+h_{f2}+d_s)(\theta_{s2}-\theta_{i2})-W(t_{ds})}{\{1-(\theta_{s2}-\theta_{i2})\}}\right]\times \qquad (5.22)$$
$$\ln\left[\frac{\frac{(D_0+h_{f2}+d_s)(\theta_{s2}-\theta_{i2})-W(t_{ds})}{\{1-(\theta_{s2}-\theta_{i2})\}}+(\theta_{s1}-\theta_{i1})d_s+(\theta_{s2}-\theta_{i2})(d_w-d_s)}{\frac{(D_0+h_{f2}+d_s)(\theta_{s2}-\theta_{i2})-W(t_{ds})}{\{1-(\theta_{s2}-\theta_{i2})\}}+W(t_{ds})}\right]$$

Once the saturation front reaches the water table, Green and Ampt infiltration theory is inapplicable. Using the theory of falling head permeameter test, the seepage loss is computed as follows.

5.3.3 Stage3: Seepage after Saturation Front Reaches the Water Table

The flow domain after the saturation front reaches the water table is shown in Fig. 5.3. It is assumed that the water table variation is insignificant consequent to recharge taking

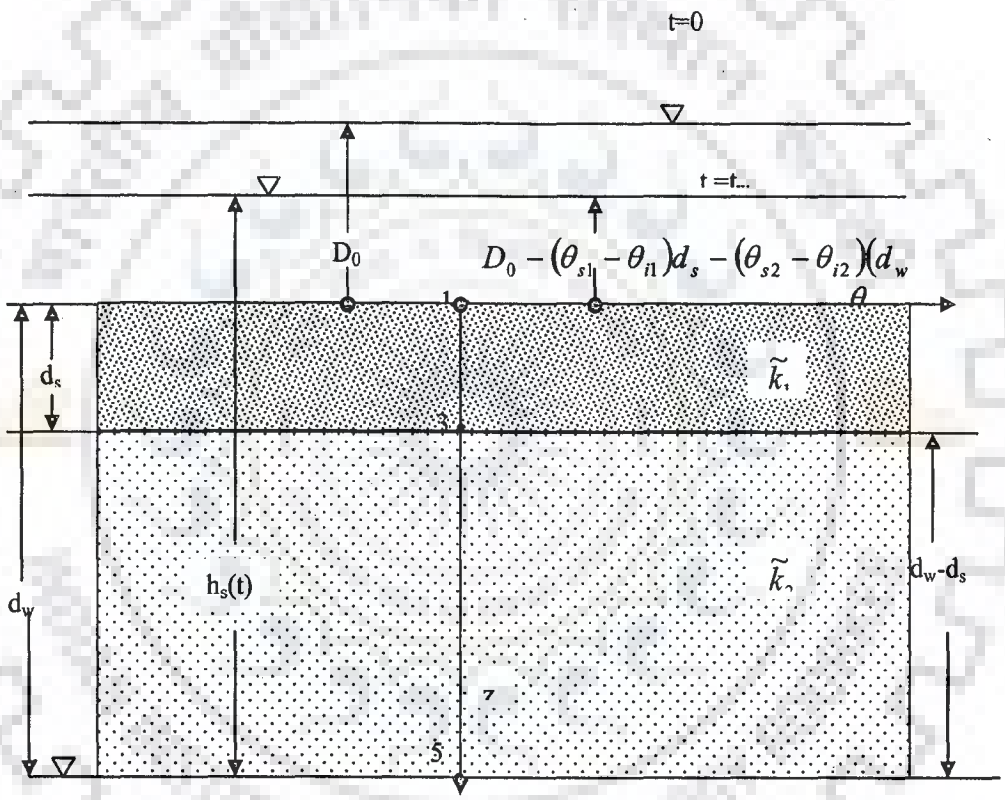

Fig. 5.3 Flow at time saturation front reaches water table

place from the tank. At the water table the pressure is atmospheric. Hence the hydraulic head difference between tank bed (at point 1) and water table (at point 5) is $h_s(t)$, which is the seepage head, which causes flow.

The two-layered porous medium, having different hydraulic conductivity in each layer, is converted to an equivalent homogeneous one with harmonic mean hydraulic conductivity, which is given by:

$$k_h = \frac{d_w}{d_s / k_1 + (d_w - d_s)/k_2} \tag{5.23}$$

At any time, $t \geq t_w$, the rate of fall of water level in the tank is the rate of seepage loss.

Hence,

$$-\frac{dh_s}{dt} = k_h \frac{h_s(t)}{d_w} \tag{5.24}$$

Integrating,

$$\ln\{h_s(t)\} = -\frac{k_h}{d_w} t + A \tag{5.25}$$

Applying the initial condition at $t = t_w$,

$$h_s(t_w) = D_0 - (\theta_{s1} - \theta_{i1})d_s - (\theta_{s2} - \theta_{i2})(d_w - d_s) + d_w \tag{5.26}$$

the constant A appearing in (5.25) is evaluated as:

$$A = \ln\{D_0 - (\theta_{s1} - \theta_{i1})d_s - (\theta_{s2} - \theta_{i2})(d_w - d_s) + d_w\} + \frac{k_h}{d_w} t_w \tag{5.27}$$

Incorporating constant A in (5.25),

$$h_s(t) = \{D_0 - (\theta_{s1} - \theta_{i1})d_s - (\theta_{s2} - \theta_{i2})(d_w - d_s) + d_w\} e^{-\frac{k_h}{d_w}(t - t_w)} \quad ; t > t_w \tag{5.28}$$

The tank gets dry at $h_s(t) = d_w$. The time at which the tanks get dry, t_{dry} is given by:

$$d_w = \{D_0 - (\theta_{s1} - \theta_{i1})d_s - (\theta_{s2} - \theta_{i2})(d_w - d_s) + d_w\} e^{-\frac{k_h}{d_w}(t_{dry} - t_w)} \tag{5.29}$$

or

$$e^{-\frac{k_h}{d_w}(t_{dry} - t_w)} = \frac{d_w}{\{D_0 - (\theta_{s1} - \theta_{i1})d_s - (\theta_{s2} - \theta_{i2})(d_w - d_s) + d_w\}} \tag{5.30}$$

or

$$t_{dry} = t_w + \frac{d_w}{k_h} \ln \frac{\{D_0 - (\theta_{s1} - \theta_{i1})d_s - (\theta_{s2} - \theta_{i2})(d_w - d_s) + d_w\}}{d_w} \tag{5.31}$$

The seepage rate is given by:

$$q(t) = k_h \frac{h_s(t)}{d_w} = \frac{k_h}{d_w} \{D_0 - (\theta_{s1} - \theta_{i1})d_s - (\theta_{s2} - \theta_{i2})(d_w - d_s) + d_w\} e^{-\frac{k_h}{d_w}(t - t_w)} \tag{5.32}$$

The cumulative seepage after the saturation front touches the water table is:

$$W(t) = W(t_w) + \int_{t_w}^{t} q(t)dt \tag{5.33}$$

Substituting (5.32) in (5.33) and integrating

$$W(t) = W(t_w) + \left[\{D_0 - (\theta_{s1} - \theta_{i1})d_s - (\theta_{s2} - \theta_{i2})(d_w - d_s) + d_w\}\right]\left\{1 - e^{-\frac{k_h}{d_w}(t - t_w)}\right\} \quad ; t > t_w \tag{5.34}$$

5.4 RESULTS AND DISCUSSION

Variations of infiltration rates and cumulative infiltration with time have been computed from a storage tank, which is underlain either by a homogeneous soil stratum or two strata with different soil characteristics, when the tank is filled for the first time to an initial depth, $D_0(m)$. Prior to the filling, the soil strata were unsaturated and the initial soil moisture content of each stratum was at its respective field capacity. Results have been presented for the following subsoil conditions:

(i) The underlying soil is homogeneous,

(ii) The top soil layer has higher hydraulic conductivity than that of the bottom layer,

(iii) The top soil layer has lower hydraulic conductivity than that of the bottom layer.

The soil moisture characteristics of the four groups of soil are taken from published data (Chow, et al, 1988) as given in Table 5.1.

5.4.1 Case-I: Tank Bed is underlain by a Homogenous Soil Layer

The temporal variations of infiltration from a storage tank underlying a homogeneous soil layer are presented in Fig. 5.4 for four soil groups. The results pertain to an initial depth $D_0 = 0.5m$. As seen from the figure, the infiltration rate tends to ∞ at time $t \to 0$ and decreases rapidly. The decrease is monotonic at time t > 4 days, the infiltration rate tending to the hydraulic conductivity of the subsoil. The depth of water in the storage tank decreases with time due to infiltration.

Table 5.1: Characteristics of different soils (Chow, et al, 1988) used for computation of infiltration

Soil type	θ_r cm3/cm^3)	θ_s (cm3/cm^3)	$\tilde{K}_s$ (m/day)	h_f (m)
Sandy loam	0.041	0.453	0.0262	0.011
Loam	0.029	0.463	0.0816	0.089
Silty clay loam	0.039	0.471	0.0240	0.273
Silty clay	0.056	0.479	0.0120	0.292

Therefore, the tank gets dry after some time varying from one day to 20 days depending on soil type. Corresponding to the initial depth $D_0 = 0.5m$, the tank underlying sandy loam gets dry after about one day of the filling. If the underlying soil happens to be silty clay, the tank would get dry after 20 days. The variation of infiltration with time follows the usual trend. These results focus on rate of infiltration under varying head. The early monotonic nature in infiltration rate is due to simultaneous decrease in depth of water in the tank and the hydraulic gradient.

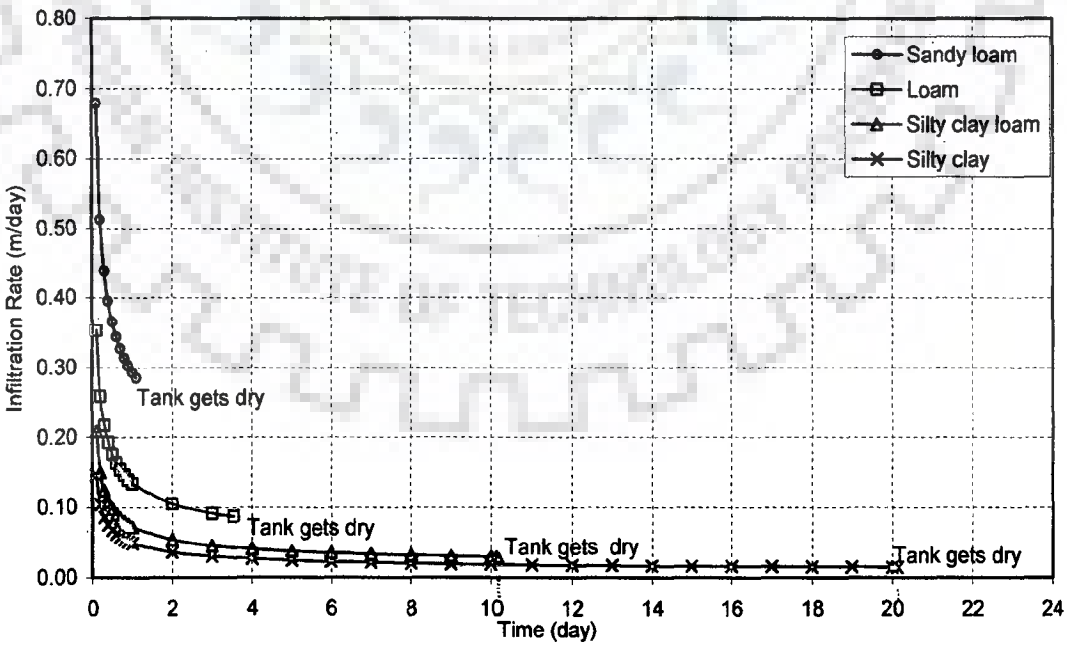

Fig. 5.4 Variation of infiltration rate (m/day) with time (day) from the storage tank bed, underlain by homogeneous soil layer, D_0 =0.5m, dw

The variations of cumulative infiltration with time for the four groups of soils are presented in Fig. 5.5. As the initial depth $D_0 = 0.5m$, the cumulative infiltrated quantity terminates at 0.5m by the time the tank gets dry.

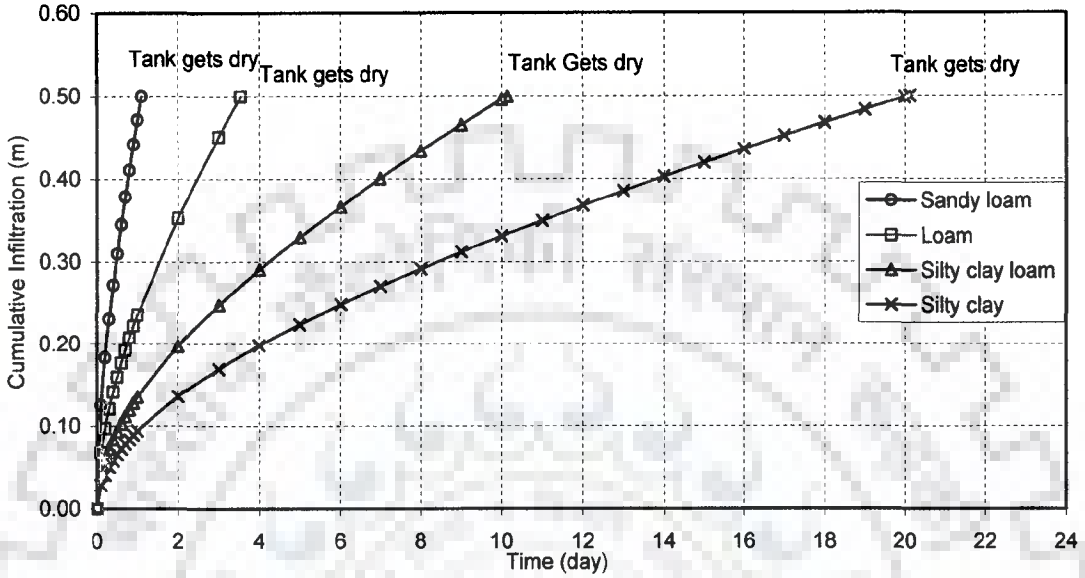

Fig. 5.5 Variation of cumulative infiltration (m) with time (day) from the storage tank bed, underlain by homogeneous soil layer, D0 =0.5m, dw

The time taken after the first filling for a tank to get dry due to infiltration alone for several initial depths, D_0, are presented for different soil groups in Fig. 5.6. Corresponding to $D_0 = 5m$, a tank underlying silty clay soil will get dry 260 days after the first filling. For D_0 =1.0m, t_{dry} =45 days. For sandy loam, the corresponding drying times are 12 and 2.3 days respectively. As seen from the figure, the drying time, t_{dry} varies quasi-linearly with initial depth of water, D_0.

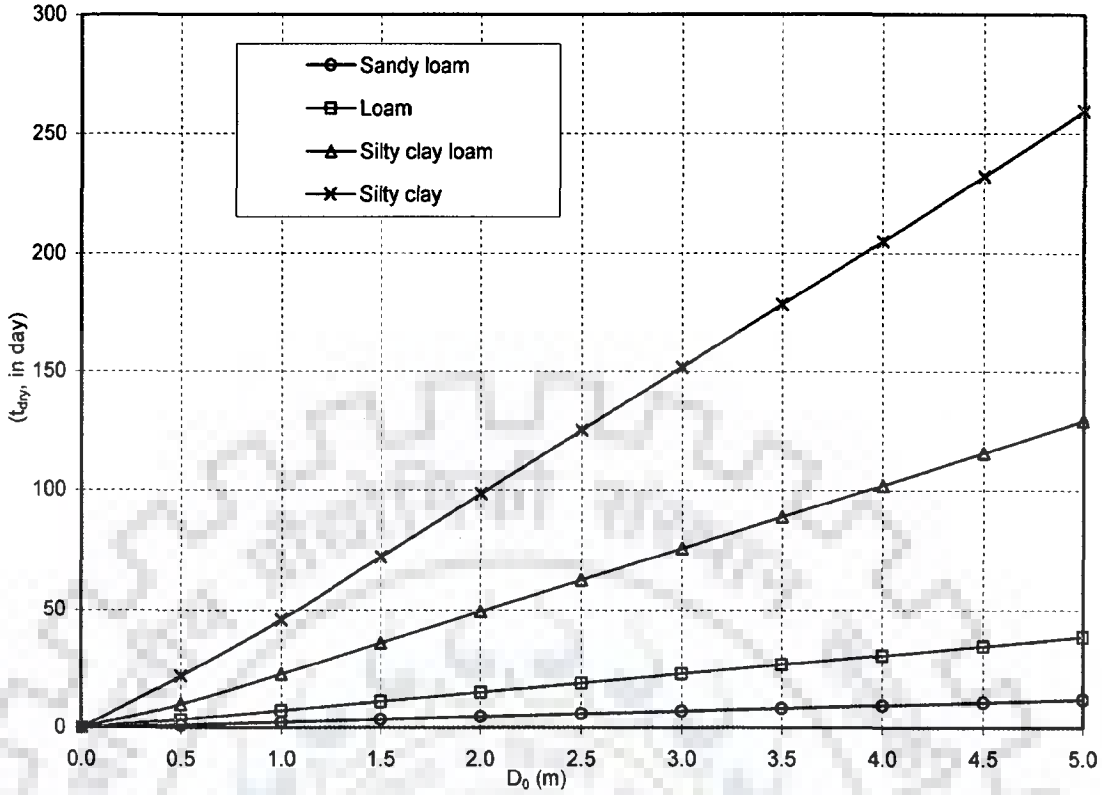

Fig.5.6 Days after which the storage tank gets dry due to infiltration alone for different initial water depth, D_0 (m), the tank bed is underlain by homogeneous soil, for dw =10.0m

In Table 5.2, movement of saturation front and the time taken by the saturation front to reach the water table, and the time after the first filling when the tank gets dry are presented in details. For the four groups of soil (i.e. sandy loam, loam, silty clay loam and silty clay) corresponding to D_0 =4.0m, t_{dry} are 9.7, 30.78, 102.14 and 204.91 days respectively. The multiplications of t_{dry} corresponding to $D_0 = 4.0m$ and the hydraulic conductivity of the underlying soil are 2.54, 2.51, 2.45 and 2.46 respectively. This indicates that the drying time is very closely inversely proportional to the hydraulic conductivity of the sub soil.

Table 5.2: Arrival time t_{ds}, t_w and drying time, t_{dry} for a storage tank underlying a homogeneous soil layer corresponding to different initial depth of water, D_0 ; d_w=10.0m

Top layer	Bottom layer	D_0(m)	t_{ds} (day)	t_w (day)	t_{dry} (day)
Sandy loam	Sandy loam	0.5	Saturation water front will not surpass the top layer		1.098
		1.0			2.320
		1.5			3.550
		2.0			4.778
		2.5	4.422	Saturation water front will not reach to the water table	6.008
		3.0	3.965		7.238
		3.5	3.595		8.469
		4.0	3.290		9.700
		5.0	2.810	8.96	12.183
Loam	Loam	0.5	Saturation water front will not surpass the top layer		3.538
		1.0			7.417
		1.5			11.307
		2.0			15.201
		2.5	15.235	Saturation water front will not reach to the water table	19.096
		3.0	13.633		22.991
		3.5	12.342		26.887
		4.0	11.278		30.783
		5.0	9.624	30.79	38.620
Silty clay loam	Silty clay loam	0.5	Saturation water front will not surpass the top layer		10.136
		1.0			22.970
		1.5			36.062
		2.0			49.233
		2.5	49.354	Saturation water front will not reach to the water table	62.440
		3.0	44.373		75.664
		3.5	40.322		88.900
		4.0	36.960		102.142
		5.0	31.690	101.84	129.25
Silty clay	Silty clay	0.5	Saturation water front will not surpass the top layer		22.118
		1.0			45.838
		1.5			72.122
		2.0			98.581
		2.5	95.670	Saturation water front will not reach to the water table	125.117
		3.0	86.099		151.693
		3.5	78.302		178.293
		4.0	71.821		204.909
		5.0	61.650	197.75	159.600

5.4.1 Case-II: Top Layer has Higher Hydraulic Conductivity than that of the Bottom Layer

The variations of infiltration rates from a storage tank with time for case-II for different soil groups are presented in Fig. 5.7. Results are also presented in Fig. 5.7 for homogeneous case. As seen from the figure, in a two layered soil system, in which, the lower layer has hydraulic conductivity less than that of the upper layer, the infiltration rate continuously decreases with time and the trend is analogous to the trend of decreasing infiltration through homogeneous soil. When the saturation front arrives at the interface, there is sharp decrease in the infiltration rate. Thus, for such layered system, where the bottom layer has less hydraulic conductivity than that of the upper overlying layer, the Green and Ampt infiltration theory is applicable. The infiltration rate decreases fast for underlying soil having lower hydraulic conductivity.

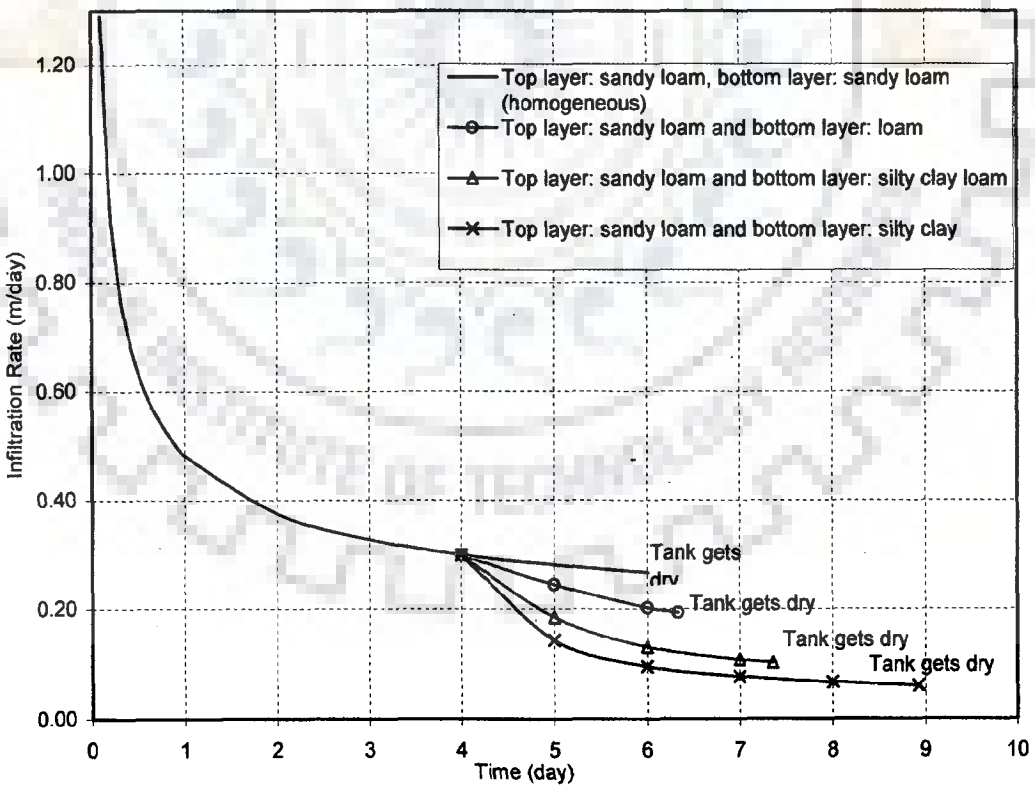

Fig. 5.7 Variation of infiltration rate (m/day) with time (day) from the storage tank bed, the top layer is underlain by different soil layers,

Variations of cumulative infiltration with time is presented in Fig. 5.8 for D_0= 2.5m. The top layer is comprised of sandy loam. The cumulative infiltration terminates at 2.5m for each soil group in the second layer, as D_0=2.5m When the saturation front arrives at the interface of the two layers, the cumulative infiltration decreases fast with time, the drying time increases. The graphs deviate from the variation corresponding to homogeneous case when the entire soils are sandy loam.

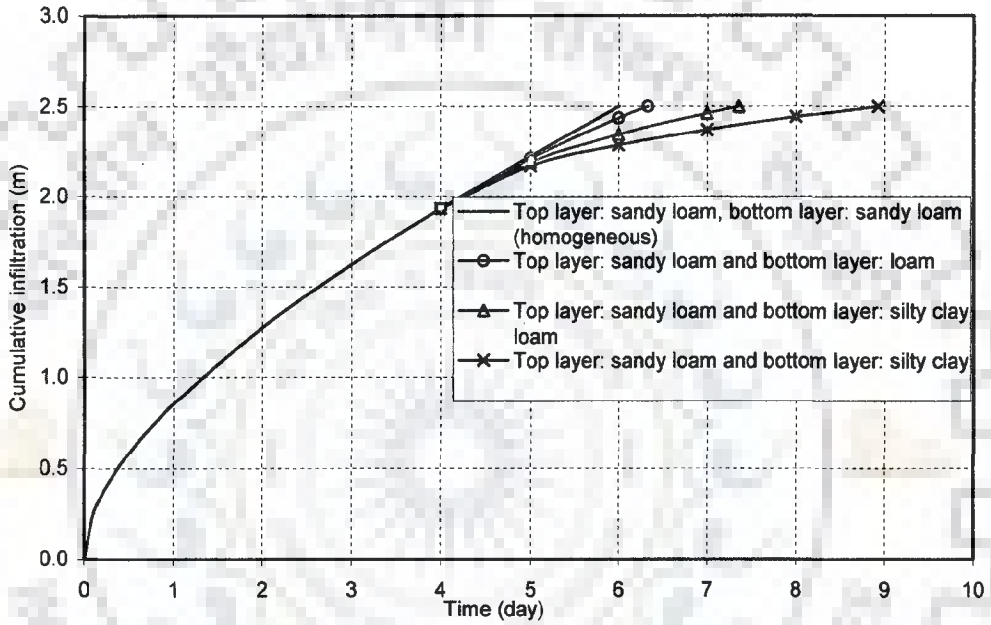

Fig. 5.8 Variation of cumulative infiltration (m) with time (day) from the storage tank, the top layer is underlain by different soil layers, for varying water depth in the tank due to infiltration alone, D_0 =2.5m , d_s=5.0m

For a two layered soil system (case-II) the time after the first filling when the tank gets dry is presented in Fig. 5.9. As seen from the figures the variation of t_{rdy} is non-linear. The drying of the storage tank gets further delayed incase the bottom soil layer has lower conductivity.

Details of movement of saturation front and drying time of storage tank for different initial depths D_0 and d_s=0.5 m and 5.0m are presented in Table 5.3 (a) and 5.3 (b). If sandy loam soil of 0.5m (d_s=0.5m) overlies silty clay soil of 9.5m up to water table, t_{dry}= 236.24 days.

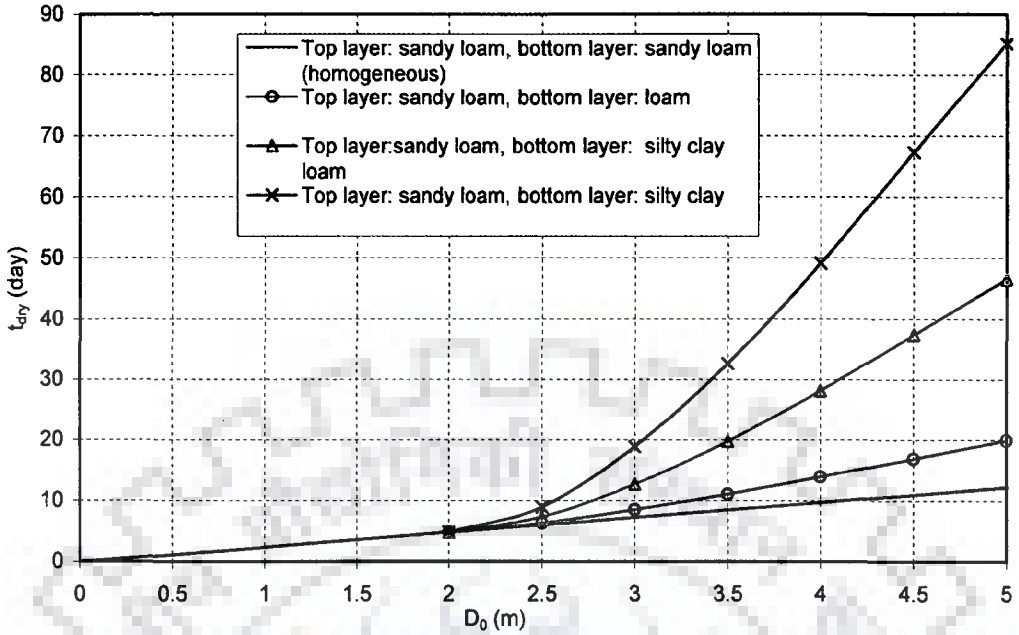

Fig. 5.9 Days after which the storage tank gets dry due to infiltration alone for different initial water depth (D_0), the top layer is underlain by a different soil layers, for d_s=5.0m

Table 5.3 (a): Arrival times t_{ds}, t_w and drying time, t_{dry} for the tank bed comprising of two heterogeneous soil layers for different initial depth of water, D_0; d_s=0.5m, d_w=10.0m

Top layer	Bottom layer	D_0(m)	t_{ds} (day)	t_w (day)	t_{dry} (day)
Sandy loam	loam	0.5	0.246	Saturation water front will not reach to the water table	1.854
		1.0	0.151		5.329
		1.5	0.109		9.061
		2.0	0.085		12.870
		2.5	0.070		16.712
		3.0	0.060		20.571
		3.5	0.052		24.441
		4.0	0.046		28.317
		4.5	0.041	30.213	32.213
		5.0	0.037	28.426	36.111
Sandy loam	Silty clay loam	0.5	0.246	Saturation water front will not reach to the water table	3.858
		1.0	0.151		14.502
		1.5	0.109		26.649
		2.0	0.085		39.293
		2.5	0.070		52.161
		3.0	0.060		65.152
		3.5	0.052		78.215
		4.0	0.046		91.325
		4.5	0.041	97.166	104.652
		5.0	0.037	91.597	118.135

Top layer	Bottom layer	D_0(m)	t_{ds} (day)	t_w (day)	t_{dry} (day)
Sandy loam	Silty clay	0.5	0.246	Saturation water front will not reach to the water table	7.009
		1.0	0.151		28.145
		1.5	0.109		52.438
		2.0	0.085		77.781
		2.5	0.070		103.6022
		3.0	0.060		129.681
		3.5	0.052		155.915
		4.0	0.046		182.251
		4.5	0.041	187.658	209.202
		5.0	0.037	176.969	236.241

Table 5.3 (b) : Arrival times t_{ds}, t_w and the drying time, t_{dry} for the tank bed comprising of two heterogeneous soil layers for different initial depth of water; d_s=5.0m, d_w=10m

Top layer	Bottom layer	D_0(m)	t_{ds} (day)	t_w (day)	t_{dry} (day)
Sandy loam	Loam	0.5	Saturation water front will not surpass the top layer		1.098
		1.0			2.320
		1.5			3.550
		2.0			4.778
		2.5	4.422	Saturation water front will not reach to the water table	6.332
		3.0	3.965		8.503
		3.5	3.595		11.075
		4.0	3.290		13.922
		4.5	3.032	14.80	16.950
		5.0	2.813	13.975	19.938
Sandy loam	Silty clay loam	0.5	Saturation water front will not surpass the top layer		1.098
		1.0			2.320
		1.5			3.550
		2.0			4.778
		2.5	4.422	Saturation water front will not reach to the water table	7.356
		3.0	3.965		12.668
		3.5	3.595		19.786
		4.0	3.290		28.151
		4.5	3.032	31.131	37.412
		5.0	2.813	29.496	46.580
Sandy loam	Silty clay	0.5	Saturation water front will not surpass the top layer		1.098
		1.0			2.320
		1.5			3.550
		2.0			4.778
		2.5	4.422	Saturation water front will not reach to the water table	8.930
		3.0	3.965		18.890
		3.5	3.595		32.670
		4.0	3.290		49.075
		4.5	3.032	53.348	67.286
		5.0	2.813	50.615	85.160

As seen from Tables 5.3(b), for ds= 5.0m the corresponding t_{dry} value is 85 days. Thus, the thickness of the upper soil layer and its hydraulic conductivity primarily governs the infiltration rate and drying time.

Temporal variations of infiltration rates, and cumulative infiltration corresponding to d_s=5.0 m, and D_0= 2.5m are presented in Figs. 5.10 and 5.11 for the case where the top soil is loam and bottom layer is either silty clay loam or silty clay.

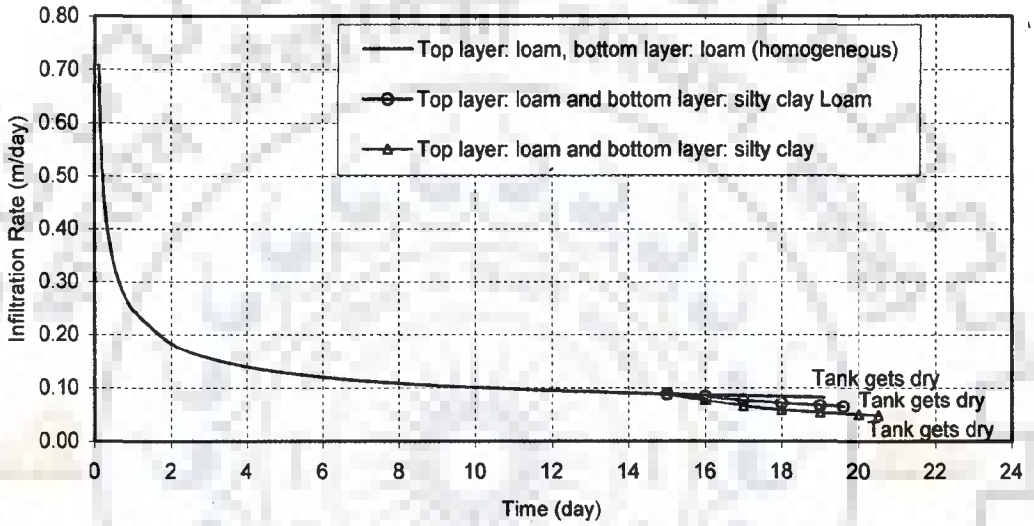

Fig. 5.10 Days after which the storage tank gets dry due to infiltration alone for different initial water depth (D_0), the top layer is underlain by a different soil layers, for d_s=5.0m

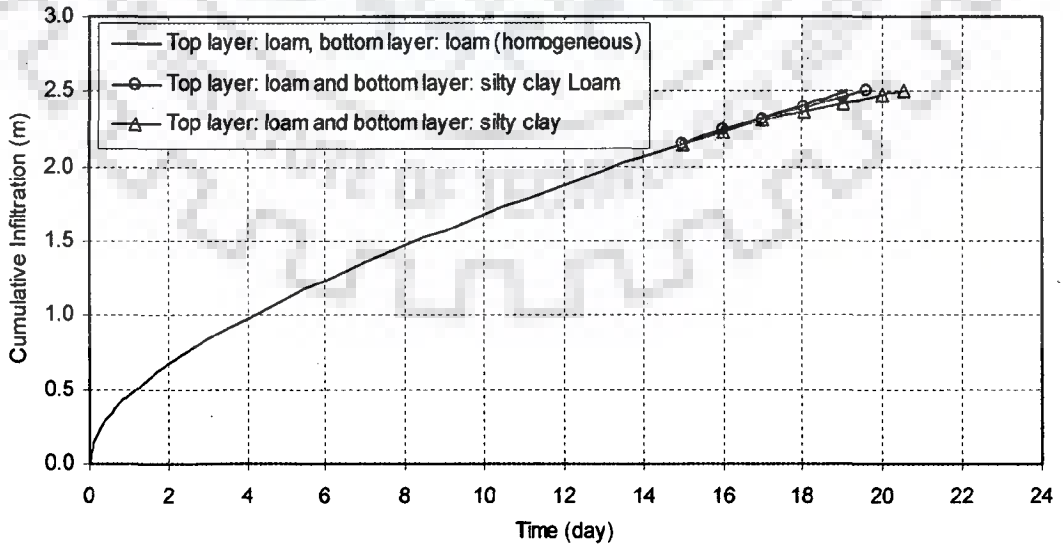

Fig. 5.11 Variation of cumulative infiltration (m) with time (day) from the storage tank, for variation of depth of water in the tank due to infiltration alone, the top layer is underlain by different soil layers, D_0= 2.5m, d_s=5.0m

As the soil moisture characteristics of the bottom layer do not differ much from those of the upper layer, the deviations in infiltration rate and cumulative infiltration, when the saturation front surpasses the interface of the two layers, are marginal as seen from Figs. 5.10 and 5.11.

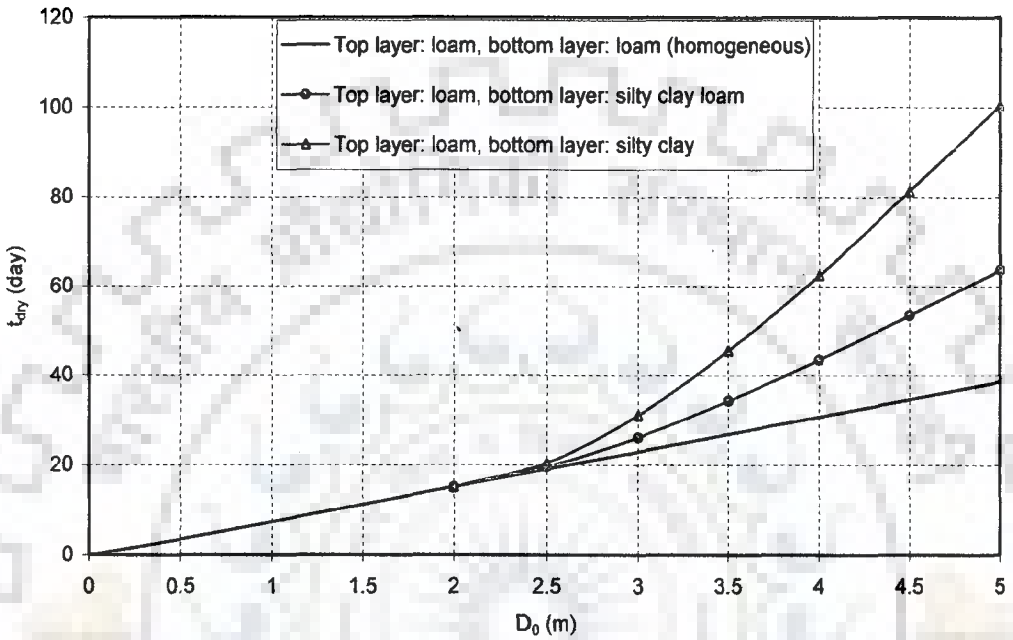

Fig. 5.12 Days after which the storage tank gets dry due to infiltration alone for different initial water depth (D_0), the top layer is underlain by different soil layers, for d_s=5.0m

The drying time of the tank is governed significantly by the conductivity of the under lying soil layer. If the bottom layer is silty clay loam, the drying time is 63 days. The drying time gets delayed and is equal to 100 if bottom layer happens to be silty clay. Once the saturation front surpasses the interface, as seen from Fig. 5.12, the variation of t_{dry} with initial depth of water D_0 is non-linear. Details of movement of saturation front and drying time of storage tank for different initial depths D_0 are presented in Table 5.4

Table 5.4: Arrival times t_{ds}, t_w and the drying time, t_{dry} for the tank bed comprising of two heterogeneous soil layers for different initial depth of water; d_s=5.0m, d_w=10m

Top layer	Bottom layer	D_0(m)	t_{ds} (day)	t_w (day)	t_{dry} (day)
Loam	Silty clay loam	0.5	Saturation water front will not surpass the top layer		3.538
		1.0			7.417
		1.5			11.307
		2.0			15.201
		2.5	15.235	Saturation water front will not reach to the water table	19.603
		3.0	13.633		26.170
		3.5	12.342		34.304
		4.0	11.278		43.504
		4.5	10.385	49.000	53.538
		5.0	9.625	46.241	63.726
Loam	Silty clay	0.5	Saturation water front will not surpass the top layer		3.538
		1.0			7.417
		1.5			11.307
		2.0			15.201
		2.5	15.235	Saturation water front will not reach to the water table	20.507
		3.0	13.633		31.138
		3.5	12.342		45.536
		4.0	11.278		62.496
		4.5	10.385	71.211	81.378
		5.0	9.625	67.211	100.358

Temporal variations of infiltration rates, and cumulative infiltration corresponding to d_s=5.0 m, and D_0= 2.5m are presented in Figs. 5.13 and 5.14 for the case where the top soil is silty clay loam and bottom layer is silty clay. As the soil moisture characteristics of the bottom layer do not differ much from those of the upper layer, the deviations in infiltration rate and cumulative infiltration, when the saturation front surpasses the interface of the two layers, are marginal as seen from Figs. 5.13 and 5.14.

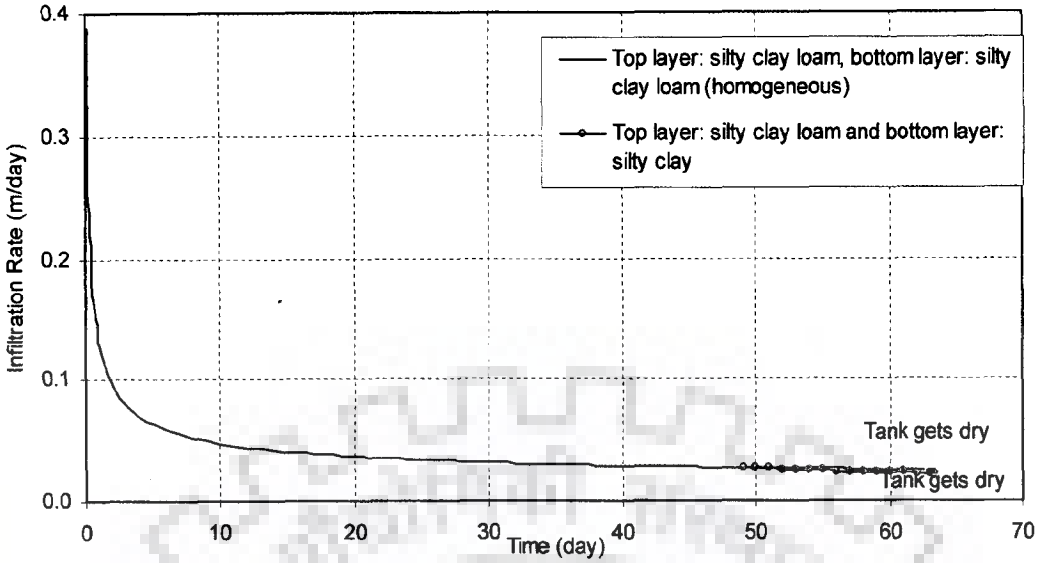

Fig. 5.13 Variation of infiltration rate (m/day) with time (day) from the storage tank bed, the top layer is underlain by different soil layers, D_0=2.5m, d_s=5.0m

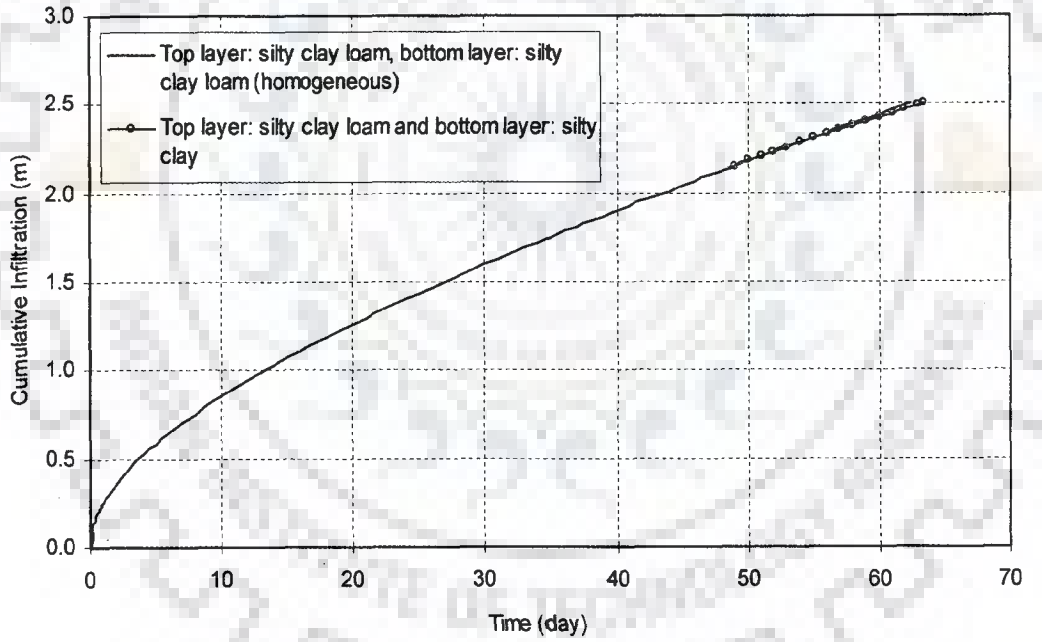

Fig. 5.14 Variation of cumulative infiltration (m) with time (day) from the storage tank, for variation in the depth of water due to infiltration alone, the top layer is underlain by different soil layers , D_0=2.5m, d_s=5.0m

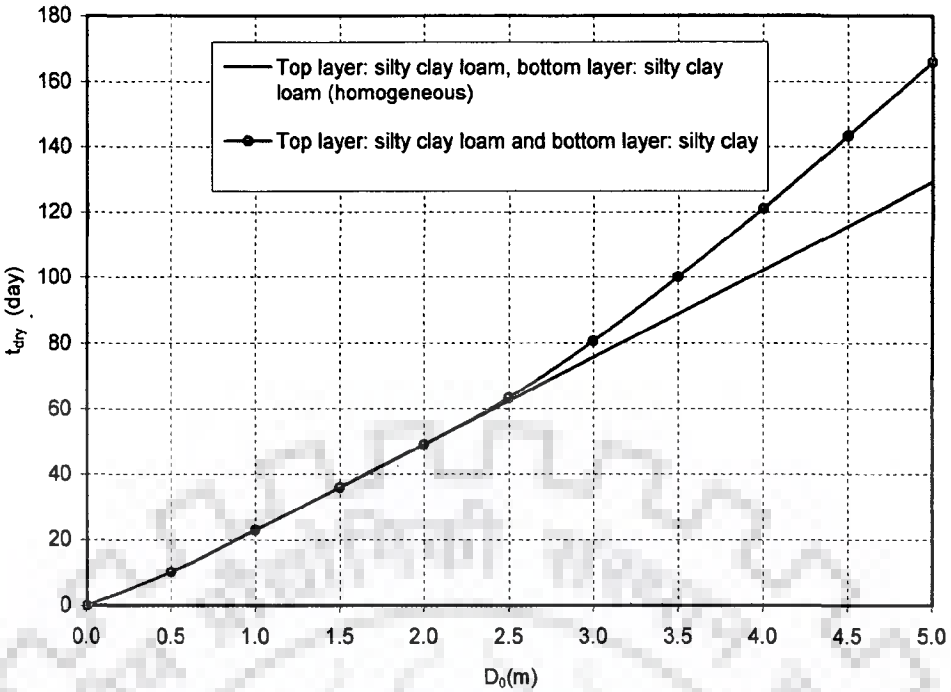

Fig. 5.15 Days after which the storage tank gets dry due to infiltration alone for different initial water depth (D_0), the top layer is underlain by different soil layers, for d_s=5.0m

Variations of t_{dry} with different initial depth of water are presented in Fig. 5.15, for d_s=5.0m, for the case where the top soil layer is silty clay loam and the bottom layer is silty clay. The drying time increases with increasing depth of water. Where the underlying soil has lower conductivity in comparison to that of the upper layer, as seen from the figure the drying time is further delayed with increasing initial water depth in the tank. For example with initial depth D_0= 2.5 m, the drying time of the storage tank is delayed by 24 hours in comparison to the homogeneous case, i.e. the underlying soil is only silty clay loam. For D_0=5.0m the time delay is 37 days (166-129). Once the saturation front surpasses the interface, as seen from Fig. 5.15, the variation of t_{dry} with initial depth of water D_0 becomes non linear. Details of movement of saturation front and drying time of storage tank for different initial depths D_0 are presented in Table 5.5

Table 5.5: Arrival times t_{ds}, t_w and the drying time, t_{dry} for the tank bed comprising of two heterogeneous soil layers for different initial depth of water; d_s=5.0m, d_w=10.0m

Top layer	Bottom layer	D_0(m)	t_{ds} (day)	t_w (day)	t_{dry} (day)
Silty clay loam	Silty clay	0.5	Saturation water front will not surpass the top layer		10.136
		1.0			22.970
		1.5			36.062
		2.0			49.233
		2.5	49.354	Saturation water front will not reach to the water table	63.357
		3.0	44.373		80.630
		3.5	40.322		100.099
		4.0	36.960		121.062
		4.5	34.121	129.450	143.356
		5.0	31.692	122.094	165.840

5.4.2 Case-III: Top Soil Layer has Lower Hydraulic Conductivity than that of the Bottom Layer

In case III, the upper soil layer has lower hydraulic conductivity than that of the lower layer. The variation of infiltration rate for the case in which the upper layer is comprised of silty clay, which has lower hydraulic conductivity, and the lower layer is comprised of sandy loam, which has higher conductivity than that of the upper layer, is presented in Figs. 5.16 and 5.17 for $d_s = 1.0m$ and 5.0m respectively. The ratio of the hydraulic conductivity of the lower layer to that of the upper layer, $\tilde{k}_2 / \tilde{k}_1 = 21.8$. As seen from the figure, the infiltration rate increases with time once the saturation front surpasses the interface of the two layers. The increase is rapid when the upper layer's thickness is small. If the upper layer thickness is 5m, the increment in infiltration rate is marginal. The infiltration rate decreases after the saturation front reaches the water table as the role of the suction head of the layers do not come into play. The decrease in

infiltration with time is due to decrease in seepage head with time consequent to infiltration.

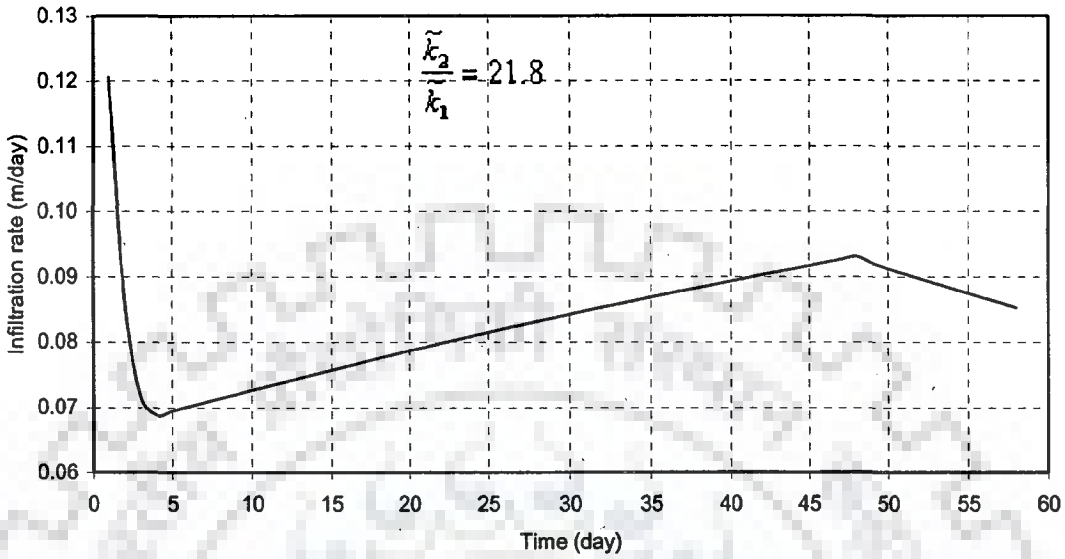

Fig.5. 16 Variation of infiltration rate (m/day) with time (day), the upper soil layer is having lower saturated hydraulic conductivity than lower layer, d_s=1.0m, D_0=5.0m

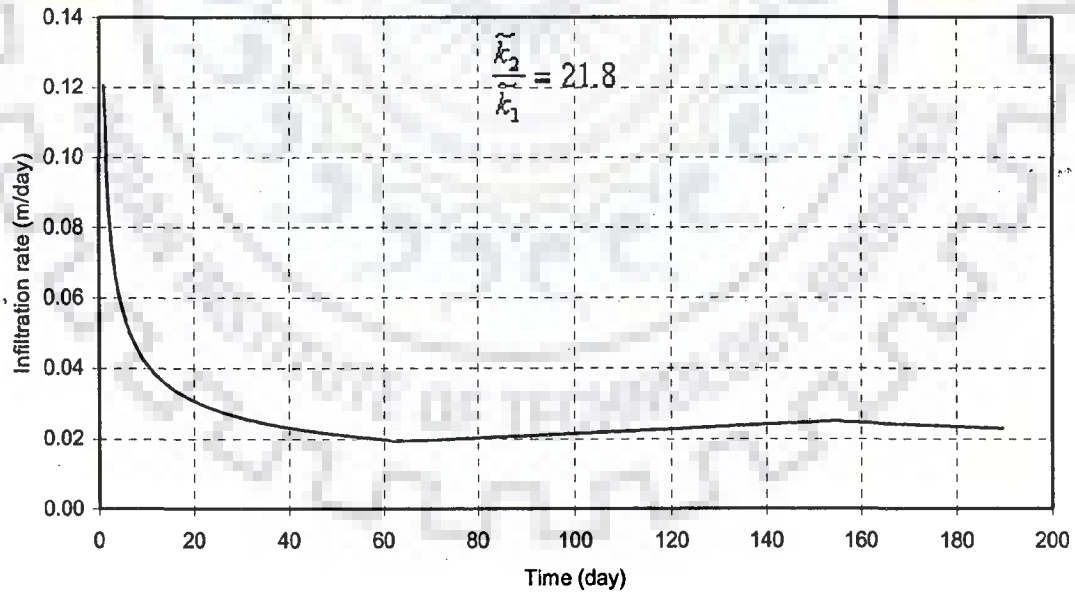

Fig. 5.17 Variation of infiltration rate (m/day) with time (day) from storage tank, the upper soil layer is having lower hydraulic conductivity than the lower layer, d_s=5.0m, D_0=5.0m

The variation of infiltration rate for a case, in which the upper layer is silty clay loam and the lower layer is sandy loam, is presented in Figs. 5.18 for $d_s = 1.0m$ and D_0=5.0m. The ratio of the hydraulic conductivity of the lower layer to that of the upper

layer, $\tilde{k}_2 / \tilde{k}_1 = 10.9$. As seen from the figure, for d_s=1.0m, there is significant increase in infiltration rate after the saturation front surpasses the interface. Temporal variation of infiltration rate for $d_s = 5.0m$ and D_0=5.0m for the above soil group is presented in Fig.5.19. For such case i.e. in which thickness of the upper layer is of the order of 5.0m the increase in the infiltration rate is marginal after the saturation front surpasses the interface of the soil layer.

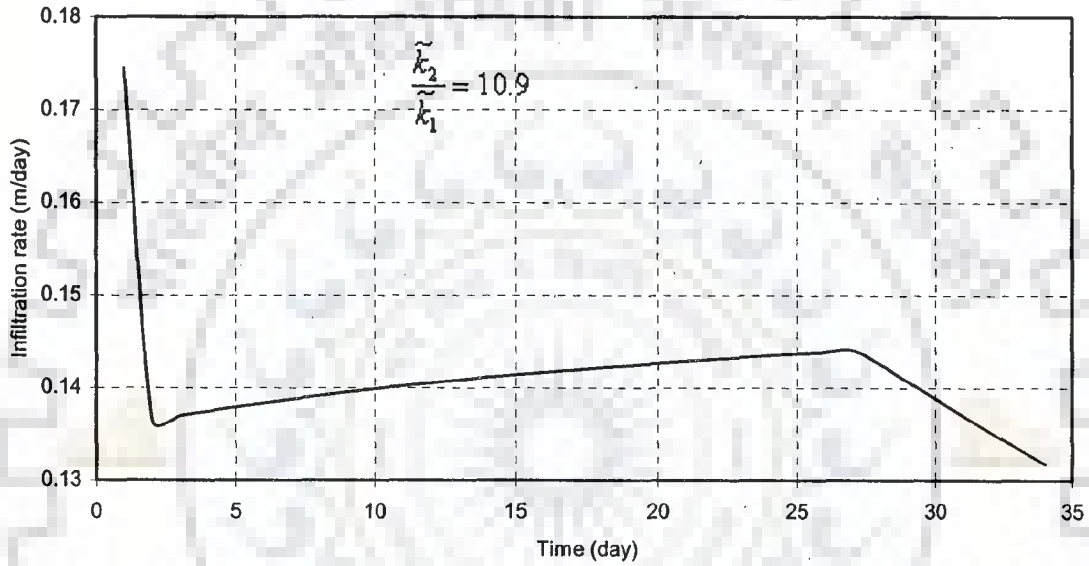

Fig. 5.18 Variation of infiltration rate (m/day) with time (day) from the storage tank, the upper soil layer having lower hydraulic conductivity than the lower layer, d_s=1.0m, D_0=5.0m

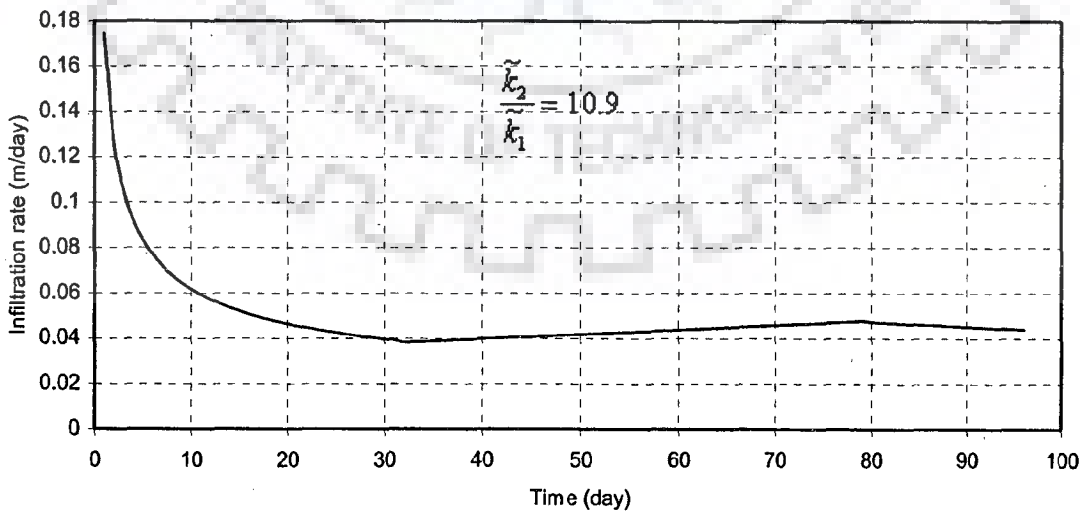

Fig. 5.19 Variation of infiltration rate (m/day) with time (day) from the storage tank, the upper soil layer having lower hydraulic conductivity than lower layer, d_s=5.0m, D_0=5.0m

Infiltration rates corresponding to large difference in hydraulic conductivities i.e. $\tilde{k}_2/\tilde{k}_1 = 100$ for $d_s = 1.0m$ and $5.0m$ are presented in Figs. 5.20 and 5.21 respectively. It is seen from these figures that, after the saturation front surpasses the interface of the layers, the infiltration rate increases with time instead of decreasing.

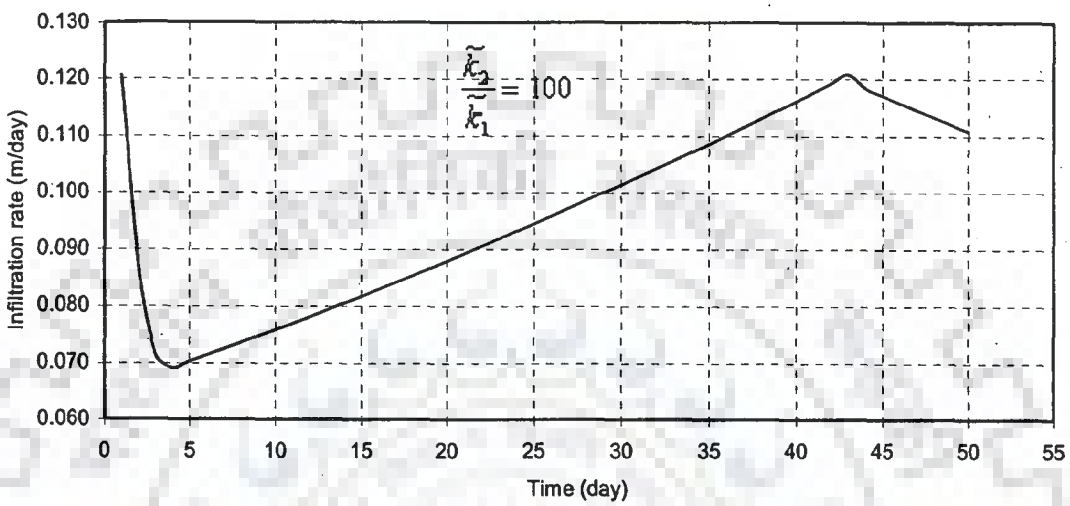

Fig.5. 20 Variation of infiltration rate (m/day) with time (day), the upper soil layer is having lower saturated hydraulic conductivity than lower layer, d_s=1.0m, D_0=5.0m

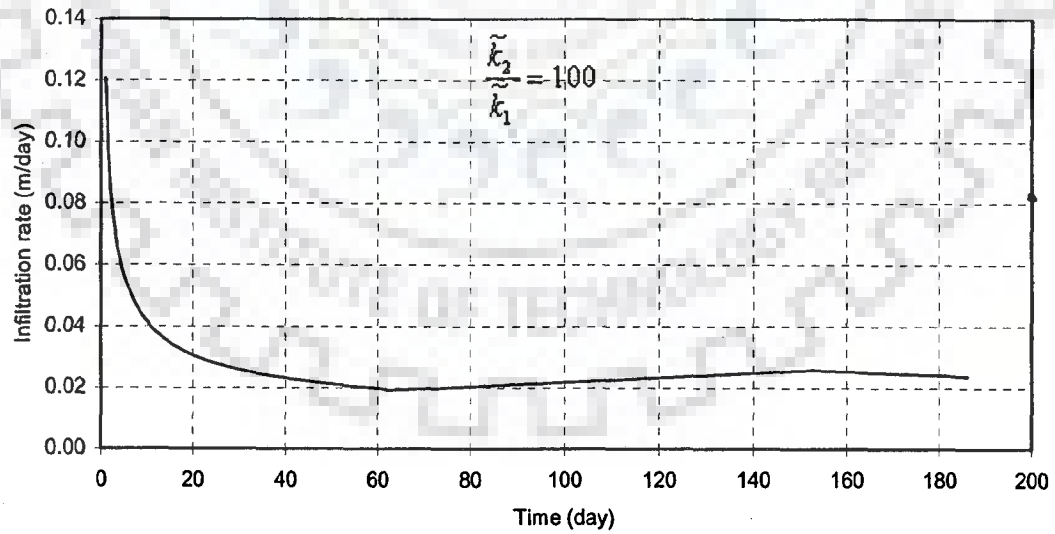

Fig. 5.21 Variation of infiltration rate (m/day) with time (day) from the storage tank, the upper soil layer is having lower saturated hydraulic conductivity than lower layer, d_s=5.0m, D_0=5.0m

Where the thickness of the upper layer is of the order of 1.0m, there is striking increase in infiltration rate if the hydraulic conductivity of the second layer is of the order of 100 times the hydraulic conductivity of the overlying soil layer.

From these features depicting conspicuous increase in infiltration rate, irrespective of the magnitude of $\tilde{k}_2 / \tilde{k}_1$ after the saturation front surpasses the upper soil layer, which has lower hydraulic conductivity and small thickness (of the order of 1.0m), it is inferred that, an assumption of complete saturation of soil behind the moving front in the underlying soil with high conductivity is in applicable.

For case-III, where the upper soil layer has thickness of the order of 1.0m, a theory is postulated in the following paragraph to predict infiltration rate which continuously decrease with time.

With an assumption that the soil behind the moving front is saturated, the Green and Ampt infiltration equation can be written as:

$$I(t) = k_h(t)\left\{1 + \frac{H(t) + h_{f2}}{z_f(t)}\right\}$$

in which the harmonic mean hydraulic conductivity, $k_h(t) = \dfrac{d_s / \tilde{k}_1 + \{z_f(t) - d_s\} / \tilde{k}_2}{z_f(t)}$

which increases as the saturation front moves deeper in the second layer. Though the hydraulic gradient $\left\{1 + \dfrac{H(t) + h_{f2}}{z_f(t)}\right\}$ decreases with time to reduce infiltration rate, the increase in harmonic mean hydraulic conductivity with time compensates the decrease as a result there is net increase in the infiltration rate. According to Polubarinova-Kochina (1962, p143), if the difference between the hydraulic conductivities of the fine sediments upper layer and the underlying soil is significant, water may percolate from the fine sediment layer in isolated jets and may not fill all the soil pores in the lower layer. The Green and Ampt approach has been effectively applied to layered soils of

decreasing permeability (Childs and Bybordi, 1969; vide. Pachepsky and Timlin 1996). In a two-layered soil system, where the underlying soil layer has higher conductivity and porosity than the overlying soil, several investigators have found that, the underlying coarse soil layer will not be saturated and water moves into the coarser soil through narrow flow channels (finger). The following theory is postulated.

According to Van Genuchtan (1980), the relationship between soil moisture content, θ and capillary suction head, $h(\theta)$ and unsaturated hydraulic conductivity, $k(\theta)$ are given by:

$$\frac{\theta-\theta_r}{\theta_s-\theta_r}=\left[1+\{\alpha\, h(\theta)\}^n\right]^{-m} \tag{5.35}$$

or

$$h(\theta)=\frac{\left\{\left[\frac{\theta-\theta_r}{\theta_s-\theta_s}\right]^{-\frac{1}{m}}-1\right\}^{\frac{1}{n}}}{\alpha}$$

where

θ = volumetric soil moisture content,

θ_s = volumetric saturated soil moisture content,

θ_r = volumetric residual soil moisture content,

α = empirical parameter cm^{-1} depends on soil type,

n *and* m are the empirical parameters depend on soil type.

$$m=1-\frac{1}{n}$$

$$k(\theta)=\tilde{k}\left(\frac{\theta-\theta_r}{\theta_s-\theta_r}\right)^l\left\{1-\left[1-\left(\frac{\theta-\theta_r}{\theta_s-\theta_r}\right)^{\frac{1}{m}}\right]^m\right\}^2 \tag{5.36}$$

where

$\tilde{k}$ = *saturated hydraulic conductivity in* $\frac{cm}{h}$

l = pore connectivity parameter $\cong 0.5$

It is postulated that behind the moving front in the second layer, the moisture content in the second layer is such that, the corresponding unsaturated hydraulic conductivity in the second layer is equal to the saturated hydraulic conductivity of the upper layer. This implies that $\tilde{k}_2$ is to be replaced by $\tilde{k}_1$; $\varepsilon = 1$ and θ_{s2} is to be replaced by θ which is to be obtained from the relation

$$\tilde{k}_1 = \tilde{k}_2 \left(\frac{\theta - \theta_{r2}}{\theta_{s2} - \theta_{r2}} \right)^l \left\{ 1 - \left[1 - \left(\frac{\theta - \theta_{r2}}{\theta_{s2} - \theta_{r2}} \right)^{\frac{1}{m}} \right]^m \right\}^2 \qquad (5.37)$$

With this modification, infiltration rates are calculated for the case where the upper soil layer is comprised of either silty clay or silty clay loam of 1.0m and 5.0m thick and under lying sandy loam. The temporal variation of infiltration rates are presented in Figs. 5.22 to 5.25. It is seen from the figures that, as the saturation front surpasses the interface, as per the postulation, the infiltration rate decreases with time in agreement to the decreasing trend given by Green and Ampt theory for homogeneous soil.

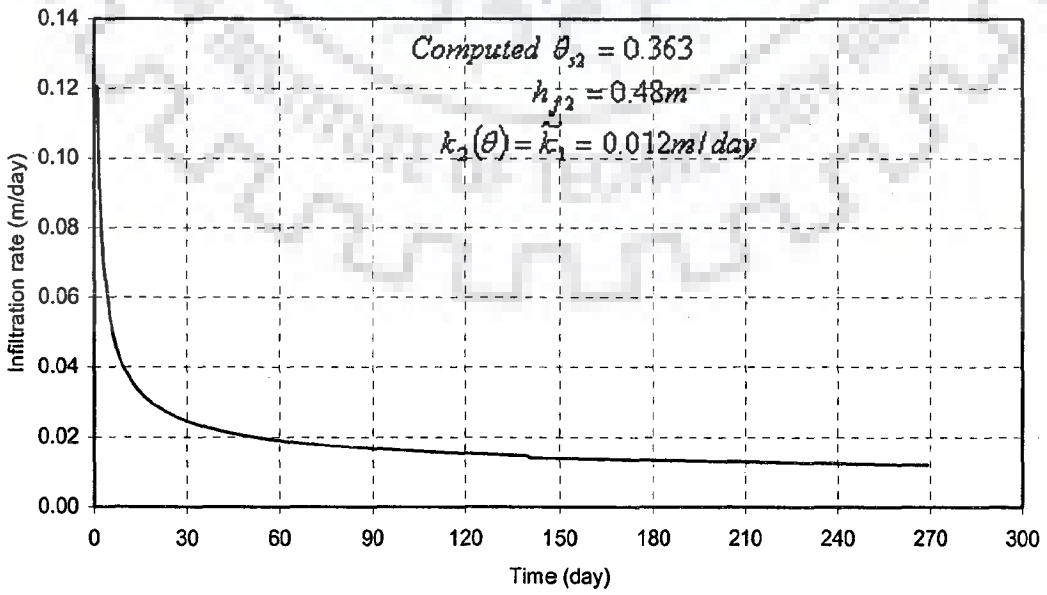

Fig. 5.22 Variation of infiltration rate (m/day) with time (day) from the storage tank bed, under the assumption $k_2(\theta) = \tilde{k}_1$, d_s=1.0m, D_0=5.0m

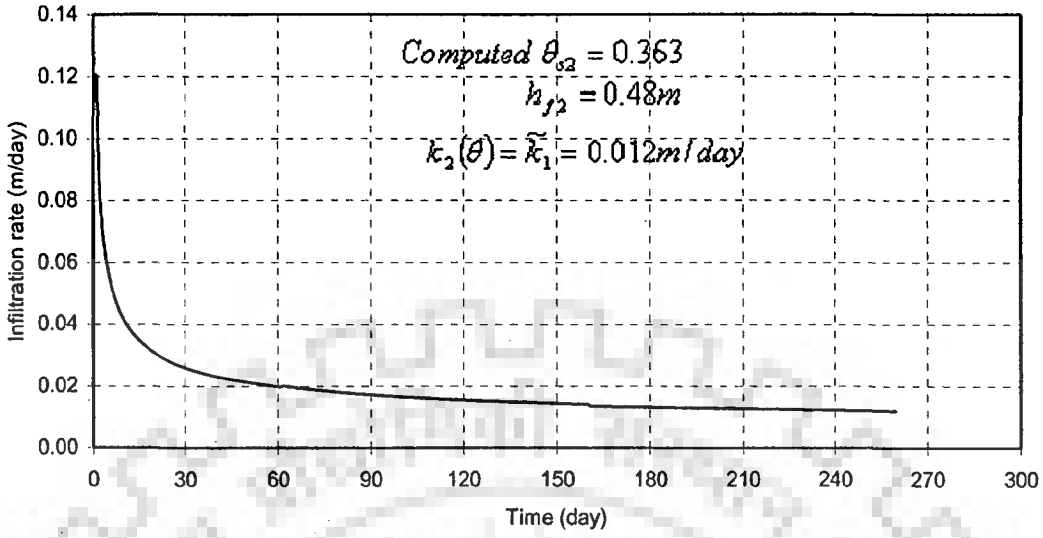

Fig. 5.23 Variation of infiltration rate (m/day) with time (day) from the storage tank bed, under the assumption $k_2(\theta) = \tilde{k}_1$, d_s=5.0m, D_0=5.0m

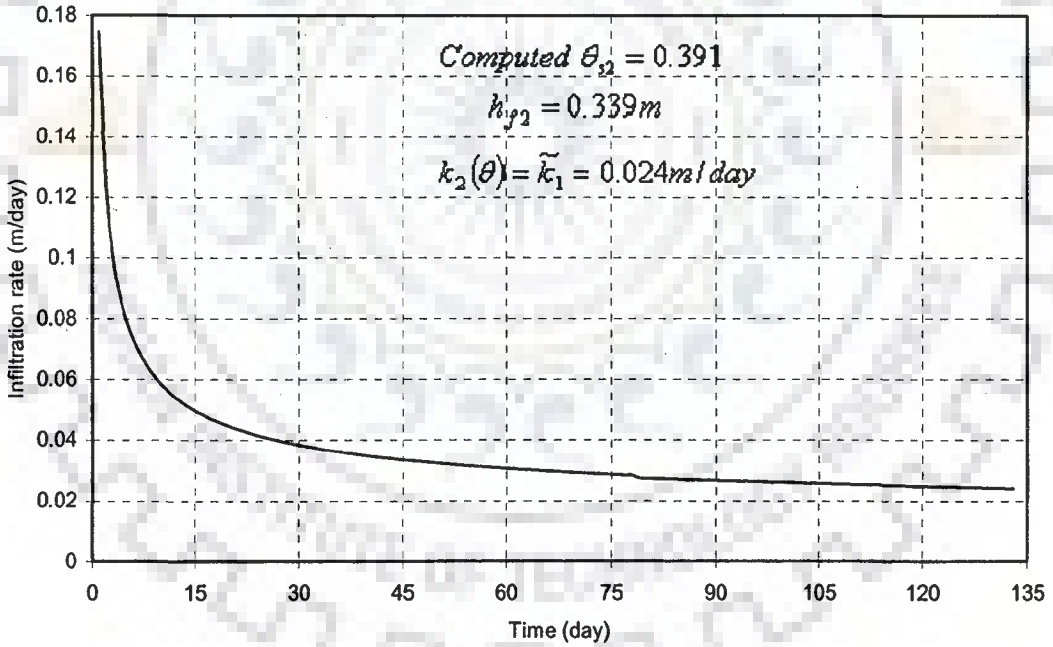

Fig. 5.24 Variation of infiltration rate (m/day) with time (day) from the storage tank bed, under the assumption $k_2(\theta) = \tilde{k}_1$, d_s=1.0m, D_0=5.0m

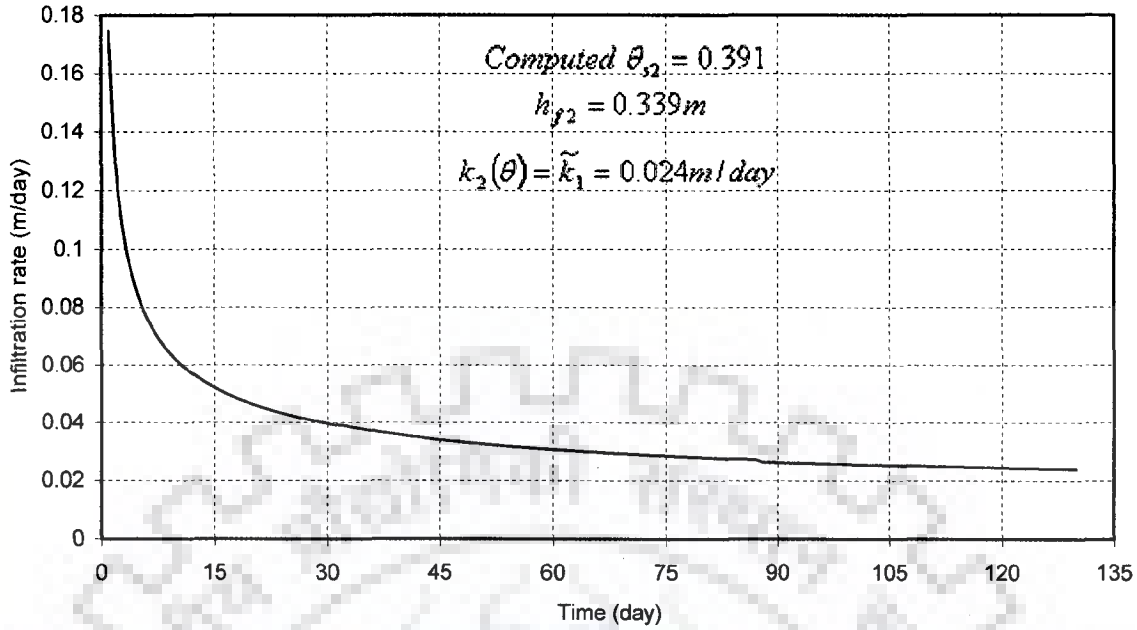

Fig. 5.25 Variation of infiltration rate (m/day) with time (day) from the storage tank bed, under the assumption $k_2(\theta) = \tilde{k}_1$, d_s=5.0m, D_0=5.0m

A comparison between infiltration rate under constant ponding depth and variable ponding depth consequent to infiltration is shown in Fig. 5.26.

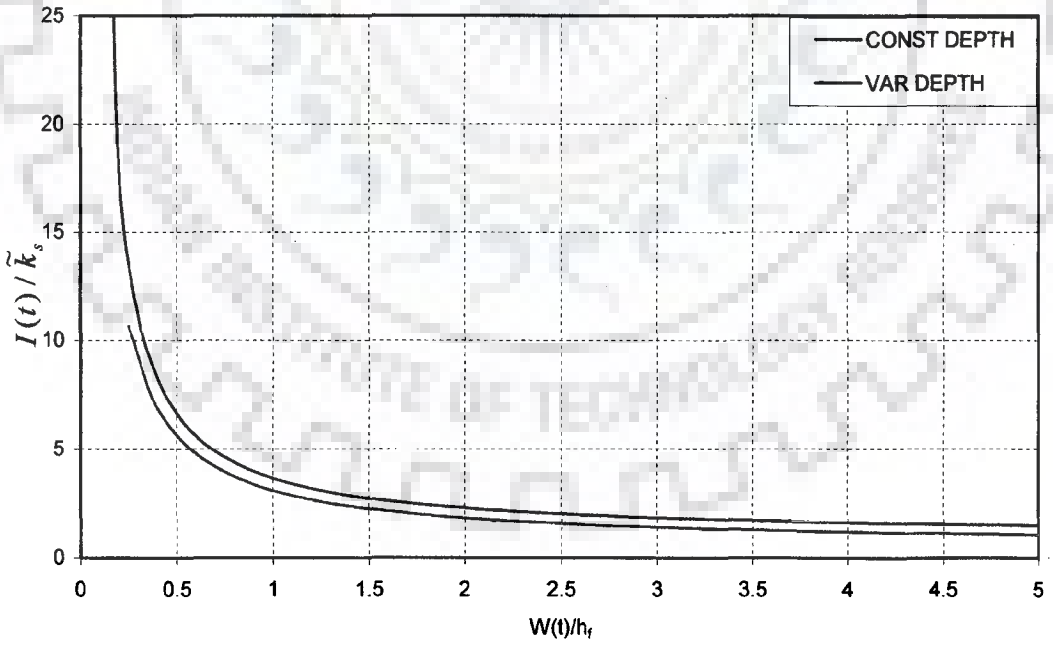

Fig. 5.26 Variation of dimensionless infiltration $I(t)/\tilde{k}_s$, with dimensionless time factor $W(t)/h_f$ for constant and variable ponding depth

5.5 CONCLUSIONS

Based on this study the following conclusions are drawn:

1. In a two layered soil system, if the upper layer happens to be layer of higher hydraulic conductivity, Green and Ampt assumptions that the soil is saturated behind a moving front is applicable irrespective of the position of the moving front in the soil layers.
2. In a two layered soil system, where the lower soil layer has higher hydraulic conductivity than that of the upper layer, the infiltration rate increases with time as the moving front surpasses the interface The increase in infiltration rate is conspicuous, irrespective of the magnitude of $\tilde{k}_2 / \tilde{k}_1$, for small thickness of the upper soil layer of the order of 1.0m. In such case assumption of the Green and Ampt theory that the soil is saturated behind the moving front in the second layer is in applicable.
3. The variation of the drying time of a storage tank underlying a homogeneous soil layer with initial depth of water during first filling is quasi-linear in nature. The drying time is very closely inversely proportional to the hydraulic conductivity of the sub soil.
4. In case of a two layered soil system, where the bottom soil layer has lower hydraulic conductivity, the variation of drying time with initial depth of filling is non-linear in nature.

CHAPTER-6

INFILTRATION FROM A STORAGE TANK FOR VARYING DEPTH OF WATER DUE TO EVAPORATION, RAINFALL, RUNOFF AND SEEPAGE

6.1 INTRODUCTION

The depth of water in a tank changes both due to seepage and evaporation losses from the tank. Consequently, the time variant seepage head is governed both by seepage and evaporation from the tank. The potential evaporation rates are governed by the depth of water in the tank besides by the prevailing meteorological parameters in the area and unknown a priori. In this chapter, the water balance of a tank is carried out using principle of Green and Ampt infiltration theory assuming the evaporation rate from the tank are exclusively estimated by Penman's method.

6.2 STATEMENT OF THE PROBLEM

A tank gets filled for the first time up to a depth D_0 (Fig. 6.1). The two layered subsoil system is in an unsaturated state initially, each layer holding the soil moisture at its respective field capacity. The evaporation is known from pan evaporation measurement. It is aimed to estimate the unsteady seepage from the tank.

6.3. ANALYSIS

6.3.1 Stage 1: Movement of Saturation Front in the Upper Fine Sediment Layer

The water depth at any time since onset of the first filling, when evaporation and seepage are taking place simultaneously is given by:

$$D_w(t) = D_0 - W(t) - \int_0^t E(\tau)d\tau \tag{6.1}$$

The infiltration rate is given by:

$$I = \tilde{k}_1 \frac{h_{f1} + z_f + D_w(t)}{z_f} = \tilde{k}_1 \frac{(\theta_{s1} - \theta_{i1})\{h_{f1} + z_f + D_w(t)\}}{(\theta_{s1} - \theta_{i1})z_f} \tag{6.2}$$

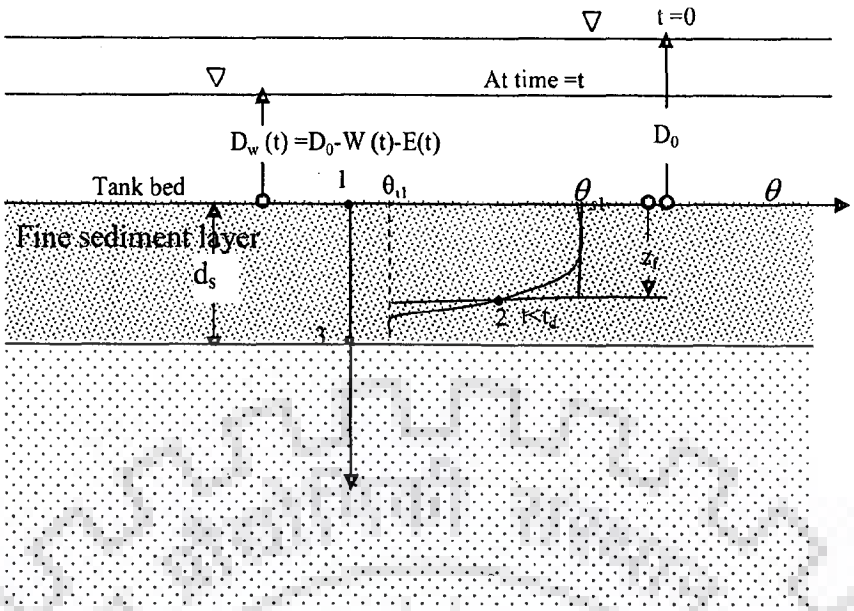

Fig. 6.1 Saturation front lies within the fine sediment layer

Incorporating (6.1) in (6.2), and substituting $(\theta_{s1} - \theta_{i1})z_f = W(t)$, and $I = \frac{dW}{dt}$, equation (6.2) reduces to

$$\frac{dW}{dt} = \tilde{k}_1 \frac{(\theta_{s1} - \theta_{i1})\left(h_{f1} + D_0 - \int_0^t E(\tau)d\tau\right) + \{1 - (\theta_{s1} - \theta_{i1})\}W(t)}{W(t)} \tag{6.3}$$

where $E(\tau)$= rate of evaporation at time τ.

Let the time domain be discretised by uniform time step of size Δt duration. Let the average rate of evaporation during the interval $(i-1)\Delta t$ to $i\Delta t$ be equal to $\bar{E}(i)$

Accordingly, $\int_0^t E(\tau)d\tau = \int_0^{(n-1)\Delta t} E(\tau)d\tau + \int_{(n-1)\Delta t}^t E(\tau)d\tau = \Delta t\sum_{i=1}^{n-1}\bar{E}(i) + \bar{E}(n)\int_{(n-1)\Delta t}^t d\tau$. The infiltration rate during $(n-1)\Delta t \le t \le n\Delta t$ is

$$\frac{dW}{dt} = \tilde{k}_1 \frac{(\theta_{s1} - \theta_{i1})\left(h_{f1} + D_0 - \Delta t\sum_{i=1}^{n-1}\bar{E}(i) - \bar{E}(n)\int_{(n-1)\Delta t}^t d\tau\right) + \{1 - (\theta_{s1} - \theta_{i1})\}W(t)}{W(t)} \tag{6.4}$$

The finite difference form of equation (6.4) at $t=n\Delta t$ is given by:

$$W(n\Delta t)-W\{(n-1)\Delta t\}=\tilde{k}_1\Delta t\frac{(\theta_{s1}-\theta_{i1})\left(h_{f1}+D_0-\Delta t\sum_{i=1}^{n}\bar{E}(i)\right)+\{1-(\theta_{s1}-\theta_{i1})\}W(n\Delta t)}{W(n\Delta t)} \quad (6.5)$$

Solving the quadratic equation and considering the positive root

$$W(n\Delta t)=\frac{\left[W\{(n-1)\Delta t\}+\tilde{k}_1\Delta t\{1-(\theta_{s1}-\theta_{i1})\}\right]}{2}+\frac{\sqrt{\left[W\{(n-1)\Delta t\}+\tilde{k}_1\Delta t\{1-(\theta_{s1}-\theta_{i1})\}\right]^2+4\tilde{k}_1\Delta t(\theta_{s1}-\theta_{i1})\left(h_{f1}+D_0-\Delta t\sum_{i=1}^{n}E(i)\right)}}{2} \quad (6.6)$$

The precipitation on any day can be incorporated in evaluating the cumulative infiltration. $W(t)$. Precipitation can be considered as negative of evaporation. Generally evaporation is recorded in each day. Assuming the time step size $\Delta t = 1$ day, and incorporating daily precipitation and runoff depth, $A(i)=P(i)+\frac{A_c}{A_{\tan k}}Q(i)$, equation (6.6) reduces to

$$W(n)=\frac{\left[W\{(n-1)\}+\tilde{k}_1\{1-(\theta_{s1}-\theta_{i1})\}\right]}{2}+\frac{\sqrt{\left[W\{(n-1)\}+\tilde{k}_1\{1-(\theta_{s1}-\theta_{i1})\}\right]^2+4\tilde{k}_1(\theta_{s1}-\theta_{i1})\left(h_{f1}+D_0-\sum_{i=1}^{n}\{E(i)-A(i)\}\right)}}{2} \quad (6.7)$$

Equation (6.7) is valid for $W(n)\le(\theta_{s1}-\theta_{i1})d_s$

6.3.1.1 Time Taken by Saturation Front to Reach the Interface of Fine Sediment Layer and Subsoil Layer

By the time the saturation front reaches the interface the cumulative infiltration is $(\theta_{s1}-\theta_{i1})d_s$. Let $W(n^*)$ be the quantity that has infiltrated at the n^{*th} day when the saturation front is just behind the interface. $W(n^*)$ and n* are known a priori from (6.7)

by comparing $W(n^*)$ with $(\theta_{s1}-\theta_{i1})d_s$. Making use of (6.4), the time Δt_1 that will be required for the cumulative infiltration to attain $(\theta_{s1}-\theta_{i1})d_s$ is given by:

$$\frac{(\theta_{s1}-\theta_{i1})d_s - W(n^*)}{\Delta t_1} =$$

$$\tilde{k}_1 \frac{(\theta_{s1}-\theta_{i1})\left(h_{f1}+D_0-\sum_{i=1}^{n^*}\{\bar{E}(i)-\bar{A}(i)\}-\Delta t_1\{\bar{E}(n^*+1)-\bar{A}(n^*+1)\}\right)+\{1-(\theta_{s1}-\theta_{i1})\}(\theta_{s1}-\theta_{i1})d_s}{(\theta_{s1}-\theta_{i1})d_s} \tag{6.8}$$

Equation (6.8) is a quadratic equation in Δt_1.Solving the quadratic equation and considering the negative root,

$$\Delta t_1 = \frac{-b-\sqrt{b^2-4ac}}{2a} \tag{6.9a}$$

With positive root Δt_1 becomes more than Δt which is not true. If both evaporation and precipitation are zero then

$$\Delta t_1 = -\frac{c}{b} \tag{6.9b}$$

where

$$a = \tilde{k}_1 \frac{\{\bar{E}(n^*+1)-\bar{A}(n^*+1)\}}{d_s}$$

$$b = -\tilde{k}_1 \frac{\left(h_{f1}+D_0-\sum_{i=1}^{n^*}\{\bar{E}(i)-\bar{A}(i)\}\right)+\{1-(\theta_{s1}-\theta_{i1})\}d_s}{d_s}$$

$$c = (\theta_{s1}-\theta_{i1})d_s - W(n^*)$$

6.3.2 Stage 2: Movement of Saturation Front beyond the Fine Sediment Layer

Starting from equation (5.13) and multiplying numerator and denominator by $(\theta_{s2}-\theta_{i2})$

$$I = \frac{dW}{dt} = \frac{\tilde{k}_2\{h_1(t)-h_4(t)\}}{\left\{(z_f(t)-d_s)+\frac{d_s}{\varepsilon}\right\}} = \frac{\tilde{k}_2\left\{D_0-W(t)-\int_0^t E(\tau)d\tau+\int_0^t A(\tau)d\tau+h_{f2}+z_f(t)\right\}(\theta_{s2}-\theta_{i2})}{\left\{(z_f(t)-d_s)+\frac{d_s}{\varepsilon}\right\}(\theta_{s2}-\theta_{i2})} \tag{6.10}$$

or

$$\frac{dW}{dt}=\frac{\tilde{k}_2\left\{D_0-W(t)-\int_0^t E(\tau)d\tau+\int_0^t A(\tau)d\tau+h_{f2}+d_s+z_f(t)-d_s\right\}(\theta_{s2}-\theta_{i2})}{\left\{(z_f(t)-d_s)+\frac{d_s}{\varepsilon}\right\}(\theta_{s2}-\theta_{i2})}$$

$$=\frac{\tilde{k}_2\left[\left\{D_0-W(t)-\int_0^t E(\tau)d\tau+\int_0^t A(\tau)d\tau+h_{f2}+d_s\right\}(\theta_{s2}-\theta_{i2})+\{z_f(t)-d_s\}(\theta_{s2}-\theta_{i2})\right]}{\left[\{z_f(t)-d_s\}+\frac{d_s}{\varepsilon}\right](\theta_{s2}-\theta_{i2})}$$

Incorporating $\{z_f(t)-d_s\}(\theta_{s2}-\theta_{i2})=W(t)-W(t_{ds})$ in above

$$\frac{dW}{dt}=\frac{\tilde{k}_2\left[\begin{aligned}&\left\{D_0-W(t)-\Delta t\sum_{i=1}^{n-1}\bar{E}(i)-\bar{E}(n)\int_{(n-1)\Delta t}^{t}d\tau+\Delta t\sum_{(i=1)}^{n-1}\bar{A}(i)+\bar{A}(n)\int_{(n-1)\Delta t}^{t}d\tau+h_{f2}+d_s\right\}(\theta_{s2}-\theta_{i2})\\&+W(t)-W(t_{ds})\end{aligned}\right]}{\left\{W(t)-W(t_{ds})+\frac{d_s}{\varepsilon}(\theta_{s2}-\theta_{i2})\right\}}$$

(6.11)

6.3.2.1 Computation of Cumulative Infiltration at the Time Saturation Front Surpasses the Upper Layer

Once the saturation front has crossed the interface at time $n^*\Delta t+\Delta t_1$, the cumulative infiltration up to $(n^*+1)\Delta t\ \ (=n^*\Delta t+\Delta t_1+\Delta t_2)$ is obtained considering a time step size of Δt_2, where $\Delta t_2=\Delta t-\Delta t_1=1-\Delta t_1$. The finite difference form of (6.11) at $t=(n^*+1)\Delta t$ is given by:

$$\frac{W\{(n^*+1)\Delta t\}-W(t_d)}{\Delta t_2}$$

$$=\frac{\tilde{k}_2\left[\begin{aligned}&\left\{\begin{aligned}&D_0-W\{(n^*+1)\Delta t\}-\Delta t\sum_{i=1}^{n^*}\bar{E}(i)-\Delta t_1\bar{E}(n^*+1)-\bar{E}(n^*+1)\int_{n^*\Delta t+\Delta t_1}^{(n^*+1)\Delta t}d\tau+\Delta t\sum_{i=1}^{n^*}\bar{A}(i)+\Delta t_1\bar{A}(n^*+1)\\&+\bar{A}(n^*+1)\int_{n^*\Delta t+\Delta t_1}^{(n^*+1)\Delta t}d\tau+h_{f2}+d_s+W\{(n^*+1)\Delta t\}-W(t_d)\end{aligned}\right\}(\theta_{s2}-\theta_{i2})\end{aligned}\right]}{\left\{W\{(n^*+1)\Delta t\}-W(t_d)+\frac{d_s}{\varepsilon}(\theta_{s2}-\theta_{i2})\right\}}$$

(6.12)

Assuming $\Delta t = 1$ day and cross multiplying

$$W(n^*+1)\left\{W(n^*+1)-W(t_d)+\frac{d_s}{\varepsilon}(\theta_{s2}-\theta_{i2})\right\}-W(t_d)\left\{W(n^*+1)-W(t_d)+\frac{d_s}{\varepsilon}(\theta_{s2}-\theta_{i2})\right\}$$

$$-\tilde{k}_2\Delta t_2\left[\left\{D_0-\sum_{i=1}^{n^*+1}\bar{E}(i)+\sum_{i=1}^{n^*+1}\bar{A}(i)+h_{f2}+d_s\right\}(\theta_{s2}-\theta_{i2})-W(t_d)\right]-\tilde{k}_2\Delta t_2\{1-(\theta_{s2}-\theta_{i2})\}W(n^*+1)=0$$

(6.13)

Further simplifying

$$W^2(n^*+1)-W(n^*+1)\left[2W(t_d)-\frac{d_s}{\varepsilon}(\theta_{s2}-\theta_{i2})+\tilde{k}_2\Delta t_2\{1-(\theta_{s2}-\theta_{i2})\}\right]$$

$$-\left[\tilde{k}_2\Delta t_2\left[\left\{D_0-\sum_{i=1}^{n^*+1}\bar{E}(i)+\sum_{i=1}^{n^*+1}\bar{A}(i)+h_{f2}+d_s\right\}(\theta_{s2}-\theta_{i2})-W(t_d)\right]-W^2(t_d)+W(t_d)\left\{\frac{d_s}{\varepsilon}(\theta_{s2}-\theta_{i2})\right\}\right]=0$$

(6.14)

Solving the quadratic equation and considering the positive root of the discriminant, (b^2-4ac),

$$W(n^*+1)=\frac{-b+\sqrt{b^2-4ac}}{2a} \tag{6.15}$$

where

$$a=1$$

$$b=-\left\{2W(t_d)-\frac{d_s}{\varepsilon}(\theta_{s2}-\theta_{i2})+\tilde{k}_2\Delta t_2\{1-(\theta_{s2}-\theta_{i2})\}\right\}$$

$$c=-\left[\tilde{k}_2\Delta t_2\left[\left\{D_0-\sum_{i=1}^{n^*+1}\bar{E}(i)+\sum_{i=1}^{n^*+1}\bar{A}(i)+h_{f2}+d_s\right\}(\theta_{s2}-\theta_{i2})-W(t_d)\right]-W^2(t_d)+W(t_d)\left\{\frac{d_s}{\varepsilon}(\theta_{s2}-\theta_{i2})\right\}\right]$$

As the negative root of the discriminant yields $-ve\ W(n^*+1)$, the negative root is disregarded. The finite difference form of equation (6.11) at $t=n\Delta t, n>n^*+1$ is given by:

$$W(n\Delta t)-W\{(n-1)\Delta t\}$$

$$=\frac{\tilde{k}_2\Delta t\left[\left\{D_0-\Delta t\sum_{i=1}^{n}\bar{E}(i)+\Delta t\sum_{i=1}^{n}\bar{A}(i)+h_{f2}+d_s\right\}(\theta_{s2}-\theta_{i2})+\{1-(\theta_{s2}-\theta_{i2})\}W(n\Delta t)-W(t_d)\right]}{\left\{W(n\Delta t)-W(t_d)+\frac{d_s}{\varepsilon}(\theta_{s2}-\theta_{i2})\right\}} \tag{6.16}$$

Cross multiplying and simplifying

$$[W(n\Delta t)-W\{(n-1)\Delta t\}]\left\{W(n\Delta t)-W(t_d)+\frac{d_s}{\varepsilon}(\theta_{s2}-\theta_{i2})\right\}$$

$$-\tilde{k}_2\Delta t\left[\left\{D_0-\Delta t\sum_{i=1}^{n}\bar{E}(i)+\Delta t\sum_{i=1}^{n}\bar{A}(i)+h_{f2}+d_s\right\}(\theta_{s2}-\theta_{i2})+\{1-(\theta_{s2}-\theta_{i2})\}W(n\Delta t)-W(t_d)\right]=0 \tag{6.17}$$

Further simplification leads to

$$W(n\Delta t)\left\{W(n\Delta t)-W(t_d)+\frac{d_s}{\varepsilon}(\theta_{s2}-\theta_{i2})\right\}-W\{(n-1)\Delta t\}\left\{W(n\Delta t)-W(t_d)+\frac{d_s}{\varepsilon}(\theta_{s2}-\theta_{i2})\right\}$$

$$-\tilde{k}_2\Delta t\left[\left\{D_0-\Delta t\sum_{i=1}^{n}\bar{E}(i)+\Delta t\sum_{i=1}^{n}\bar{A}(i)+h_{f2}+d_s\right\}(\theta_{s2}-\theta_{i2})-W(t_d)\right]-\tilde{k}_2\Delta t\{1-(\theta_{s2}-\theta_{i2})\}W(n\Delta t)=0 \tag{6.18}$$

or

$$W^2(n\Delta t)-W(n\Delta t)\left\{W(t_d)-\frac{d_s}{\varepsilon}(\theta_{s2}-\theta_{i2})+W\{(n-1)\Delta t\}+\tilde{k}_2\Delta t\{1-(\theta_{s2}-\theta_{i2})\}\right\}$$

$$-W\{(n-1)\Delta t\}\left\{-W(t_d)+\frac{d_s}{\varepsilon}(\theta_{s2}-\theta_{i2})\right\}$$

$$-\tilde{k}_2\Delta t\left[\left\{D_0-\Delta t\sum_{i=1}^{n}\bar{E}(i)+\Delta t\sum_{i=1}^{n}\bar{A}(i)+h_{f2}+d_s\right\}(\theta_{s2}-\theta_{i2})-W(t_d)\right]=0 \tag{6.19}$$

Solving the above quadratic equation for $W(n)\Delta t$ and considering the positive root

$$W(n\Delta t)=0.5\left[W\{(n-1)\Delta t\}+W(t_d)+\tilde{k}_2\Delta t\{1-(\theta_{s2}-\theta_{i2})\}-\frac{d_s}{\varepsilon}(\theta_{s2}-\theta_{i2})\right]$$

$$+0.5\sqrt{\left\{W\{(n-1)\Delta t\}+W(t_d)+\tilde{k}_2\Delta t\{1-(\theta_{s2}-\theta_{i2})\}-\frac{d_s}{\varepsilon}(\theta_{s2}-\theta_{i2})\right\}^2 +4\left[\tilde{k}_2\Delta t\left\{\left(D_0-\Delta t\sum_{i=1}^{n}E(i)+\Delta t\sum_{i=1}^{n}A(i)+h_{f2}+d_s\right)(\theta_{s2}-\theta_{i2})-W(t_d)\right\}+W\{(n-1)\Delta t\}\left(-W(t_d)+\frac{d_s}{\varepsilon}(\theta_{s2}-\theta_{i2})\right)\right]} \tag{6.20}$$

The negative root of the discriminant yields negative $W(n)$, therefore, the negative root is disregarded. Assuming the time step size $\Delta t = 1$ day, (6.20) reduces to

$$W(n)=0.5\left[W(n-1)+W(t_d)+\tilde{k}_2\{1-(\theta_{s2}-\theta_{i2})\}-\frac{d_s}{\varepsilon}(\theta_{s2}-\theta_{i2})\right] +0.5\sqrt{\left\{W\{(n-1)\}+W(t_d)+\tilde{k}_2\{1-(\theta_{s2}-\theta_{i2})\}-\frac{d_s}{\varepsilon}(\theta_{s2}-\theta_{i2})\right\}^2 +4\left[\tilde{k}_2\left\{\left(D_0-\sum_{i=1}^{n}(E(i)-A(i))+h_{f2}+d_s\right)(\theta_{s2}-\theta_{i2})-W(t_d)\right\} +W\{(n-1)\}\left(-W(t_d)+\frac{d_s}{\varepsilon}(\theta_{s2}-\theta_{i2})\right)\right]} \tag{6.21}$$

6.3.2.2 Time Taken by Saturation Front to Reach the Water table

By the time the saturation front reaches the water table, the cumulative infiltration, $W(t_w)$, is $(\theta_{s1}-\theta_{i1})d_s+(\theta_{s2}-\theta_{i2})(d_w-d_s)$. Let $W(n^\circ)$ be the quantity that has infiltrated by the end of the n° th day when the saturation front is just behind the water table. $W(n^\circ)$ and n° are known a priori from (6.21) by comparing $W(n)$ with $(\theta_{s1}-\theta_{i1})d_s+(\theta_{s2}-\theta_{i2})(d_w-d_s)$. Making use of (6.11) the time Δt_3 beyond $n^\circ\Delta t$ that will be required for the cumulative infiltration to attain $W(t_w)=[(\theta_{s1}-\theta_{i1})d_s+(\theta_{s2}-\theta_{i2})(d_w-d_s)]$ is given by:

$$\frac{W(t_w)-W(n^\circ)}{\Delta t_3}= \frac{\tilde{k}_2\left[\left\{D_0-W(t_w)-\sum_{i=1}^{n^\circ}\bar{E}(i)-\bar{E}(n^\circ+1)\Delta t_3+\sum_{i=1}^{n^\circ}\bar{A}(i)+\bar{A}(n^\circ+1)\Delta t_3+h_{f2}+d_s\right\}(\theta_{s2}-\theta_{i2})+W(t_w)-W(t_{ds})\right]}{\left\{W(t_w)-W(t_{ds})+\frac{d_s}{\varepsilon}(\theta_{s2}-\theta_{i2})\right\}} \tag{6.22}$$

Equation (6.22) is a quadratic equation in Δt_3. Solving the quadratic equation and considering the negative root,

$$\Delta t_3 = \frac{-b - \sqrt{b^2 - 4ac}}{2a} \tag{6.23a}$$

The positive root yields Δt_3 greater than Δt, so the positive root is disregarded.

If both evaporation and precipitation are zero then

$$\Delta t_3 = -\frac{c}{b} \tag{6.23b}$$

where

$$a = \tilde{k}_2 \left\{ \bar{E}(n^* + 1) \right\} (\theta_{s2} - \theta_{i2})$$

$$b = -\tilde{k}_2 \left[\left\{ D_0 - W(t_w) - \sum_{i=1}^{n^*} \bar{E}(i) + \sum_{i=1}^{n^*} \bar{A}(i) + h_{f2} + d_s \right\} (\theta_{s2} - \theta_{i2}) + W(t_w) - W(t_{ds}) \right]$$

$$c = \left\{ W(t_w) - W(n^*) \right\} \left\{ W(t_w) - W(t_{ds}) + \frac{d_s}{\varepsilon} (\theta_{s2} - \theta_{i2}) \right\}$$

6.3.3 Stage3: Seepage after Saturation Front Reaches the Water Table

The flow domain after the saturation front reaches the water table is shown in Fig. 6.2. It is assumed that the water table variation is insignificant consequent to recharge taking place from the tank. At the water table the pressure is atmospheric. Hence, the hydraulic head difference between tank bed (at point 1) and water table (at point 5) is $h_s(t)$, the seepage head, which causes flow. At time $t = t_w$ the seepage head is:

$$h_s(t_w) = D_0 - (\theta_{s1} - \theta_{i1}) d_s - (\theta_{s2} - \theta_{i2})(d_w - d_s) - \int_0^{t_w} E(t) dt + \int_0^{t_w} A(t) dt + d_w \tag{6.24}$$

The seepage head will decrease because of recharge to the groundwater table and due to evaporation and would increase due to precipitation. Hence, the variation in seepage head will be given by:

$$-\frac{dh_s}{dt} = k_h \frac{h_s(t)}{d_w} + E(t) - A(t) \tag{6.25}$$

or

$$\frac{dh_s}{Ch_s(t)+E(t)-A(t)} = -dt \tag{6.26}$$

where $C = \frac{k_h}{d_w}$

Let the time domain be discretised with time step Δt. Let the evaporation rate and precipitation rate be separate constant, but vary from time step to time step.

For $(t_w - \Delta t_3) \le t \le (n^\circ + 1)\Delta t$, $E(t) = E(n^\circ + 1)$, $A(t) = A(n^\circ + 1)$

Incorporating $E(t), A(t)$ in (6.26)

$$\frac{dh_s}{Ch_s(t)+E(n^\circ+1)-A(n^\circ+1)} = -dt \tag{6.27}$$

Integrating and incorporating the limits

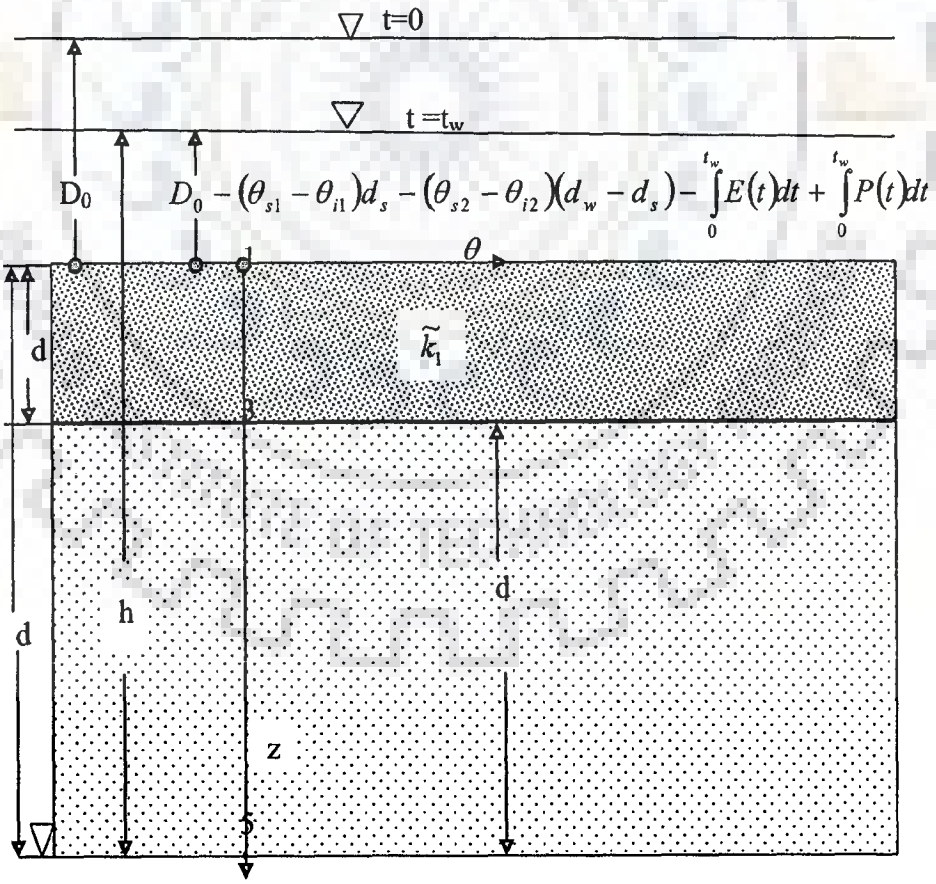

Fig. 6.2 Flow when saturation front reaches water table

$$\int_{D_0-W(t_w)-\sum_{i=1}^{n^\circ}\{E(i)-A(i)\}-\{E(n^\circ+1)-A(n^\circ+1)\}\Delta t_3+d_w}^{h_s(n^\circ+1)} \frac{C\,dh_s}{Ch_s(t)+E(n^\circ+1)-A(n^\circ+1)} = -C\int_{n^\circ\Delta t+\Delta t_3}^{(n^\circ+1)\Delta t} dt = -C(\Delta t-\Delta t_3)$$

(6.28)

$$\ln\frac{C\left[h_s(n^\circ+1)\right]+E(n^\circ+1)-A(n^\circ+1)}{C\left[D_0-W(t_w)-\sum_{i=1}^{n^\circ}\{E(i)-A(i)\}-\{E(n^\circ+1)-A(n^\circ+1)\}\Delta t_3+d_w\right]+E(n^\circ+1)-A(n^\circ+1)} = -C(\Delta t-\Delta t_3)$$

(6.29)

Solving for $h_s(n^\circ+1)$ and taking $\Delta t = 1$ day

$$h_s(n^\circ+1) = \left\{\left[D_0-W(t_w)-\sum_{i=1}^{n^\circ}\{E(i)-A(i)\}-\{E(n^\circ+1)-A(n^\circ+1)\}\Delta t_3+d_w\right]+\left[\frac{E(n^\circ+1)-A(n^\circ+1)}{C}\right]\right\}e^{-C(1-\Delta t_3)} - \left[\frac{E(n^\circ+1)-A(n^\circ+1)}{C}\right]$$

(6.30)

$h_s(n^\circ+1)$ is the seepage head at the end of $(n^\circ+1)^{th}$ day.

For $(n^\circ+1)\le t\le(n^\circ+2)$

$$\int_{h_s(n^\circ+1)}^{h_s(n^\circ+2)} \frac{C\,dh_s}{Ch_s(t)+E(n^\circ+2)-A(n^\circ+2)} = -C\int_{n^\circ+1}^{n^\circ+2} dt = -C \qquad (6.31)$$

Integrating and incorporating the limits

$$\ln\{Ch_s(t)+E(n^\circ+2)-A(n^\circ+2)\}\Big|_{h_s(n^\circ+1)}^{h_s(n^\circ+2)} = -C \qquad (6.32a)$$

Simplifying

$$h_s(n^\circ+2) = \left\{h_s(n^\circ+1)+\frac{1}{C}\{E(n^\circ+2)-A(n^\circ+2)\}\right\}e^{-C}-\frac{1}{C}\{E(n^\circ+2)-A(n^\circ+2)\} \qquad (6.32b)$$

$h_s(n)$ is found in succession starting from $(n^\circ+1)^{th}$ day.

The infiltration rate at $t = n\Delta t$; $n \ge n^\circ+1$ is given by:

$$I(n\Delta t) = Ch_s(n\Delta t) \qquad (6.33)$$

The cumulative infiltration up to $n\Delta t$, $W(n\Delta t)$ is given by:

$$W(n\Delta t) = W(t_w)$$
$$+0.5\times\left[C\left\{D_0 - W(t_w) - \sum_{i=1}^{n^\circ}\{E(i)-A(i)\} - \{E(n^\circ+1)-A(n^\circ+1)\}\Delta t_3 + d_w\right\} + Ch_s(n^\circ+1)\right](\Delta t - \Delta t_3)$$
$$+\sum_{i=(n^\circ+1)}^{n} 0.5\times C\{h_s(i)+h_s(i+1)\}\Delta t \qquad (6.34)$$

6.4 DRAINAGE AFTER THE TANK GETS DRY FOR THE FIRST TIME

Let the storage tank get dry at time t_{dry}. There after redistribution of soil moisture occurs beneath the tank bed. It is assumed that the soil moisture within the drained column is uniform. This assumption has been presumed on the basis of the analysis given by (Ogden and Saghafian, 1997).

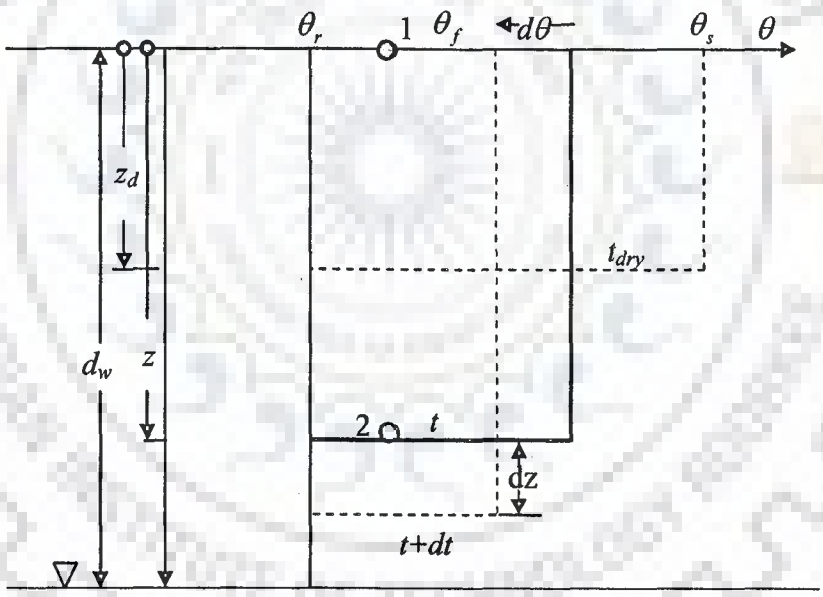

Fig. 6. 3 Green and Ampt theory during drainage

Considering mass balance (Fig.6.3) over a time period t to $t+dt$,

$$-d\theta\, z = dz(\theta - \theta_r) \qquad (6.35)$$

$d\theta$ is a negative quantity as θ decreases with time. Equation (6.35) can be written as

$$-\frac{d\theta}{\theta-\theta_r} = \frac{dz}{z}$$

Integrating

$$-\ln(\theta-\theta_r)=\ln z+C \tag{6.36}$$

At $z=z_d$, $\theta=\theta_s$. Hence,

$$-\ln(\theta_s-\theta_r)=\ln z_d+C \tag{6.37a}$$

or

$$C=-\ln(\theta_s-\theta_r)-\ln z_d \tag{6.37b}$$

Substituting the constant A in (6.36)

$$-\ln(\theta-\theta_r)=\ln z-\ln(\theta_s-\theta_r)-\ln z_d \tag{6.38}$$

or

$$\ln\frac{\theta_s-\theta_r}{\theta-\theta_r}=\ln\frac{z}{z_d} \tag{6.39}$$

or

$$\frac{\theta_s-\theta_r}{\theta-\theta_r}=\frac{z}{z_d} \tag{6.40}$$

or

$$z=\frac{z_d(\theta_s-\theta_r)}{\theta-\theta_r} \tag{6.41}$$

When the soil moisture in the vertical attains the field capacity, the draining front will move to

$$z(\theta_f)=z_d\frac{\theta_s-\theta_r}{\theta_f-\theta_r} \tag{6.42}$$

If the draining front $z(\theta_f)$ is greater than d_w, the draining front will encounter the water table before the moisture content attains the field capacity.

The moisture content θ_w, when the draining front reaches the water table, is given by:

$$d_w=\frac{z_d(\theta_s-\theta_r)}{\theta_w-\theta_r} \tag{6.43}$$

or

$$\theta_w = \theta_r + \frac{(\theta_s - \theta_r)z_d}{d_w} \tag{6.44}$$

6.5 TRAVEL TIME OF THE DRAINING FRONT

The hydraulic head at point 1, at time t is $-h_c(\theta)$ as the tank is dry and at point 2 the hydraulic head is $-h_c(\theta) - z$.

The hydraulic gradient $= \frac{-h_c(\theta) - z + h_c(\theta)}{z} = -1$, and Darcy velocity is given by

$$V(t) = -k(\theta)\frac{-h_c(\theta) - z + h_c(\theta)}{z} = k(\theta) \tag{6.45}$$

The quantity of water drained during the time period *dt* is:

$$V(t)dt = k(\theta)dt = dz(\theta - \theta_r) \tag{6.46}$$

From (6.41)

$$dz = -z_d(\theta_s - \theta_r)\frac{d\theta}{(\theta - \theta_r)^2} \tag{6.47}$$

Incorporating (6.47) in (6.46)

$$k(\theta)dt = -z_d(\theta_s - \theta_r)\frac{d\theta}{(\theta - \theta_r)^2}(\theta - \theta_r) \tag{6.48}$$

Rearranging

$$dt = \frac{-z_d(\theta_s - \theta_r)}{k(\theta)}\frac{d\theta}{(\theta - \theta_r)} = -\frac{z_d}{k(\theta)}\frac{d\theta}{\left(\frac{\theta - \theta_r}{\theta_s - \theta_r}\right)} \tag{6.49}$$

If the draining front reaches the water table, the moisture content in the drained column will be θ_w Let the corresponding time to reach the water table be t_{dw}

Integrating (6.49) within the limit t_{dry} to t_{dw} and θ_s *to* θ_w, the following expression is obtained:

$$[t]_{t_{dry}}^{t_{dw}} = -z_d \int_{\theta_s}^{\theta_w} \frac{d\theta}{k(\theta)\left(\frac{\theta - \theta_r}{\theta_s - \theta_r}\right)} \tag{6.50}$$

Substituting the expression for θ_w from (6.44) in (6.50)

$$t_{dw} - t_{dry} = -z_d \int_{\theta_s}^{\theta_r + \frac{(\theta_s - \theta_r) z_d}{d_w}} \frac{d\theta}{k(\theta)\left(\frac{\theta - \theta_r}{\theta_s - \theta_r}\right)} \tag{6.51}$$

or

$$t_{dw} - t_{dry} = z_d \int_{\theta_r + \frac{(\theta_s - \theta_r) z_d}{d_w}}^{\theta_s} \frac{d\theta}{k(\theta)\left(\frac{\theta - \theta_r}{\theta_s - \theta_r}\right)} \tag{6.52}$$

Incorporating the expression for $k(\theta)$ (Van Genugtan, 1980) in (6.52)

$$t_{dw} = t_{dry} + z_d \int_{\theta_r + \frac{(\theta_s - \theta_r) z_d}{d_w}}^{\theta_s} \frac{d\theta}{\tilde{k}\left(\frac{\theta - \theta_r}{\theta_s - \theta_r}\right)^{l+1} \left\{1 - \left[1 - \left(\frac{\theta - \theta_r}{\theta_s - \theta_r}\right)^{\frac{1}{m}}\right]^m\right\}^2} \tag{6.53}$$

The integration is performed numerically.

If the rainfall occurs before t_{dw}, then the moisture content just before the occurrence of rainfall is given by:

$$t_{rain} = t_{dry} + z_d \int_{\theta_{rain}}^{\theta_s} \frac{d\theta}{\tilde{k}\left(\frac{\theta - \theta_r}{\theta_s - \theta_r}\right)^{l+1} \left\{1 - \left[1 - \left(\frac{\theta - \theta_r}{\theta_s - \theta_r}\right)^{\frac{1}{m}}\right]^m\right\}^2} \tag{6.54}$$

Here the unknown θ_{rain} is obtained by an iteration procedure.

6.6 INFILTRATION RATE AFTER THE SECOND FILLING

Because of the rain the storage tank will receive water and a new saturation front would proceed from the tank bed. Thus, there will be simultaneous movement of saturation front and the draining front. Using Green and Ampt infiltration theory, the movement of saturation front is predicted and temporal variation in the depth of water in the storage tank is predicted.

$$I(t) = \frac{\mathrm{dW(t)}}{\mathrm{dt}} = \tilde{k}_1 \frac{h_{f1}\{\theta(t)\} + z_f(t) + D_w(t)}{z_f(t)} \tag{6.55}$$

Cumulative quantity can be approximated as:

$$W(t) \cong \frac{1}{2}[\{\theta_{s1} - \theta(t_r)\} + \{\theta_{s1} - \theta(t)\}] z_f(t) \cong \left[\theta_{s1} - \frac{1}{2}\{\theta(t_r) + \theta(t)\}\right] z_f(t) \qquad (6.56)$$

Multiplying the numerator and the denominator in (6.55) by $\left[\theta_{s1} - \frac{1}{2}\{\theta(t_r) + \theta(t)\}\right]$

$$\frac{dW}{dt} = \tilde{k}_1 \left[\theta_{s1} - \frac{1}{2}\{\theta(t_r) + \theta(t)\}\right] \frac{[h_{f1}\{\theta(t)\} + z_f(t) + D_w(t)]}{\left[\theta_{s1} - \frac{1}{2}\{\theta(t_r) + \theta(t)\}\right] z_f(t)} \qquad (6.57)$$

or

$$\frac{dW}{dt} = \tilde{k}_1 \frac{\left[\theta_{s1} - \frac{1}{2}\{\theta(t_r) + \theta(t)\}\right][h_{f1}\{\theta(t)\} + D_w(t)] + \left[\theta_{s1} - \frac{1}{2}\{\theta(t_r) + \theta(t)\}\right] z_f(t)}{\left[\theta_{s1} - \frac{1}{2}\{\theta(t_r) + \theta(t)\}\right] z_f(t)} \qquad (6.58)$$

Incorporating (6.56) in (6.58)

$$\frac{dW}{dt} = \tilde{k}_1 \frac{\left[\theta_{s1} - \frac{1}{2}\{\theta(t_r) + \theta(t)\}\right][h_{f1}\{\theta(t)\} + D_w(t)] + W(t)}{W(t)} \qquad (6.59)$$

The depth of water in the storage tank is given by:

$$D_w(t) = D_0 - W(t) - \int_0^t E(\tau)d\tau + \int_0^t A(\tau)d\tau =$$
$$D_0 - W(t) - \int_0^{(n-1)\Delta t} E(\tau)d\tau - \int_{(n-1)\Delta t}^t E(\tau)d\tau + \int_0^{(n-1)\Delta t} A(\tau)d\tau + \int_{(n-1)\Delta t}^t A(\tau)d\tau \qquad (6.60)$$

Incorporating (6.60) in (6.59)

$$\frac{dW}{dt} = \tilde{k}_1 \frac{\left[\theta_{s1} - \frac{1}{2}\{\theta(t_r) + \theta(t)\}\right]\left[h_{f1}\{\theta(t)\} + D_0 - W(t) - \int_0^{(n-1)\Delta t} E(\tau)d\tau - \int_{(n-1)\Delta t}^t E(\tau)d\tau + \int_0^{(n-1)\Delta t} A(\tau)d\tau + \int_{(n-1)\Delta t}^t A(\tau)d\tau\right] + W(t)}{W(t)} \qquad (6.61)$$

Let the time span be discretised with time step size Δt. The finite difference form of equation (6.61) at $t = n\Delta t$ is given by

$$\frac{W(n\Delta t)-W\{(n-1)\Delta t\}}{\Delta t}=$$

$$\left[\theta_{s1}-\frac{1}{2}\{\theta(t_r)+\theta(n\Delta t)\}\right]\left[h_{f1}\{\theta(n\Delta t)\}+D_0-\int_0^{(n-1)\Delta t}\bar{E}(\tau)d\tau-\int_{(n-1)\Delta t}^{n\Delta t}\bar{E}(\tau)d\tau+\int_0^{(n-1)\Delta t}\bar{A}(\tau)d\tau+\int_{(n-1)\Delta t}^{n\Delta t}\bar{A}(\tau)d\tau\right]+$$

$$\tilde{k}_1\frac{\left[1-\left\{\theta_{s1}-\frac{1}{2}\{\theta(t_r)+\theta(n\Delta t)\}\right\}\right]W(n\Delta t)}{W(n\Delta t)} \qquad (6.62)$$

$\theta(n\Delta t)$ is unknown. Therefore, as an approximation $\theta(n\Delta t)$ is taken as $\theta\{(n-1)\Delta t\}$

$$\frac{W(n\Delta t)-W\{(n-1)\Delta t\}}{\Delta t}=$$

$$\left[\theta_{s1}-\frac{1}{2}\{\theta(t_r)+\theta((n-1)\Delta t)\}\right]\left[h_{f1}\{\theta((n-1)\Delta t)\}+D_0-\Delta t\sum_{i=1}^{n}\bar{E}(i)+\Delta t\sum_{i=1}^{n}\bar{A}(i)\right]+$$

$$\tilde{k}_1\frac{\left[1-\left\{\theta_{s1}-\frac{1}{2}\{\theta(t_r)+\theta((n-1)\Delta t)\}\right\}\right]W(n\Delta t)}{W(n\Delta t)} \qquad (6.63)$$

Simplifying

$$W^2(n\Delta t)-W(n\Delta t)W\{(n-1)\Delta t\}-\tilde{k}_1\Delta t\left[1-\left\{\theta_{s1}-\frac{1}{2}\{\theta(t_r)+\theta((n-1)\Delta t)\}\right\}\right]W(n\Delta t)$$

$$-\tilde{k}_1\Delta t\left[\theta_{s1}-\frac{1}{2}\{\theta(t_r)+\theta((n-1)\Delta t)\}\right]\left[h_{f1}\{\theta((n-1)\Delta t)\}+D_0-\Delta t\sum_{i=1}^{n}\bar{E}(i)+\Delta t\sum_{i=1}^{n}\bar{A}(i)\right]=0$$

or

$$W^2(n\Delta t)-\left[W\{(n-1)\Delta t\}+\tilde{k}_1\Delta t-\tilde{k}_1\Delta t\left\{\theta_{s1}-\frac{1}{2}\{\theta(t_r)+\theta((n-1)\Delta t)\}\right\}\right]W(n\Delta t)$$

$$-\tilde{k}_1\Delta t\left[\theta_{s1}-\frac{1}{2}\{\theta(t_r)+\theta((n-1)\Delta t)\}\right]\left[h_{f1}\{\theta((n-1)\Delta t)\}+D_0-\Delta t\sum_{i=1}^{n}\bar{E}(i)+\Delta t\sum_{i=1}^{n}\bar{A}(i)\right]=0$$

(6.64)

$$W(n)=\frac{-b+\sqrt{b^2-4ac}}{2a}$$

where

$$a=1$$

$$b=-\left[W\{(n-1)\Delta t\}+\tilde{k}_1\Delta t-\tilde{k}_1\Delta t\left\{\theta_{s1}-\frac{1}{2}\{\theta(t_r)+\theta((n-1)\Delta t)\}\right\}\right]$$

$$c = -\tilde{k}_1 \Delta t \left[\theta_{s1} - \frac{1}{2}\{\theta(t_r) + \theta((n-1)\Delta t)\} \right] \left[h_{f1}\{\theta((n-1)\Delta t)\} + D_0 - \Delta t \sum_{i=1}^{n} \bar{E}(i) + \Delta t \sum_{i=1}^{n} \bar{A}(i) \right]$$

$$z_f(n) = \frac{W(n)}{\left[\theta_{s1} - \frac{1}{2}\{\theta(t_r) + \theta(t)\} \right]} \cong \frac{W(n)}{\left[\theta_{s1} - \frac{1}{2}\{\theta(t_r) + \theta(n-1)\} \right]} \tag{6.65}$$

Considering draining of the vertical column

$$-k\{\theta(t)\} \frac{-h_c\{\theta(t)\} - z_d(t) + z_f(t) + h_c\{\theta(t)\}}{z_d(t) - z_f(t)} dt = dz_d\{\theta(t) - \theta_i\} \tag{6.66}$$

or

$$k\{\theta(t)\}dt = dz_d\{\theta(t) - \theta_i\}$$

$$\frac{dz_d}{dt} = \frac{k\{\theta(t)\}}{\theta(t) - \theta_i} \tag{6.67}$$

Writing the finite difference form at $t = n\Delta t$

$$\frac{z_d(n) - z_d(n-1)}{\Delta t} = \frac{k\{\theta(n)\}}{\theta(n) - \theta_i} \cong \frac{k\{\theta(n-1)\}}{\theta(n-1) - \theta_i} \tag{6.68}$$

$$\frac{z_d(n) - z_d(n-1)}{\Delta t} \cong \frac{k\{\theta(n-1)\}}{\theta(n-1) - \theta_i}$$

$$z_d(n) = z_d(n-1) + \frac{k\{\theta(n-1)\}}{\theta(n-1) - \theta_i} \Delta t \tag{6.69}$$

Considering mass balance

$$-d\theta\{z_d(t) - z_f(t)\} = dz_d\{\theta(t) - \theta_i\} \tag{6.70}$$

or

$$-\frac{d\theta}{\theta(t) - \theta_i} = \frac{dz_d}{z_d(t) - z_f(t)}$$

or

$$-d\theta = \{\theta(n) - \theta(n-1) + \theta(n-1) - \theta_i\} \frac{dz_d}{z_d(n) - z_f(n)}$$

or

$$-* - d\theta = \{- d\theta + \theta(n-1) - \theta_i\} \frac{dz_d}{z_d(n) - z_f(n)}$$

or

$$- d\theta + d\theta \frac{dz_d}{z_d(n) - z_f(n)} = \{\theta(n-1) - \theta_i\} \frac{dz_d}{z_d(n) - z_f(n)}$$

or

$$\frac{-\lfloor z_d(n) - z_f(n) \rfloor + dz_d}{z_d(n) - z_f(n)} d\theta = \{\theta(n-1) - \theta_i\} \frac{dz_d}{z_d(n) - z_f(n)}$$

Substituting $dz_d = z_d(n) - z_d(n-1)$

$$\frac{\{z_d(n) - z_d(n-1) - \lfloor z_d(n) - z_f(n) \rfloor\}}{z_d(n) - z_f(n)} d\theta = \{\theta(n-1) - \theta_i\} \frac{z_d(n) - z_d(n-1)}{z_d(n) - z_f(n)} \quad (6.71)$$

or

$$d\theta = \frac{\{\theta(n-1) - \theta_i\}\{z_d(n) - z_d(n-1)\}}{\{z_d(n) - z_d(n-1) - \lfloor z_d(n) - z_f(n) \rfloor\}} \quad (6.72)$$

or

$$d\theta = -\frac{\{\theta(n-1) - \theta_i\}\{z_d(n) - z_d(n-1)\}}{z_d(n-1) - z_f(n)} \quad (6.73)$$

$$\theta(n) = \theta(n-1) + d\theta \quad (6.74)$$

Using (6.65), (6.69), (6.74) z_f (n), z_d (n) and $\theta(n)$ can be predicted in succession starting from time step 1. The time step Δt can be chosen as 1 hour as hourly evaporation is computed from heat balance equation.

6.7 RESULTS AND DISCUSSION

The daily variations in depth of water in the storage tank consequent to simultaneous infiltration, evaporation (obtained by Penman's method), rainfall and runoff after the first filling have been computed for various sub soil characteristics. The day of first occurrence of drying of the storage tank has been ascertained. The tank is filled to an initial depth D_0 at $t = 0$ for the first time. Prior to the filling, the soil strata were

unsaturated and the initial soil moisture content of each stratum was at its respective field capacity. Results have been presented for the following subsoil conditions:

(i) The underlying soil is homogeneous.

(ii) The top soil layer has higher hydraulic conductivity than that of the bottom layer.

(iii) The top soil layer has lower hydraulic conductivity than that of the bottom layer.

The soil moisture characteristics of the four groups of soil are taken from published data (Chow, et al, 1988) as given in Table 5.1.

6.7.1 Case-I: The Tank underlain by a Homogeneous Soil Layer

The temporal variations of depth of water in a storage tank underlain by a homogeneous soil layer are presented in Figs. 6.4, 6.5 and 6.6 for four soil groups, for D_0=2.0m, 3.0m and 5.0m respectively. Evaporation losses, runoff to the tank from the contributing catchment and infiltration have been taken into account while computing the depth of water in the tank.

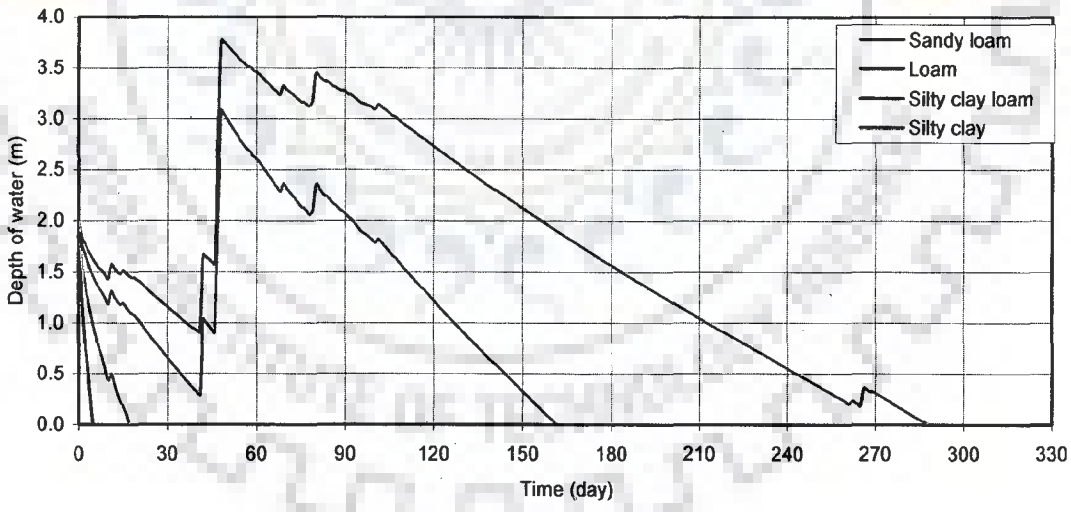

Fig.6. 4 Variation in depth of water in the storage tank with time due to combined effect of infiltration, rainfall, runoff and evaporation, the tank bed is underlain by a homogeneous soil layer, D_0=2m, and d_w=10m

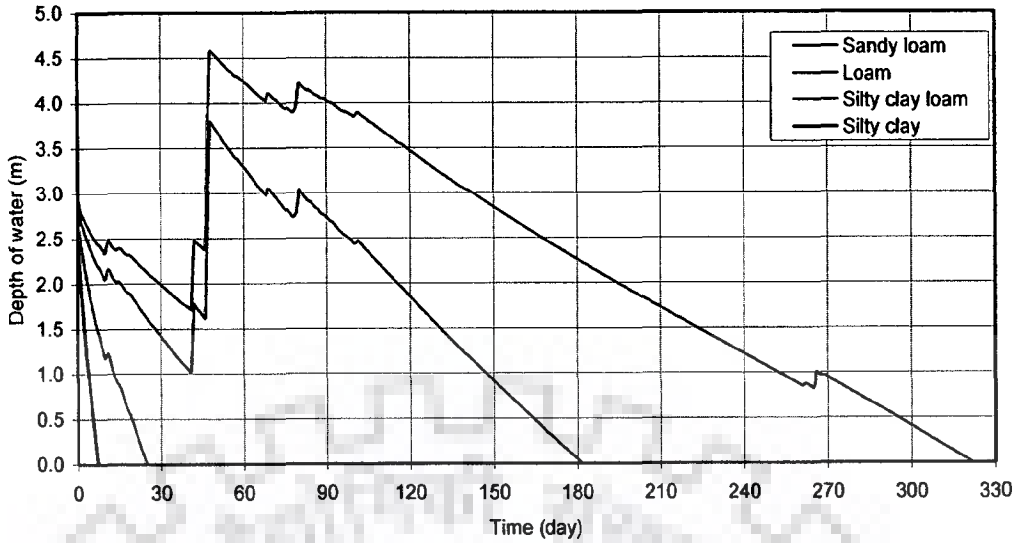

Fig.6. 5 Variation in depth of water in the storage tank with time due to combined effect of infiltration, rainfall, runoff and evaporation, the tank bed is underlain by a homogeneous soil layer, D_0=3m, and d_w=10m

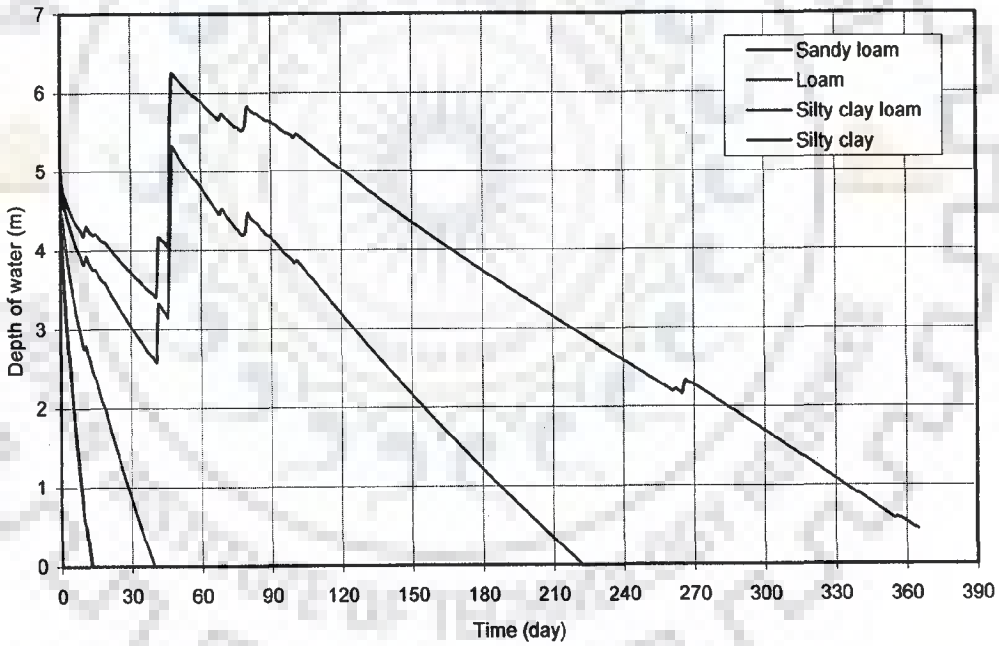

Fig.6.6 Variation in depth of water in the storage tank with time due to combined effect of infiltration, rainfall, runoff and evaporation, the tank bed is underlain by a homogeneous soil layer, D_0=5m, and d_w=10m

As seen from the figures, where the tank is underlain by silty clay and D_0=5.0m, the tank does not get dry during the year. At the end of the year, the depth of water in the tank is about 0.5 m. The loss from a tank is mainly due to infiltration. The

intermediate rise in the depth of water in the tank is due to occurrence of rainfall event and corresponding runoff. The linear trend in the variation is due to uniform rate of infiltration during the post rainfall period.

The variations of infiltration with respect to time are presented in Figs. 6.7 to 6.9. The infiltration rate approaches a steady state value prior to the tank gets dry.

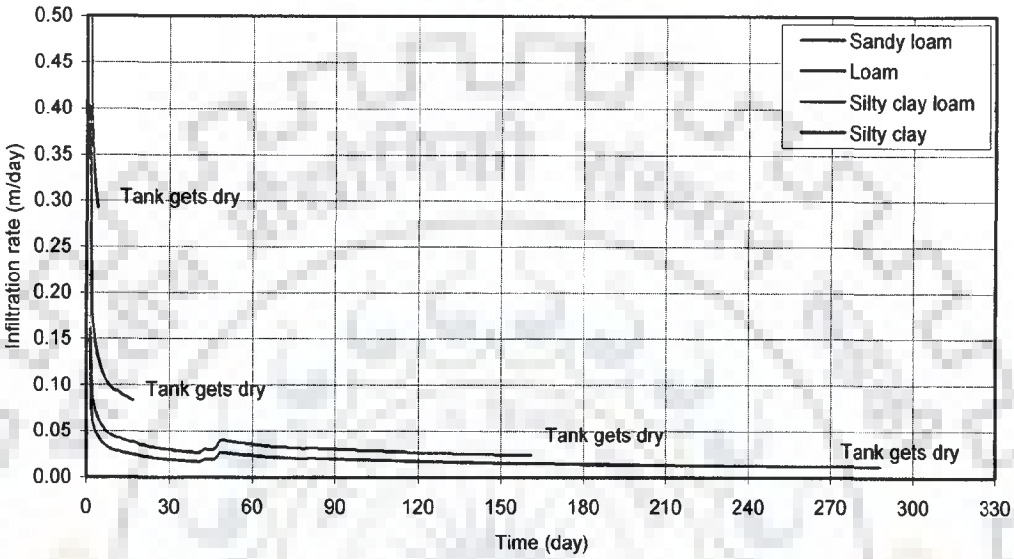

Fig.6. 7 Variation of infiltration rate with time, tank bed is underlain by a homogeneous soil layer, for D_0=2m, d_w =10m

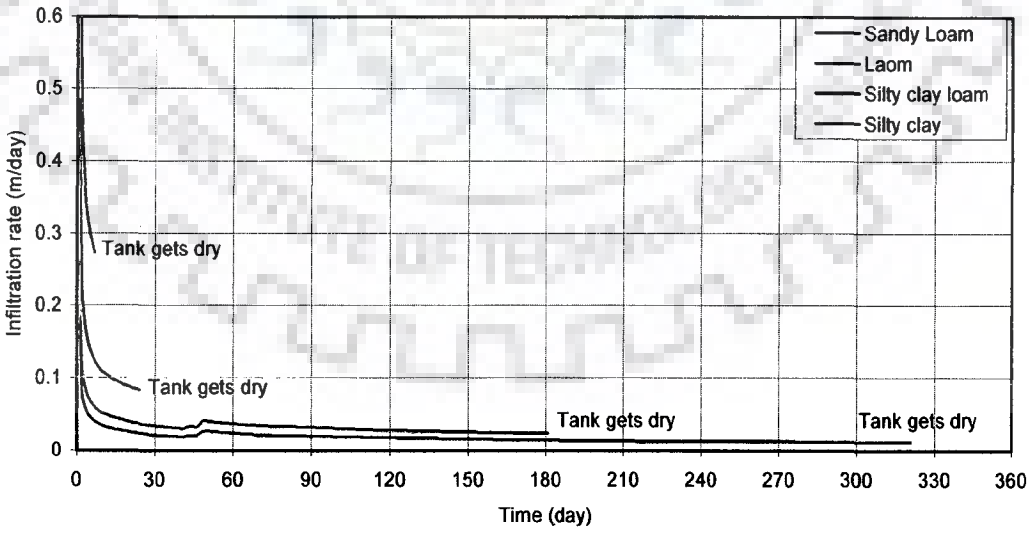

Fig.6. 8 Variation of infiltration rate with time, tank bed is underlain by a homogeneous soil layer, for D_0=3m, d_w =10m

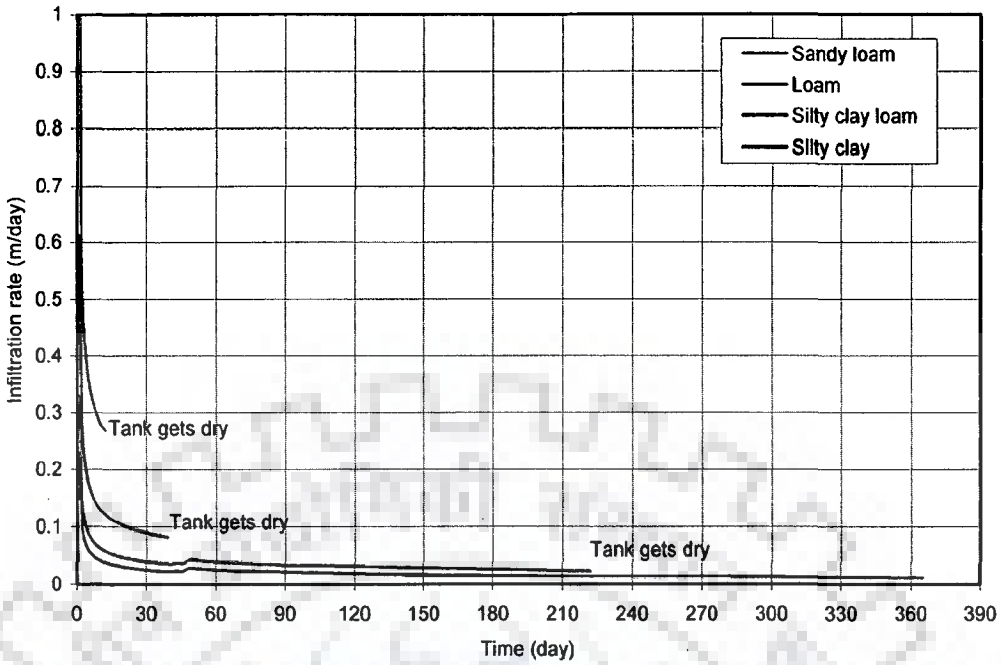

Fig. 6.9 Variation of infiltration rate with time, tank bed is underlain by a homogeneous soil layer, for D_0=5m, d_w =10m

The tank water balance components (infiltration, evaporation, rainfall and runoff) and the storage component i.e. depth of water in the tank for the four group of soils (sandy loam, loam, silty clay loam, silty clay) till the tank gets dry for the first time after the initial filling are presented in Figs. 6.10 through 6.21 for D_0 = 2.0m, 3.0m and 5.0m respectively. It can be ascertained that the tank gets dry mainly due to infiltration as the losses due evaporation is much less than that due to infiltration. These results also can be used for quantifying groundwater recharge rate.

At any time the water balance components satisfy the mass balance equation. The marginal error in satisfying water balance equation is presented in Fig. 6.22.

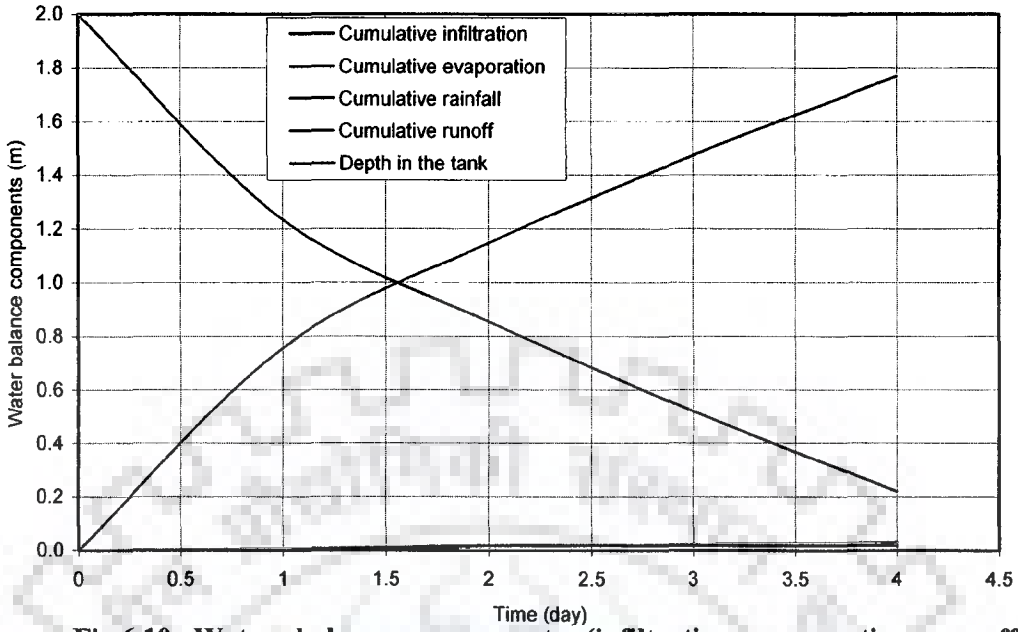

Fig.6.10 Water balance components (infiltration, evaporation, runoff, rainfall and depth of water in tank), the tank bed is underlain by sandy loam soil, for D_0=2m, d_w=10m

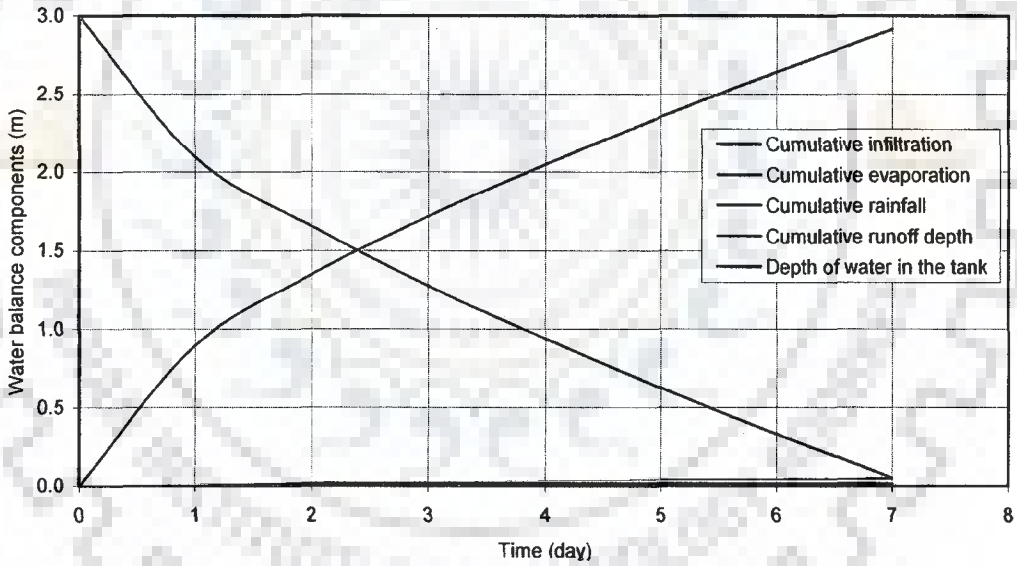

Fig.6.11 Water balance components (infiltration, evaporation, runoff, rainfall and depth of water in tank), the tank bed is underlain by sandy loam soil, for D_0=3m, d_w=10m

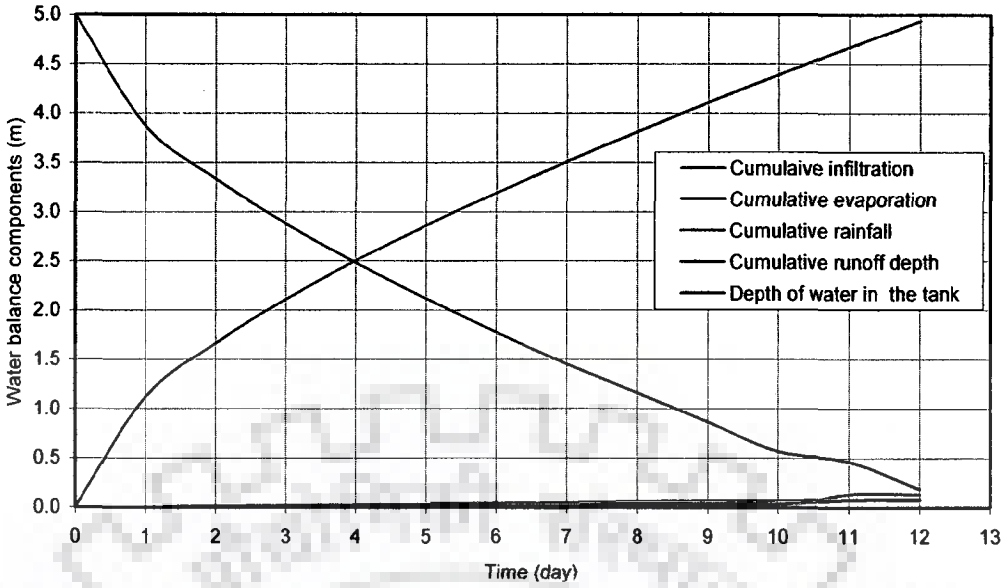

Fig.6.12 Water balance components (infiltration, evaporation, runoff, rainfall and depth of water in tank), the tank bed is underlain by sandy loam soil, for D_0=5m, d_w =10m

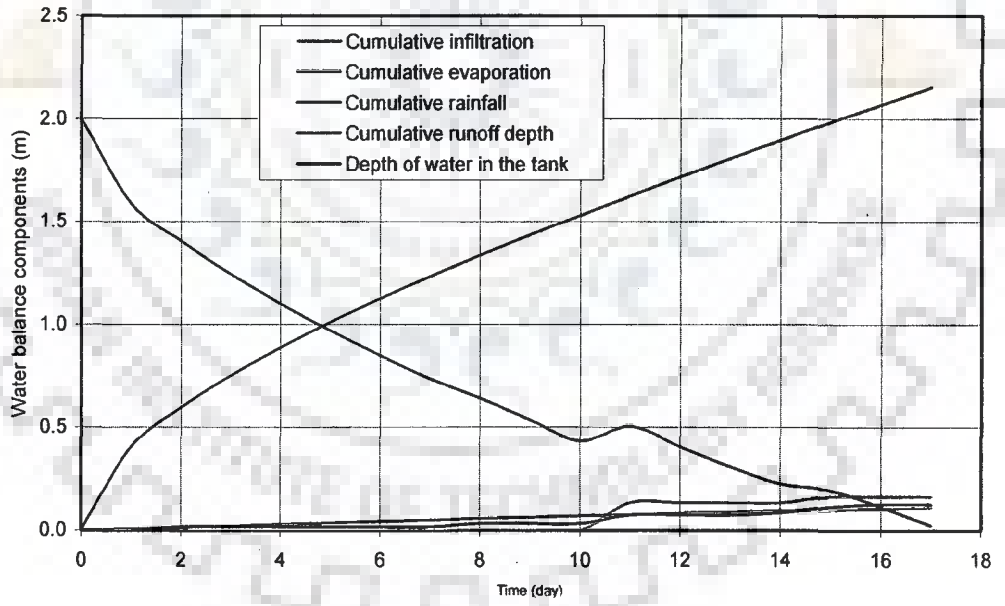

Fig.6.13 Water balance components (infiltration, evaporation, runoff, rainfall and depth of water in tank), the tank bed is underlain by loam soil, for D_0=2m, d_w =10m

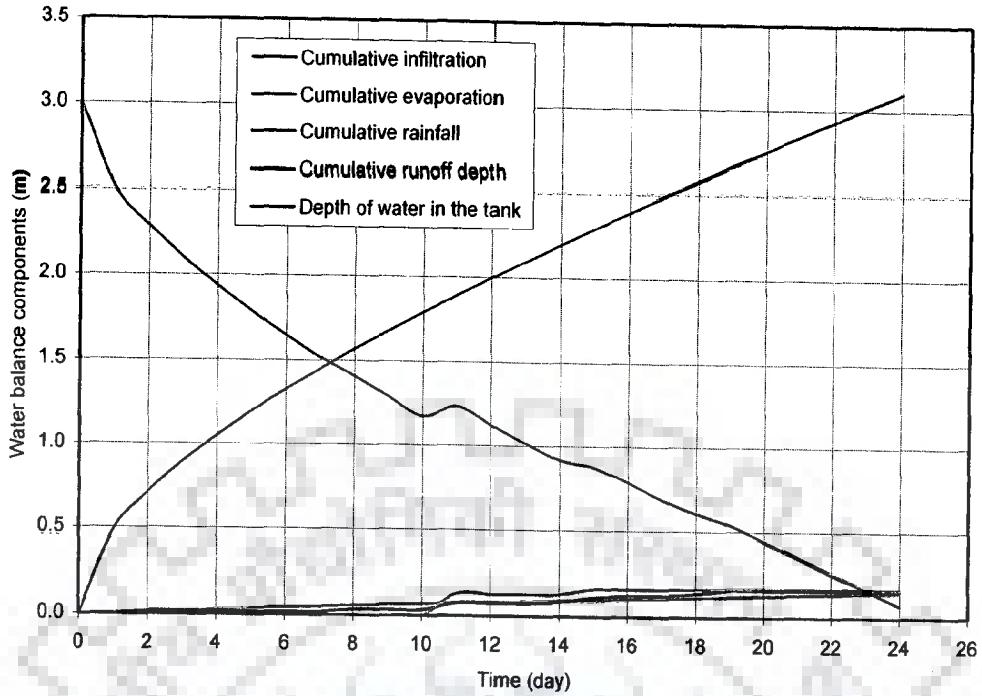

Fig.6.14 Water balance components (infiltration, evaporation, runoff, rainfall and depth of water in tank), the tank bed is underlain by loam soil, for D_0=3m, d_w=10m

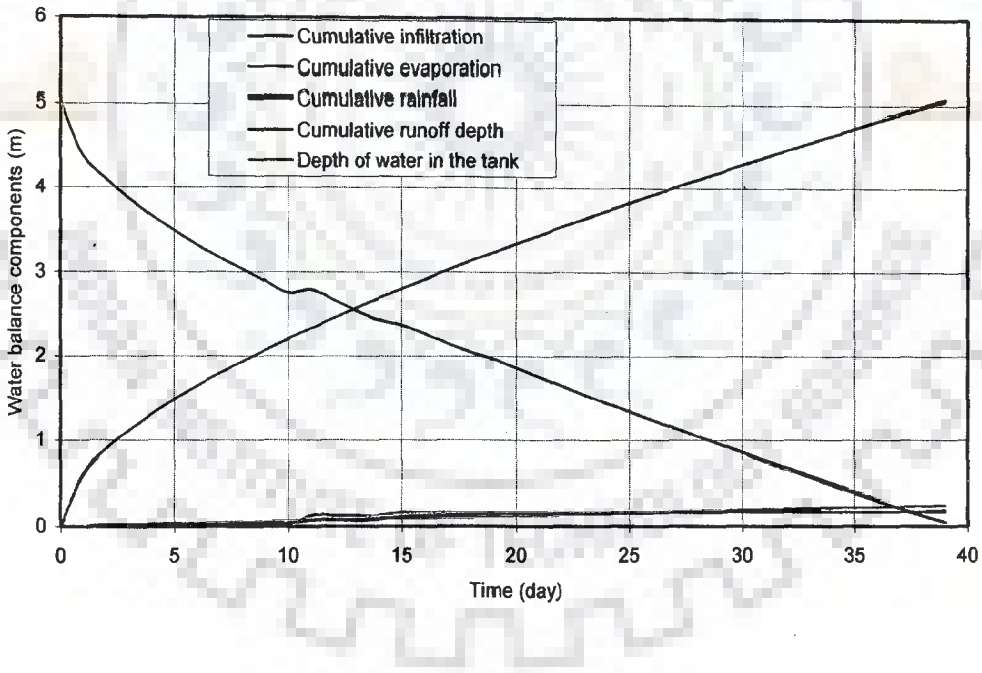

Fig.6.15 Water balance components (infiltration, evaporation, runoff, rainfall and depth of water in tank), the tank bed is underlain by loam soil, for D_0=5m, d_w=10m

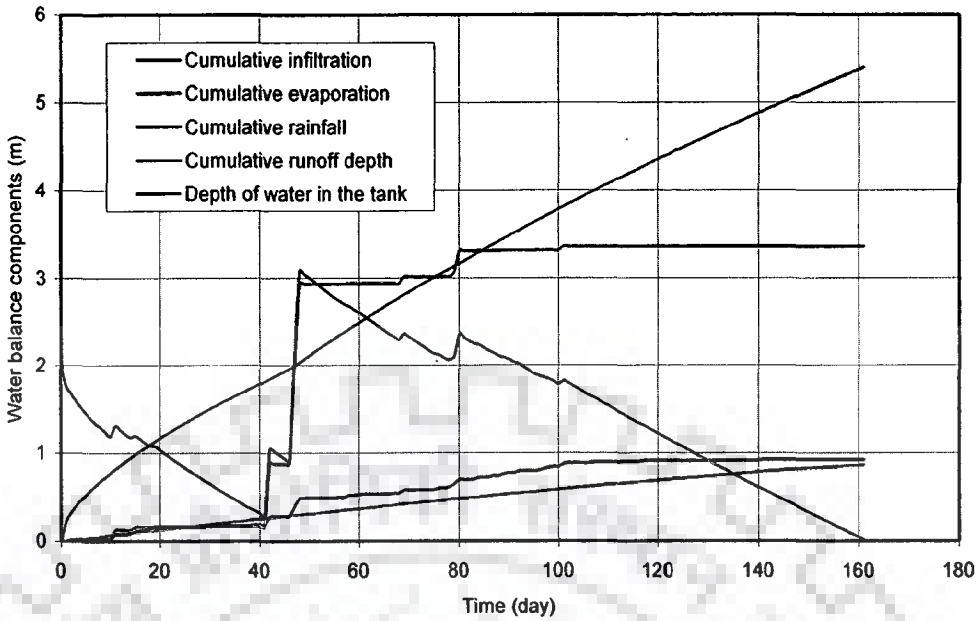

Fig.6.16 Water balance components (infiltration, evaporation, runoff, rainfall and depth of water in tank), the tank bed is underlain by silty clay loam soil, for D_0=2m, d_w=10m

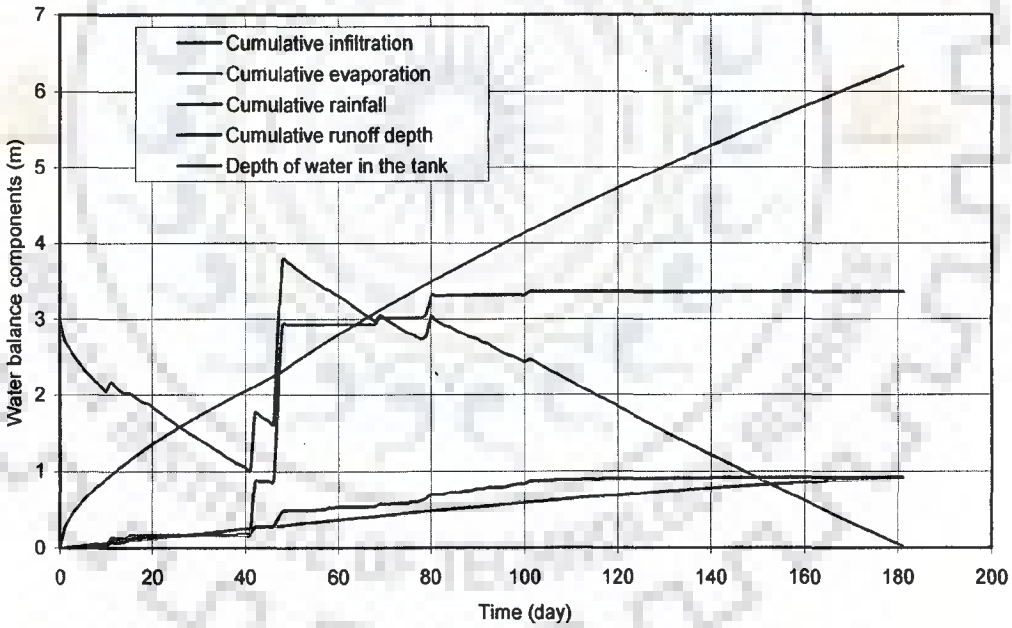

Fig.6.17 Water balance components (infiltration, evaporation, runoff, rainfall and depth of water in tank), the tank bed is underlain by silty clay loam soil, for D_0=3m, d_w=10m

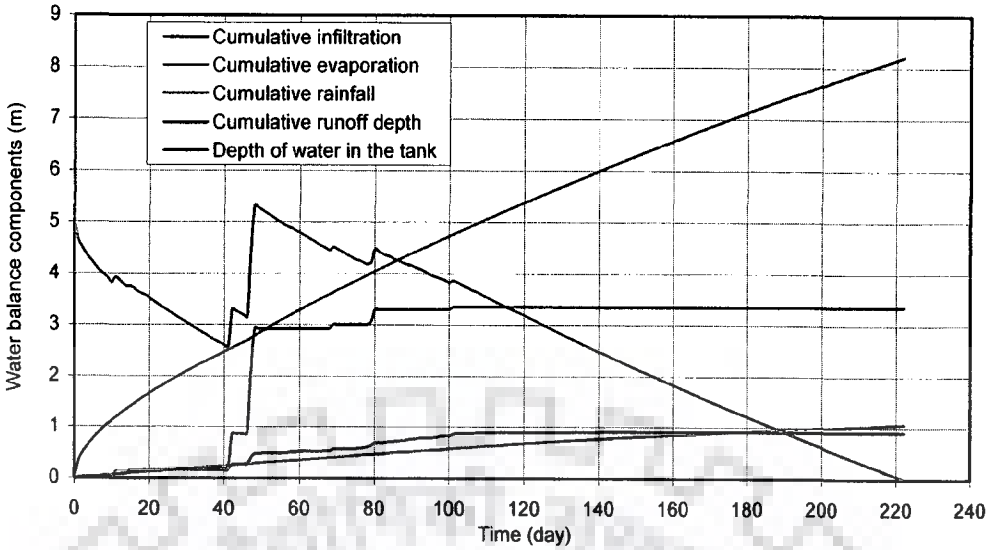

Fig.6. 18 Water balance components (infiltration, evaporation, runoff, rainfall and depth of water in tank), the tank bed is underlain by silty clay loam soil, for D_0=5m, d_w =10m

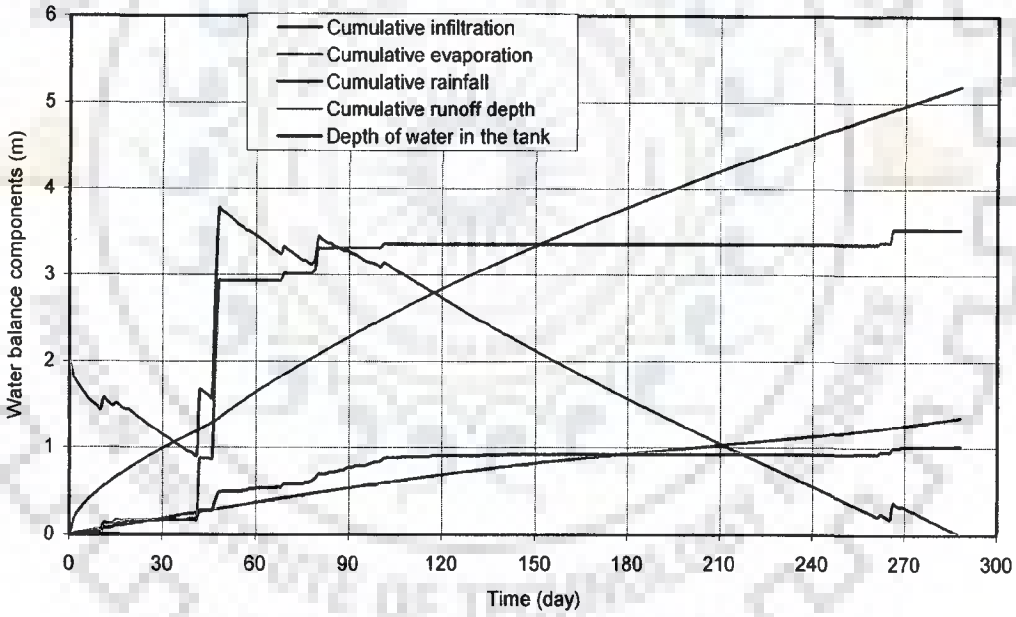

Fig.6.19 Water balance components (infiltration, evaporation, runoff, rainfall and depth of water in tank), the tank bed is underlain by silty clay soil, for D_0=2m, d_w =10m

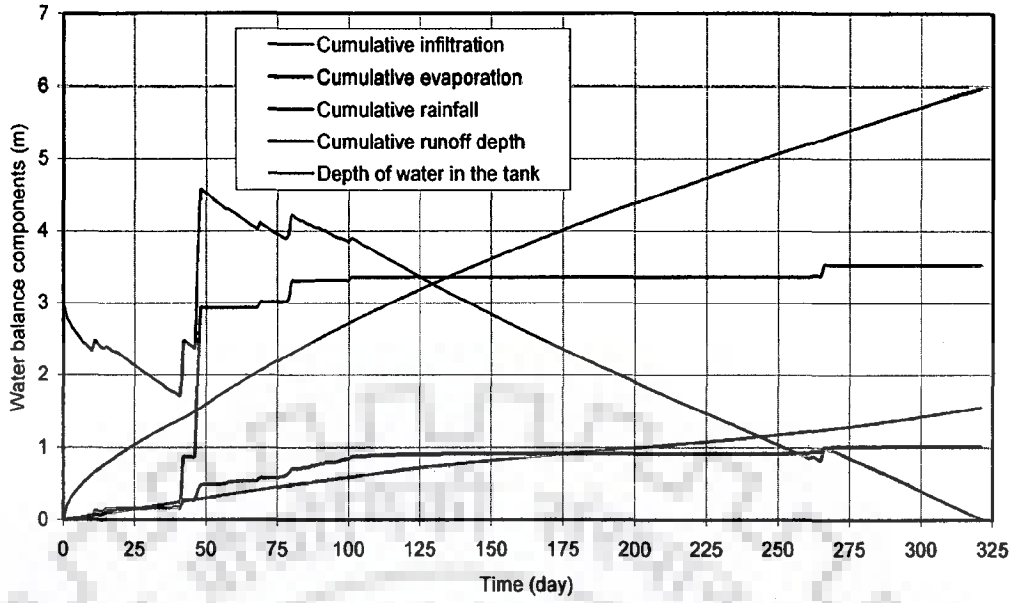

Fig.6.20 Water balance components (infiltration, evaporation, runoff, rainfall and depth of water in tank), the tank bed is underlain by silty clay, for D_0=3m, d_w=10m

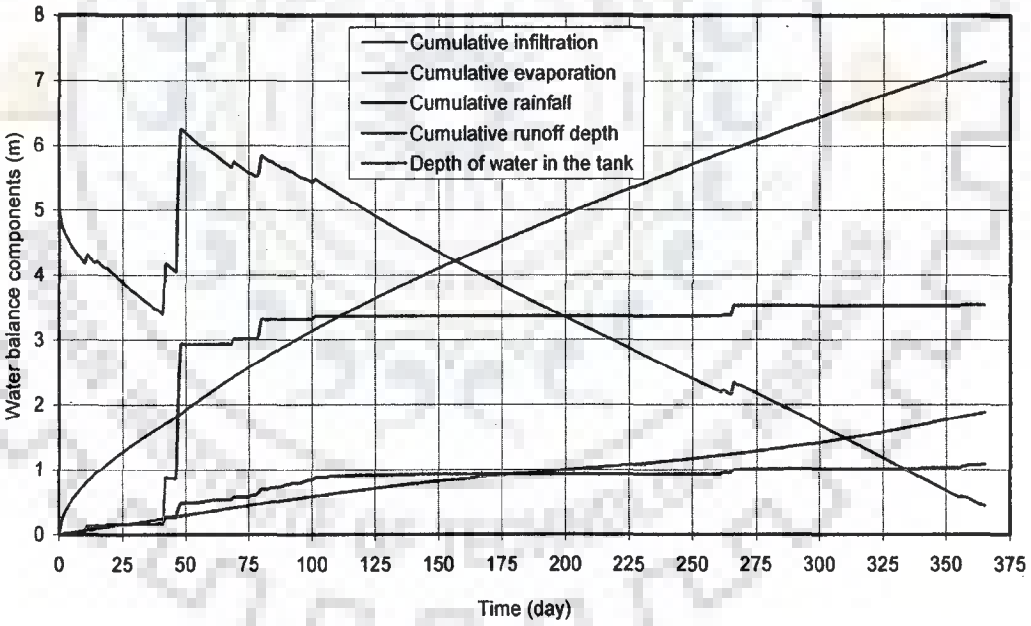

Fig.6.21 Water balance components (infiltration, evaporation, runoff, rainfall and depth of water in tank), the tank bed is underlain by silty clay soil, for D_0=5m, d_w=10m

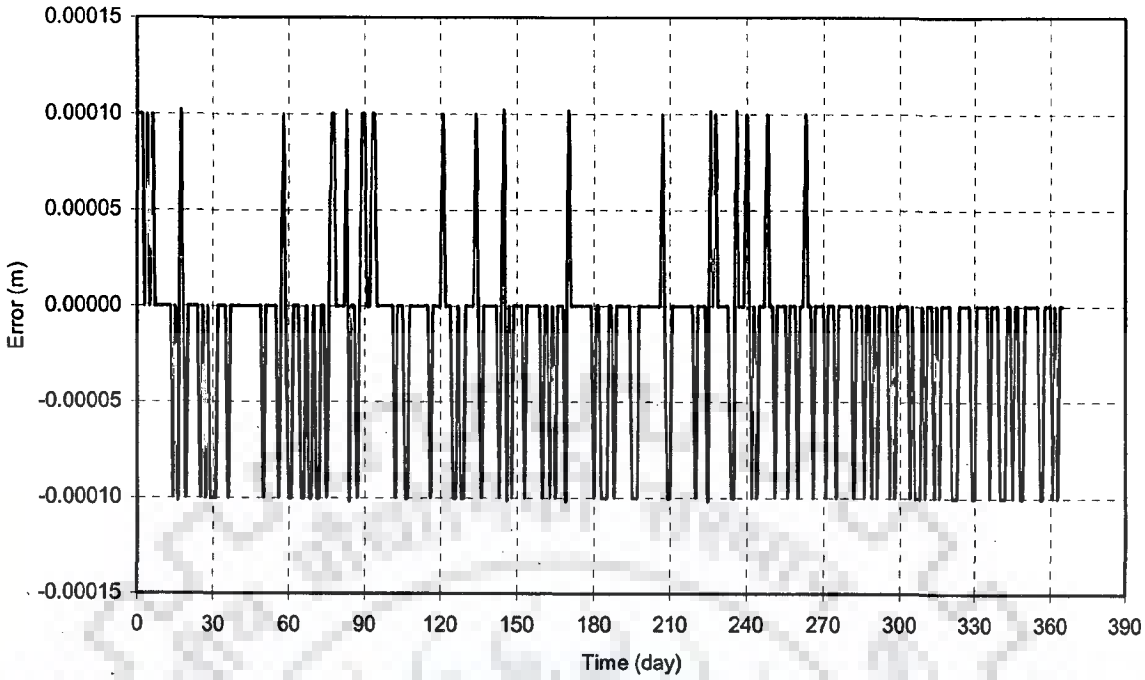

Fig.6.22 Errors during computation of water balance, tank bed underlain by silty clay soil, for D_0=5m and d_w =10m

6.7.2 Case-II: Top Soil Layer has Higher Hydraulic Conductivity than that of the Bottom Layer

The temporal variations in the depth, infiltration rate and the water balance components for case-II are presented in the following paragraphs in three soil groups.

6.7.2.1 First soil group: Top Soil Layer is sandy Loam; Bottom Layer Either is Sandy Loam or Loam or Silty Clay Loam or Silty Clay

The daily variations in the depth of water in the storage tank for case-II are presented in Figs. 6.23 and 6.24 for D_0 = 3.0m and 5.0m. As seen from the figures, if the storage tank is underlain by sandy loam (1st layer) and loam (2nd layer), then the tank acts as a recharge pond as it gets dry very shortly within about 25 days. If the 1st layer is sandy loam and the second layer is either silty clay loam or silty clay then water can be stored for a period of about 130 days or 198 days for D_0=5.0m. If the initial depth of water D_0=3.0m, the tank gets dry within 24 days in all the soil groups. Therefore, if the top soil happens to be sandy loam, the storage tank is performing more as a recharge pond for an initial filling depth of 3.0 m.

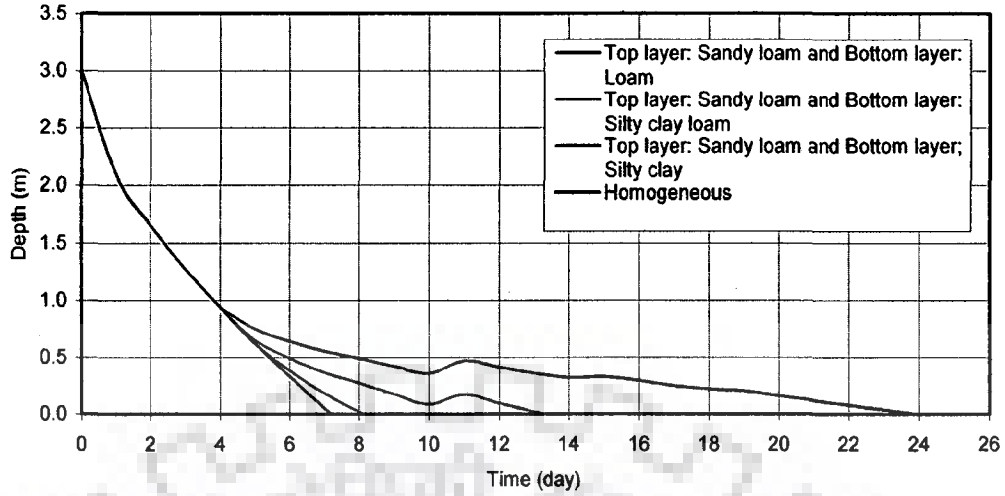

Fig. 6.23 Variation of depth of water in the storage tank with time due to combined effect of infiltration, rainfall, runoff and evaporation, the tank bed is underlain by two different soil layers, D_0=3m, d_s=5m, d_w=10m

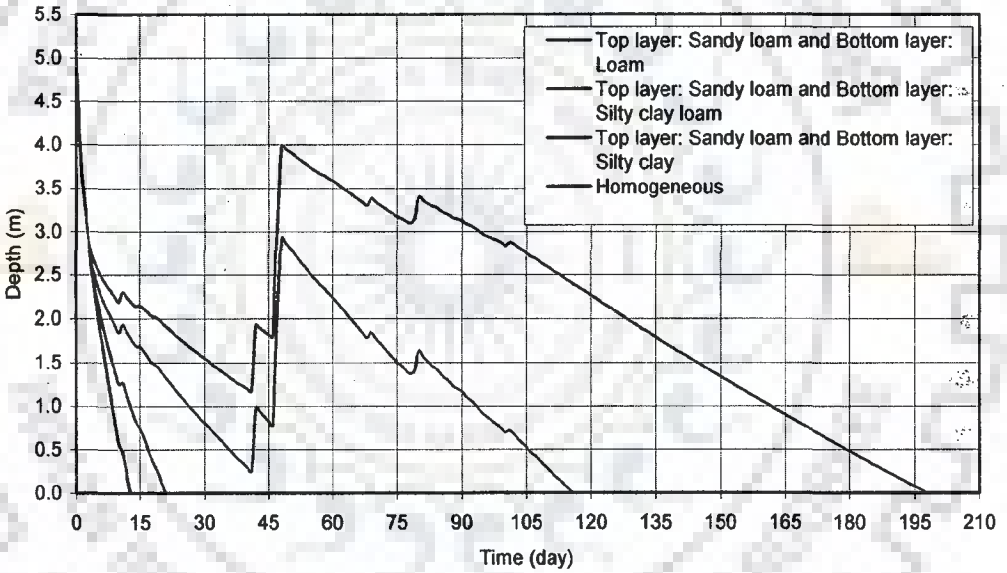

Fig.6. 24 Variation of depth of water in the storage tank with time due to combined effect of infiltration, rainfall, runoff and evaporation, the tank bed is underlain by two different soil layers, D_0=5m, d_s=5m, d_w=10m

The variations of infiltration rate with time for case-II are presented in Figs. 6.25 and 6.26 for D_0=3.0m and 5.0m. The top soil layer being same, the infiltration rates are same till the saturation front reaches the interface. The saturation front reaches the interface at about 4 days after the filling.

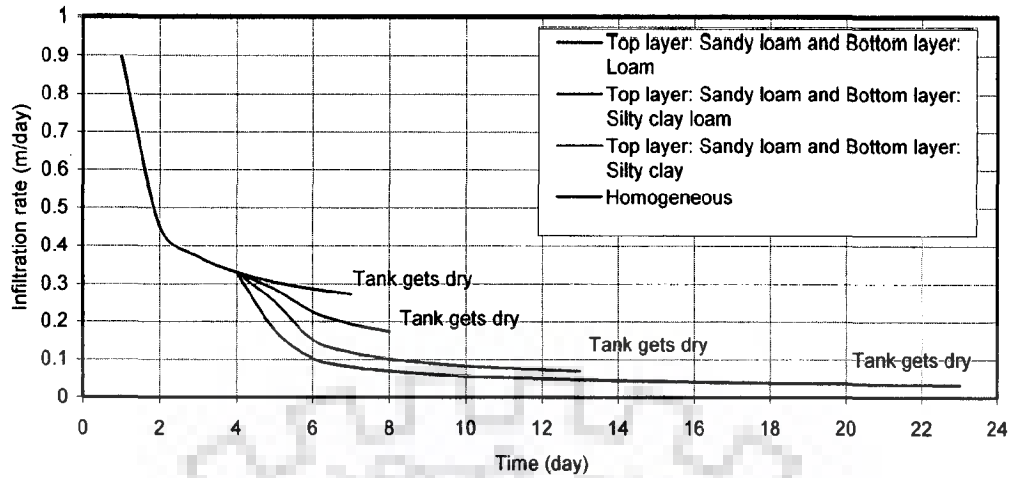

Fig.6. 25 Variation of infiltration rate with time, tank bed is underlain by two different soil layers for D_0=3m, d_s=5m and d_w=10m

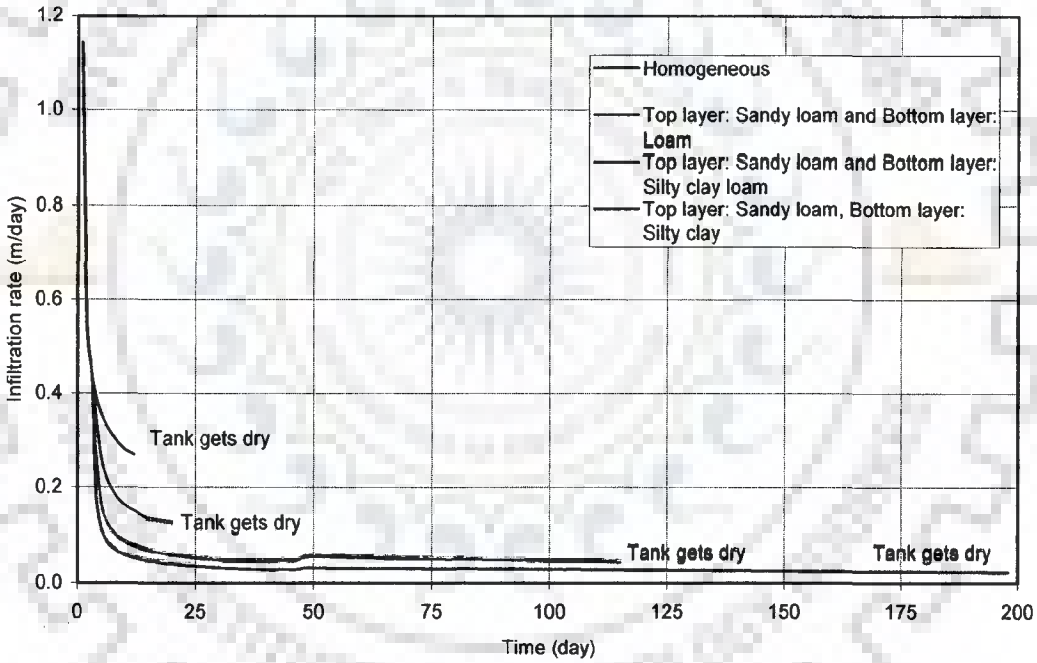

Fig.6. 26 Variation of infiltration rate with time, tank bed is underlain by two different soil layers for D_0=5m, d_s=5m and d_w=10m

For a higher filling depth i.e. D_0=5.0m, the storage tank, which is underlain by sandy loam (1st layer) and silty clay (2nd layer), retains water upto about 198 days. However, the depth of water before drying (at the end of 180 days) is about 0.5m. Therefore, tanks in such hydro-geological conditions will not be able to retain water

throughout the year unless intermittent rainfall occurs. The tanks under case-II condition perform partly as a storage tank and partly as recharging tanks.

The water balance has been verified in Figs. 6.27 through 6.32.

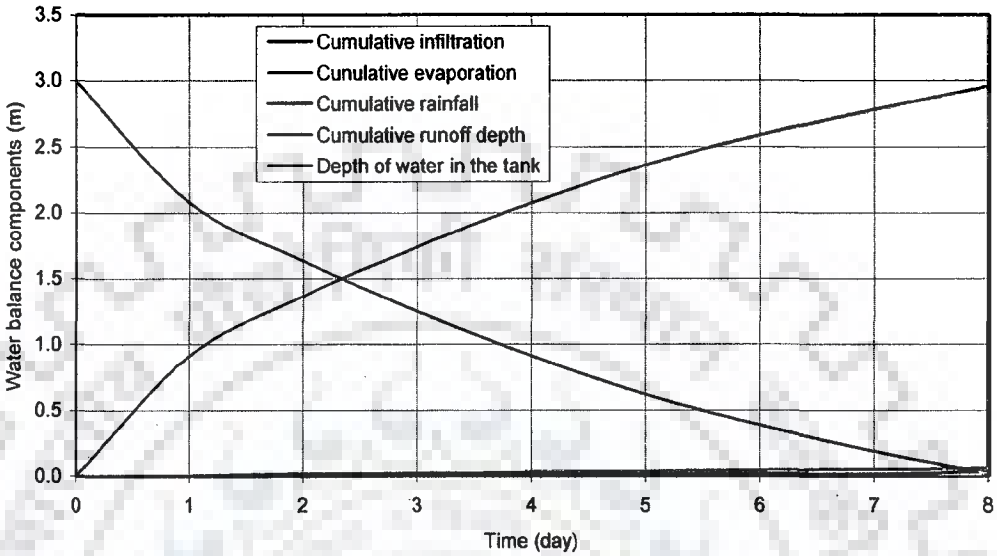

Fig.6. 27 Water balance components (infiltration, evaporation, runoff, rainfall, depth of water in tank), the tank bed is underlain by: top layer- sandy loam and bottom layer- loam for D_0=3m, d_s=5m, d_w=10m

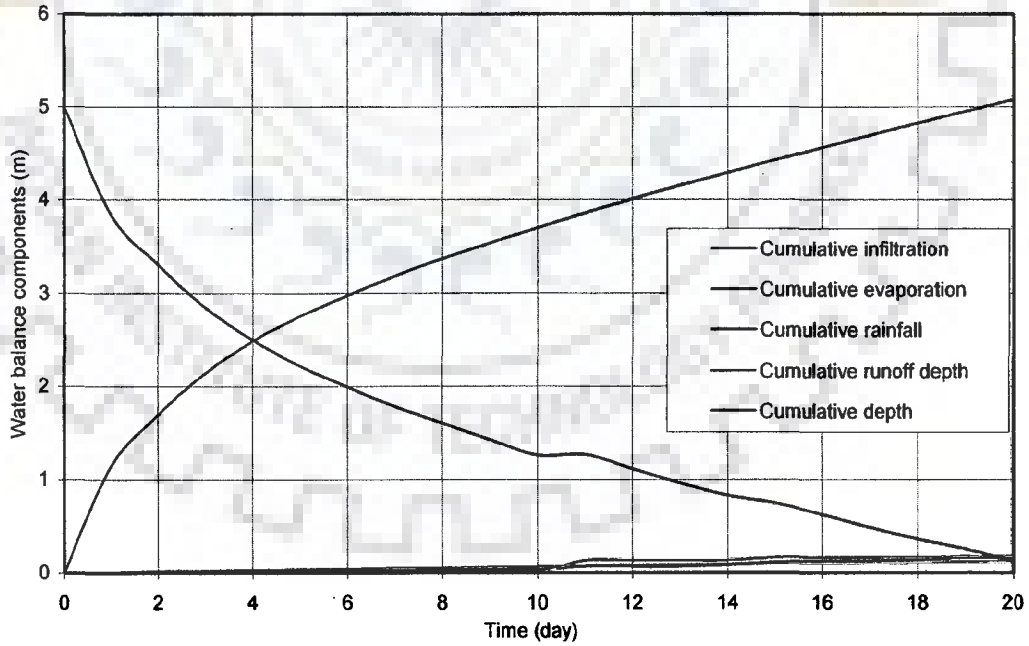

Fig.6. 28 Water balance components (infiltration, evaporation, runoff, rainfall, depth of water in tank), the tank bed is underlain by: top layer- sandy loam and bottom layer- loam for D_0=5m, d_s=5m, d_w=10m

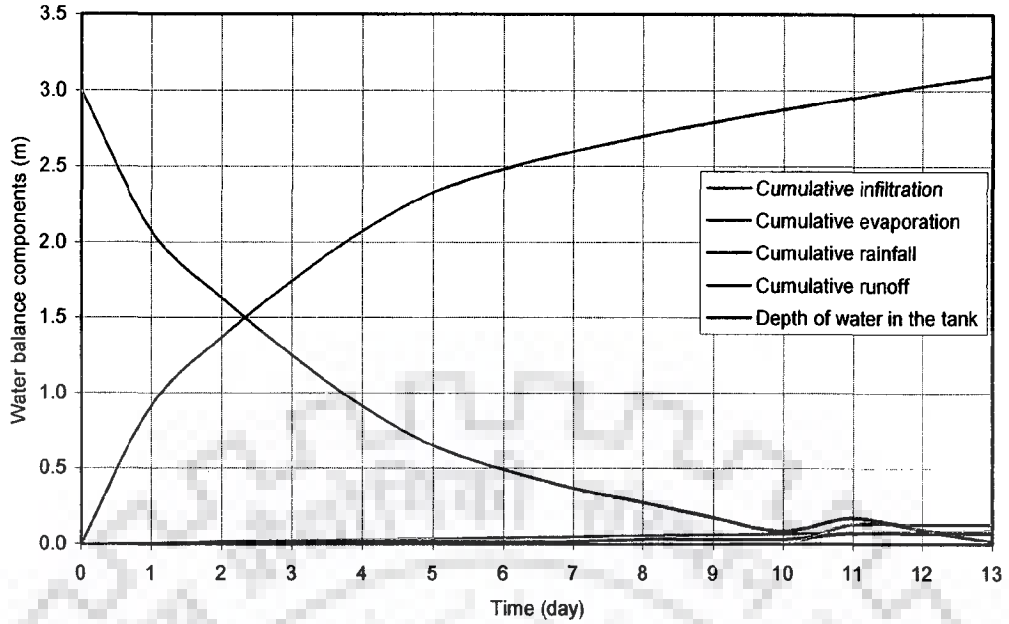

Fig.6. 29 Water balance components (infiltration, evaporation, runoff, rainfall, depth of water in tank), the tank bed is underlain by: top layer-sandy loam and bottom layer-silty clay laom for D_0=3m, d_s=5m, d_w=10m

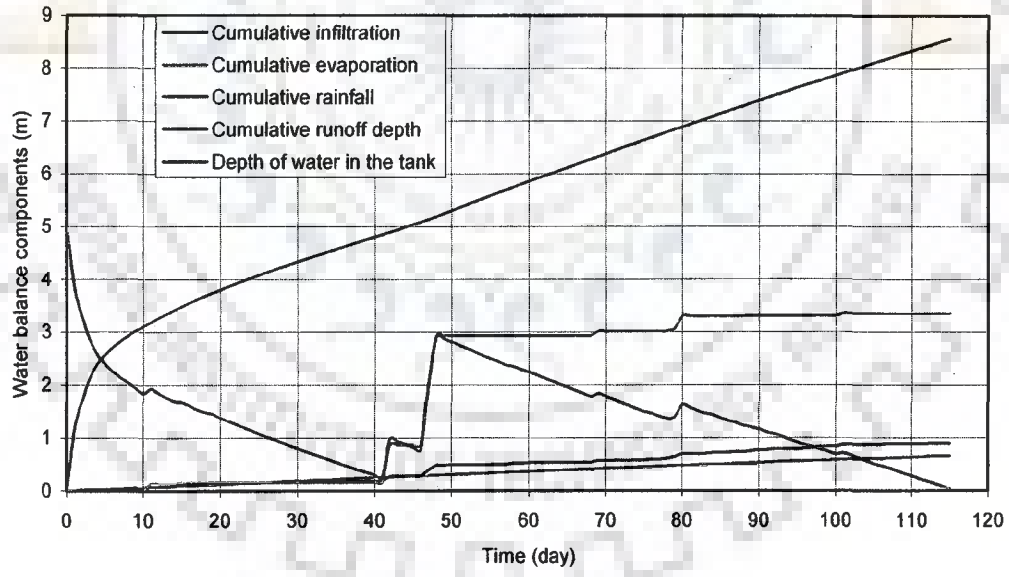

Fig.6. 30 Water balance components (infiltration, evaporation, runoff, rainfall, depth of water in tank), the tank bed is underlain by: top layer-sandy loam and bottom layer-silty clay laom for D_0=5m, d_s=5m, d_w=10m

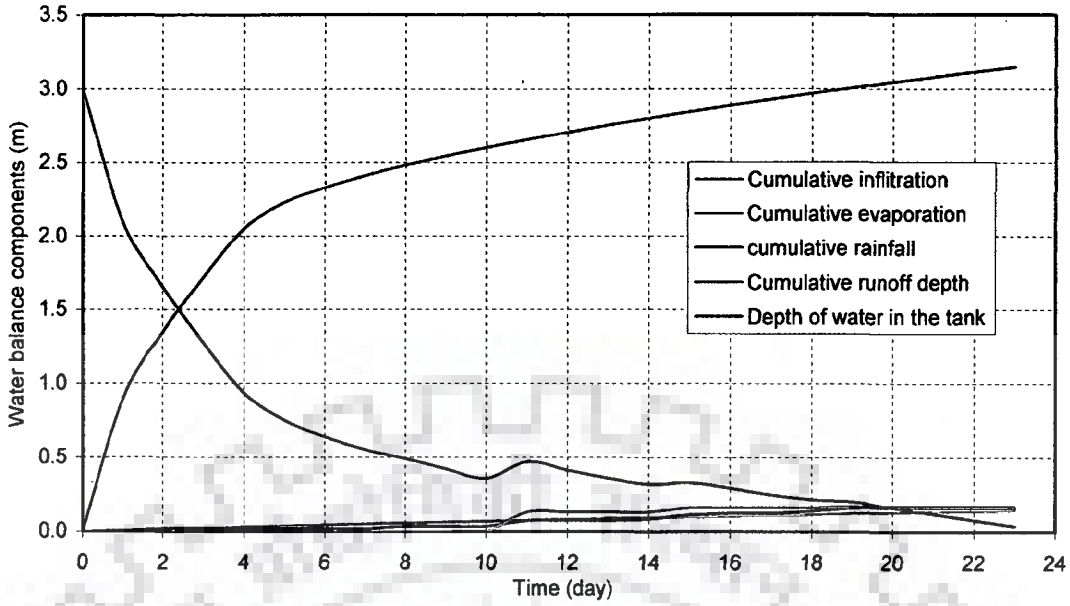

Fig.6. 31 Water balance components (infiltration, evaporation, runoff, rainfall, depth of water in the tank), the tank bed is underlain by: top layer- sandy loam and bottom layer-silty clay for D_0=3m, d_s=5m, d_w=10m

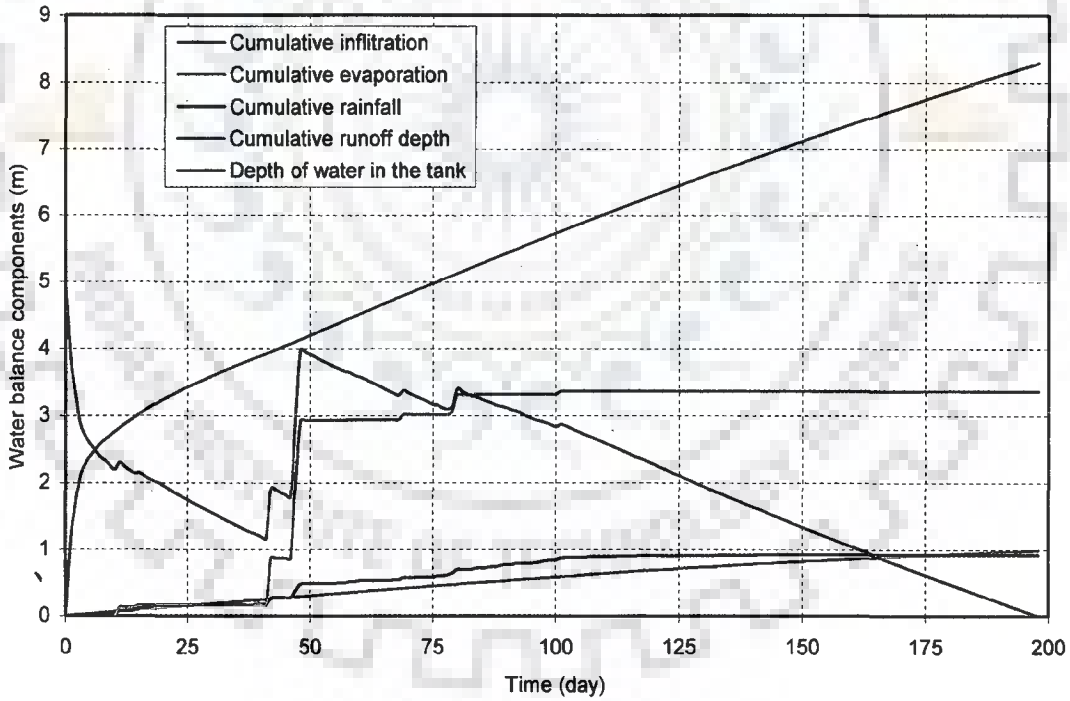

Fig.6. 32 Water balance components (infiltration, evaporation, runoff, rainfall, depth of water in the tank), the tank bed is underlain by: top layer- sandy loam and bottom layer-silty clay for D_0=5m, d_s=5m, d_w=10m

The error in water balance equation has been presented in Fig. 6.33 for D_0 =5.0m, d_s=5.0m and d_w=10.0m.

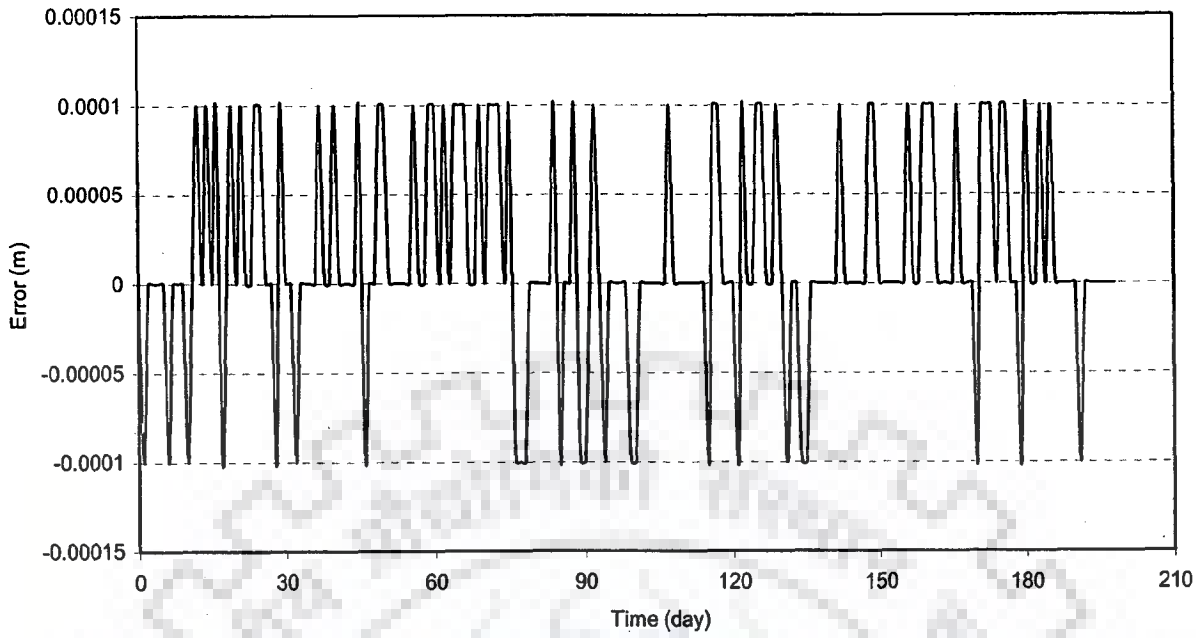

Fig. 6.33 Error during computation of water balance, the tank bed is underlain by: top layer- sandy loam and bottom layer-silty clay for D_0=5m, d_s=5m and d_w=10m

6.7.2.2 Second Soil Group: Top Soil Layer is Loam; Bottom Layer is Either Loam or Silty Clay Loam or Silty Clay

The variations of depth of water with time, due to combined effect of infiltration, rainfall, runoff, and evaporation, in case the top soil layer is loam and the bottom layer is either loam or silty clay loam or silty clay, are presented in Figs. 6.34 and 6.35 for D_0=3.0m and 5.0m respectively. The bottom layer affects the temporal variation in depth once the saturation front surpasses the top layer. The saturation front reaches the interface at t= 13 days for D_0=3.0m. The variation in depth of water with time is quasi-linear once the saturation front reaches the interface. This is because; the infiltration rate reaches a near uniform rate after the saturation front surpasses the top soil layer which is of considerable depth.

Comparing Figs. 6.34 and 6.35, for D_0=3.0m the storage tank gets dried at about 35 days after the first filling where as for D_0=5.0m drying time is about 215 days. The effect of the less pervious bottom layer comes into play, though the rate of infiltration

in the beginning of filling is more due to higher depth of water in the storage tank. The occurrences of isolated peaks are due to rainfall events.

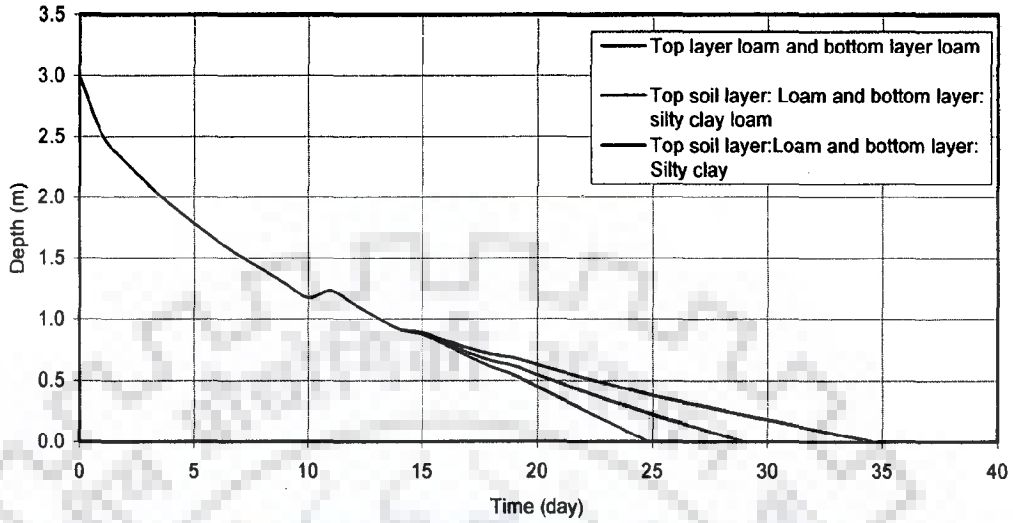

Fig.6.34 Variation of depth of water in the storage tank with time due to combined effect of infiltration, rainfall, runoff, evaporation , the tank bed is underlain by two different soil layers for D_0=3m,d_s=5m and d_w=10m

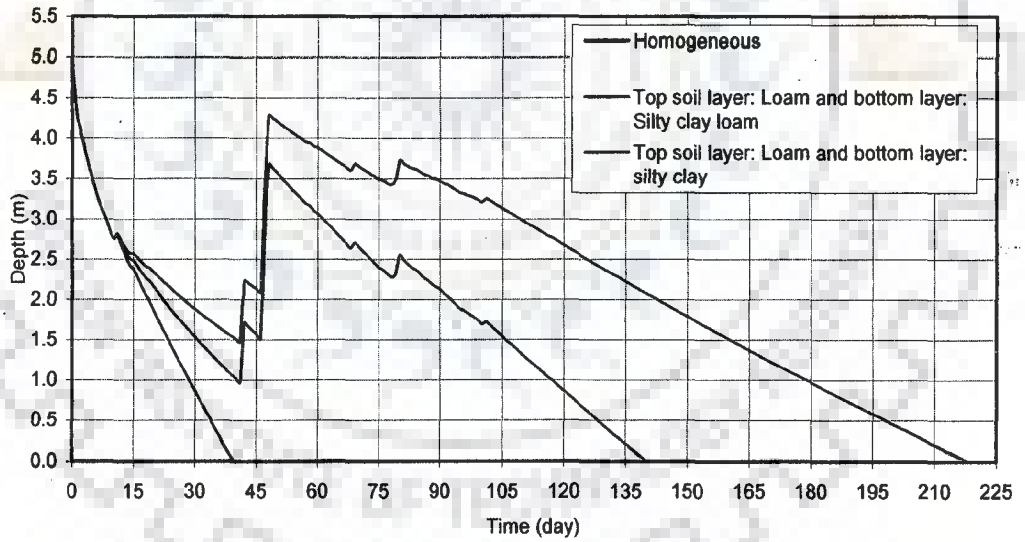

Fig.6.35 Variation of depth of water in the storage tank with time due to combined effect of infiltration, rainfall, runoff, evaporation , the tank bed is underlain by two different soil layers for D_0=5m,d_s=5m and d_w=10m

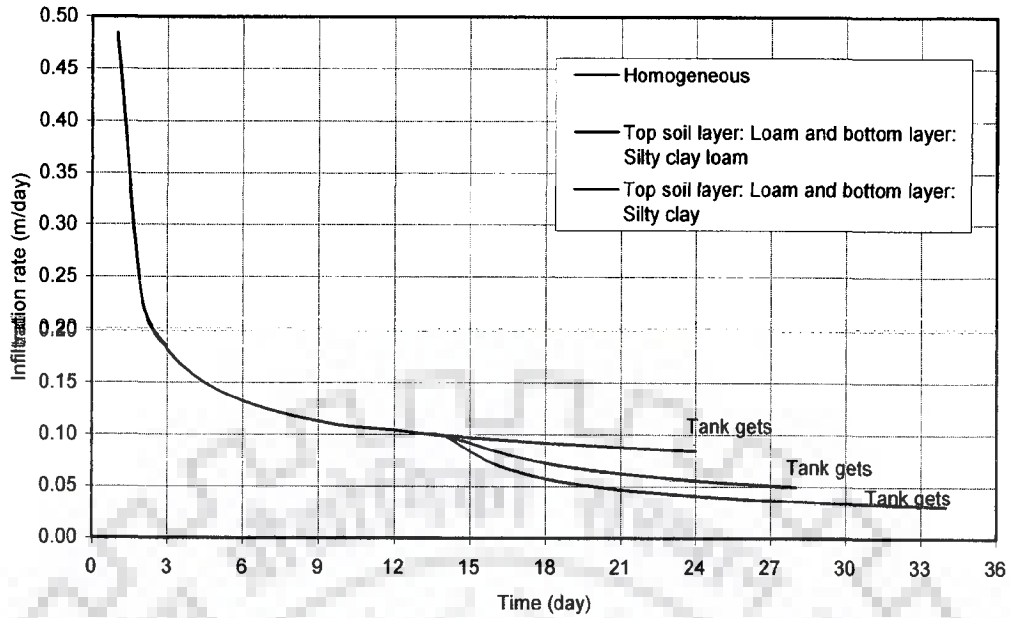

Fig.6.36 Variation of infiltration rate with time, tank bed is underlain by two different soil layers for D_0=3m, d_s=5m and d_w=10m

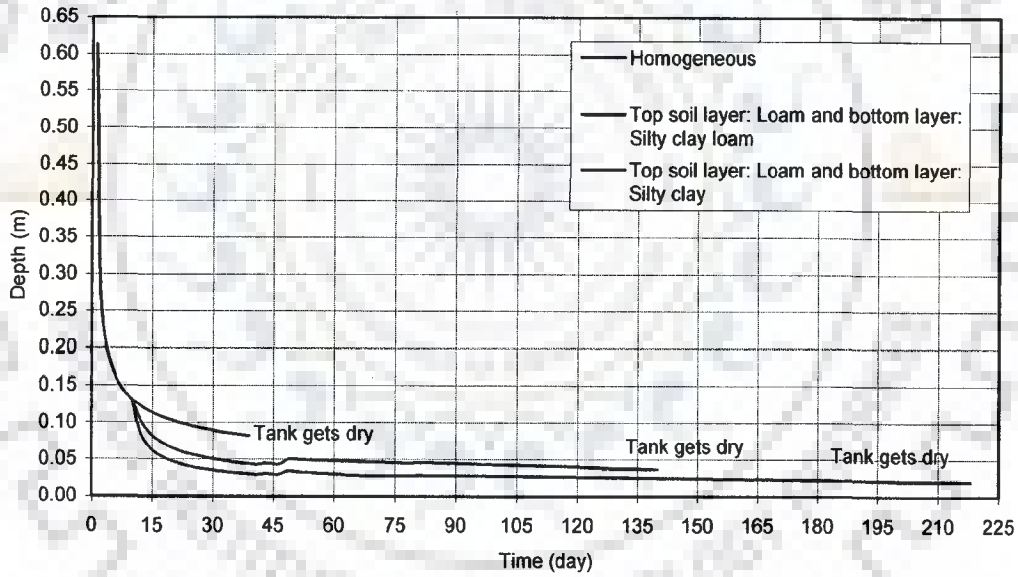

Fig.6.37 Variation of infiltration rate with time, tank bed is underlain by two different soil layers for D_0=5m, d_s=5m and d_w=10m

The variations of infiltration rate with time are presented in Figs. 6.36 and 6.37. Due to intermediate rainfall, there is minor change in the rate of infiltration. The infiltration rates are nearly uniform 45 days after the first filling. The water balance components for the second soil group are presented in Figs. 6.38 through 6.41.

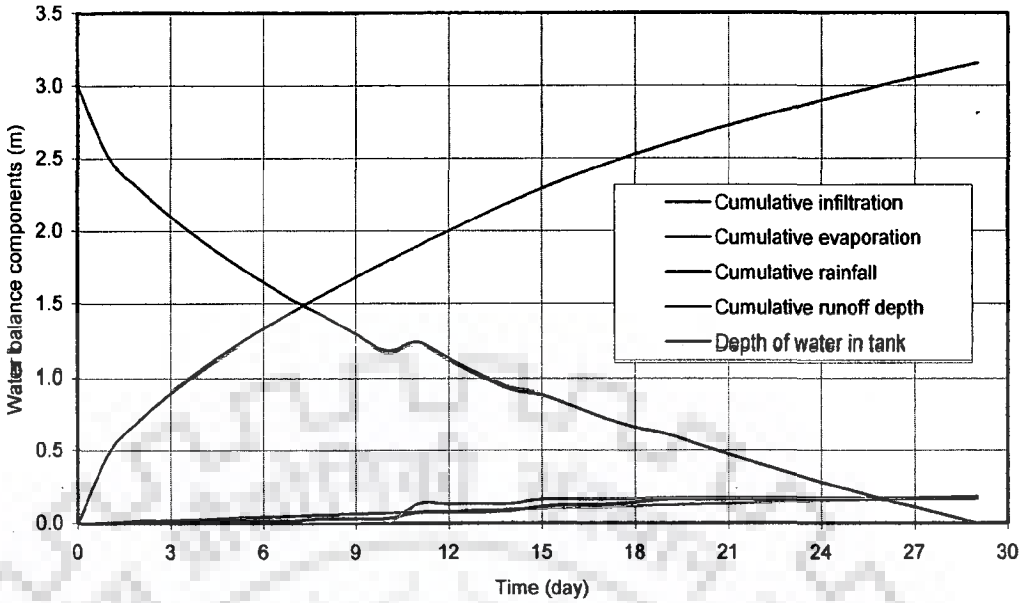

Fig.6.38 Water balance components (infiltration, evaporation, rainfall, runoff, depth of water in the tank), the tank bed is underlain by: top layer-loam and bottom layer-silty clay loam for D_0=3m, d_s=5m and d_w=10m

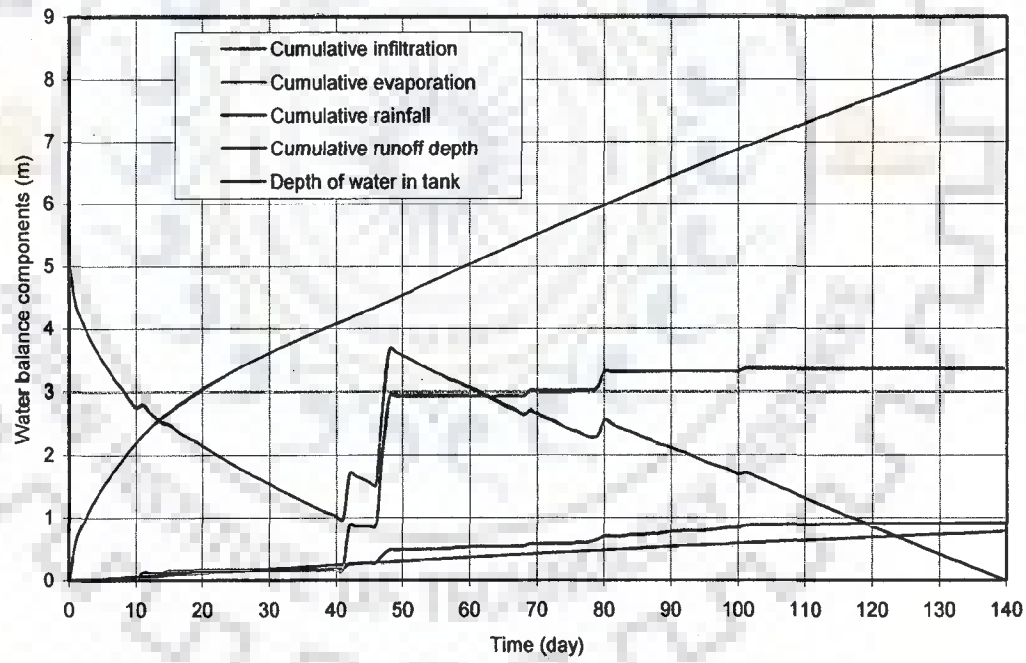

Fig.6.39 Water balance components (infiltration, evaporation, rainfall, runoff, depth of water in the tank), the tank is underlain by: top layer-loam and bottom layer-silty clay loam for D_0=5m, d_s=5m and d_w=10m

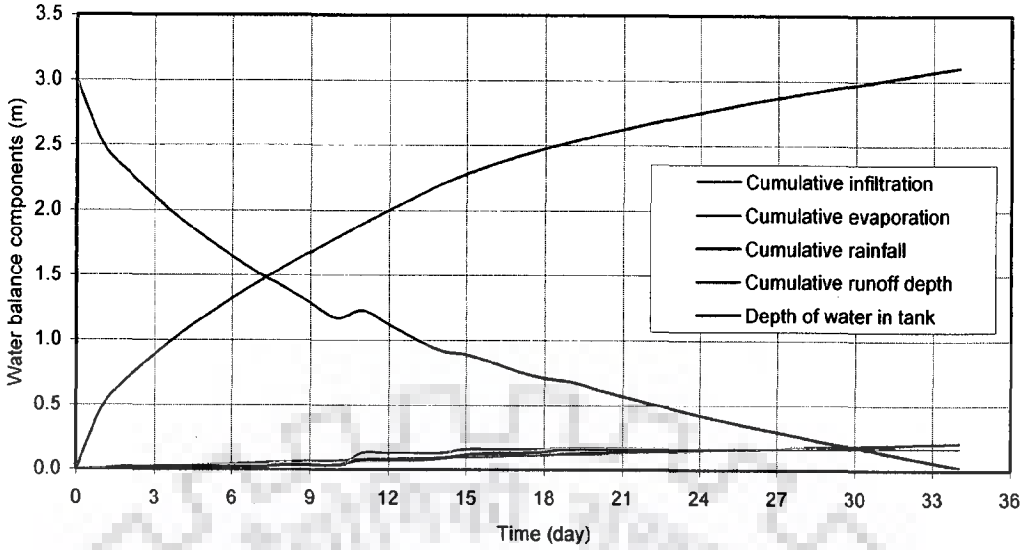

Fig. 6.40 Water balance component (infiltration, evaporation, rainfall, runoff, depth of water in tank), the tank bed is underlain by: top layer-loam and bottom layer-silty clay for D_0=3m, d_s=5m and d_w=10m

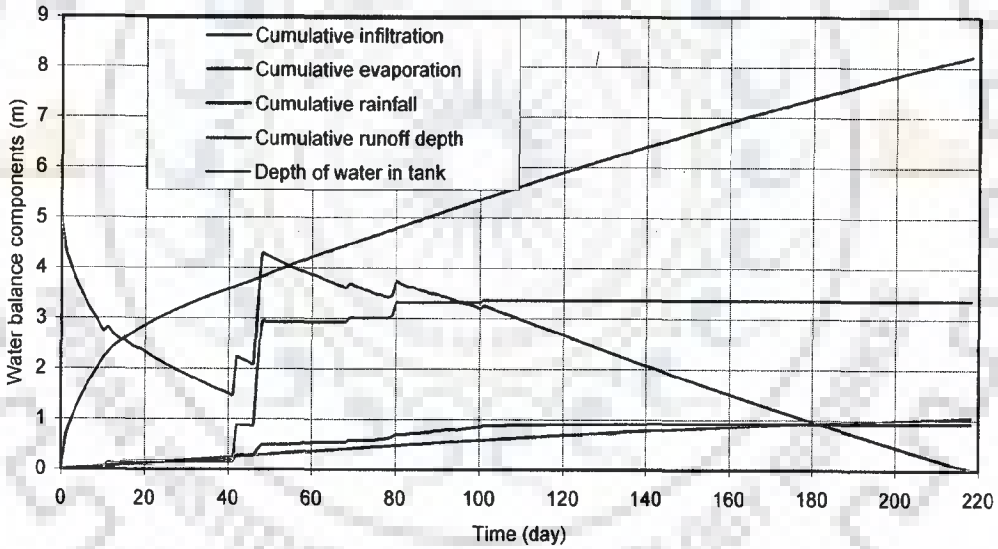

Fig. 6.41 Water balance component (infiltration, evaporation, rainfall, runoff, depth of water in tank), the tank bed is underlain by: top layer-loam and bottom layer-silty clay for D_0=5m, d_s=5m and d_w=10m

The error in the computation of water balance is presented in Fig. 6.42.

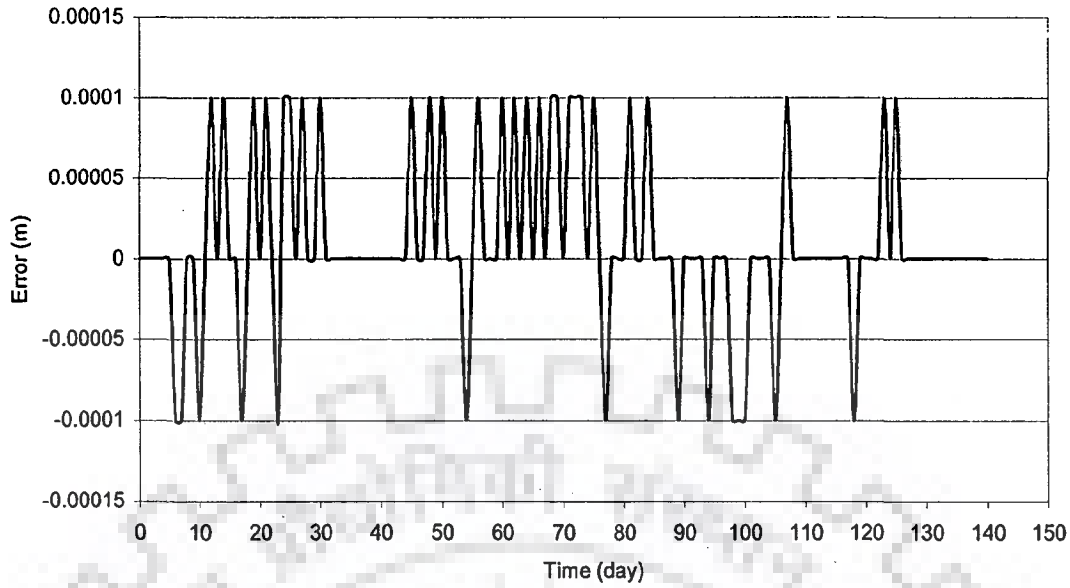

Fig.6.42 Error during computation of water balance, the tank bed is underlain by: top soil layer-loam and bottom layer-silty clay for D_0=5m, d_s=5m and d_w=10m

6.7.2.3 Third Soil Group: Top Soil Layer is Silty Clay Loam; Bottom Layer is either Silty Clay Loam or Silty clay

The variations in depth with time due to combined effect of infiltration, rainfall, runoff, evaporation are presented in Figs. 6.43 and 6.44 respectively for D_0=3.0m and D_0=5.0m. If the tank is underlain either by silty clay loam or silty clay water can be stored in the storage tank for irrigation purpose. However, for aquaculture, the tank should be refilled from surface water sources other than rainfall in order to maintain required depth of water for aquatic plants and pisciculture and recreation purposes.

The corresponding variation of infiltration rate with time is presented in Figs. 6.45 and 6.46. As seen from figures, infiltration rate is decreasing uniformly with time towards the end of the time when the tank gets dry. The rise of infiltration rate is due to intermediate rainfall events.

The water balance components (infiltration, evaporation, rainfall, runoff and depth of water in the tank) are presented in Figs. 6.47 and 6.48 for D_0 =3.0m and 5.0m.

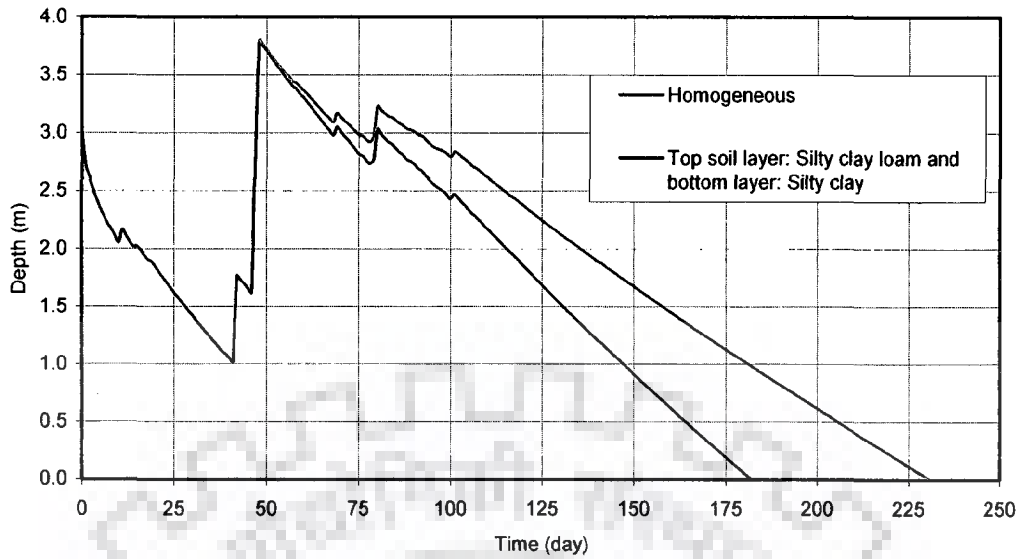

Fig.6.43 Variation of depth in the storage tank with time due to combined effect of infiltration, rainfall, runoff, evaporation, the tank bed is underlain by two different soil layers for D_0=3m, d_s=5m and d_w=10m

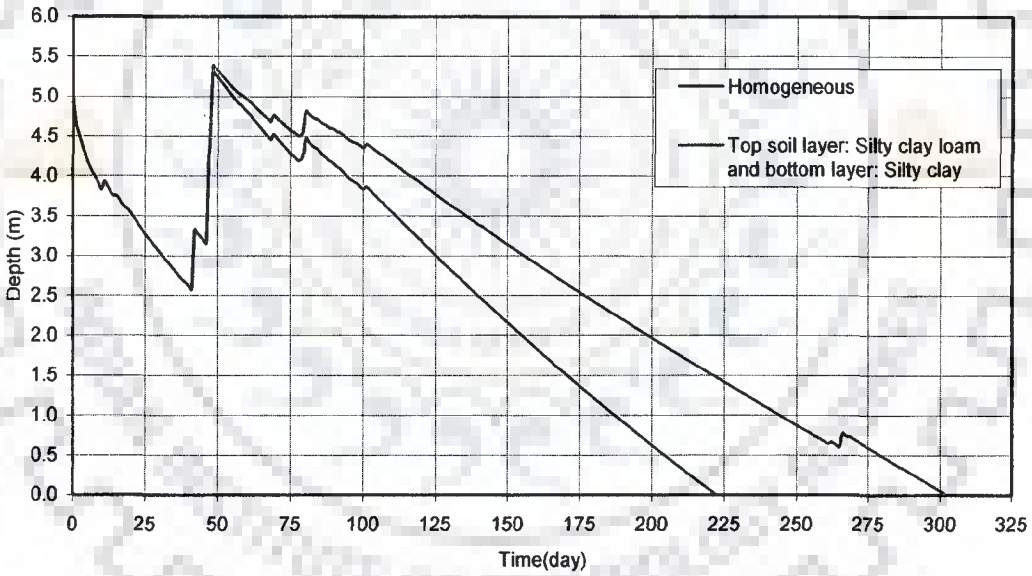

Fig.6.44 Variation of depth in the storage tank with time due to combined effect of infiltration, rainfall, runoff, evaporation , the tank bed is underlain by two different soil layers for D_0=5m, d_s=5m and d_w=10m

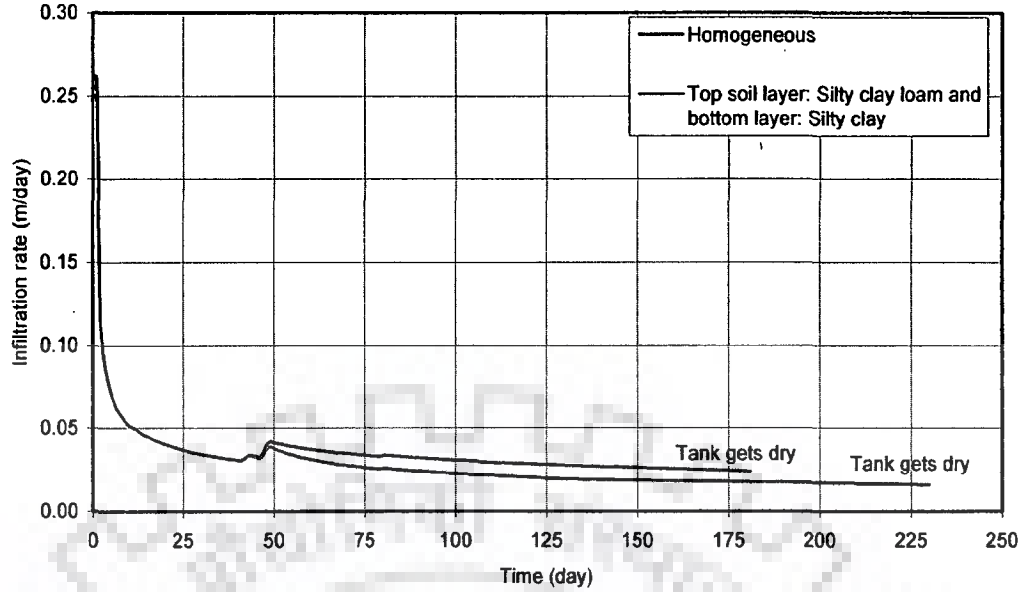

Fig. 6.45 Variation of infiltration rate with time, tank bed is underlain by two different soil layers for D_0=3m, d_s=5m and d_w=10m

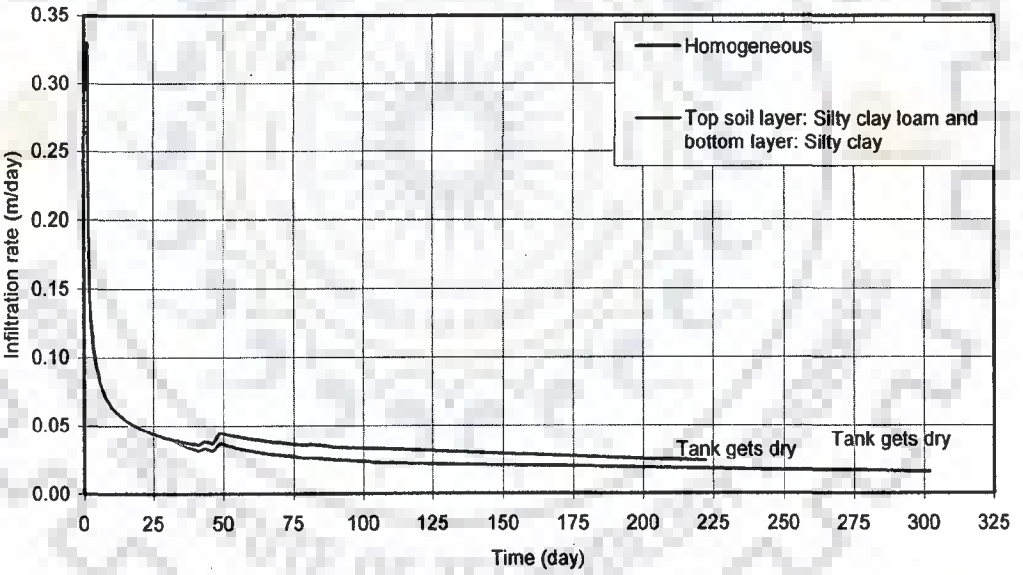

Fig. 6.46 Variation of infiltration rate with time, tank bed is underlain by two different soil layers for D_0=5m, d_s=5m and d_w=10m

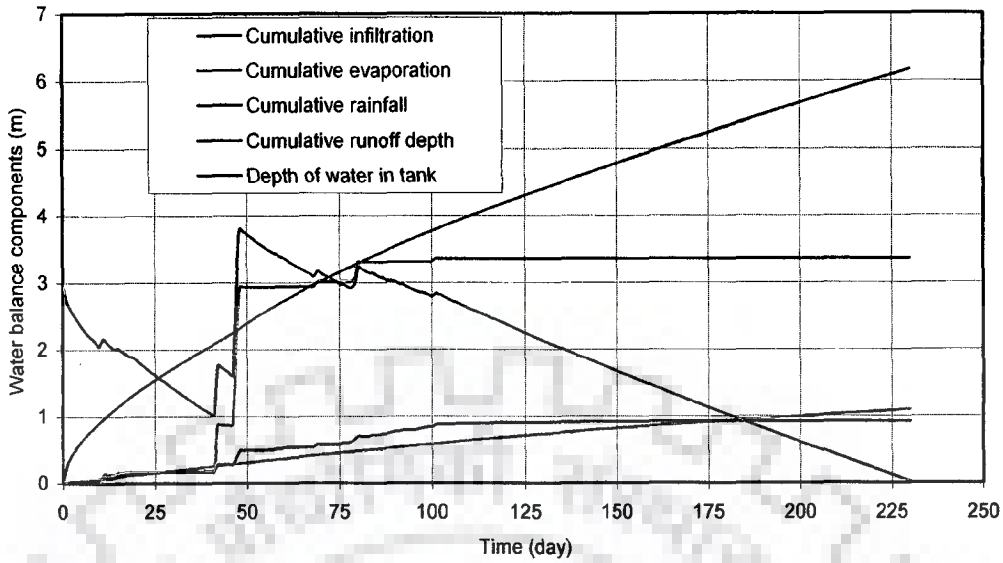

Fig.6.47 Water balance components (infiltration, rainfall, runoff, evaporation, depth of water in the tank), the tank bed is underlain by: top soil layer-silty clay loam and bottom layer-silty clay for D_0=3m, d_s=5m and d_w=10m

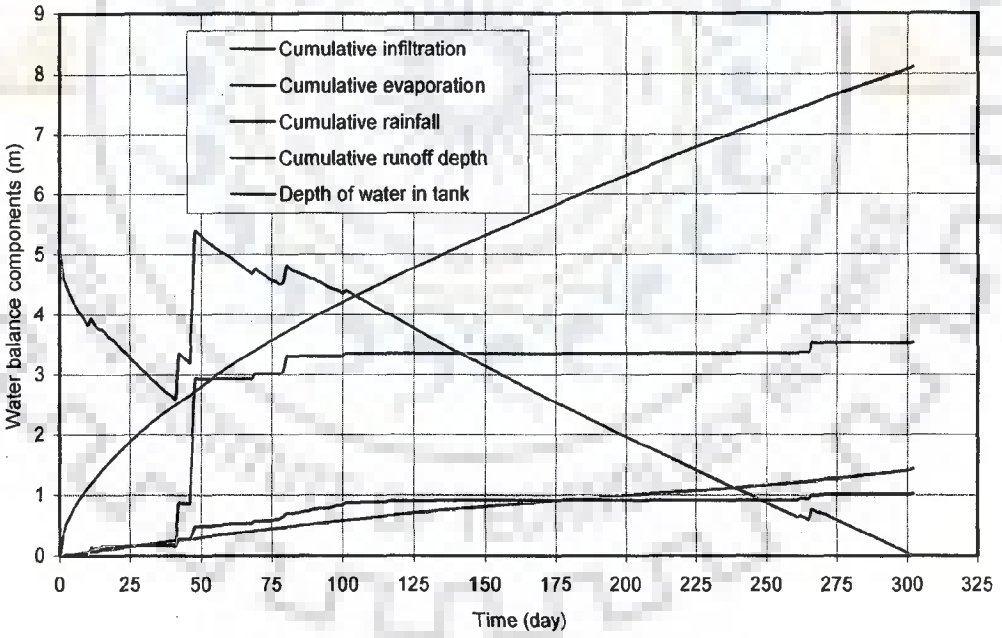

Fig.6.48 Water balance components (infiltration, rainfall, runoff, evaporation, depth of water in the tank), the tank bed is underlain by: top soil layer-silty clay loam and bottom layer-silty clay for D_0=5m, d_s=5m and d_w=10m

The error during computation of water balance is presented in Fig. 6.49.

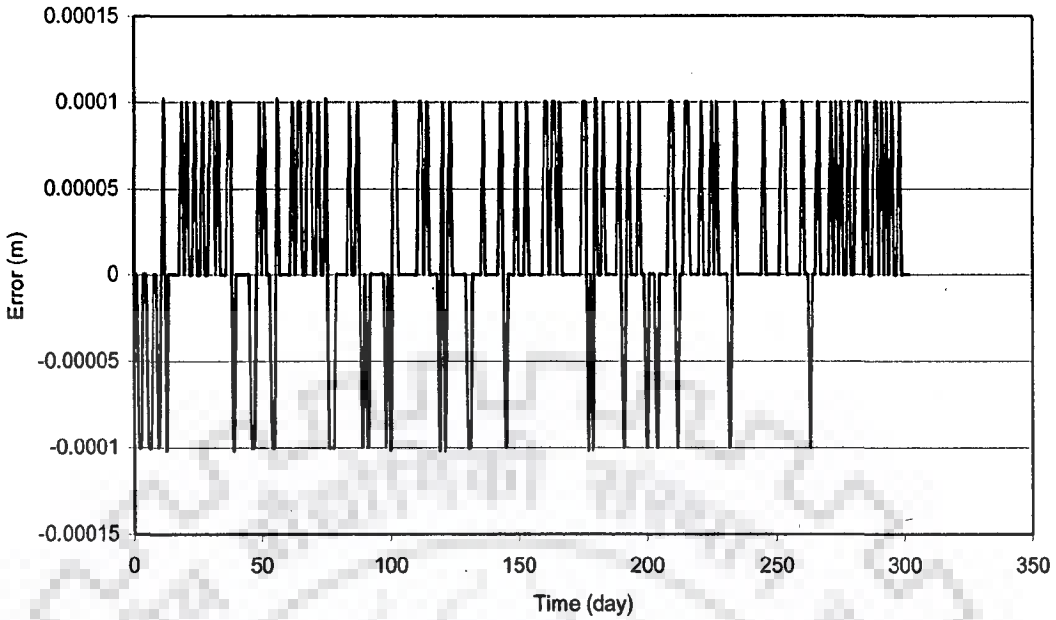

Fig.6.49 Error during computation of water balance, the tank bed is underlain by: top soil layer-silty clay loam and bottom layer-silty clay for D_0=5m, d_s=5m and d_w=10m

6.7.3 Case-III: Top Soil Layer has Lower Hydraulic Conductivity than that of the Bottom Layer

As described earlier when the upper soil layer is very less pervious compared to the bottom layer, the water percolates in the highly permeable bottom layer in an unsaturated state. Assuming that water percolates in the second layer at that moisture content at which the unsaturated hydraulic conductivity of the bottom layer is same as that of the saturated hydraulic conductivity of the top layer, the infiltration rates and the variation in depth of water in the storage tank due to combined effect of infiltration, rainfall, runoff, and evaporation are computed and presented in Figs. 6.50 and 6.51 respectively for $\tilde{k}_2 / \tilde{k}_1 = 21.8$, d_s=1.0m, D_0=3.0m. In Fig. 6.50, also the variation in infiltration rate without the above postulation is presented. As seen from the figure, the infiltration rate after the saturation front reaches interface increases rapidly prior to the occurrence of any rainfall event; this is in contradiction to the general behaviour of the exponentially decreasing rate of infiltration with time. With postulation, the

characteristic of the infiltration curve follows the accepted Horton's equation for infiltration. The postulated theory needs to be supported by experimental investigation.

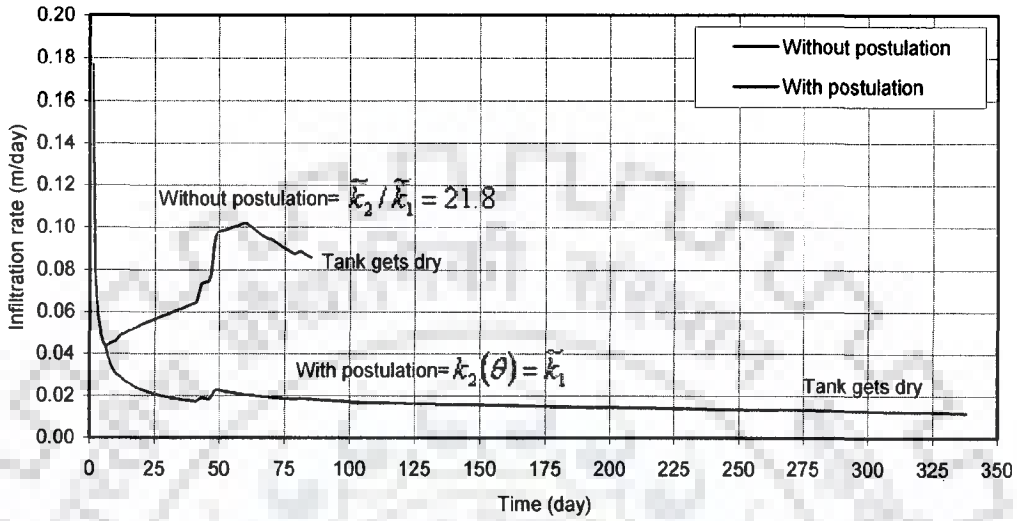

Fig. 6.50 Variation of infiltration rate with time the upper soil layer having lower saturated hydraulic conductivity than the lower layer for d_s=1m, D_0=3m and d_w=10m

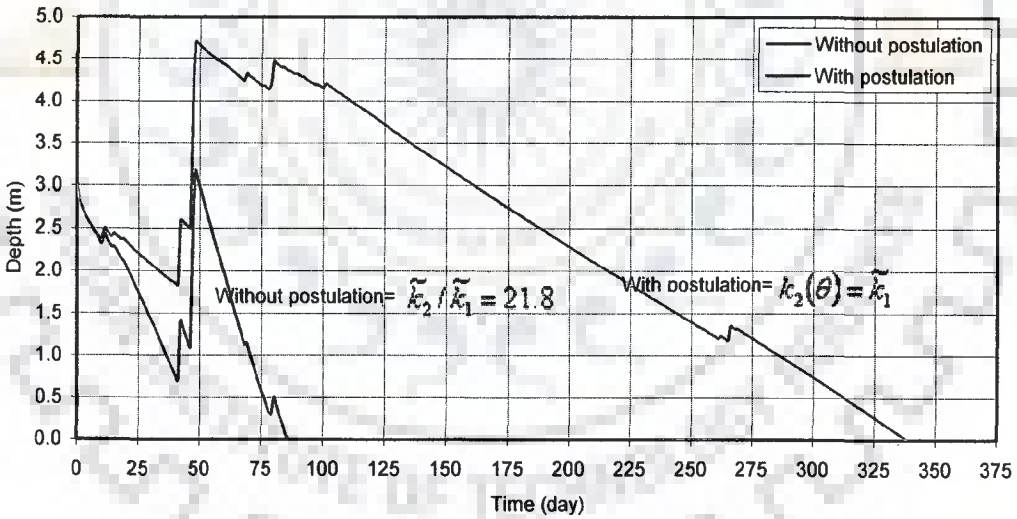

Fig.6.51 Variation of depth of water in the tank with time due to combined effect of infiltration, rainfall, runoff and evaporation , the upper soil layer having less saturated hydraulic conductivity than lower layer for d_s=1m, D_0=3m and d_w=10m

For another thickness of the top less pervious layer, the infiltration rates and depth of water with and without postulation are presented in Figs. 6.52 and 6.53. When the thickness of the top layer is more, the soil layer would tend to a homogeneous layer

as far as the infiltration rate is concerned. However, without postulation the infiltration curve does not strictly follow Horton's infiltration equation. With postulation the drying time can be ascertained realistically.

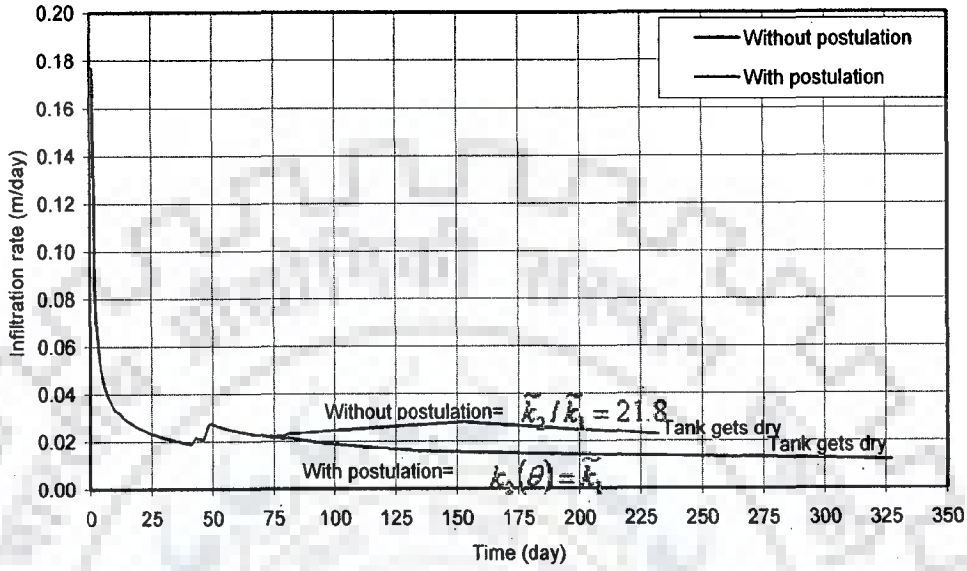

Fig.6.52 Variation of infiltration rate with time, the upper soil layer having less saturated hydraulic conductivity than lower layer for

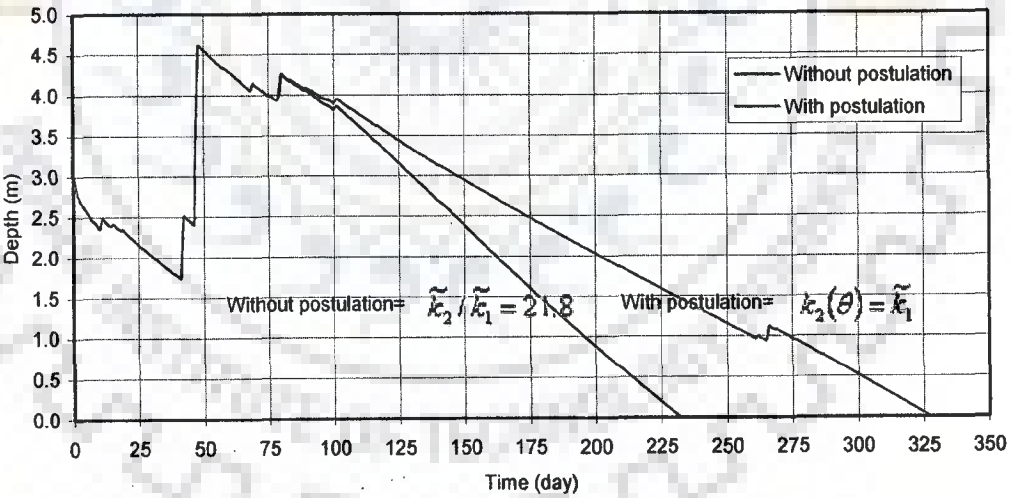

Fig.6.53 Variation of depth of water in the tank with time due to combined effect of infiltration, rainfall, runoff and evaporation, the upper soil layer having less saturated hydraulic conductivity than lower layer for d_s=5m and D_0=3m

For a very high ratio of $\tilde{k}_2/\tilde{k}_1 = 100$, the infiltration rate is presented in Fig. 6.54, for d_s =1.0m and D_0=3.0m, magnifies the in applicability of Green and Amp

postulation increases with time instead of decreasing. The corresponding variations in the depth of water in the tank with time are presented in Fig. 6.55.

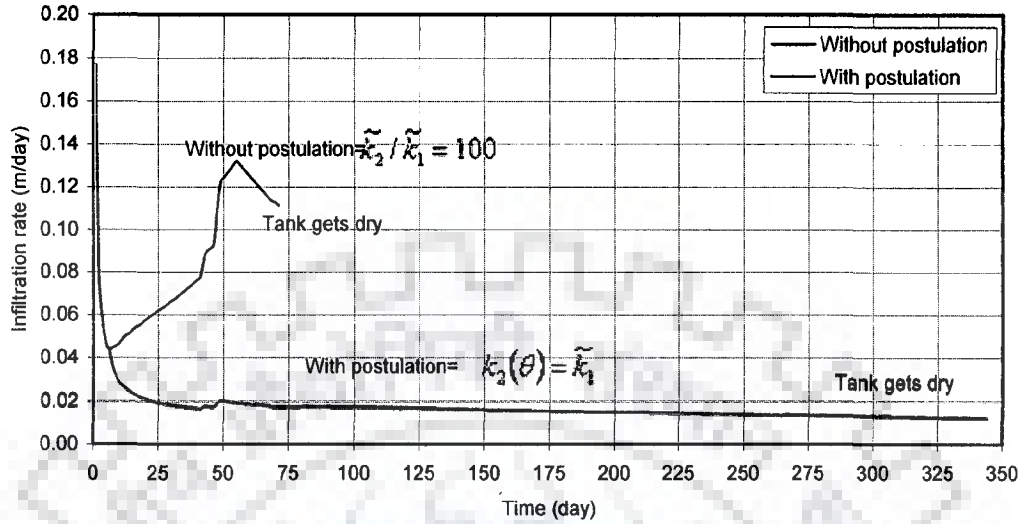

Fig.6.54 Variation of infiltration rate with time, the upper soil layer having lower saturated hydraulic conductivity than lower layer for hypothetical soil, for d_s=1m and D_0=3m

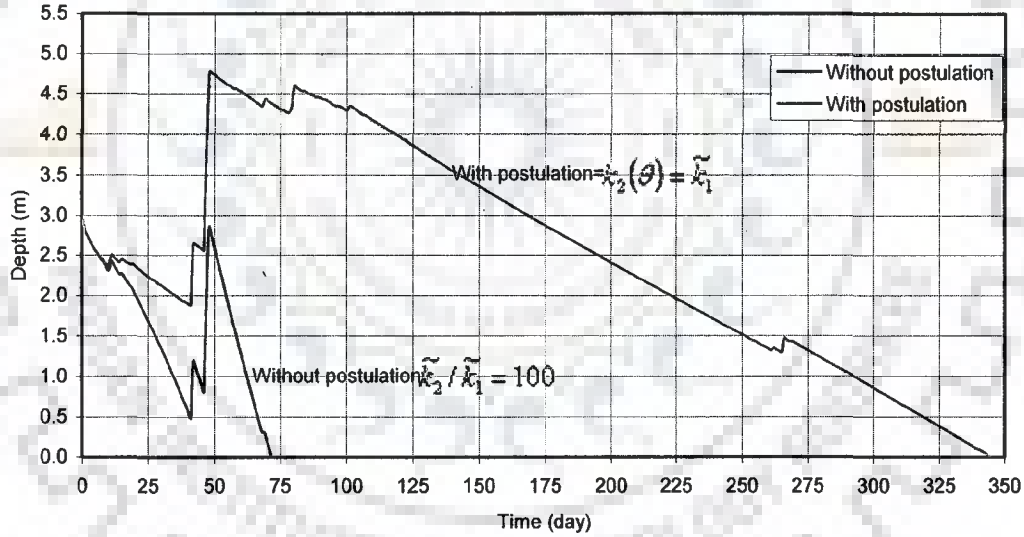

Fig.6.55 Variation of depth of water in the tank with time due to combined effect of infiltration, rainfall, runoff and evaporation , the upper soil layer having less hydraulic conductivity than lower layer, for a hypothetical soil, for d_s=1m and D_0=3m

As seen from Fig. 6.56 the variation of infiltration with time without postulation and with postulation is almost identical irrespective of the ratio of the hydraulic conductivity, for higher thickness of the upper soil layer. The corresponding variation in the depth of water is presented in Fig. 6.57.

conductivity, for higher thickness of the upper soil layer. The corresponding variation in the depth of water is presented in Fig. 6.57.

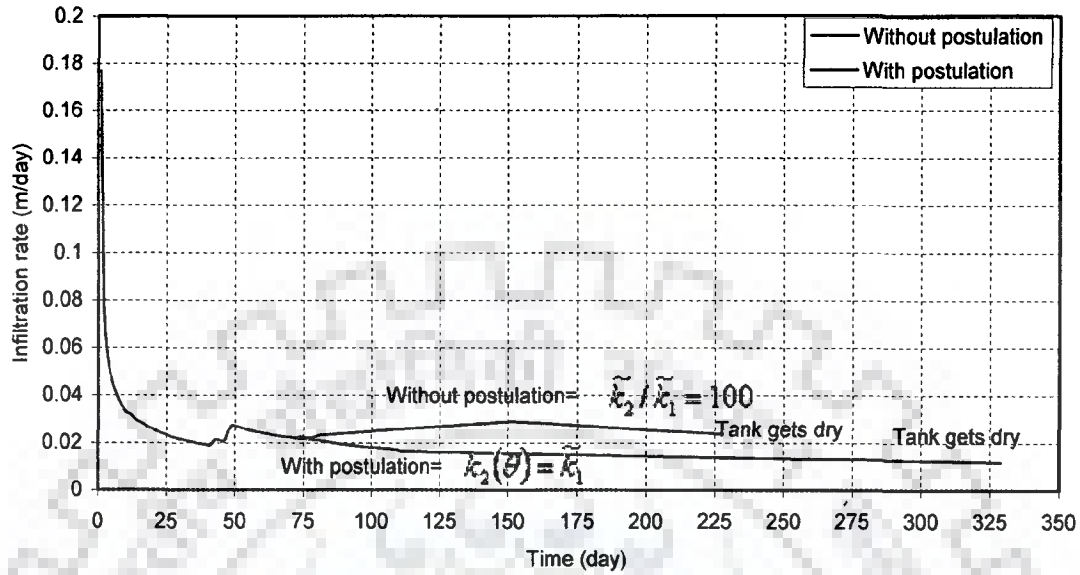

Fig.6.56 Variation of infiltration rate with time, the upper soil layer having less saturated hydraulic conductivity than lower layer for a hypothetical soil for d_s=5m , D_0=3m

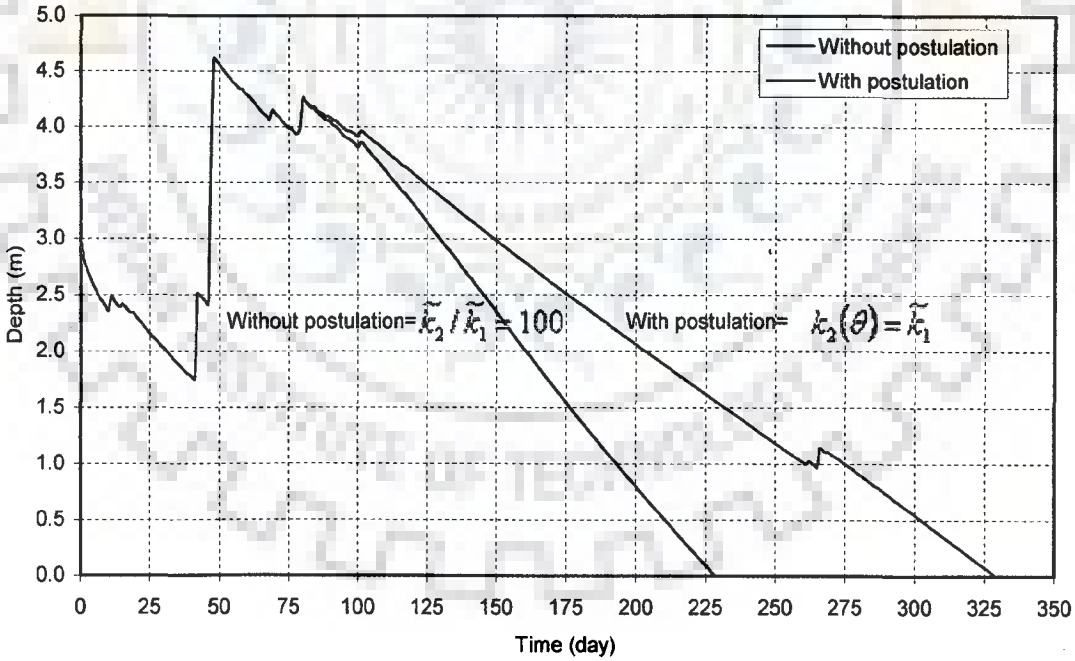

Fig.6.57 Variation of depth of water in the tank with time, the upper soil layer having less saturated hydraulic conductivity than lower layer for a hypothetical soil, for d_s=5m, D_0=3m

6.7.4 Drainage after the Storage Tank Gets Dry for the First Time

The temporal variations in depth of water have been presented in previous section until the storage tank gets dry for the first time after the initial filling. For example, as seen in Fig. 6.34, for D_0= 3.0 m, the tank gets dry before the occurrence of the first rainfall event in the year. However, for D_0=5.0m, the tank does not get dry before occurrence of several rainfall events. Incase of the tank, which gets dry before the occurrence of a rainfall event, drainage of the saturated soil column under the storage tank would occur after the drying of the tank. The movement of draining front is presented in Fig. 6.58 for the case, in which the tank bed is underlain by a single layer of sandy loam soil. When the tank gets dry at t= 114 hour, the saturation front had reached a depth of 4.7 m from the tank bed. Therefore, the depth to draining front is 4.7 m at t=114 hour. The rate of increase in draining depth decreases with time. The movement of the draining front is fast and later on becomes slow. At the end of t=985 hour the draining front reaches a depth of 6.8 m. The corresponding temporal variation of volumetric soil moisture content within the drained layer is presented in Fig. 6.59.

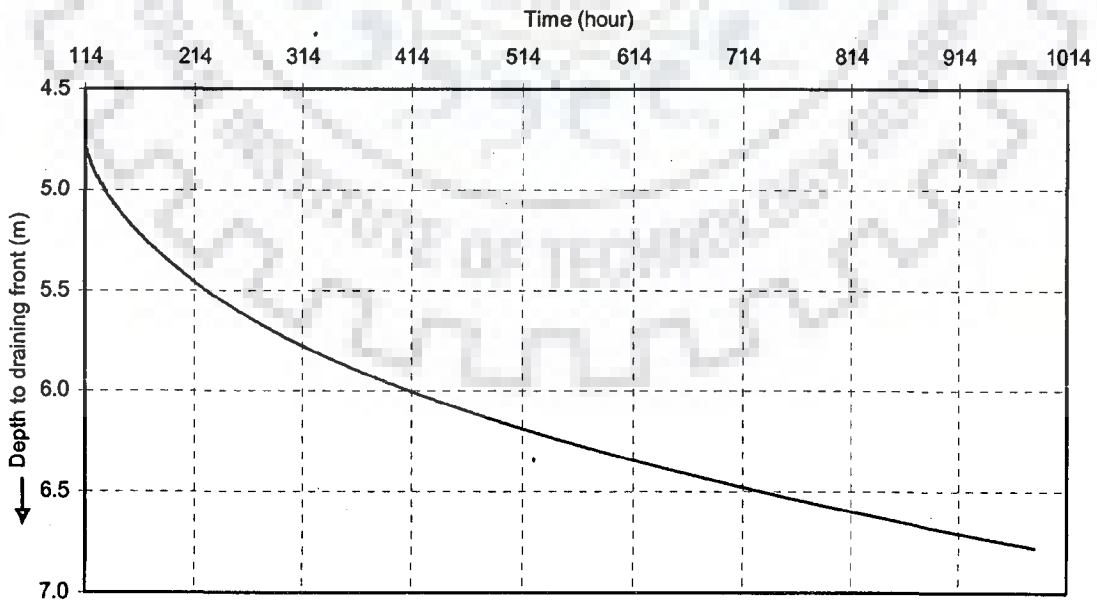

Fig.6.58 Depth to draining front during inter-storm period

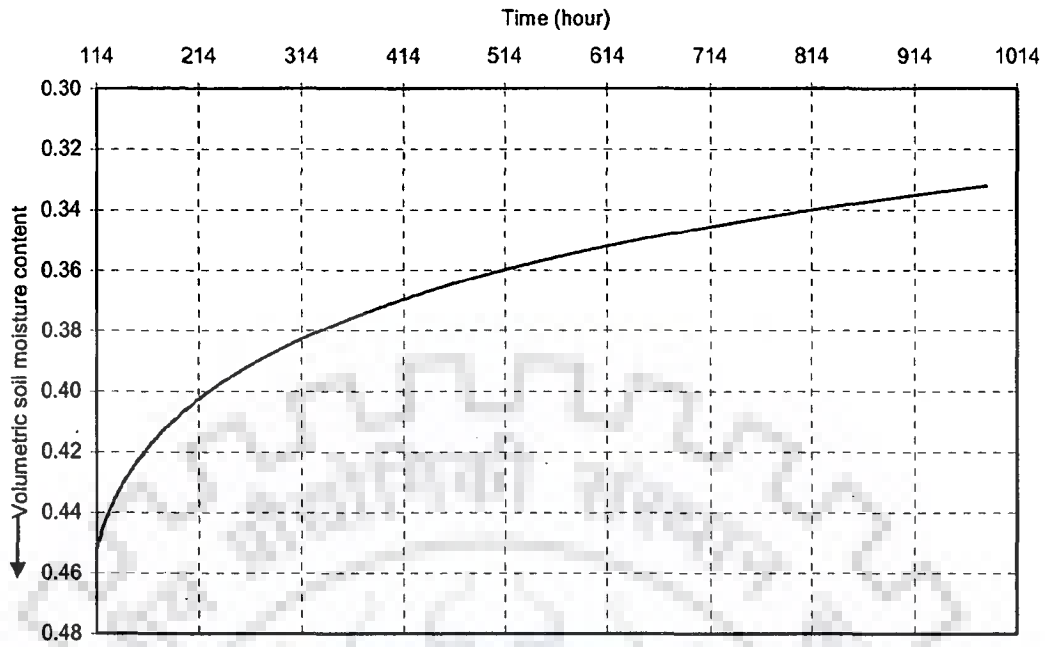

Fig. 6.59 Volumetric soil moisture content during inter-storm period

Again when the tank gets filled up for the second time at t=985 hour, a saturation front proceeds from the tank bed and there are simultaneous movement of the saturation front and the draining front. In Fig. 6.60, the temporal variations of depth to saturation front and depth to draining front are presented. The tank gets dry again at t= 1042 hour. After t=1042 hour the draining of the upper saturated layer would commence. The temporal variation in volumetric moisture content within the drained soil column is presented in Fig. 6.61.

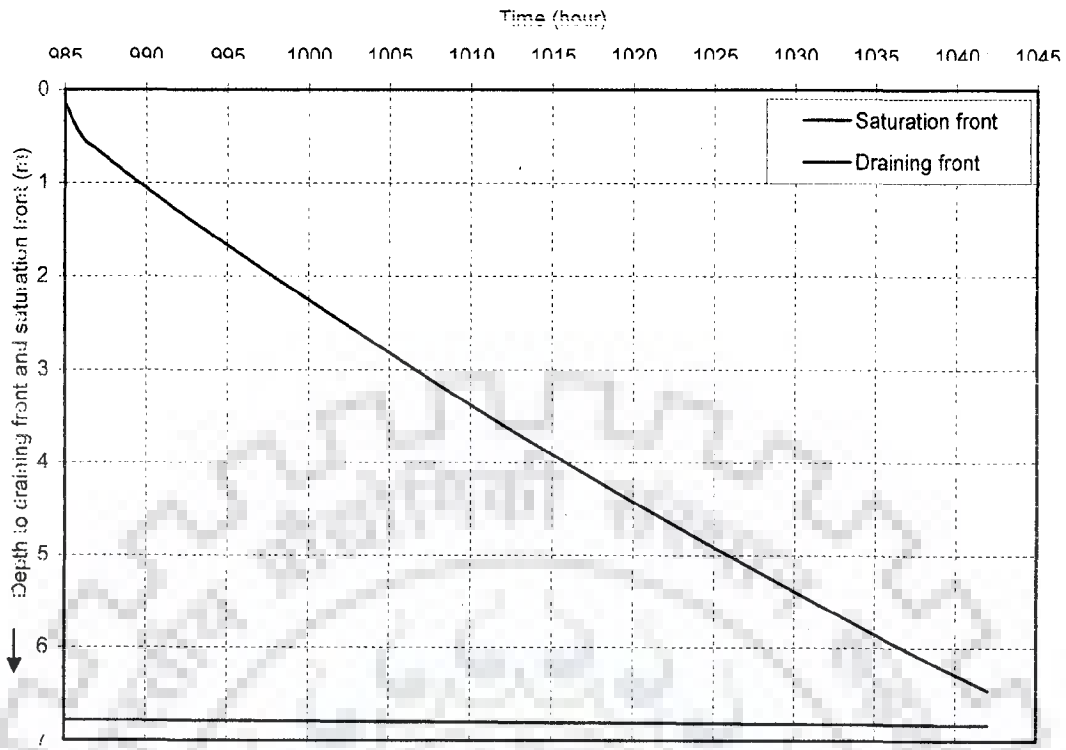

Fig. 6.60 Depth to draining front and saturation front after second filling

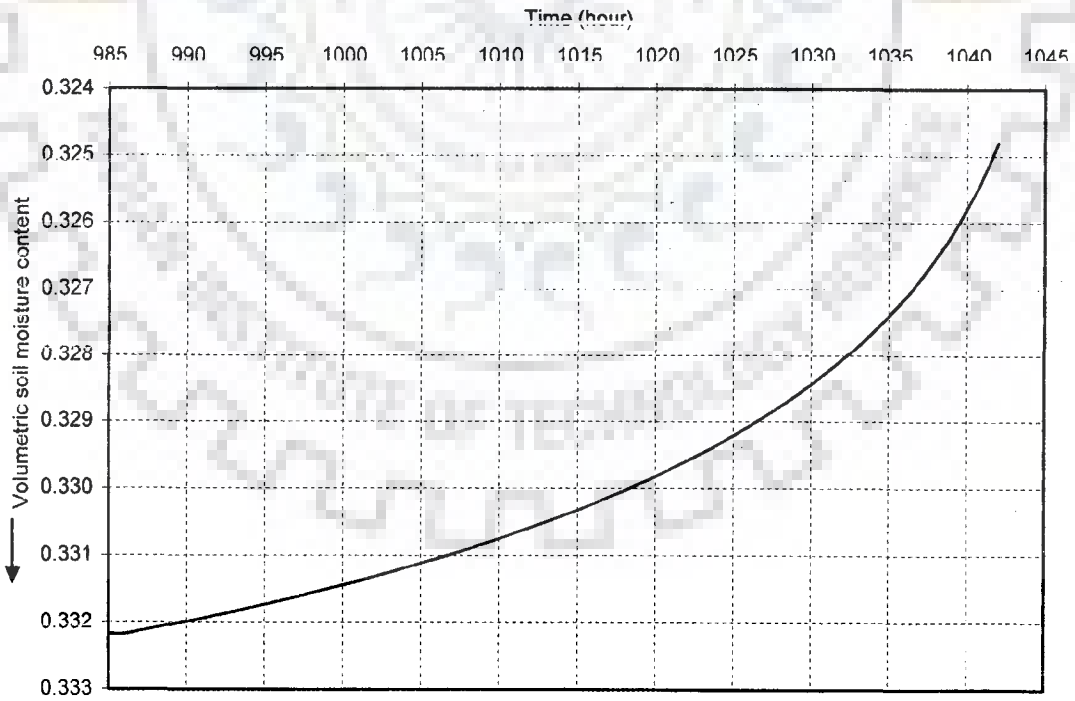

Fig. 6.61Variation of volumetric soil moisture content with time for draining soil column

The variation in the infiltration rate with time after the second filling is presented in Fig. 6.62. The rainfall and contribution from catchment continues from 985 hour to 1008 hour. The rainfall and runoff stops at 1008 hours. For this reason there is a change in the trend of temporal variation of infiltration. The water balance components are presented in Fig. 6.63. The components satisfy the mass balance equation.

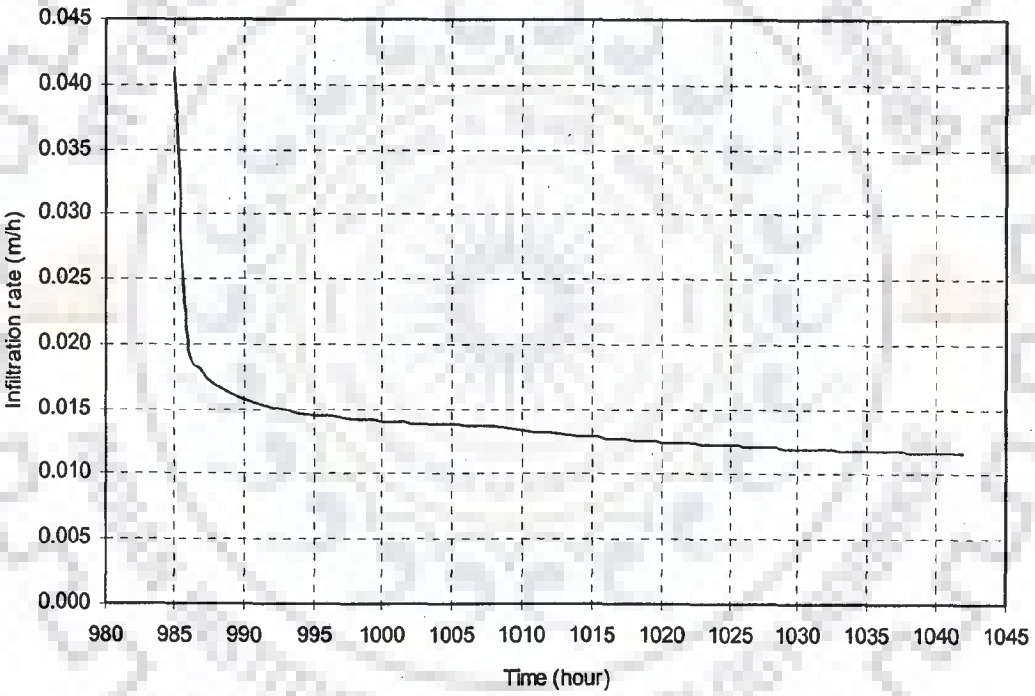

Fig.6. 62 Variation of infiltration rate with time after second filling

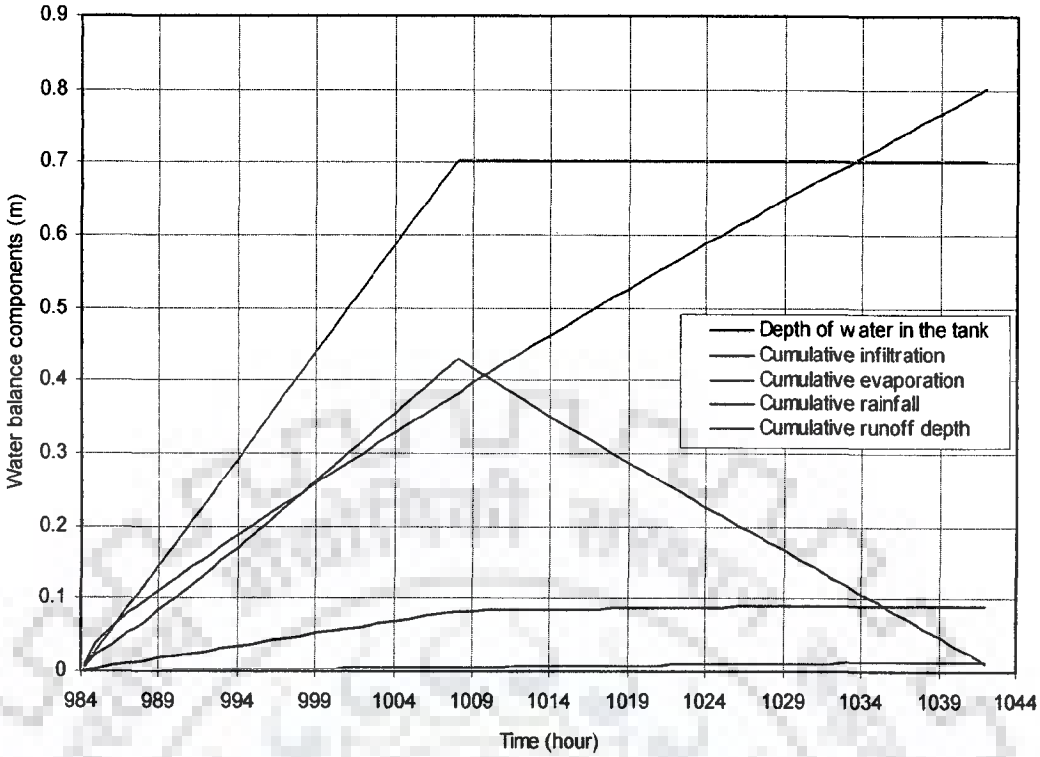

Fig. 6.63 Water balance components (depth of water in the tank, infiltration, evaporation, rainfall and runoff) of the tank, the tank bed is underlain by a homogeneous soil layer after second filling

6.8 CONCLUSIONS

Based on this study the following conclusions can be drawn:

1. Green and Ampt infiltration theory is inapplicable for computing infiltration from a storage tank underlain by a layered soil system if the upper soil layer is less permeable than the lower layer, as the simulated infiltration rate does not follow the decreasing trend of infiltration given by Horton's equation. With a postulation that water front moves in unsaturated state in the lower layer at a moisture content corresponding to which the unsaturated hydraulic conductivity of the lower layer is same as the saturated hydraulic conductivity of the upper layer, the simulated infiltration rate follows the

decreasing trend as given by Horton's infiltration equation. The proposed postulation needs experimental verification.

2. The storage tank besides storing water also acts as a groundwater recharging structure if the subsoil happens to be sandy loam and loam. Incase, the subsoil is silty clay and initial depth of filling is about 5.0m, depth of water in the storage tank at the end of about 300 days after the first filling is of the order of 0.5m. If the subsoil is of clay type water will be available in the storage tank through out the year.
3. The model proposed here is suitable for predicting water availability in a storage tank. The model integrates infiltration, evaporation, surface runoff and rainfall in the water balance computation.

CHAPTER-7

WATER AVAILIBLITY IN ASHA SAGAR STORAGE TANK- A CASE STUDY IN A DROUGHT PRONE AREA

7.1 INTRODUCTION

Asha Sagar storage tank is located in Bhawanipatna town in Kalahandi district, Orissa, India (between 19^0 8' N to 20^0 25' N latitude and 82^0 32' East to 83^0 47' East longitude). Kalahandi district is located in a severe drought prone area. The storage tank was constructed in 1880-81 by the then king of Kalahandi, his highness Udit Pratap Deo, in the name of his Queen Asha Manjari Devi for public use and irrigation (Indian express news, 2007). Physiographically Kalahandi district can be broadly divided into two different natural divisions namely the hilly tracts and the plain area. The climate of this district is extreme type climate. Summer season is intensely hot and winter is very cold. The average annual rainfall is 1378.3 mm. The variation in the annual rainfall from year to year is not very large (Sahu, 2006). Though the average annual rainfall is considerable, agricultural drought occurs because the rainfall is not evenly distributed during monsoon period. The drought effect can be mitigated by conserving the water in ponds and storage tanks to be used for irrigation purpose at the time of need. The climatic water balance of the region shows that water deficit is prevalent from November to May in almost all locations (WTCER, 2001). As canal irrigation and tube well irrigation are not feasible due to topographical, geological and hydrological constraints, rainwater harvesting and conservation have the potential to provide water for irrigation during water scarcity period (Bhatnagar et al., 1996; Srivastava and Panda, 1998; Srivastava, 1996a, b, 2001). In this present study, water availability in Asha Sagar storage tank is investigated. A rigorous hourly water balance has been carried out for a normal year of rainfall considering losses due to infiltration, evaporation and spill and inflow from the contributing catchment and direct rainfall.

7.2 THE ASHA SAGAR STORAGE TANK

The water surface area of the Asha Sagar storage tank, obtained from topographical map, is 37.5 ha. The dead storage level (D.S.L) in the storage tank is 30.175m; the full reservoir level which is the crest level of an existing broad crested spillway is 31.7m; the maximum permissible water level in the storage tank is 32.615m and the top bund level is 33.83m. The height of spillway above dead storage level is 1.525m.The depth to ground water prior to monsoon period is about 5m. The catchment, which contributes runoff to the tank, has an area of 900 ha. The meteorological data pertaining to the storage tank for a water year are collected from Krishi Vigyan Kendra (KVK), Bhawanipatna, under Orissa University of Agricultural and Technology (O.U.A.T.).

The satellite image downloaded from Google Earth for Asha Sagar storage tank is shown in Fig. 7.1. There are three prominent land use pattern in the catchment, these are: agriculture, forest and settlement. The drainage and the land use pattern of the cachment are shown in Figs. 7.2 and 7.3 respectively. Based on the basic infiltration rate 6.0 cm /hr (Srivastava et al., 2004), the soils in the study area are classified as 'Hydrological soil group A'. The weighted curve number for AMC-II condition for the study area is found to be 75.

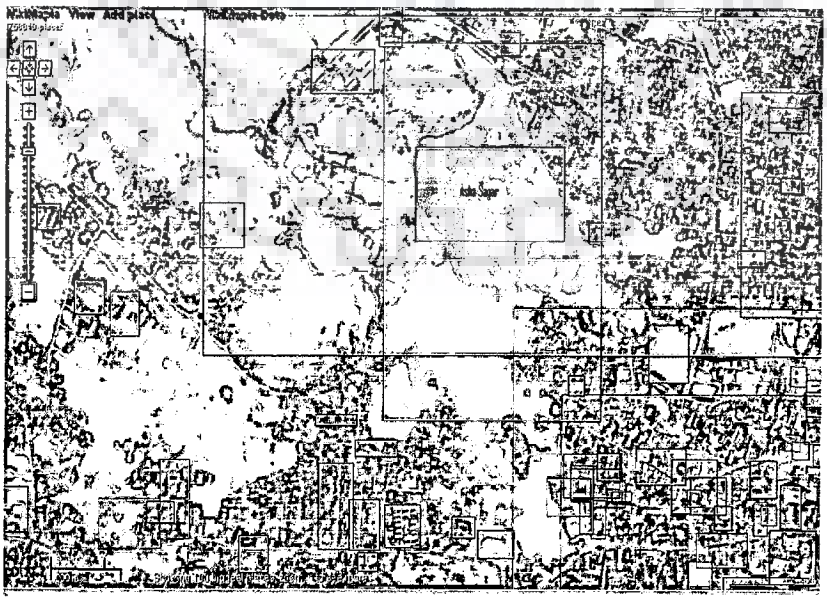

Fig. 7.1 Satellite image of Asha Sagar storage tank

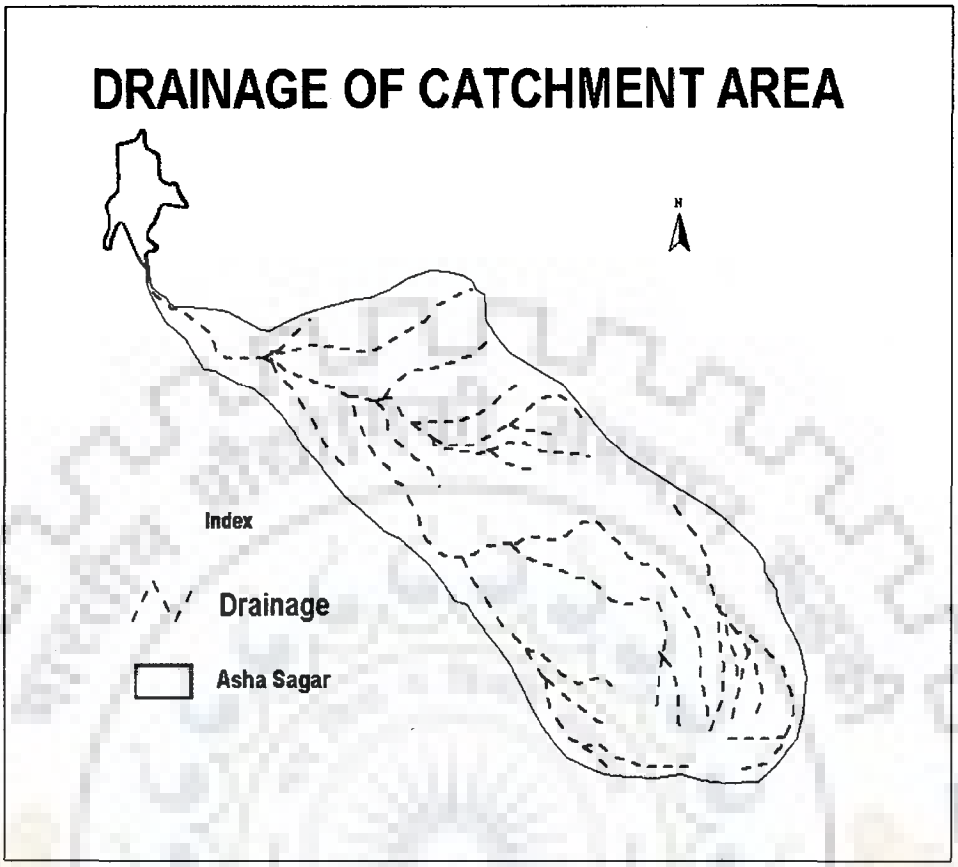

Fig. 7.2 Drainage of catchment area

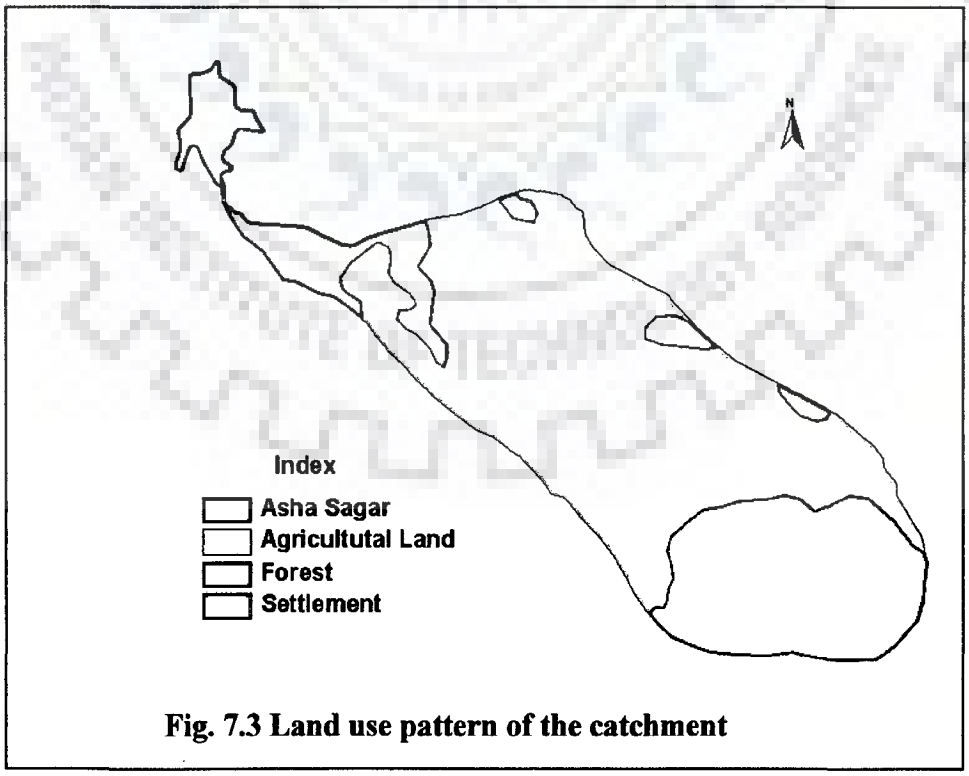

Fig. 7.3 Land use pattern of the catchment

7.3 ANALYSIS

7.3.1 Infiltration from the Tank Bed

The water depth in the storage tank, $D_w(t)$, at any time, t, since onset of the first filling, owing to evaporation, rainfall, runoff, seepage and outflow through spillway taking place simultaneously, is given by:

$$D_w(t) = D_0 + \int_0^t P(\tau)d\tau + \frac{A_c}{A_{\tan k}}\int_0^t Q(\tau)d\tau - W(t) - \int_0^t E(\tau)d\tau - \int_0^t O(\tau)d\tau \qquad (7.1a)$$

or $$D_w(t) = D_0 + \int_0^t A(\tau)d\tau - W(t) - \int_0^t E(\tau)d\tau - \int_0^t O(\tau)d\tau \qquad (7.1b)$$

where

$$A(\tau) = P(\tau) + \frac{A_c}{A_{\tan k}}Q(\tau)$$

$O(\tau)$ = reduction in depth of water in the storage tank due to outflow through spillway,

A_{tank} = area of the tank,

A_c = area of the catchment.

Following the derivation of (6.3) from chapter-VI:

$$\frac{dW}{dt} = \tilde{k}_1 \frac{(\theta_{s1}-\theta_{i1})\left[h_{f1} + D_0 + \int_0^t A(\tau)d\tau - \int_0^t E(\tau)d\tau - \int_0^t O(\tau)d\tau\right] + \{1-(\theta_{s1}-\theta_{i1})\}W(t)}{W(t)} \qquad (7.2)$$

Let the time domain be discretised by uniform time step of size Δt duration.

$$\frac{dW}{dt} = \tilde{k}_1 \frac{(\theta_{s1}-\theta_{i1})\left[h_{f1} + D_0 + \Delta t\sum_{i=1}^{n-1}\bar{A}(i) + \bar{A}(n)\int_{(n-1)\Delta t}^{t} d\tau - \Delta t\sum_{i=1}^{n-1}\bar{E}(i) - \bar{E}(n)\int_{(n-1)\Delta t}^{t} d\tau - \Delta t\sum_{i=1}^{n-1}\bar{O}(i) - \bar{O}(n)\int_{(n-1)\Delta t}^{t} d\tau\right] + \{1-(\theta_{s1}-\theta_{i1})\}W(t)}{W(t)} \qquad (7.3)$$

The finite difference form of equation (7.3) at $t=n\Delta t$ is given by:

$$W(n\Delta t) - W\{(n-1)\Delta t\} =$$

$$\tilde{k}_1\Delta t \frac{(\theta_{s1}-\theta_{i1})\left[h_{f1} + D_0 + \Delta t\sum_{i=1}^{n}\bar{A}(i) - \Delta t\sum_{i=1}^{n}\bar{E}(i) - \Delta t\sum_{i=1}^{n}\bar{O}(i)\right] + \{1-(\theta_{s1}-\theta_{i1})\}W(n\Delta t)}{W(n\Delta t)} \qquad (7.4)$$

$W(n\Delta t)$ is to be solved in succession starting from $n=1$. Assuming that the $D_w(i)$ is constant during i^{th} time step but varies from step to step, the equivalent outflow depth

due to spill from the storage tank during i^{th} time step, $\overline{O}(i)$, is computed using Doerngsfeld and Barker equation (Chow, 1959)

$$\overline{O}(i)=0.433\sqrt{2g}\left\{\frac{D_w(i)}{D_w(i)+H_{sp}}\right\}^{0.5}\left\{D_w(i)-H_{sp}\right\}^{1.5}\times W_{sp}/A_{\tan k} \tag{7.5}$$

where

$D_w(i)$ = depth of water in the storage tank during i^{th} time step,

g = acceleration due to gravity (m per unit time step square),

H_{sp} = height of crest from dead storage level,

W_{sp} = width of the broad crested spill way.

Because, $D_w(n)$ and $W(n)$ are implicitly related and also $O(n)$ and $D_w(n)$ are implicitly related, we compute $O(n)$ using $D_w(n-1)$ value.

Solving the quadratic equation and considering the positive root

$$W(n\Delta t)=\frac{\left[W\{(n-1)\Delta t\}+\tilde{k}_1\Delta t\{1-(\theta_{s1}-\theta_{i1})\}\right]}{2}+\frac{\sqrt{\left[W\{(n-1)\Delta t\}+\tilde{k}_1\Delta t\{1-(\theta_{s1}-\theta_{i1})\}\right]^2+4\tilde{k}_1\Delta t(\theta_{s1}-\theta_{i1})\left(h_{f1}+D_0+\Delta t\sum_{i=1}^{n}A(i)-\Delta t\sum_{i=1}^{n}E(i)-\Delta t\sum_{i=1}^{n}O(i)\right)}}{2} \tag{7.6}$$

By the time the saturation front reaches the water table, the cumulative infiltration, $W(t_w)$, is $(\theta_{s1}-\theta_{i1})d_w$. Let $W(n^\circ)$ be the quantity that has infiltrated at the n^{oth} day when the saturation front is just behind the interface. $W(n^\circ)$ and n° are known a priori from (7.6) by comparing $W(n^\circ)$ with $(\theta_{s1}-\theta_{i1})d_w$. Making use of (7.3), the time Δt_1 that will be required for the cumulative infiltration to attain $W(t_w)=[(\theta_{s1}-\theta_{i1})d_w]$ is given by:

$$\frac{(\theta_{s1}-\theta_{i1})d_w-W(n^\circ)}{\Delta t_1}=\tilde{k}_1\frac{(\theta_{s1}-\theta_{i1})\left(h_{f1}+D_0-\sum_{i=1}^{n^\circ}\left\{\overline{E}(i)+\overline{O}(i)-\overline{A}(i)\right\}-\Delta t_1\left\{\overline{E}(n^\circ+1)+\overline{O}(n^\circ+1)-\overline{A}(n^\circ+1)\right\}\right)+\{1-(\theta_{s1}-\theta_{i1})\}(\theta_{s1}-\theta_{i1})d_w}{(\theta_{s1}-\theta_{i1})d_w} \tag{7.7}$$

Equation (77) is a quadratic equation in Δt_1. Solving the quadratic equation and considering the negative root,

$$\Delta t_1 = \frac{-b - \sqrt{b^2 - 4ac}}{2a} \tag{7.7a}$$

With positive root Δt_1 becomes more than Δt which is not true.

If both evaporation and precipitation are zero then

$$\Delta t_1 = -\frac{c}{b} \tag{7.7b}$$

where

$$a = \tilde{k}_1 \frac{\left\{\overline{E}(n^\circ + 1) + \overline{O}(n^\circ + 1) - \overline{A}(n^\circ + 1)\right\}}{d_w}$$

$$b = -\tilde{k}_1 \frac{\left(h_{f1} + D_0 - \sum_{i=1}^{n^\circ} \left\{\overline{E}(i) + \overline{O}(i) - \overline{A}(i)\right\}\right) + \left\{1 - (\theta_{s1} - \theta_{i1})\right\} d_w}{d_w}$$

$$c = (\theta_{s1} - \theta_{i1}) d_w - W(n^\circ)$$

7.3.2 Seepage after Saturation Front Reaches the Water Table

It is assumed that the water table variation is insignificant consequent to recharge taking place from the tank. At the water table the pressure is atmospheric. Hence, the hydraulic head difference between tank bed (at point 1) and water table (at point 5) as described in chapter-VI is $h_s(t)$, the seepage head, which causes flow. At time $t = t_w$ the seepage head is:

$$h_s(t_w) = D_0 - (\theta_{s1} - \theta_{i1}) d_s - \int_0^{t_w} E(t)dt - \int_0^{t_w} O(t)dt + \int_0^{t_w} A(t)dt + d_w \tag{7.8}$$

The seepage head will decrease because of recharge to the groundwater table and due to evaporation and outflow and would increase due to precipitation and runoff. Hence, the variation in seepage head will be given by:

$$-\frac{dh_s}{dt} = \tilde{k}_1 \frac{h_s(t)}{d_w} + E(t) + O(t) - A(t) \tag{7.9}$$

or

$$\frac{dh_s}{Ch_s(t) + E(t) + O(t) - A(t)} = -dt \tag{7.10}$$

where $C = \frac{\tilde{k}_1}{d_w}$

Let the time domain be discretised with time step Δt. Let the evaporation rate and precipitation rate be separate constant, but vary from time step to time step.

For $(t_w - \Delta t_1) \le t \le (n^\circ + 1)\Delta t$, $E(t) = E(n^\circ + 1)$, $A(t) = A(n^\circ + 1)$, $O(t) = O(n^\circ + 1)$

Incorporating $E(t), A(t)$ *and* $O(t)$ in (7.10)

$$\frac{dh_s}{Ch_s(t) + E(n^\circ + 1) + O(n^\circ + 1) - A(n^\circ + 1)} = -dt \tag{7.11}$$

Integrating and incorporating the limits

$$\int_{D_0 - W(t_w) - \sum_{i=1}^{n^\circ}\{E(i) + O(i) - A(i)\} - \{E(n^\circ+1) + O(n^\circ+1) - A(n^\circ+1)\}\Delta t_1 + d_w}^{h_s(n^\circ+1)} \frac{C\,dh_s}{Ch_s(t) + E(n^\circ + 1) + O(n^\circ + 1) - A(n^\circ + 1)}$$

$$= -C \int_{n^\circ \Delta t + \Delta t_1}^{(n^\circ+1)\Delta t} dt = -C(\Delta t - \Delta t_1) \tag{7.12}$$

or

$$\ln \frac{Ch_s(n^\circ + 1) + E(n^\circ + 1) + O(n^\circ + 1) - A(n^\circ + 1)}{C\left[D_0 - W(t_w) - \sum_{i=1}^{n^\circ}\{E(i) + O(i) - A(i)\} - \{E(n^\circ + 1) + O(n^\circ + 1) - A(n^\circ + 1)\}\Delta t_1 + d_w\right] + E(n^\circ + 1) + O(n^\circ + 1) - A(n^\circ + 1)}$$

$$= -C(\Delta t - \Delta t_1) \tag{7.13}$$

Solving for $h_s(n^\circ + 1)$ and taking $\Delta t = 1$ day

$$h_s(n^\circ + 1) = \left\{\left[D_0 - W(t_w) - \sum_{i=1}^{n^\circ}\{E(i) + O(i) - A(i)\} - \{E(n^\circ + 1) + O(n^\circ + 1) - A(n^\circ + 1)\}\Delta t_1 + d_w\right] + \left[\frac{E(n^\circ + 1) + O(n^\circ + 1) - A(n^\circ + 1)}{C}\right]\right\} e^{-C(1 - \Delta t_1)} - \left[\frac{E(n^\circ + 1) + O(n^\circ + 1) - A(n^\circ + 1)}{C}\right] \tag{7.14}$$

$h_s(n^\circ + 1)$ is the seepage head at the end of $(n^\circ + 1)^{th}$ day.

For $(n^\circ + 1) \le t \le (n^\circ + 2)$

$$\int_{h_s(n^\circ+1)}^{h_s(n^\circ+2)} \frac{C\,dh_s}{Ch_s(t)+E(n^\circ+2)+O(n^\circ+2)-A(n^\circ+2)} = -C\int_{n^\circ+1}^{n^\circ+2} dt = -C \tag{7.15}$$

Integrating and incorporating the limits

$$\ln\{Ch_s(t)+E(n^\circ+2)+O(n^\circ+2)-A(n^\circ+2)\}\Big|_{h_s(n^\circ+1)}^{h_s(n^\circ+2)} = -C \tag{7.16}$$

Simplifying

$$h_s(n^\circ+2)=\left\{h_s(n^\circ+1)+\frac{1}{C}\{E(n^\circ+2)+O(n^\circ+2)-A(n^\circ+2)\}\right\}e^{-C} - \frac{1}{C}\{E(n^\circ+2)+O(n^\circ+2)-A(n^\circ+2)\} \tag{7.17}$$

$h_s(n)$ is found in succession starting from $(n^\circ+1)^{th}$ day. The infiltration rate at $t=n\Delta t \quad ;n\geq n^\circ+1$ is given by:

$$I(n\Delta t)=Ch_s(n\Delta t) \tag{7.18}$$

The cumulative infiltration up to $n\Delta t$, $W(n\Delta t)$ is given by:

$$W(n\Delta t)=W(t_w) +0.5\times\left[C\left\{D_0-W(t_w)\sum_{i=1}^{n^\circ}\{E(i)+O(i)-A(i)\}-\{E(n^\circ+1)+O(n^\circ+1)-A(n^\circ-1)\}\Delta t_1+d_w\right\}+Ch_s(n^\circ+1)\right](\Delta t-\Delta t_1) + \sum_{i=(n^\circ+1)}^{n}0.5\times C\{h_s(i)+h_s(i+1)\}\Delta t \tag{7.19}$$

7.4 RESULTS AND DISCUSSION

7.4.1 Steps for Computation of Components of Water Balance Equation

- The water balance is carried out from June 1st to May 31st.
- The initial depth of water in the storage tank prior to onset of monsoon has been taken as 0.5m.
- Hourly evaporation is estimated. For computing evaporation, the heat balance has been performed assuming the depth of water during the hour of the heat balance to be equal to the depth of water in the previous hour as described in chapter-3.

- As some rainfall occurs prior to June, initial curve number is found assuming AMC-II condition. The initial curve number is estimated to be 75.
- Assuming initial soil moisture to be at field capacity, considering the meteorological data, the change in soil moisture storage in a depth of 120.0cm is calculated and curve number is updated as described in chapter-4.
- Infiltration rate is computed using Green and Ampt infiltration theory as described in chapter -6
- Hourly water balance is done considering these components.

Rainfall data pertaining to the study area are presented in Fig. 7.4. The variation in curve number during the water year is presented in Fig. 7.5. The curve number remains uniform at 89 from October to the middle of February when a rainfall event occurs. Owing to rainfall in the second half of February the curve number has increased and again stabilized at 87 by the end of March. The difference in the stabilized values is due to difference in potential evaporation rates during the succeeding periods prior to rainfall events. The corresponding runoff depths are presented in Fig. 7.6.

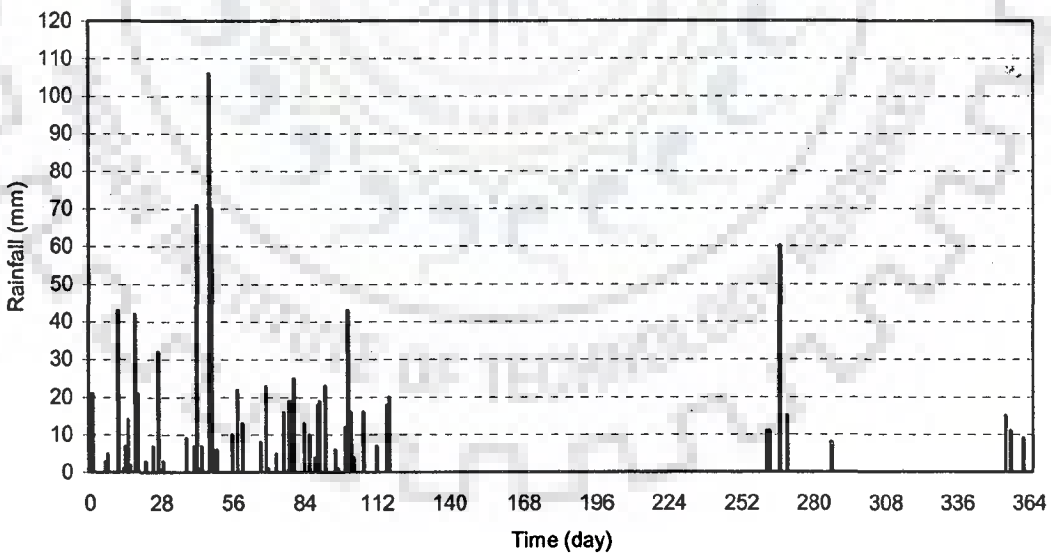

Fig. 7.4 Rainfall during the year

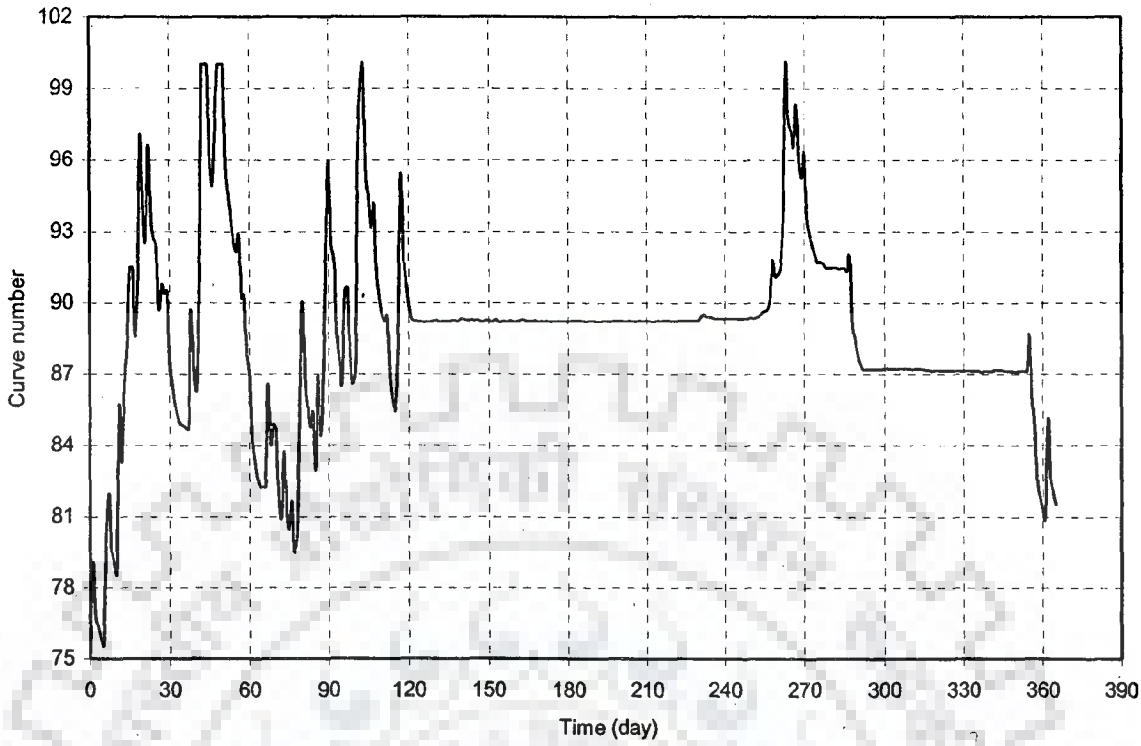

Fig.7. 5 Variations in curve number during a year

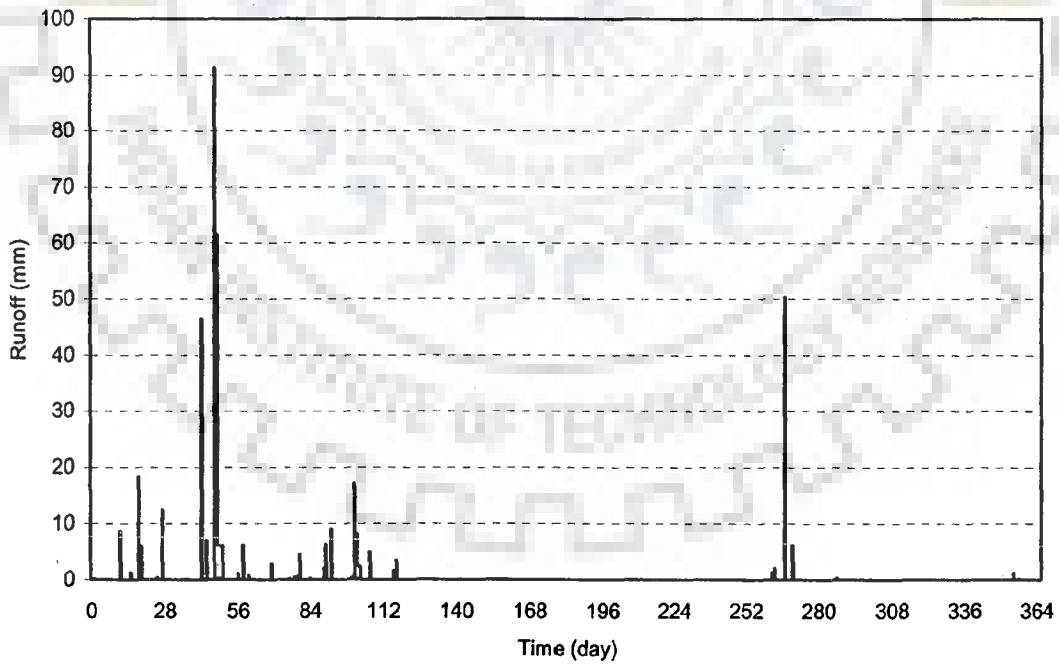

Fig.7. 6 Runoff generated by updating curve number during a year

7.4.2 Water Balance for the Existing Crest Level Height

The existing crest level height is 1.525m. The average daily water temperatures computed from heat balance are presented in Fig. 7.7. The temperature of the water

stored in the tank depends upon depth of water. As the storage tank gets dry after 232 days i.e. in the month of January, the graphs of temperature and evaporation terminates on 232 day. During the starting period of simulation, the daily average water temperature is at maximum (about 36^0C) which happens to be in summer period. During winter period before the tank gets dry, the water temperature is at the minimum (about 15^0C). Thus high temperature is not a constraint for pisciculture in this storage tank as the optimum temperature for fish growing in India ranges from 16^0C to 40^0C (Yadev, 2006). But, the depth of water in the storage tank is to be maintained by supplying water from some other external source. The temporal variation in evaporation from the storage tank is presented in Fig. 7.8.

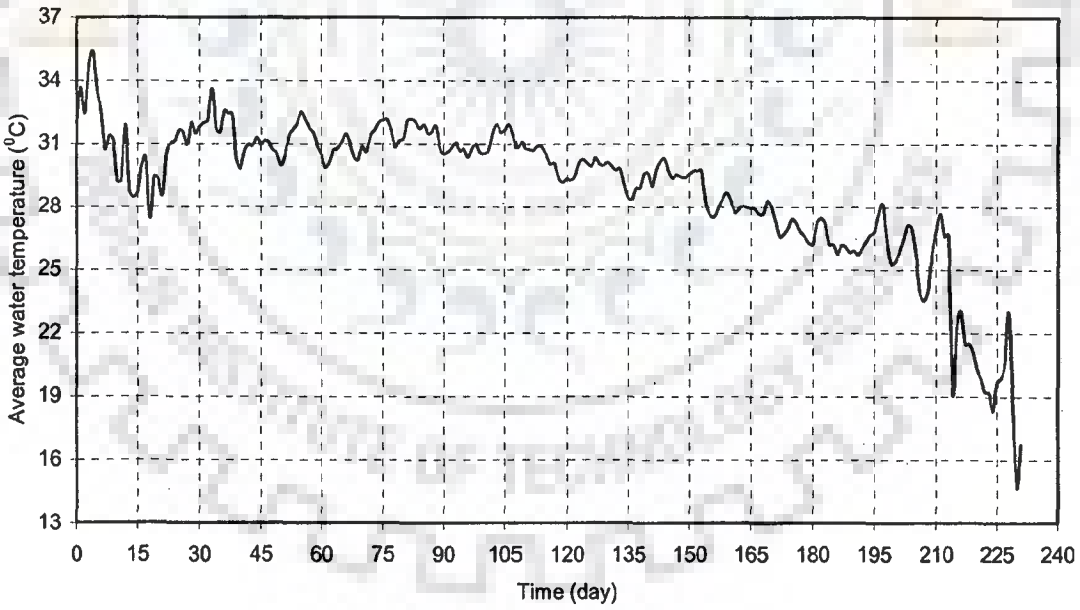

Fig. 7.7 Daily average water temperature in the storage tank where the height of the spillway crest is 1.525m above the D.S.L.

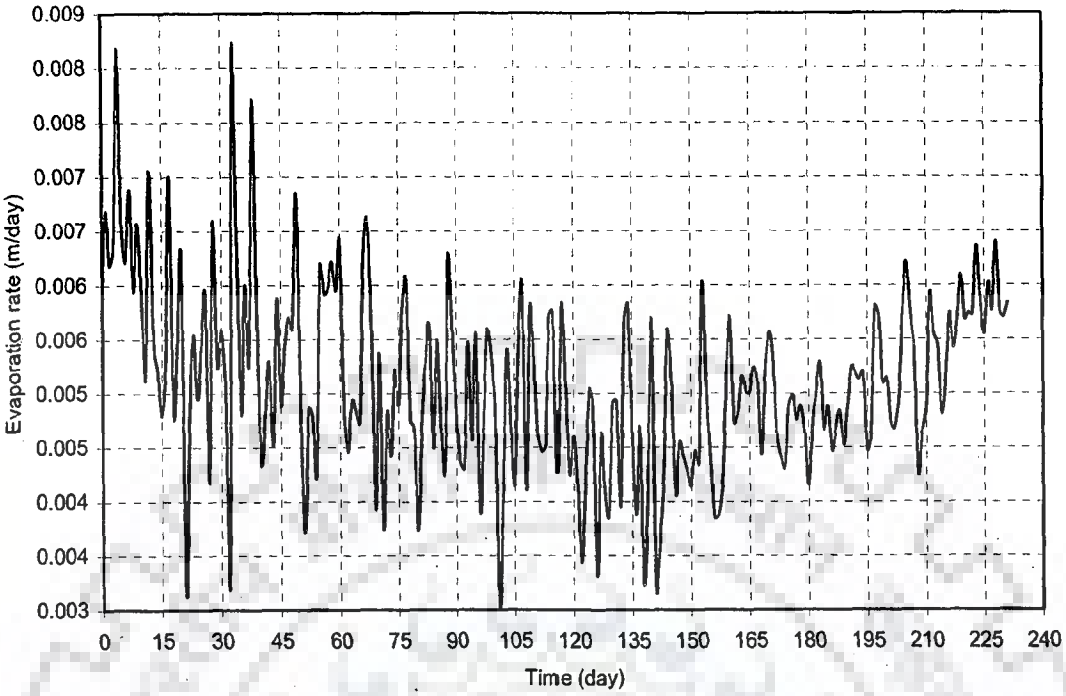

Fig. 7.8 Evaporation rate from the storage tank where the height of the spillway crest is 1.525m above the D.S.L.

The variations of the infiltration rate and cumulative infiltration are presented in Figs. 7.9 and 7.10. The infiltration rate and cumulative infiltration follow the usual trend.

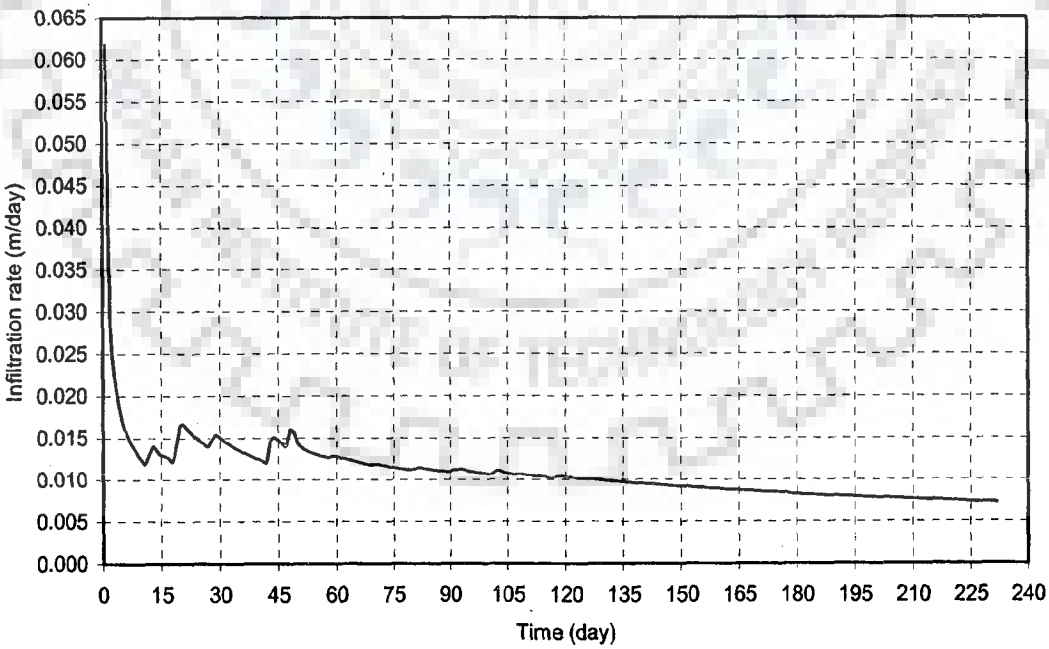

Fig. 7.9 Variations of the infiltration rate with time from the storage tank where the height of spillway crest is 1.525m above the D.S.L.

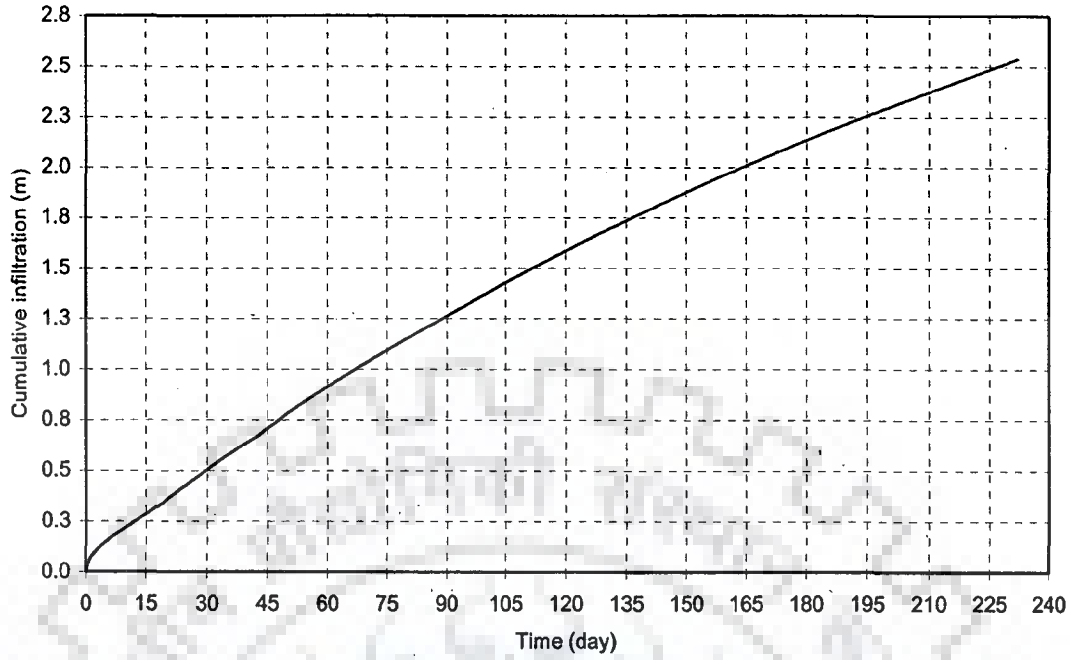

Fig. 7.10 Variations of the cumulative infiltration with time in the storage tank where the height of the spillway crest is 1.525m above the

Temporal variation of depth of water in the storage tank is presented in Fig. 7.11. Thus the present crest level is inadequate as the storage tank gets dry. The components of the water balance are presented in Fig. 7.12. The components satisfy the mass balance equation.

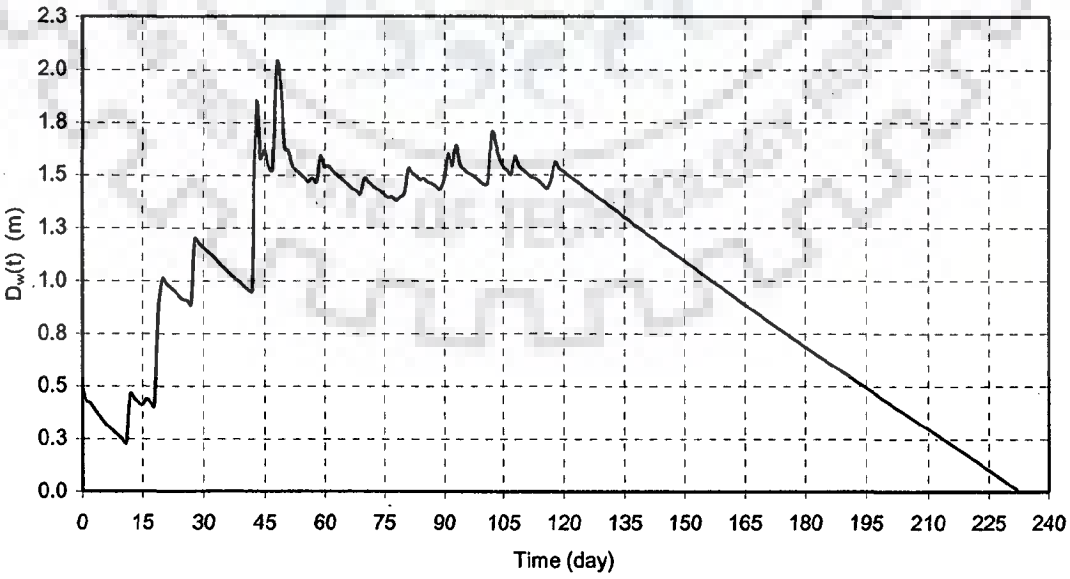

Fig. 7.11 Variations in the depth of water with time in the storage tank where the height of the spillway crest is 1.525m above the D.S.L.

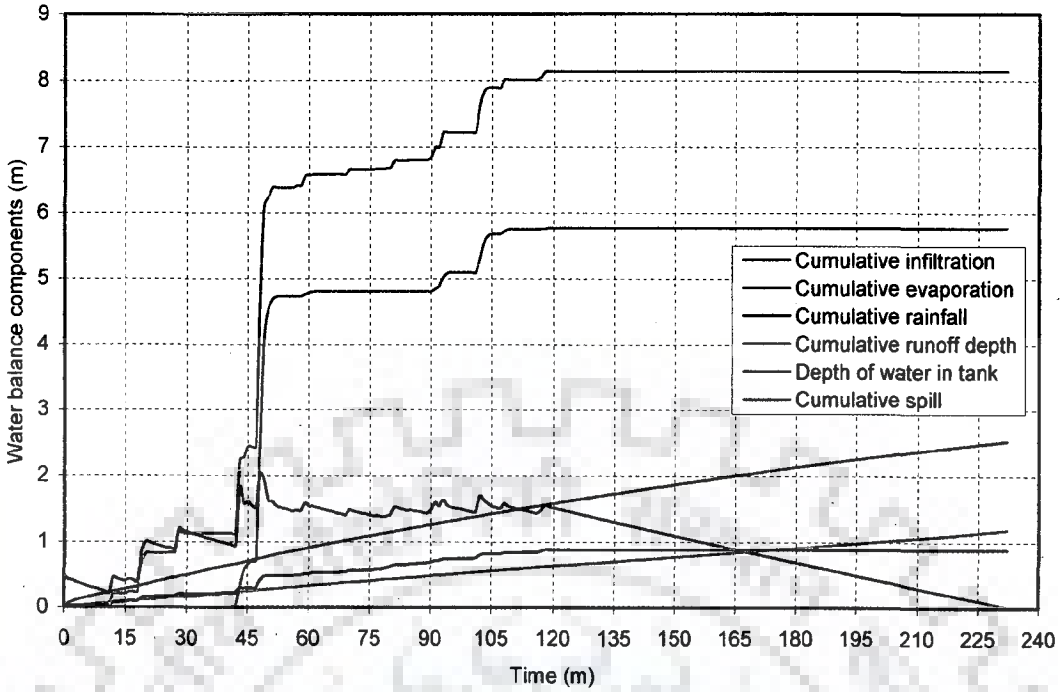

Fig. 7.12 Water balance components in the storage tank where the height of the spillway crest is 1.525m above the D.S.L.

7.4.3 Water Balance for a Crest Level Height of 3.155m

Corresponding to this crest height, daily average water temperature and water balance components are presented in Figs. 7.13 through 7.18. The maximum temperature is about 35.5 ^{0}C and the minimum temperature about 22 ^{0}C. Thus the water temperature is not a constraint for pisciculture in this storage tank. At the end of the year, about 1.0m depth of water is available in the tank. Therefore, this crest height is adequate for growth of aquatic life. In this case, water stored in the storage tank is not sufficient for irrigation supply. However, the spilled water can be collected down stream to be stored and subsequently used for irrigation.

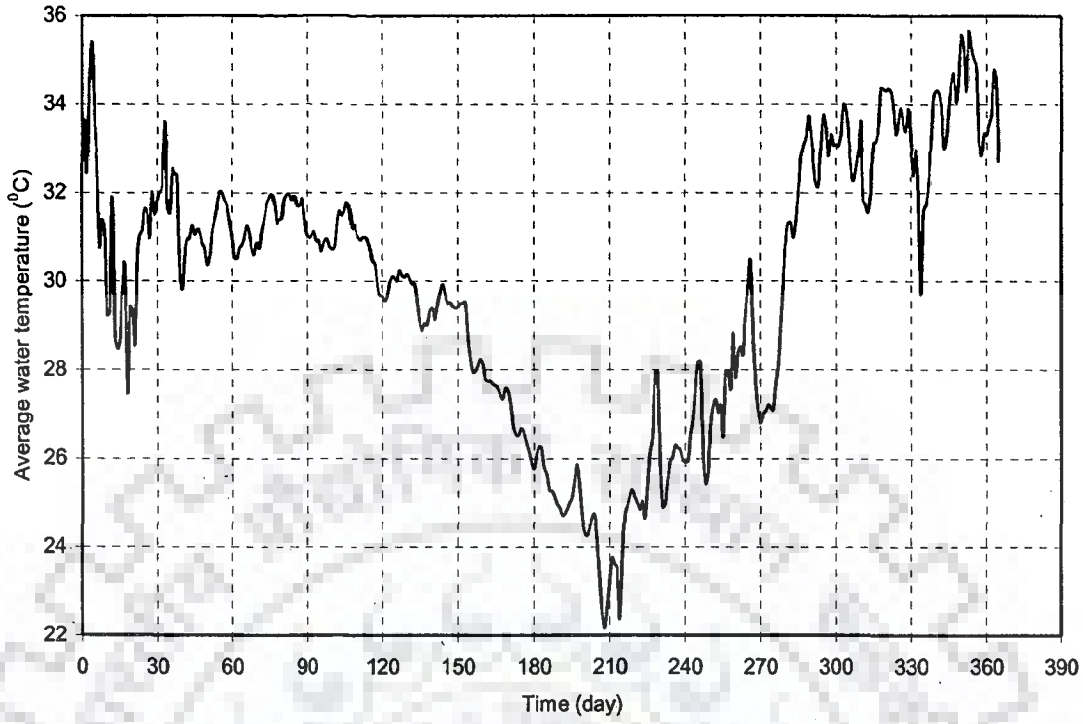

Fig. 7.13 Daily average water temperature in the storage tank where the height of the spillway crest 3.155m above the D.S.L.

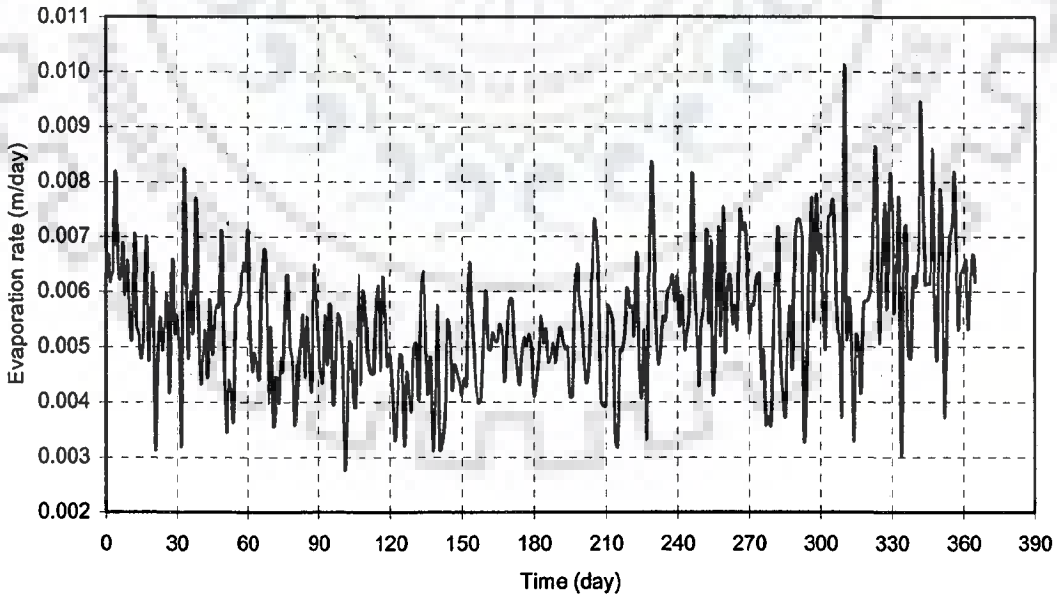

Fig. 7.14 Evaporation rate from the storage tank in a year where the height of the spillway crest is 3.155m above D.S.L.

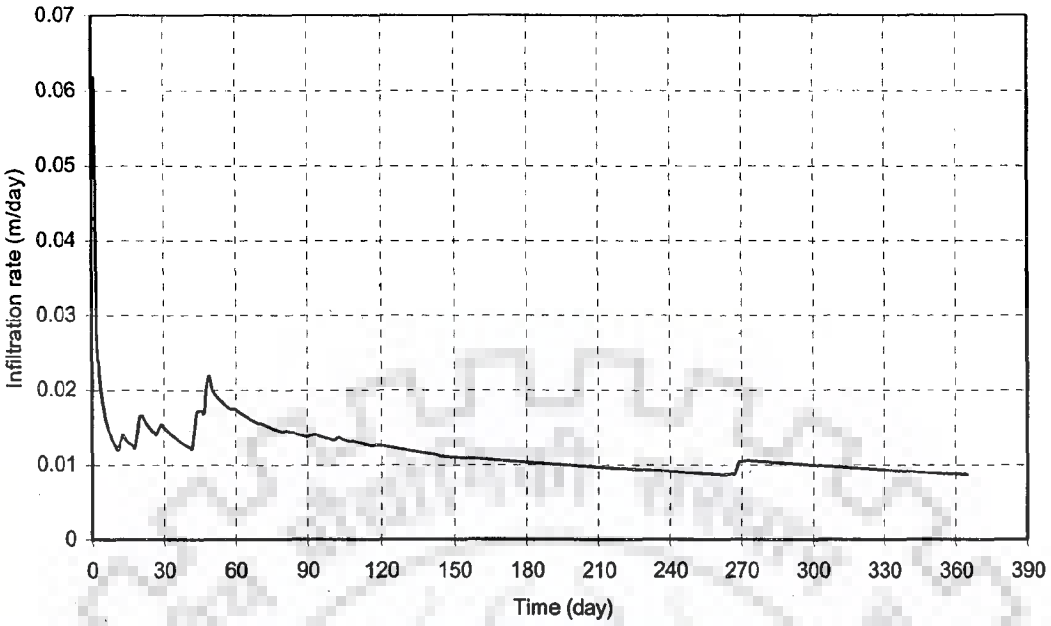

Fig. 7.15 Variations in the infiltration rate with time from the tank bed where the height of the spillway crest is 3.155m above the D.S.L.

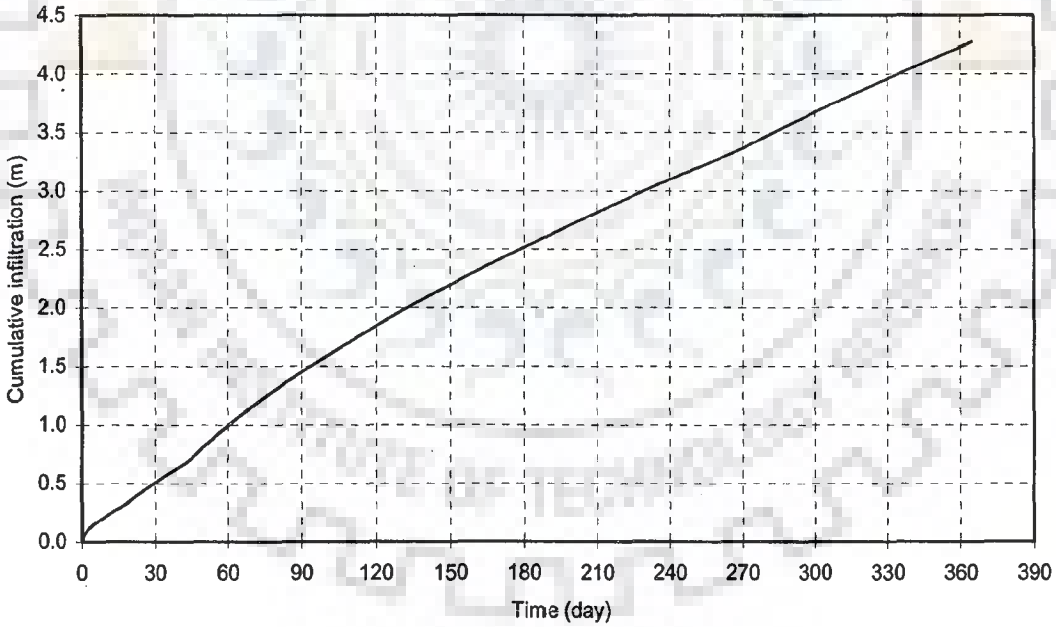

Fig. 7.16 Variations of cumulative infiltration with time where the height of the spillway crest is 3.155m above the D.S.L

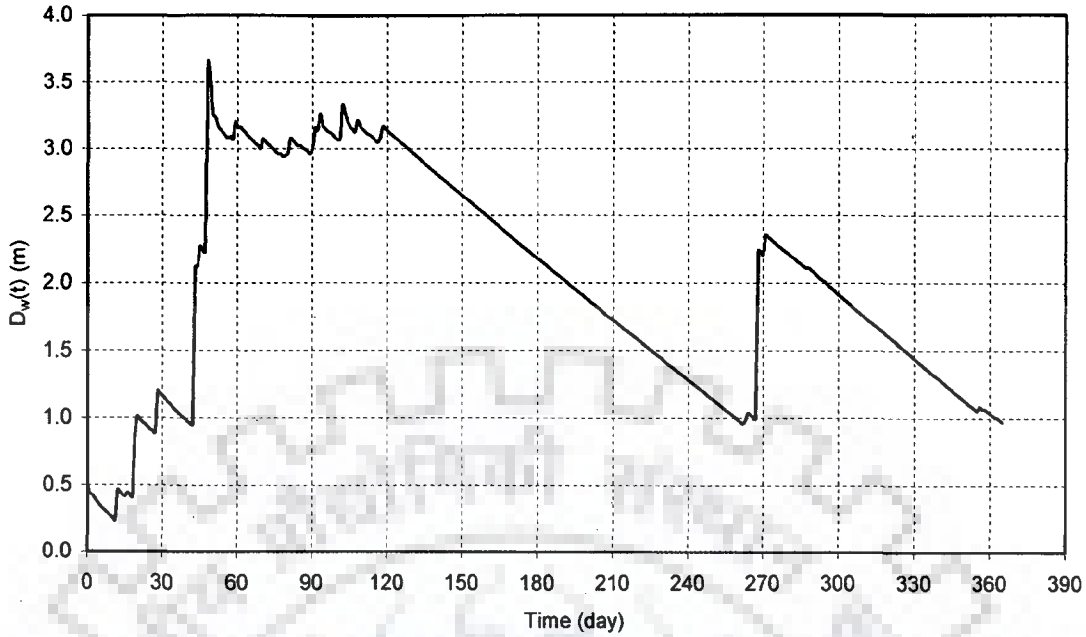

Fig. 7.17 Variations in the depth of water in the storage tank with time where the height of the spillway crest is 3.155m above the D.S.L.

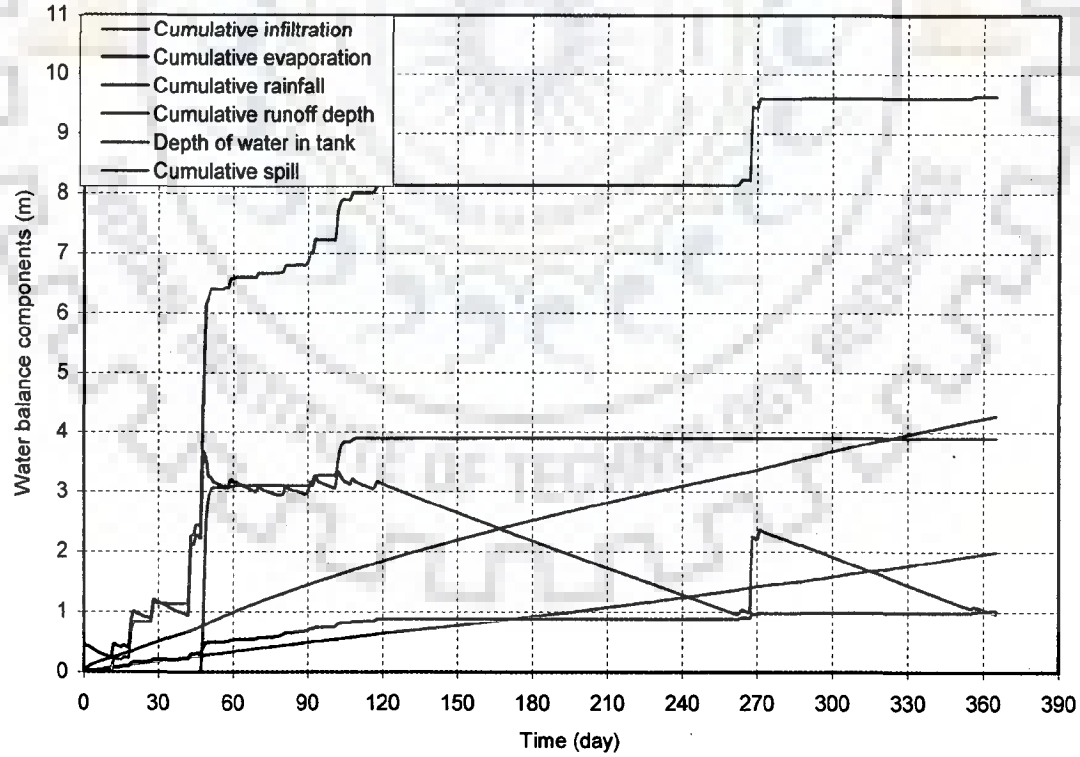

Fig. 7.18 Water balance components in the storage tank where the height of the spillway crest is 3.155m above the D.S.L.

7.4.3 Water Balance for a Crest Level Height of 6.8m

If a crest height of 6.8m is provided then all the water which is collected from contributing catchment is retained in the storage tank. The storage tank losses water due to evaporation and infiltration. The storage tank acts both as recharge pond and evaporation pond. The depth of water at the end of year is about 3.5m. In this case, water can be supplied in a limited way for irrigation purposes after the end of monsoon. Corresponding to this crest height, daily average water temperature and water balance components are presented in Figs. 7.19 through 7.24.

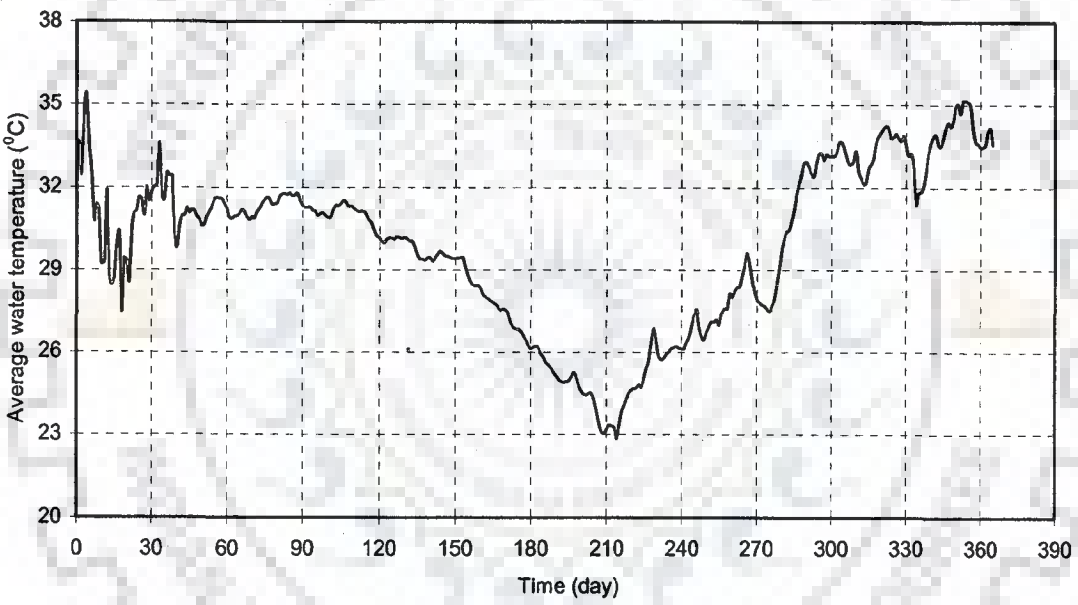

Fig. 7.19 Daily average water temperature in the storage tank where the height of spillway crest is 6.8m above D.S.L

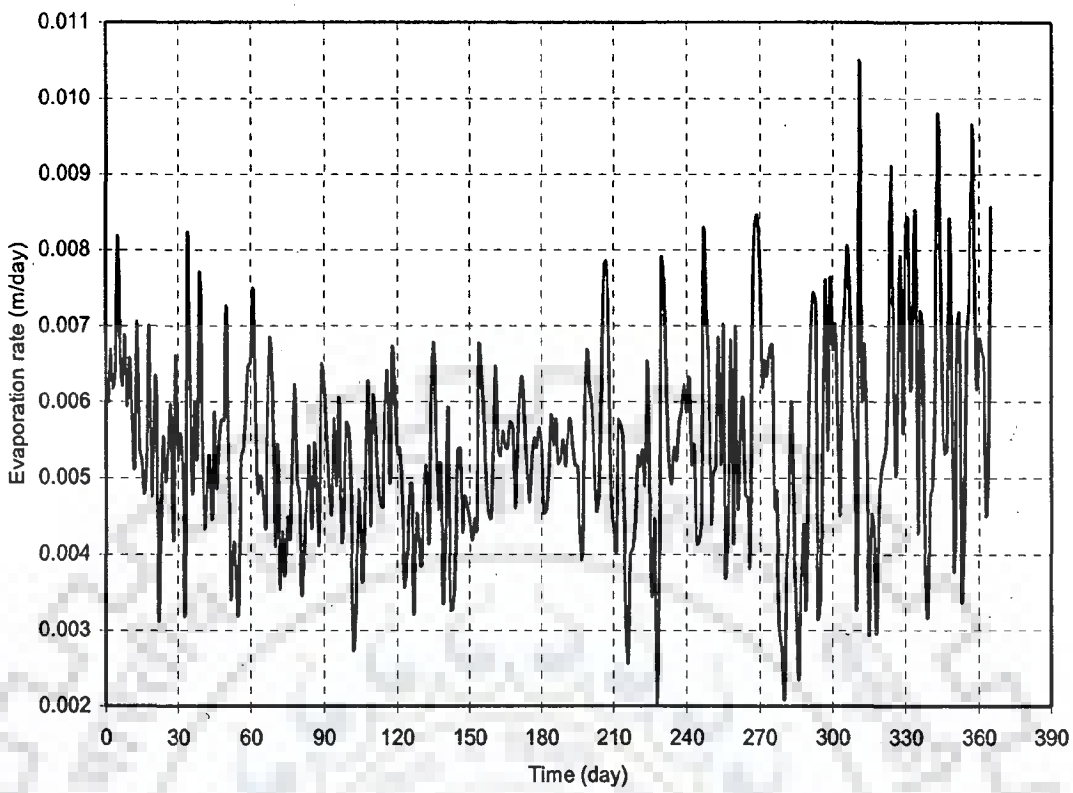

Fig. 7.20 Evaporation rate from the storage tank in a year where the height of the spillway crest is 6.8m above the D.S.L.

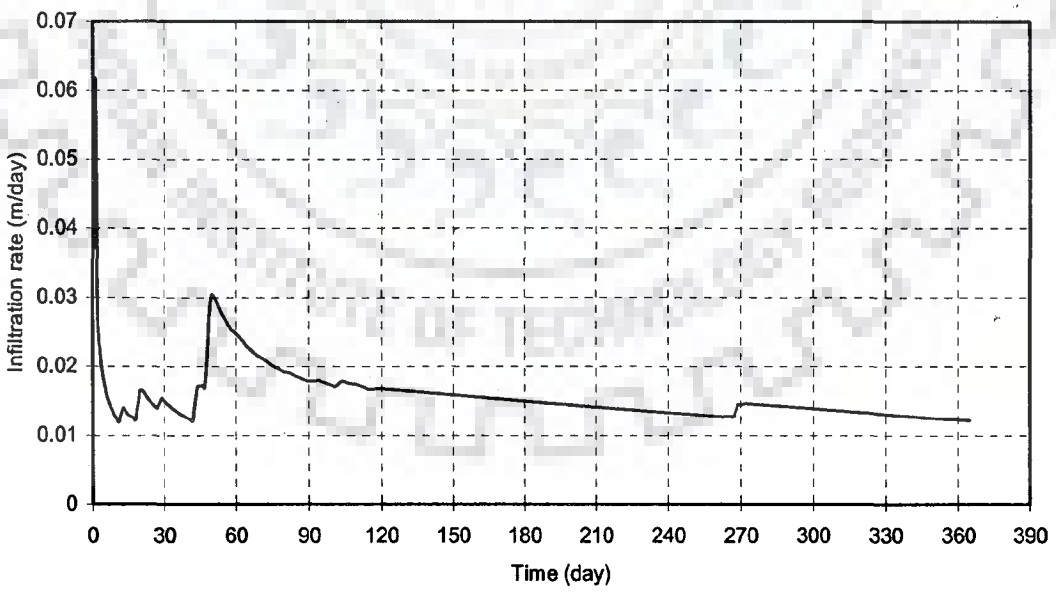

Fig. 7.21 Variations of infiltration rate with time from the storage tank where the height of spillway crest is above 6.8m from D.S.L.

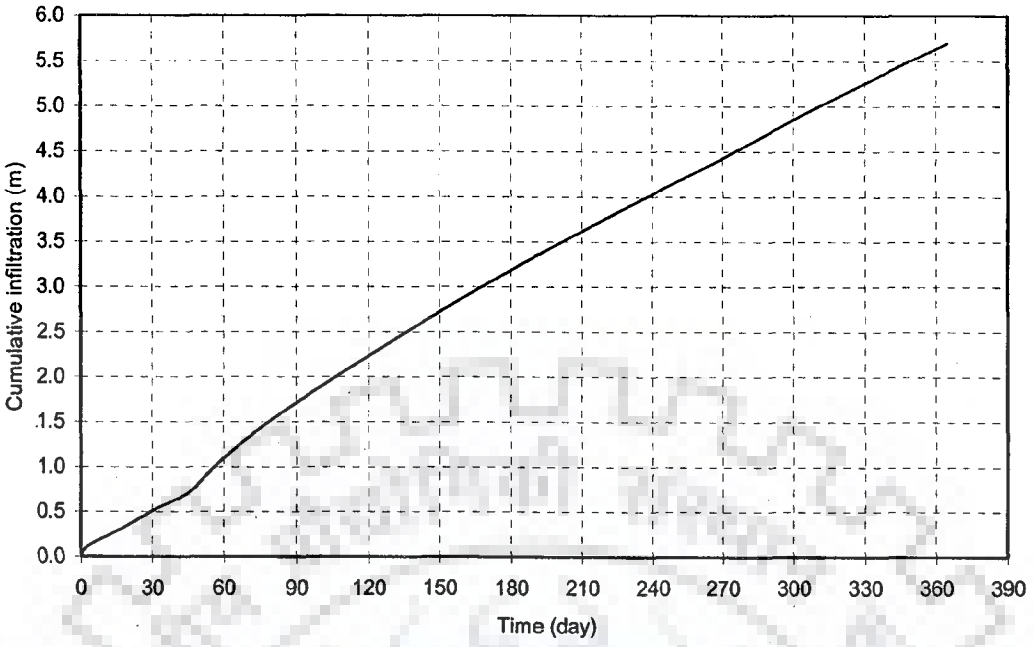

Fig. 7.22 Variations of cumulative infiltration with time in the storage tank where the height of the spillway crest is 6.8m above D.S.L.

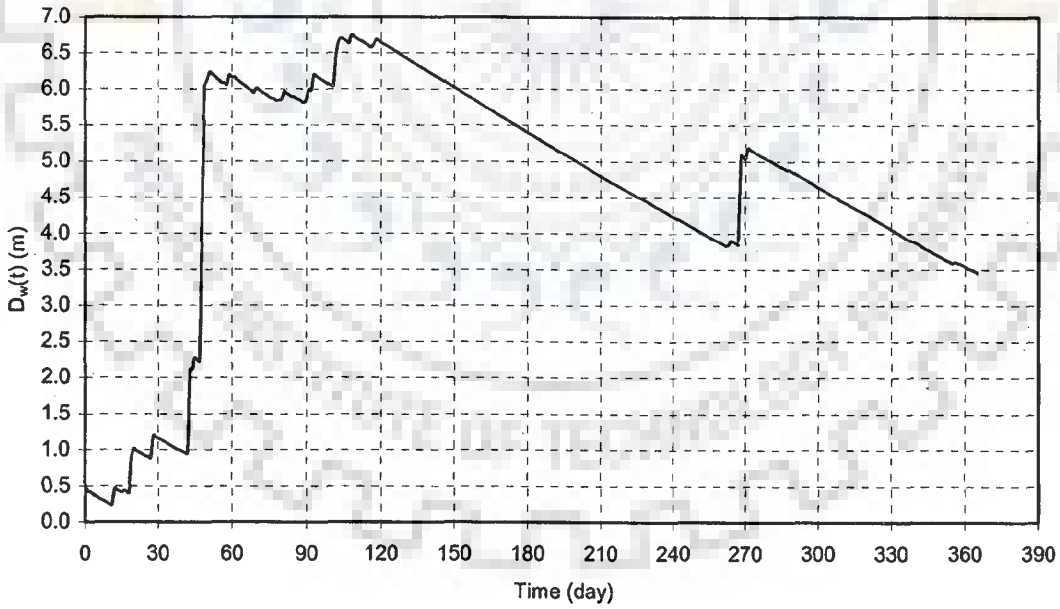

Fig.7.23 Variations in the depth of storage tank with time where the height of the spillway crest is 6.8m above D.S.L.

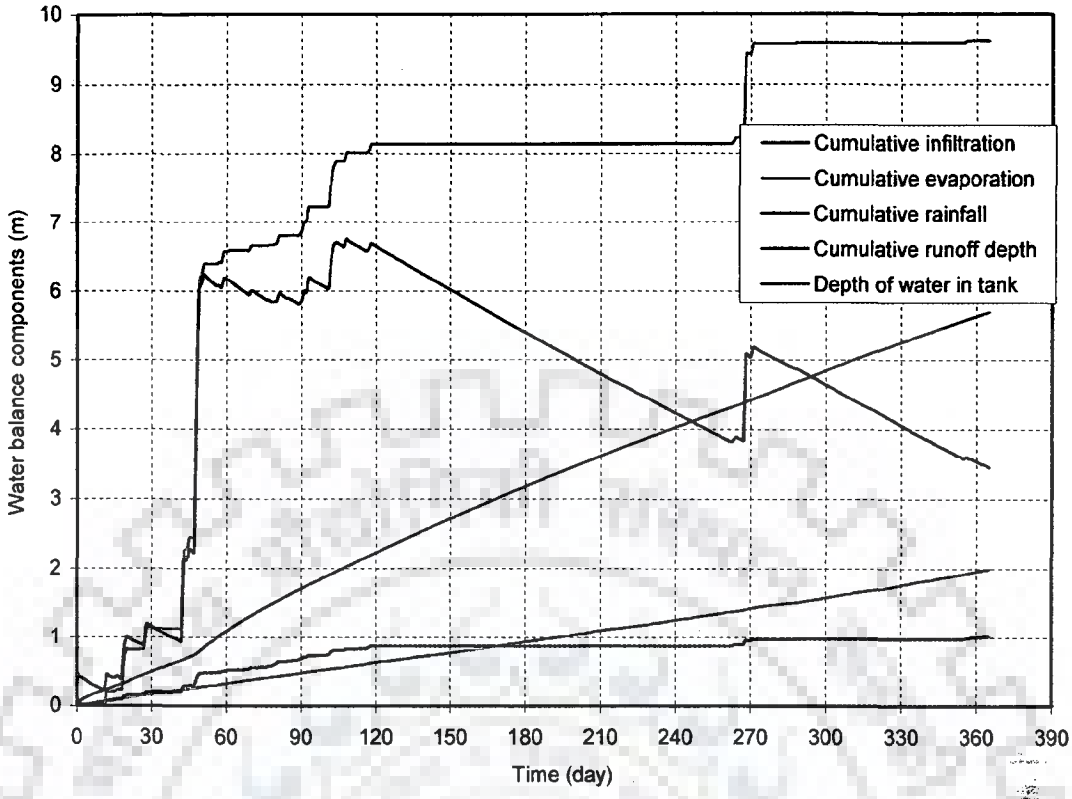

Fig.7.24 The water balance components of the storage tank, where the height of spillway crest is 6.8m above D.S.L.

The volume of water available at the end of monsoon (30th of September) and volume of water lost due to infiltration and evaporation in the post monsoon period (1st October to 31st May) for different spillway crest level height are presented in Table 7.1. Only if the crest level is raised to 6.8m (and accordingly the bund height is raised upto a height of 7.3m) the volume of excess water (2.48x 10^6m^3-1.16x10^6m^3) which can be stored is about 1.32x 10^6m^3. The storage tank has a command area of 121 ha. Thus, the command area can be irrigated during drought period by rising the corresponding crest level height and bund height.

Table 7.1 Comparison of volume of water available at the end of monsoon and volume of water lost due to infiltration and evaporation in the post monsoon period for spillway height =1.525.0m, 3.155m and 6.8m

	Spillway height =1.525m	**Spillway height=3.155m**	**Spillway height=6.8m**
Volume of water available at the end of monsoon	5.63×10^5 m^3	1.16×10^6 m^3	2.48×10^6 m^3
Volume of water lost due to infiltration in the post monsoon period	3.53×10^5 m^3	9.06×10^5 m^3	1.29×10^6 m^3
Volume of water lost due to evaporation in the post monsoon period	2.05×10^5 m^3	5.07×10^5 m^3	5.03×10^5 m^3

7.4 CONCLUSIONS

The following conclusions are drawn from the above study.

1. A case study has been presented for carrying out water balance in a storage tank.
2. The present height of the spillway crest need to be raised from 1.525m to 6.8m to store the potential runoff from the contributing catchment for supplying water for irrigation during post monsoon period to a command area of 121 ha and for supporting pisciculture.

CHAPTER-8

SUMMARY AND CONCLUSIONS

8.1 GENERAL

The processes level models pertaining to a water balance study in a storage tank are: (i) evaporation from water body, (ii) evaporation and drainage from upper soil layer of the runoff contributing catchment, (iii) runoff contribution from the catchment of the storage tank, (iv) infiltration from tank bed and (v) outflow through spillway. These processes level models have been integrated and water availability in a storage tank is determined in this thesis. Based on the study the following conclusions are drawn:

1. The heat balance method is more rigorous as the method computes zero evaporation on the day, the water temperature in the tank coincides with the dew point temperature of the atmosphere. The Penman's method computes an average evaporation rate as compared to heat balance method.
2. For shallow depth of water in the storage tank (less than 3m), variation in depth of water due to evaporation has small effect on evaporation rate from the water body.
3. Curve number changes considerably during a water year. Updating curve numbers results in accurate determination of runoff from a catchment. The curve number can be updated successfully considering evaporation and drainage from the top soil layer during inter-storm period besides accounting the part of rainfall not appearing as runoff. In SCS method an assumption of a constant curve number during the monsoon period underestimates the runoff depth considerably from a catchment.
4. Green and Ampt assumptions, that the soil is saturated behind a moving front in a two layered soil system, is valid, if the upper layer happens to be layer of

higher hydraulic conductivity. Incase the upper layer in two layered soil system has lower hydraulic conductivity than that of the underlying layer, the soil moisture behind the moving front in the first layer is equal to the saturation moisture content of the upper layer. When the moving front surpasses the upper layer, the moisture content behind the moving front in the lower layer is less than the saturated moisture content of the underlying layer. Green and Ampt infiltration theory is inapplicable for computing infiltration from a storage tank, underlain by a layered soil system if the upper soil layer is less permeable than that of the lower layer, as the simulated infiltration rate does not follow the decreasing trend of infiltration given by Horton's equation.

5. With a postulation that water front moves in unsaturated state in the lower layer at a moisture content corresponding to which the unsaturated hydraulic conductivity of the lower layer is same as the saturated hydraulic conductivity of the upper layer, the simulated infiltration rate follows the decreasing trend as given by Horton's infiltration equation. The proposed postulation needs experimental verification.
6. The variation of the drying time of a storage tank in a homogeneous soil layer with initial depth of water during first filling is quasi-linear in nature. The drying time is very closely inversely proportional to the hydraulic conductivity of the sub soil. But, in case of a two layered soil system, where the bottom soil layer has lower hydraulic conductivity, the variation of drying time with initial depth of filling is non-linear in nature.
7. Water balance is carried out in an existing storage tank in a drought prone area. The present height of the spillway crest needs to be raised from 1.525m to 3.155m to maintain a minimum depth of 1m in the storage tank at the end of the water year. Otherwise, the tank would remain dry during the later half of the

water year. If the crest level will be raised to a height of 6.8m, all the potential runoff from the contributing catchment will get stored and water can be supplied for irrigation during post monsoon period to a command area of 121 ha, besides supporting for pisciculture in the storage tank.

8.2 SUGGESTIONS FOR FUTURE WORK

The following aspects need to be studied for improving the water balance model:

1. While updating the curve number for forested catchment evapotranspiration should be accounted.
2. If water table lies at a shallow depth below the storage tank, the seepage loss from the storage tank after the saturation front reaches the water table would be controlled by water table position. The water balance model should incorporate storage tank and aquifer interaction for computation of recharge from the storage tank.

REFRENCES

1. Agrawal, M. K., Panda, S. N., Panigrahi, B. (2004). Modeling water balance parameters for rainfed rice. Journal of Irrigation and Drainage Engineering. 130 (2), pp. 129-139.
2. Allen, J. B. (1968). An analysis of evaporation at lake Hefner, 1965-1966 based on the water budget, energy budget, and evaporation tanks. Ph.D. dissertation, Oklahoma State University.
3. Allen, R. G. (1868). A penman for all seasons. Journal of Irrigation and Drainage Engineering, Vol. 112, No. 4, pp. 348-367.
4. Al-Ghobari, H.M. (2000). Estimation of reference evapotranspiration for southern region of Saudi Arabia. Irrig. Sci. 19, pp. 81–86.
5. Ambast, S.K., Keshari, A.K., Gosain, A. K. (2002). An operational model for estimating regional evapotranspiration through surface energy partitioning (RESEP). International Journal of Remote Sensing. 22 (23), pp. 4917-4930.
6. Andreas, Güntner, Krol, M. S., Araújo, José C. de, Bronstert, A. (2004). Simple water balance modeling of surface reservoir systems in a large data-scarce semiarid region. Hydrological Sciences. 45 (5). pp. 901-918.
7. Anbumozhi, V., Matsumoto K. and Yamaji E., (2001), 'Towards improved performance of irrigation tanks in semi-arid regions of India: Modernisation opportunities and challenges', *Irrigat. DrainageSyst.* 15, pp.293–309.
8. Aron, G., Miller, A. C. Jr., and Lakatos, D. F. (1977). Infiltration formula based on SCS curve number. J. Irrigation and Drainage Division, ASCE, 103(IR4), pp. 419-427.
9. Audu. (1999). Development of application of runoff model for water harvesting in north eastern Nigeria, Research report, Cranfield University.

10. Batchelor, C. H. (1984). The accuracy of evapotranspiration estimated with the FAO modified penman equation. Irrigation Science, 5 (4). pp. 223-233.

11. Bhatnagar, P.R., Srivastava, R.C., Bhatnagar, V.K., 1996. Management of runoff stored in small tanks for transplanted rice production in mid hills of N-W Himalayas. Agric. Water Manage. 30, 107–118.

12. Blodgett, T.A., Lenters, J.D., Isacks, B.L. (1997). Constraints on the origin of paleolake expansions in the Central Andes. Earth Interactions1.

13. Bonta, J. V. (1997). Determination of watershed curve number using derived distributions. Journal of Irrigation and Drainage Engineering, ASCE, 123(1), pp. 28–36.

14. Bouwer, H. (1969). Infiltration of Water into Non-uniform Soil. Journal of Irrigation and Drainage. Division of ASCE 95(IR4). pp. 451-462.

15. Boszany, M. (1989). Generalization of SCS curve number method. J. Irrigation and Drainage Engineering, ASCE, 115(1). pp. 139-144.

16. Brown, L.C., and Barnwell Jr., T.O. (1987). The enhanced water quality models QUAL2E and QUAL2E-UNCAS: Documentation and user Manual. EPA/600/3-87/007. U.S. Environmental Protection Agency. Athens. G.A.

17. Brutsaert, W., Stricker, H. (1979). An advection-aridity approach to estimate actual regional evapotranspiration. Water Resources Research 15 (2), pp. 443–450.

18. Brutsaert, W. (1982). Evaporation into the atmosphere: theory, history and application, D. Reidel, Boston, Mass.

19. Burman, R. D., Pochop, L. O., and Borrelli, J. (1984). Development of evapotranspiration crop coefficients, climatological data, and evapotranspiration models for the upper Green River, Annual Progress Report to Wyoming Water Development Commission and the Wyoming Water Research Center, Univ. Wyo. Agr. Engr. Dept.

20. Cathcart, T. P. and Wheaton, F. W. (1987) Modeling temperature distribution in freshwater ponds. *Aquacultural Engineering,* 6. pp. 237-257.

21. Chen, C. (1982). An evaluation of the mathematics and physical significance of the Soil Conservation Service Curve Number Procedure for estimating runoff volume. Proc. Int. Symp. on Rainfall-Runoff Relationship, V. P. Singh(Ed.).Water Resources Publications, Littleton, Colo., pp. 387-418.

22. Childs, E.C. and M. Bybordi. (1969). The vertical movement of water in stratified porous material 1. Infiltration. Water Resources Research 5(2), pp. 446-459

23. Choi, J. Y., Engel, B. A., and Chung, H. W. (2002). Daily stream flow modeling and assessment based on curve number technique. Hydrological Processes, 16, pp. 3131-3150.

24. Chow, V. T. (1959). Open Channel Hydraulics. McGraw-Hill, Inc.

25. Chow, V.T. (1964). Handbook of Applied Hydrology, Mc Graw Hill, New York.

26. Chow, V. T., Maidment, D .R., and Mays, L. W. (1988). Applied Hydrology. McGraw-Hill International Editions, New York, pp.572.

27. Copper, P. I. (1969). The absorption of solar energy radiation in solar stills, Solar Energy. 12. pp 333.

28. Chu, S.T. (1978). Infiltration during an unsteady rain. Water Resources Research 14(3), pp. 461- 466.

29. Chu, X, and Marino, A.M., (2005). Determination of ponding condition and infiltration into layered soils under unsteady rainfall. Journal of Hydrology. 313, pp. 195-207.

30. Dalton, J. (1802). Experimental essays on the constitution of mixed gases: on the force of steam or vapor from water or other liquids in different temperatures, both in a Torricelli vacuum and in air; on evaporation; and on expansion of gases by heat, Manchester Lit.Phil. Soc. Mem. Proc., 5. pp. 536-602.

31. deBruin, H. A. R. (1978). A simple model for shallow lake evaporation, Journal of Applied Meteorology. 17, pp. 1132-1134.

32. deBruin, H.A.R., and Keijman, J.Q. (1979). The Priestley-Taylor evaporation model applied to large, shallow lake in the Netherlands. J. Appl. Meteorol. 18, pp. 898–903.

33. de Jager, J. M. and Walmsley, R. D. (1984) A model to predict water temperature in plastic-covered outdoor mass algal culture systems. *Aquacultural Engineering* 3, pp. 191-206.

34. Deshmukh, D.S. (2008).GIS based study of geomorphology, landuse and water resources in small watersheds. un published Ph.D. thesis, submitted to Indian Institute of Technology Roorkee, India.

35. Dharmasena, P.B. (1989). Optimum utilization of the storage in village tanks. Tropical Agriculturist 145, pp. 1–11.

36. Dharmasena, P.B. (1991). Present use of land and water resources in village tank farming (a case study in Maha Kanumulla cascade).Journal of Soil Science Society, Sri Lanka 7, pp. 1–17.

37. Dhyani, B.L., J. S. Samra, G. P.Juyal, Ram Babu and V.S. Katiyar. (1997). Socio-Economic Analysis of a Participatory Integrated Watershed Management in Garhwal Himalaya (Fakot Watershed). Central Soil and Water Conservation Research and Training Institute, ICAR, Dehradun.

38. Doorenbos J. and W. O. Pruitt. (1977). Crop water requirements. Irrigation and Drainage Paper No. 24, FAO (United Nations), Rome, pp.144.

39. Eagleson, P.S. (978). Climate, Soil, and Vegetation. A simplified model of soil moisture movement in the liquid phase. Water Resources Research 14(5), pp. 722-730.

40. Eiker, E.E. (1972). Heat Exchange Program. Program No. 722-F5-E1010, US Corps of Engineers, Baltimore District. Baltimore. MD.

41. Environmental Laboratory. (1985). CE QUAL-R1. a numerical one dimensional model of reservoir water quality , user's manual , Instruction Report E-82-1, U.S. Army Corps of Engineers Water ways Experiment Station, Vicksburg, MS.

42. Flerchinger, G.N., F.J. Watts, and G.L. Bloomsburg. (1988). Explicit solution to Green-Ampt equation for non-uniform soils. Journal of Irrigation and Drainage. Division of ASCE 114(3), pp. 561-565.

43. Ganji, A., Khalili, D., Karamouz, M., Ponnambalam, K., Javan, M. (2008) A fuzzy stochastic dynamic Nash game analysis of policies for managing water allocation in a reservoir system. Water Resources Management 22, pp. 51–66.

44. Garbrecht, J., Ogden, F.L., DeBarry, P.A. and Maidment, D.A. (2001). GIS and distributed watershed models. I, Data Coverages and Sources. Journal of Hydrologic Engineering, Nov. /Dec., pp. 506-512.

45. Garen, D., and Moore, D. S. (2005). Curve number hydrology in water quality modeling, use, abuse, and future directions. J. American Water Resources Association, 41(2), pp. 377-388.

46. Geetha et al., (2007), Geetha.

47. George, B.A., Reddy, B.R.S., Raghuwanshi, N.S., Wallender, W.W. (2002). Decision support system for estimating reference evapotranspiration. J. Irrig. Drain. Eng. 128 (1), pp. 1-10.

48. Gray, D.M. (1970). Handbook on the principles of hydrology; with special emphasis directed to Canadian conditions in the discussions, applications, and presentation of data. Water Information Center, Port Washington, NY

49. Green, W. H and C.A. Ampt. (1911). Studies on Soil Physics I. The Flow of Air and Water through Soils. Journal of Agricultural Science IV (Part I 1911), pp. 1-24.

50. Greogory, J. M., and Fedler, C. B. (1986). Model evaluation research verification (MERV). ASAE Paper No. 86-5032, Presented at the Summer Meeting, ASAE, California Polytechnic Institute, San Luis Obispo, CA

51. Gupta, R.S. (1989). Hydrology and Hydraulic Systems. Prentice Hall. NJ

52. Hamon, W.R. (1961). Estimating potential evapotranspiration. Proc. Amer. Soc. civ. Engrs. 87, pp. 107–120.

53. Harbeck, G.E.J., Kohler, M.A., Koberg, G.E. (1958). Water-loss investigations: Lake Mead studies. Professional Paper 298, US Geological Survey.

54. Harboe, R., Gautam, T. R., Onta, P. R. (1994). Conjunctive operation of hydroelectric and thermal power plants. Journal of Water Resources Planning Management .120(6), pp. 778–793.

55. Hawkins, R.H. (1978). Runoff curve numbers with varying site moisture. J. Irrigation and Drainage Division, ASCE, 104(IR4), pp. 389-398.

56. Hawkins, R. H. (1993). Asymptotic determination of runoff curve numbers from data. Journal of Irrigation and Drainage Engineering, ASCE, 119(2), pp. 334–345.

57. Hawkins, R. H., Hjelmfelt, A. T .Jr. and Zevenbergen, A.W. (1985). Runoff probability, storm depth and curve numbers. J. Irrigation and Drainage Engineering, 111(4), pp. 330-340.

58. Hawkins, R. H., Jiang, R., and Woodward, D. E. (2001). Investigation of the runoff curve number abstraction ratio, Water Resources for 21st Century: A National Hydrology and Hydraulic Engineering Workshop, Tucson, AZ.

59. Henderson-Sellers, B. (1984). Engineering Limnology. Pitman, London.

60. Hjelmfelt, A.T. Jr.(1980). Empirical investigation of curve number technique. J. Hydraulic Division, ASCE. 106(9), pp.1471-1477.

61. Hjelmfelt, A. T. Jr (1991) Investigation of curve number procedure. J Hydraulic Engrg 117(6):725–737

62. Hostetler, S.W., Bartlein, P.J. (1990). Simulation of lake evaporation with application to modeling lake level variations of Harney– Malheur Lake, Oregon. Water Resources Research 26 (10). pp. 2603–2612.

63. Hugo, A. L. (2002). Reservoir design and operation with variable lake hydrology. Journal of Water Resources Planning Management. 128(6), pp. 399–405.

64. Hussein, A.S.A. (1999). Grass ET estimates using Penman-type equations in Central Sudan. J. Irrig. Drain. Eng. 125 (6), pp. 324–329.

65. Husenappa, V., Juyal, G. P., and Sastry, G. (1981). Water harvesting through ponds. Indian Farming, 10, pp. 27-29.

66. Idso, S. B. (1981). Relative rates of evaporative water losses from open and vegetation covered mater bodies. Water Resources Bulletin, American Water Resources Assoc.17 (1), pp. 46-48.

67. Ikebuchi, S., Seki, M., Ohtoh, A. (1988). Evaporation from lake Biwa. Journal of Hydrology. 102. pp. 427–449.

68. Indian Express News. 15th March, 2007.

69. Itakura, J. (1995). Water balance model for planning rehabilitation of a tank cascade irrigation system in Sri Lanka. IIMI Working Paper No. 3, International Irrigation Management Institute, Sri Lanka, ISBN: 92-9090-320-1.

70. James, L.G. and C.L. Larson. (1976). Modeling infiltration and redistribution of soil water during intermittent application. Transactions of ASAE. 19(3), pp. 482-488.

71. Jayatilaka, C.J., Sakthivadivel, R., Shinogi, Y., Makin, I.W., Witharana P. (2003). A simple water balance modeling approach for determining water availability in an irrigation tank cascade system. Journal of Hydrology. 273, pp. 81-102.

72. Jensen, M. E. (Editor), (1973). Consumptive use of water and irrigation water requirements. Irrigation and Drainage Div., American Society of Civil Engineers, New York, NY.

73. Jensen, J. R., Mannan, S. M. A., Uddin, S. M. N. (1993). Irrigation requirement of transplanted monsoon rice in Bangladesh. Agricultural Water Management, 23(3), pp. 199–212.

74. Jones, F. E. (1992). Evaporation of water - emphasis on applications and measurements. Lewis Publishers Inc, Chelsea, MI.

75. Kashyap, P.S., and Panda, R.K. (2001). Evaluation of evapotranspiration methods and development of crop coefficients for potato crop in a sub-humid region. Agric. Water Mange. 50, pp. 9–25.

76. Kenabatho, P. K., and Parida, B. P. (2005) Evaporation losses as a major factor in determining allowable releases from water supply reservoirs: the case of Botswana's major reservoirs, River basin management III. WIT Trans Ecol Environ. 83, pp. 631–638.

77. Kitamura, Y. (1984). Consumptive use of water for paddy field irrigation in the dry zone areas of Sri Lanka: Nekkensiryo No.63, Tropical Agricultural Research Center, Ministry of Agriculture, Forestry and Fisheries, Japan (In Japanese with English Summary).

78. Kitamura, Y. (1990). Management of irrigation systems for rice double cropping culture in the tropical monsoon area. Technical Bulletin of the Tropical Agricultural Research Center No. 27, Tropical Agricultural Research Center, Ministry of Agriculture, Forestry and Fisheries, Japan.

79. Klemetson, S. L. and Rogers, G. L. (1985) Aquaculture pond temperature modelling. *Aquacultural Engineering,* 4. pp. 191-208.

80. Knapp, H. V., Yu, Y. S., and E. C. Pogge. (1984). Monthly evaporation for Milford lake in Kansas. Journal of Irrigation Engineering. 110 (2), pp. 138-148.

81. Knisel, W.G. (1980). CREAMS, a field scale model for chemicals, runoff, erosion from agricultural management system, Conservation Research Report, USDA, 26, pp. 643.

82. Kohler, M. A., Nordenson, T. J., and Fox, W. E. (1955). Evaporation from Pans and Lakes, U. S. Dept. Commerce, Weather Bureau Research Paper, pp. 38.

83. Kohler, M. A. and Parmele, L. H. (1967). Generalized estimates of free- water estimates. Water Resources Research. 3, pp. 997-1005.

84. Krant, J. F., Motzkin, F. and Gordin, H. (1982) Modelling temperatures and salinities of mixed seawater fish ponds. *Aquaculture,* 27, 377-388.

85. Krol, M. S., Jaeger, A. & Bronstert, A. 2003. Integrated modeling of climate change impacts in Northeastern Brazil. In: Global Change and Regional Impacts: Water Availability and Vulnerability of Ecosystems and Society in the Semiarid Northeast of Brazil (Ed. by T. Gaiser, M. S. Krol, H. Frischkorn & J. C. de Araújo), Springer-Verlag, Berlin, Germany. pp. 43–56

86. Kumar, M., Kumar, P., Tiwari, K. N. and Pal, D. K. (1997). Establishing SCS runoff curve number form IRS digital database. J. Indian society of remote sensing, 19(4), pp. 246-251.

87. Kumar, M, Raghuwanshi N. S., Singh, R., Wallender, W. W., Pruitt, W. O. (2002) Estimating evapotranspiration using artificial neural network. J Irrig Drain Eng., 128(4), pp. 224–33.

88. Laird, N.F., Kristovich, D.A.R. (2002). Variations of sensible and latent heat fluxes from a great lakes buoy and associated synoptic weather patterns. Journal of Hydrometeorology 3 (1), 3–12

89. Li, R.M., M.A. Stevens, and D.B. Simons. (1976). Solutions to Green-Ampt Infiltration Equation. Journal of Irrigation and Drainage. Division of ASCE 102(IR2), pp. 239-248.

90. Linacre, E. T. (1977). A simple formula for estimating evaporation rates in various climates, using temperature data alone, Agricultural Meteorology. 18, pp. 409-424.

91. Liou, K.N. (2002). An introduction to atmospheric radiation. Second edition. Academic press. An imprint of Elsevier Science.

92. Losodo, T. M. (1988) Characterization and modelling of thermal and oxygen stratification in aquaculture ponds. Ph.D. Dissertation, University of California, Davis, CA.

93. Mahfouf, J. F., Noilhan, J. (1991): Comparative study of various formulations of evaporation from bare soil using in situ data. *J. Appl. Meteor.* 30. pp. 1354-1365.

94. Mather. J.R. (1978). The climatic water budget in environmental analysis. Lexington Books, Lexington, MA, pp 239.

95. Martin, J. L. and McCutcheon, S. C. (1999). Hydrodynamics and transport for water quality modeling. CRC Press, Inc. Lewis Publisher, USA

96. McCuen, R. H. (2002). Approach to confidence interval estimation for curve numbers. J. Hydrologic Engineering. 7 (1), pp. 43-48.

97. McGuinness, J.L., Bordne, E.F. (1972). A comparison of lysimeter derived potential evapotranspiration with computed values. Technical Bulletin 1452, US Department of Agriculture Agricultural Research Service, Washington, DC.

98. Mein, R.G. and Larson, C. L. (1973). Modeling infiltration during a steady rain. Water Resources Research. 9(2), pp. 384-394.

99. Meyer, A. F. (1928). The element of hydrology. John Wiley and Sons, New York.

100. Miller, N, and Cronshey, R. (1989). Runoff curve numbers, the next step, Proc., Int. Conf. on Channel Flow and Catchment Runoff, University of Virginia, Charlottesville, Va.

101. Mishra, G.C. and Kansal, M.L. Asolekar, S. R, (2005). Water balance study of Mansagar Lake. Report submitted to Ministry of Rajasthan, Govt. of India.

102. Mishra, S. K., and Singh, V.P. (2002a). SCS-CN method, Part 1, Derivation of SCS-CN based models, Acta Geophysica Polonica. 50(3), pp. 457-477.

103. Mishra S. K. and Singh V. P. (2003a). Soil Conservation Service Curve Number (SCS-CN) Methodology. Kluwer Academic Publishers, Dordrecht, ISBN 1-4020-1132-6.

104. Mishra, S.K., and Singh, V. P. (2004a). Long-term hydrologic simulation based on the Soil Conservation Service Curve Number. Hydrological Processes. 18, pp. 1291-1313.

105. Mishra, S. K., and Singh, V. P. (2004b). Validity and extension of the SCS-CN method for computing infiltration and rainfall excess rates. Hydrological Process. 18, pp. 3323-3345.

106. Mishra, S. K., and Singh, V. P. (2006). A re-look at NEH-4 curve number data and antecedent moisture condition criteria. Hydrological Processes. 18, pp. 3323-3354.

107. Mishra, S. K., Jain, M. K., Pandey, R. P., and Singh, V.P. (2003a). Evaluation of AMC dependant SCS-CN models using large data of small watersheds. Water and Energy International. 60(3), pp. 13-23.

108. Mishra, S. K., Jain, M. K., Pandey, R. P., and Singh, V. P. (2005). Catchment area based evaluation of the AMC dependant SCS-CN based rainfall-runoff models. Hydrological Processes. 19, pp. 2701-2718.

129. Philip, J.R. (1992). Falling head ponded infiltration. Water Resources Research. 28(8), pp. 2147- 2148.

130. Philip, J.R. (1993). Variable-head ponded infiltration under constant or variable rainfall. Water Resources Research. 29(7), pp. 2155-2165.

131. Polubarinova-Kochina. (1962). Theory of Groundwater Movement. Princeton University Press. Princeton NJ. pp. 606-509.

132. Ponce, V. M., and Hawkins, R. H. (1996). Runoff curve number, has it reached maturity? Journal of Hydrologic Engineering-ASCE. 1(1), pp. 11–19.

133. Priestley, C. H. B., and Taylor, R. J. (1972). On the assessment of surface heat flux and evaporation using large-scale parameters, Monthly Weather Review. 100, pp. 81-92.

134. Ragan, R. M., and Jackson, T. J. (1980). Runoff synthesis using landsat and SCS model, Journal of Hydrologics Division, ASCE. 106 (HY5), pp. 667–678.

135. Raghuwanshi, N.S. and Wallender, W, W. (1998) Converting from pan evaporation to evapotranspiration. Journal of Irrigation and Drainage Engineering. 124 (5) pp 275-277

136. Rallison, R E. (1980). Origin and evaluation of the SCS runoff equation. Proc., Symp. Watershed Management, ASCE, Idaho. pp. 912-924.

137. Rallison, R.E., and Cronshey, R.C. (1979). Discussion of "Runoff curve number with site varying moisture" by R.H. Hawkins, *Journal of Irrigation and Drainage Division, ASCE* 105 (IR4), pp. 439–441

138. Rasmussen, A.H., Hondzo, M., and Stefan, H.G. (1995). A test of several evaporation equations for water temperature simulations in lakes. Water Resources Bulletin. 31 (6), pp. 1023–1028.

139. Ravi, V., and William, J.R. (1998). Estimation of infiltration rate in the vadose zone: Compilation of simple mathematical models. EPA/600/R-97/128a. U.S. Environmental Protection Agency Cincinnati, OH.

140. Roberson, J. A., Cassidy, J. J. and Chaudhy M. H. (1988). Hydraulic Engineering. Boston. Houghton Miffin Co. pp. 662.

141. Rosenberry, D.O., Sturrock, A.M., Winter, T.C. (1993). Evaluation of the energy budget method of determining evaporation at Williams Lake, Minnesota, using alternative instrumentation and study approaches. Water Resources Research 29 (8), pp. 2473– 2483.

142. Rosenberry, D.O.,Winter, T. C., Buso, D.C., Likens, G. E. (2007). Comparison of 15 evaporation methods applied to a small mountain lake in the northeastern USA. Journal of Hydrology. 340, pp 149-166

143. Ryan, P. J., Harleman, D. R. F., and Stolzenbach, K. D. (1974). Surface heat loss from cooling ponds. Water Resour. Res. 10, pp. 930–938.

144. Sahu, J. P. Land use pattern of Kalahandi District. Orissa Review. pp. 64-76. 2006.

145. Sahu, R. K., Mishra, S.K., Eldho, T.I. and Jain, M.K. (2007). An advanced soil moisture accounting procedure for SCS curve number method. Hydrolgical Processes. 21, pp. 2872-2881.

146. Salvucci, G.D., and D. Entekhabi. (1994). Explicit expressions for Green-Ampt (Delta function diffusivity) infiltration rate and cumulative storage. Water Resour. Res., 30: pp. 2661-2663.

147. Saxena, R. K., Verma, K. S., Chary, G. R., Shristava, R. and Barthwal, A. K. (2000). IRS-1C data application in watershed characterization and management, Int. J. of Remote Sensing. 21(17), pp. 3197-3208.

148. Schneider, L.E., and McCuen, R.H. (2005). Statistical guidelines for curve number generation. J. Irrigation and Drainage Engineering, ASCE. 131(3), pp. 282-290.

149. Schumann, A. H., Funke, R. and Schultz, G. A. (2000) Application of geographical information system for conceptual rainfall runoff modeling, J. of Hydrology. 240, pp. 45-61.

150. Sharda, D. Kumar R., Venkatatatnam, M. V. L. and Rao, M. (1993). Watershed prioritization for soil conservation – A GIS approach, Geo Carto International (1), pp. 27-34.

151. Sharda, V.N., and Juyal, G. P. (2008). Water harvesting techniques, design of small dams and hydraulic components. Lecture Material, http://www.waterforfood.org/gga/Lecture%20Material/VNSharda_WaterHarvesting.pdf

152. Sharda, V. N., Juyal, G. P., and Singh, P.N. (2002). Hydrologic and sedimentologic behavior of a conservation bench terrace system in a sub-humid climate. American Society of Agricultural and Biological Engineers. 45 (5), pp. 1433-1441.

153. Sharif, M. (1989). Development of a physically exact energy balance method for estimating evaporation from free water surfaces. Ph.D dissertation, Texas Tech University.

154. Sharm, K.D. (1987). Modified runoff curve numbers for bare crust forming sandy soils. Australian Journal of Soil Research. 25 (4), pp. 541 – 545.

155. Shiau, J. T., and Lee, H. C. (2005). Derivation of optimal hedging rules for a water-supply reservoir through compromise programming. Water Resources Management. 19, pp. 111–132.

156. Shinogi, Y., Makin, I.W., and Witharana, P. (1998). Simulation of the water balance in a dry zone tank cascade. Paper presented at the National Conference of

the Status and Future Direction of Water Research in Sri Lanka, November 4–6, 1998, at BMICH, Colombo, Sri Lanka.

157. Simanton, J.R., Hawkins, R.H., Mohseni-Saravi, M., and Renard, K.G. (1996). Runoff curve number variation with drainage area, Walnut Gulch, Arizona, Soil and Conservation Division, Trans. ASAE. 39(4), pp. 1391-1394.

158. Sivapragasam, C., Vasudevan, G., Maran, J., Bose, C., Kaza, S., and Ganesh, N. (2009). Modeling evaporation-seepage losses for reservoir water balance in semi arid regions. Water Resources Management. 23, pp. 853-867.

159. Slack, R. B., and Welch, R. (1980). Soil conservations service runoff curve number estimates from Landsat data, Water Resources Bulletin. 16 (5), pp. 887–893.

160. Smith, R.E., and Parlange, J.Y. (1978) A parameter-efficient hydrologic infiltration model. Water Resources Research. 14(3), pp. 5-538.

161. Smith, R.E. (1997). Discussion of 'runoff curve number: has it reached maturity?' by V.M. Ponce and R.H. Hawkins. Journal of Hydrologic Engineering, ASCE. 2(3), pp. 145-148.

162. Soil Conservation Service (SCS). (1956, 1964, 1971, 1972, 1993). Hydrology, National Engineering Handbook, Supplement A, Section 4, Chapter 10, Soil Conservation Service, USDA, Washington, DC.

163. Soil Conservation Service, (1967). Irrigation Water Requirements, Technical Release No. 21, U. S. Dept. Agri., Engineering Div., Revised Sept. 1970.

164. Sonu, J. (1986). Vertical infiltration into stratified soil for groundwater accretion. Proceeding of Budapest Symposium. IAHS Publication No. 156. pp. 365-374.

165. Sorrell, R. C. and P.E. (2003). Computing flood discharges for small ungaged watersheds. Michigan Department of Environmental Quality Geological and Land Management Division. pp. 1-31.

166. Spiegel, M. R. (1995). Theory and problems of statistics, 2nd Ed, Schaum's Series, New York.

167. Springer, E. P., McGurk, B. J., Hawkins, R. H., and Goltharp, G. B. (1980). Curve numbers from watershed data. Proc., Irrigation and Drainage Symp. on Watershed Management, ASCE, New York, N.Y. pp. 938-950.

168. Srivastava, R. C. (2000). Methodology for design of water harvesting system for high rainfall areas. Agricultural Water Management. 47, pp. 37–53.

169. Srivastava, R.C. Singahandhupe, R.B. and Mohanty, R.K. (2004). Integrated farming approach for runoff recycling systems in humid plateau areas of eastern India. Agricultural Water Management. 64. pp 197-212.

170. Srivastava, R.C., Panda, R.K., 1998. Potential and prospects of runoff recycling based irrigation system in plateau region of eastern India. Indian J. Soil Conserv. 26 (2), 104–108.

171. Srivastava, R.C., 1996a. Amethodology for optimizing design of integrated tank irrigation system. J.Water Resour. Plann. Manage. 122 (6), 394–402.

172. Srivastava, R.C., 1996b. Design of runoff recycling irrigation system for rice cultivation. J. Irrigation Drain. Eng. (ASCE) 122 (6), 331–335.

173. Srivastava, R.C., 2001. A methodology for design of water harvesting system in high rainfall areas. Agric. Water Manage. 47 (1), 37–53.

174. Steenhuis, T. S., Winchell, M., Rossing, J., Zollweg, J. A. and Walter, M. F. (1995). SCS runoff equation revisited for variable source runoff areas. J. Irrigation and Drainage Engineering. 121(3), pp. 234-238.

175. Stewart, R. B., and Rouse, W. R. (1976). A simple method for determining the evaporation from shallow lakes and ponds, Water Resources Research. 12, pp. 623-628.

176. Still, D. A., and Shih, S. F. (1985). Using landsat data to classify land use for assessing the basin wise runoff index. Water Resource Bulletin. 21, pp. 931-940.

177. Streeter, V. L., and Wylie, E. B. (1988). Fluid Mechanics, 1st Metric Ed, McGraw Hill, New York.

178. Subramanya, K. (2006) Engineering hydrology, 2nd Ed. McGraw Hill, New Delhi.

179. Sun Y-H, Yang S-L, Yeh WWG, Louie PWF (1996) Modeling reservoir evaporation losses by generalized networks. J Water Resour Plan Manage 122(3):pp. 222–226.

180. Swartzendruber, D. (1974). Infiltration of constant-flux rainfall into soil as analyzed by the approach of Green and Ampt. Soil Science. 117, pp. 272-281

181. Szumiec, M. (1979). Hydrometerology in pond fish culture. In: Pillay, T.V.R. (Ed.), Advances in Aquaculture. FAO, Fishing News Books, London. pp. 117–120.

182. Tasumi, M., Matsuno, Y., Otsuki, Y., Van der Hoek, Y., and Sakthivadivel, R. (1999). The role of return flows in a tank cascade system in Sri Lanka. Working Paper, International Water Management Institute (IWMI), Colombo, Sri Lanka.

183. Thom, A. S., and H. R. Oliver. (1977). On Penman's equation for estimating regional evaporation. Quarterly Journal of Royal Meteorological Society. 103, pp. 345- 357.

184. Tiwari, G.N. (2005). Solar Energy. Second Reprint. Narosa Publishing House, New Delhi.

185. Tiwari, K. N., Kumar, P., Sibastian, M., and Paul, D. K. (1991). Hydrological modeling for runoff determination, Remote Sensing Technique, J. Water Resources Planning and Management. 7(3), pp. 178-184.

186. Tripathi, M.P., Raghuwanshi, N.S., and Rao, G. P. (2005). Effect of watershed subdivision on simulation of water balance components. Hydrological Processes. 20 (5). pp. 1137-1156.

187. U.S. Army Corps of Engineers. (1994). Engineering and design flood runoff analysis. Department of the Army, Washington .Manual No.1110-2-1417.Chapter 6.

188. U. S. Geological Survey. (1954). Water loss investigations - lake Hefner studies. Technical Report, U. S. Geological Survey Professional Paper No. 269.

189. U. S. Geological Survey. (1954). Water loss investigations - lake Hefner studies. Base Data Report, U. S. Geological Survey Professional Paper No. 270.

190. Utah State University Report. (1994). Consumptive Use of Irrigated Crops in Utah. Utah Agricultural Experiment Station Research Report No. 145, Utah State University, Logan, Utah.

191. Usgodaarachi, T., Weerasinghe, A.D., and Sakthivadivel, R. (1996). Reservoir Operation Simulation (Extended) Systems, ROSES—Version 3.00, User Manual, International Irrigation Management Institute, P.O. Box 2075, Colombo, Sri Lanka.

192. van Mullem, J. A. (1989). Runoff and peak discharges using Green–Ampt infiltration model. J. Hydrol. Engng, ASCE. 117(3), pp. 354-370.

193. van Bavel, C. H. M. (1966). Potential evaporation: the combination concept and its experimental verification. Water Resources Research. 2 (3), pp. 455-467.

194. van Genugten, M.Th. (1980). A closed form equation for predicting the hydraulic conductivity of unsaturated soil. Soil Sc. Soc. Am. J. 44. pp. 892-898.

195. Ventura, F., Spano, D., Duce, P., and Snyder, R.L. (1999). An evaluation of common evapotranspiration equations. Irrig. Sci. 18, pp. 163–170.

196. Verma, H. N. and Sarma, P. B. S. (1990). Design of storage tanks for water harvesting in rainfed areas. Agricultural Water Management. 18, pp. 195–207.

197. Walpole, R. E., and R. H. Myers. (1993). Probability and statistics for engineers and scientists, 5th Ed., Prentice Hall, Englewood Cliffs, New Jersey.

198. Wunderlich, W.O. (1972). Heat and mass transfer between a water surface and atmosphere, TN Report No.14. Tennssee Valley Authority, Water Resources Engineering Laboratory. Norris, TN.

199. Water Resources Engineers, Inc. (1967). Prediction of thermal energy distribution in streams and reservoirs, Prepared for the California Department of Game and fish. Environmental protection agency Athens, GA.

200. Wegner, D. (1999). A report on evaporation and ground water seepage. In: Columbia EARTHSCAPE (An online resource on the global environment).

201. Weiss, A. (1983). A quantitative approach to the Pruitt and Doorenbos version of the Penman equation. Irrigation Science. 4 (4), pp. 267-275.

202. White, D. (1988). Grid based application of runoff curve numbers. J. Water Resources Planning and Management, ASCE. 114(6), pp. 601-612.

203. Willeke, G.E. (1997). Discussion of 'runoff curve number: has it reached maturity?' by V.M. Ponce and R.H. Hawkins. Journal of Hydrologic Engineering, ASCE. 2(3), pp. 145-148.

204. Winter, T.C., Buso, D.C., Rosenberry, D.O., Likens, G.E., Sturrock, A.M., Mau, D.P. (2003). Evaporation determined by the energy-budget method for Mirror Lake, New Hampshire. Limnology and Oceanography 48 (3), 995–1009.

205. Winter, T.C. (1981). Uncertainties in estimating the water balance of lakes. Water Resources Bulletin 17 (1), 82–115.

206. Winter, T.C., Rosenberry, D.O., Sturrock, A.M. (1995). Evaluation of 11 equations for determining evaporation for a small lake in north central United States. Water Resources Research 31,983–993.

207. Woodward, D. E. and Gburek, W. J. (1992). Progress report ARS/SCS curve number work group, Proc., ASCE, Water Forum 92, ASCE, New York. pp. 378-382.

208. WTCER, 2001. Report of Consultancy Project on Comprehensive Water Resource Development Planning for Two Gram Panchayats of Kalahandi and Raygada of Orissa.Water Technology Centre for Eastern Region (ICAR), India, p. 50.

209. Yadev, B. Pond, its management and productivity. Fish and Fisheries. 2nd Ed. Daya Books. Pp 253. (2006).

210. Yadav, B.K. and Keshari, A.K. (2006). A coupled mathematical water and salt balance model of flat bay. Asian Journal of Water, Environment and Pollution. 4 (2), pp. 59-55.

211. Yu, Y.S., Knapp, H.V. (1985). Weekly, monthly, and annual evaporations for Elk City Lake. Journal of Hydrology. 80. pp.93–110.

212. Yuan, Y., Mitchell, J. K., Hirschi, M. C., Cooke, R. A. C. (2001). Modified SCS curve number method for predicting sub-surface drainage flow. Trans. ASAE. 44(6), pp. 1673-1682.

213. Yurekli, K., Kurunc, A., and Simsek, H. (2004). Prediction of daily maximum stream flow based on stochastic approaches. Journal of Spatial Hydrology. 4 (2), pp.1-12.

A.1 Calculation of Extraterrestrial Radiation

Solar radiation before subjected to the mechanism of atmospheric absorption and scattering is known as extraterrestrial radiation. The variation of extraterrestrial radiation with time is due to the revolution of earth around the sun in an elliptical path with sun at one of the foci. The eccentricity of the earth's orbit is defined as the ratio of the distance between the two foci to the major axis of the ellipse and is given by as follow (Liou, 2002):

$$e = \frac{\left(a^2 - b^2\right)^{\frac{1}{2}}}{a} \tag{A.1}$$

where

e= eccentricity of the earth's orbit

a= Semi-major axis of the ellipse

b= Semi-minor axis of the ellipse

The eccentricity varies from 0.01 to 0.04 with mean value of about 0.017 (Liou, 2002). The intensity of extraterrestrial radiation (H_0) can be estimated on the any day of the year in terms of solar constant (G_{SC}) as follow:

$$H_0 = G_{SC}\left(\frac{r_0}{r}\right)^2 \tag{A.2}$$

where

H_0= extraterrestrial radiation in W/m^2

G_{SC}= solar constant in W/m^2

r_0= mean distance from earth to sun in meter

r= distance from earth to sun on the nth day in meter

A.2 Calculation of Solar Constant

The radiant energy flux received per second by a surface of unit area held normal to the direction of sun's rays at the mean sun-earth distance outside the atmosphere is known as solar constant. It is assumed by many researchers as constant through out the year and adopted to be 1367 W/m^2. But in reality solar constant is not a constant unit, as the distance from the sun to earth is not constant through out the year.

The distance from sun to earth at nth day can be derived from the geometry of the ellipse which has been seen in Fig.A.1.as follows (Liou, 2002):

$$r = \frac{a(1-e^2)}{1+e\cos\upsilon} \qquad \text{(A.3)}$$

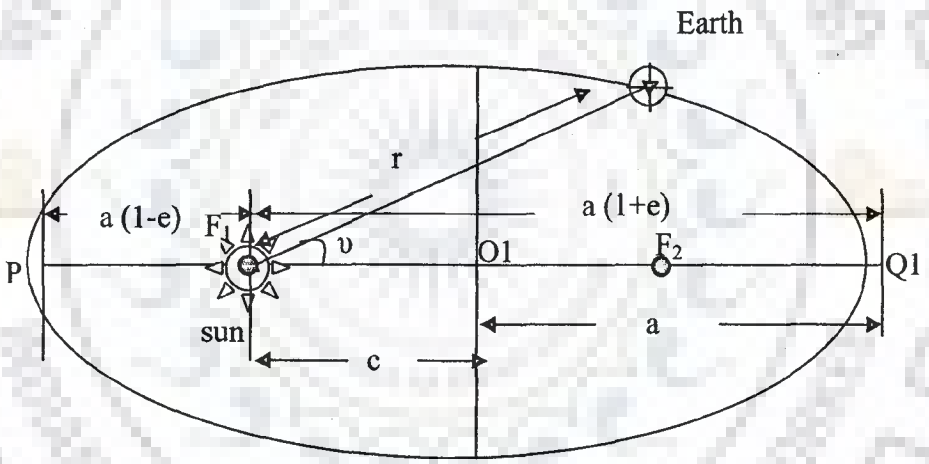

Fig. A.1 Sun-Earth Geometry, (Liou, 2002)

where

υ =the anomaly of the earth at a given time and which is equal to $\frac{2\pi n}{365}$, and 'n' = 1 for the 1st day of January and 365 for the 31st of December.

The semi-major axis of the earth's orbit is invariant. The mean distance between the sun and earth may be set as the invariant semi-major axis i.e. $r_0 = a$ (Liou, 2002). Now by substituting the value of r, r_0, and υ in (A.3):

$$H_0 = G_{SC}\left[\frac{a\left(1+e\cos\frac{2\pi n}{365}\right)}{a\left(1-e^2\right)}\right]^2 \tag{A.4}$$

or

$$H_0 = G_{SC}\left[\frac{a\left(1+e\cos\frac{2\pi n}{365}\right)}{a\left(1-e^2\right)}\right]^2 = G_{SC}\frac{\left(1+e\cos\frac{2\pi n}{365}\right)^2}{\left(1-e^2\right)^2}$$

or

$$H_0 = G_{SC}\frac{1+e^2\left(\cos\frac{2\pi n}{365}\right)^2+2e\cos\frac{2\pi n}{365}}{\left(1-e^2\right)^2} \tag{A.5}$$

Substituting the value of e =0.017 in the (A.5):

$$H_0 = G_{SC}\frac{1+(0.017)^2\left(\cos\frac{2\pi n}{365}\right)+2\times 0.017\times\cos\frac{2\pi n}{365}}{\left\{1-(0.017)^2\right\}^2} \tag{A.6}$$

or

$$H_0 = G_{SC}\frac{1+2.89\times10^{-4}\left(\cos\frac{2\pi n}{365}\right)^2+0.034\cos\frac{2\pi n}{365}}{0.99942\approx 1} \tag{A.7}$$

By neglecting the term $2.89\times10^{-4}\left(\cos\frac{2\pi n}{365}\right)^2$ in (A.7) as its negligible quantity the expression for the extraterrestrial radiation is obtained as follows:

$$H_0 = G_{SC}\left(1+0.034\cos\frac{2\pi n}{365}\right). \tag{A.8}$$

This is the extraterrestrial radiation reaching to the top of the earth's atmosphere per unit area normal to the sun's rays per second on the nth day as shown in the Fig.A.2.

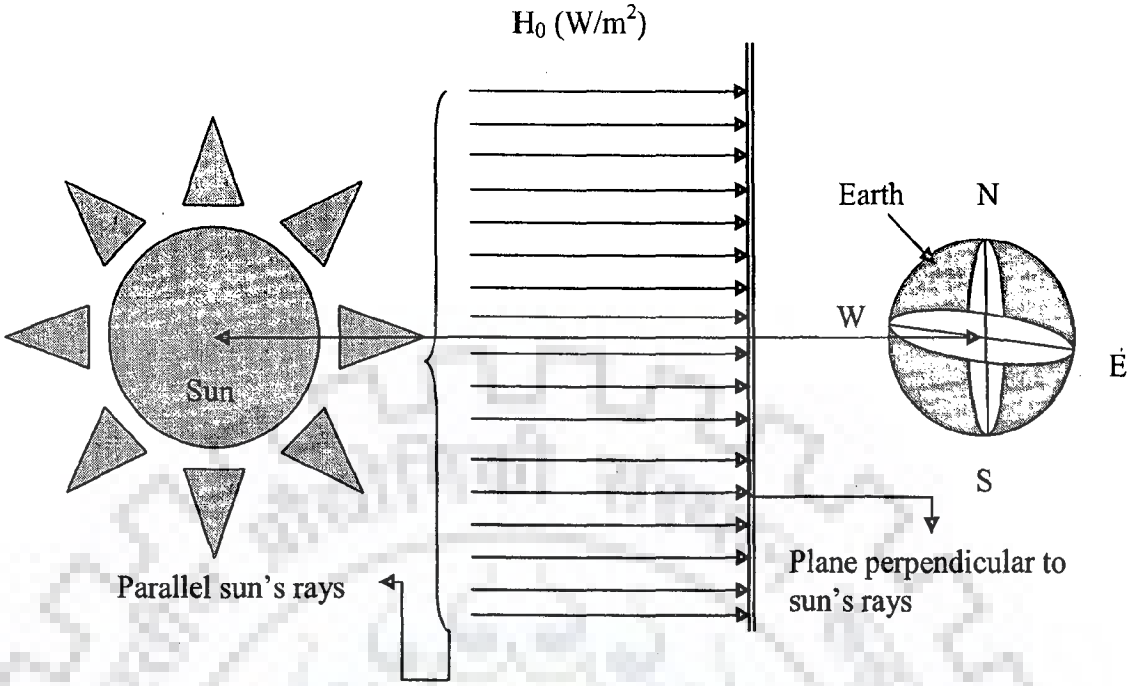

Fig.A.2 Sun's rays incident on the earth, http://www.itacanet.org/eng/elec/solar/sun2.pdf

A.3 Cosine Effect

It's true that not all points on the earth's surface are perpendicular to the sun's rays. Hence, the extraterrestrial radiation reaching to the earth surface depends primarily on the solar zenith angle and to some extent on the variable distance of the earth from the sun and it is smaller than H_0 due to cosine effect (Fig. A.3). In the Fig.A.3 plane A is the horizontal plane on the earth surface, plane B is the horizontal plane parallel plane to plane A in the outer surface of earth's atmosphere, and Plane C is the perpendicular plane which is normal to the sun's rays.

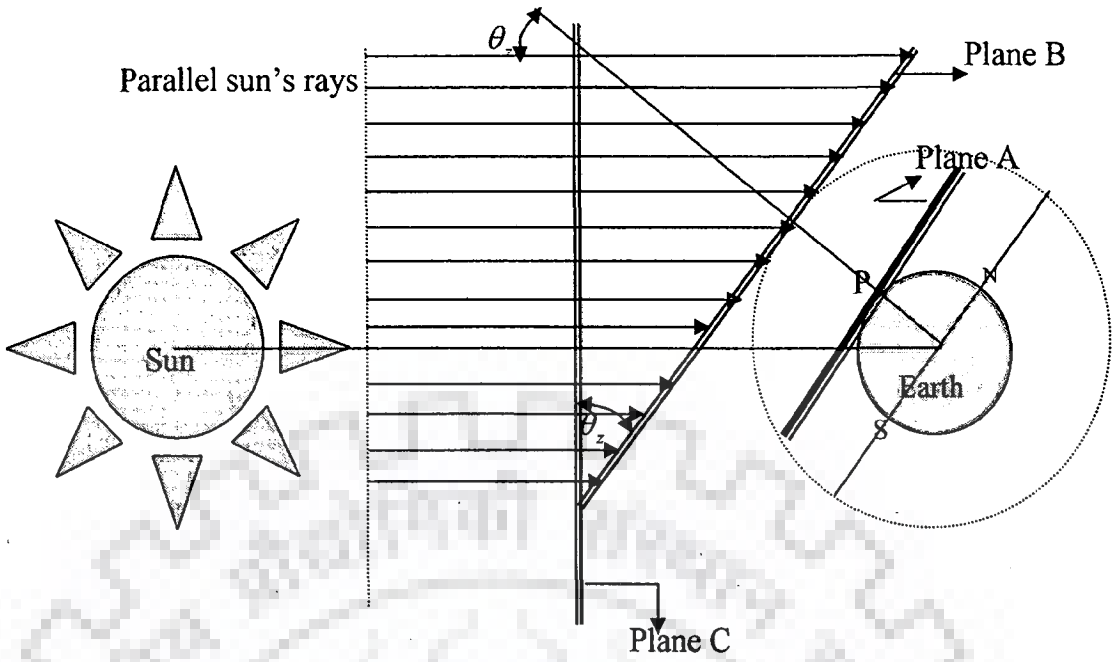

Fig.A.3 Cosine Effect, http://www.itacanet.org/eng/elec/solar/sun2.pdf

H_0 is the extraterrestrial radiation flux on the normal plane and extraterrestrial radiation flux in the horizontal plane can be calculated from the following equation.

$$H_{OH} = H_0 \cos\theta_z \tag{A.9}$$

where

H_{OH} = extraterrestrial radiation on a horizontal plane in W/m^2

H_0 = extraterrestrial radiation on a normal plane in W/m^2

θ_z = solar zenith angle in degree shown in Fig.A.3

A.4 Solar Zenith Angle

The position of the sun is defined by the solar zenith angle, which is determined from the known angle. In Fig.A.4, let P be the point of observation and OZ is the zenith through the point of observation. Assume that sun is in the direction of OS or PS and let D be the point directly under the sun.

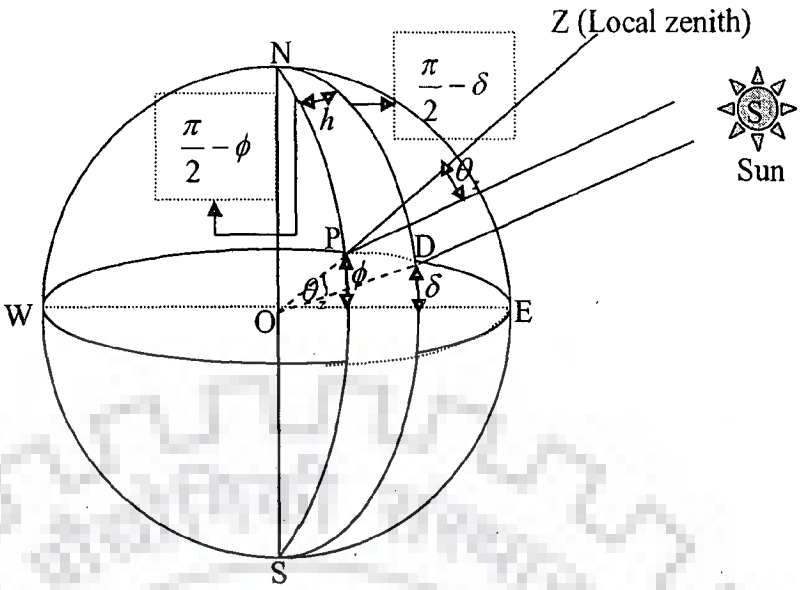

Fig.A.4 Relationship of the solar zenith angle, the latitude, solar declination angle and the hour angle, (Liou, 2002)

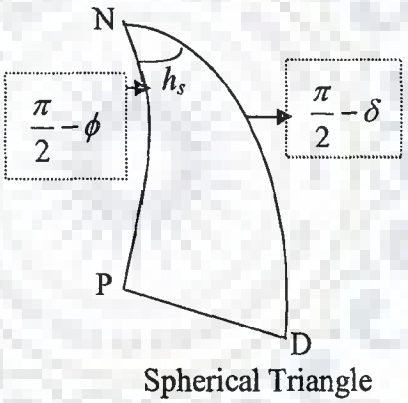

Fig.A.5 Triangle on the celestial plane, (Eagleson, 1970)

Then the plane of OZ and OS will be intersecting the surface of the earth in a great circle. The angle measured by the arc PD of this circle and this is equal to the sun's zenith distance θ_z. In the spherical triangle NPD, (Fig.A.5) the arc ND is equal to 90^0 minus the solar inclination δ, which is the angular distance of sun. It is positive for north and negative for south of the equator. The arc NP is equal to 90^0 minus the latitude ϕ of the observation point. The angle h is the hour angle or the angle through

which the earth must turn to bring the meridian of P directly under the sun and it is given by $h_s = \frac{2\pi t}{day}$, where t is the time period.

By applying the cosine law to the NPD spherical triangle, the following expression is obtained:

$$\cos\theta_z = \cos\left(\frac{\pi}{2}-\phi\right)\cos\left(\frac{\pi}{2}-\delta\right)+\sin\left(\frac{\pi}{2}-\phi\right)\sin\left(\frac{\pi}{2}-\delta\right)\cos h_h \qquad \text{(A.10)}$$

or

$$\cos\theta_z = \sin\phi\sin\delta+\cos\phi\cos\delta\cos h_h \qquad \text{(A.11)}$$

where

ϕ = latitude of the location in degree

δ = solar declination angle in degree

h_h= hour angle in degree

Substituting the expression for H_0 and $\cos\theta_z$ in (A.9), from (A.8) and (A.11) respectively, the expression for the extraterrestrial radiation in horizontal plane is obtained as:

$$H_{OH} = G_{SC}\left(1+0.034\cos\frac{2\pi n}{365}\right)\times\left(\sin\phi\sin\delta+\cos\phi\cos\delta\cos h_h\right) \qquad \text{(A.12)}$$

The declination angle δ is given as (Copper, 1969):

$$\delta = 23.45\sin\left(2\pi\frac{284+n}{365}\right) \qquad \text{(A.13)}$$

A.5 Hour Angle

At solar noon at any latitude, the hour angle h_h equal to *0* (Liou, 2002) except at the poles where solar zenith angle, $\vartheta_z = \frac{\pi}{2}$ i.e. during sunrise and sunset. From (A.11),

thus the half-day H (i.e. from sunrise to noon or from noon to sunset) is defined by the following expression:

$$\cos H = -\tan\phi \tan\delta \qquad \text{(A.14)}$$

where

H = Hour angle during sunrise to noon or noon to sunset in degree

Thus hour angle is defined as the angle through which the earth must be rotated to bring the meridian of the plane directly under the sun. In other wards, it is the angular displacement of the local meridian, due to the rotation of the earth on its axis at 15^0 per hour. The hour angle is zero at solar noon, negative in the morning and positive in the noon. The expression for the hour angle is given by as follow:

$$h_h = (ST - 12) \times 15^0 \qquad \text{(A.15)}$$

where

ST is the local standard time

Solar time is the time used in all of the sun-angle relationships which does not coincide with local clock time. Hence it is necessary to convert standard time to solar time by two corrections. First correction is a constant correction for the difference in longitude between the observer's meridian and the meridian on which the local standard time is based. The earth takes 4 minutes to transverse 1^0 of longitude. The second correction is from the equation of time, which takes into account the perturbation in the earth's rate of rotation which affect the time of observer's meridian to cross the sun. The difference in minutes between solar time and standard time is given by as follow:

$$Solar\,Time - S\tan dard\,Time = E_a \times 4(L_{st} - L_{loc}) + E_t \qquad \text{(A.16)}$$

where

L_{st}= the standard meridian for local time zone (for India it is 81^0 54') in degree

L_{loc}= the longitude of the location in question in degree (longitude correction will be negative if the local longitude in question is west of standard meridian)

E_t= Equation of time in minute

E_a= the correction factor, for west of meridian it is *-1* and east of meridian it is *+1*

Equation of time (E) can be expressed as follows:

$$E_t = 229.2(0.000075 + 0.001868\cos B - 0.032077\sin B - 0.014615\cos 2B - 0.04089\sin 2B) \quad \text{(A.17a)}$$

where

$$B = n - 1\left(\frac{360}{365}\right) \quad \text{(A.17b)}$$

A.6 Calculation of Standard Sunrise and Sunset Time

From (A.16) we can find the sunset hour angle and hence the time of sunset can be calculated as follow:

$$H = \cos^{-1}(-\tan\phi\tan\delta) \quad \text{(A.18)}$$

Solar time of sunset in hour will be

$$t_{ss} = \frac{H}{15} + 12 \quad \text{(A.19)}$$

Hence standard time for sunset will be

$$t_{ssi} = \left\{\left(\frac{H}{15} + 12\right) - \left[\frac{E_a \times 4(L_{st} - L_{loc}) + E_t}{60}\right]\right\} \quad \text{(A.20)}$$

and the standard time of sunrise will be

$$t_{sri} = \left\{\left(12 - \frac{H}{15}\right) - \left[\frac{E_a \times 4(L_{st} - L_{loc}) + E_t}{60}\right]\right\} \quad \text{(A.21)}$$

Thus hour angle from sunrise to sunset can be calculated by using (A.15), where *ST* will vary from t_{ssi} *to* t_{sri} i.e. the hourly standard time for sunrise to sunset.

A.7 Hourly Extraterrestrial Radiation on the Horizontal Plane

If we define the extraterrestrial radiation on a horizontal plane received at the top of the atmosphere per unit area as H_H, then the solar flux density on a horizontal plane may be written as:

$$H_{OH}(t) = \frac{dH_H}{dt} \tag{A.22}$$

Thus, the extraterrestrial radiation for a given period of time i.e. t_1 to t_2 can be written as follow:

$$H_H = \int_{t_1}^{t_2} H_{OH}(t)\,dt \tag{A.23}$$

or

$$H_H = \int_{t_1}^{t_2} H_0 \cos\theta_z(t)\,dt \tag{A.24}$$

Angular velocity, υ of the earth is given by the following equation:

$$\upsilon = \frac{dh_h}{dt} = \frac{2\pi}{day} \tag{A.25}$$

or

$$dt = \frac{dh_h}{\upsilon} = \frac{dh_h \times day}{2\pi} \tag{A.26}$$

Substituting the expression for $\cos\theta_z$ from (A.11) and the expression for *dt* from (A.26) in (A.24):

$$H_H = H_0 \int_{h_{h1}}^{h_{h2}} (\sin\phi\sin\delta + \cos\phi\cos\delta\cos h_h)\frac{dh_h \times day}{2\pi}$$

or

$$H_H = \frac{H_0 \times day}{2\pi}\left[\int_{h_{h1}}^{h_{h2}} \sin\phi \sin\delta \, dh + \int_{h_{h1}}^{h_{h2}} \cos\phi \cos\delta \cos h_h \, dh_h\right]$$

or

$$H_H = \frac{H_0 \times day}{2\pi}\left[\sin\phi \sin\delta \int_{h_{h1}}^{h_{h2}} dh_s + \int_{h_{h1}}^{h_{h2}} \cos\phi \cos\delta \cosh_h \, dh_h\right]$$

or

$$H_H = \frac{H_0 \times day}{2\pi}\left[\sin\phi \sin\delta \left[h_h\right]_{h_{h1}}^{h_{h2}} + \cos\phi \cos\delta \left[\sinh_h\right]_{h_{h1}}^{h_{h2}}\right]$$

or

$$H_H = \frac{H_0 \times day}{2\pi}\left[\sin\phi \sin\delta (h_{h2} - h_{h1}) + \cos\phi \cos\delta (\sinh_{h2} - \sinh_{h1})\right] \quad \text{(A.27)}$$

Here $(h_{h2} - h_{h1})$ is in degree, to convert it into radian multiplied by $\frac{\pi}{180}$ in (A.27), the following expression is obtained:

$$H_H = \frac{H_0 \times day}{2\pi}\left[\cos\phi \cos\delta (\sinh_{h2} - \sinh_{h1}) + \frac{\pi}{180}(h_{h2} - h_{h1}) \sin\phi \sin\delta\right] \quad \text{(A.28)}$$

Substituting the expression for H_0 in (A.28) from (A.8):

$$H_H = G_{SC}\left(1 + 0.034\cos\frac{2\pi n}{365}\right)\frac{day}{2\pi}\left[\cos\phi\cos\delta(\sinh_{h2} - \sinh_{h1}) + \frac{\pi}{180}(h_{h2} - h_{h1})\sin\phi\sin\delta\right] \quad \text{(A.29)}$$

As the solar constant G_{SC} is in W/m^2 unit, hence the extraterrestrial radiation on a horizontal plane (H_H) in hourly basis can be calculated follow:

$$H_H = G_{SC}\left(1' + 0.034\cos\frac{2\pi n}{365}\right)\frac{24}{2\pi} \times \left[\cos\phi \cos\delta (\sinh_{h2} - \sinh_{h1}) + \frac{\pi}{180}(h_{h2} - h_{h1}) \sin\phi \sin\delta\right]$$

or

$$H_H = G_{SC}\left(1+0.034\cos\frac{2\pi n}{365}\right)\frac{12}{\pi}\times \left[\cos\phi\cos\delta(\sinh_{h2}-\sinh_{h1})+\frac{\pi}{180}(h_{h2}-h_{h1})\sin\phi\sin\delta\right] \quad \text{(A.30)}$$

In (A.30) a correction factor (τ) should be introduced for diurnal exposure to the radiation flux. The correction factor will be 1.0 for the time, when the hour angle less than sunset time and greater than sun rise time, and during all other times it will be 0.0 (Martin and James, 1999).

Hence, extraterrestrial radiation on a horizontal plane in an hour as:

$$H_H = G_{SC}\left(1+0.034\cos\frac{2\pi n}{365}\right)\frac{12}{\pi}\times \left[\cos\phi\cos\delta(\sin h_{h2}-\sin h_{h1})+\frac{\pi}{180}(h_{h2}-h_{h1})\sin\phi\sin\delta\right]\times\tau \quad \text{(A.31)}$$

A.8 Derivation of Long Wave Radiation

Stefan-Boltzman constant σ is derived by Plank's law of radiation as follows (Tewari, 2005):

$$E_{b\lambda} = \frac{C_1}{\lambda^5}\times\frac{1}{\left[e^{\frac{C_2}{\lambda T}}-1\right]} \quad \text{(A.32)}$$

where

$E_{b\lambda}$ = energy emitted by the black body in $\frac{W}{m^2\,\mu m}$

$C_1 = 3.742 \times 10^8 \frac{W\mu m^4}{m^2} = 3.742 \times 10^{-16}\ W\ m^2$

$C_2 = 1.4387 \times 10^4\ \mu mK = 0.01439\ m\ ^0K$

(C_1 and C_2 are Plank's first and second radiation constant respectively)

T = temperature of the surface ^0K

The long wave radiation is estimated from integrating (A.32) by taking limit of the wave length from 0 to ∞ (Stefan-Boltzman law) as follows:

$$H_L = \int_0^\infty E_{b\lambda} d\lambda \tag{A.34}$$

$$H_L = \int_0^\infty \frac{C_1}{\lambda^5} \frac{1}{\left[e^{\frac{C_2}{\lambda T}} - 1\right]} d\lambda \tag{A.35}$$

Let us substitute $x = \frac{C_2}{\lambda T}$ (A.36)

Hence, $dx = -\frac{C_2}{T}\frac{1}{\lambda^2} d\lambda$ (A.37)

or

$$d\lambda = -\frac{T\lambda^2}{C_2} dx, \text{ for } \lambda = \infty, x = 0 \text{ and } \lambda = 0, x = \infty \tag{A.38}$$

Incorporating the expression of $d\lambda$ in (A.35) from (A.38) with proper limit

$$H_L = C_1 \int_\infty^0 \frac{1}{\lambda^5} \frac{1}{\left(e^x - 1\right)} \left(\frac{-T\lambda^2}{C_2}\right) dx = \frac{C_1}{C_2} T \int_0^\infty \frac{1}{\lambda^3} \frac{1}{\left(e^x - 1\right)} dx$$

or

$$H_L = \frac{C_1}{C_2} T \int_0^\infty \frac{1}{\lambda^3} \frac{dx}{\left(e^x - 1\right)} \tag{A.39}$$

Incorporating the expression for λ and dx from (A.36) and (A.37) in (A.39), the following expression is obtained:

$$H_L = \frac{C_1}{C_2} T \int_0^\infty \frac{1}{\left(\frac{C_2}{xT}\right)^3} \frac{dx}{\left(e^x - 1\right)} = \frac{C_1}{C_2} T \frac{T^3}{(C_2)^3} \int_0^\infty \frac{x^3}{\left(e^x - 1\right)} dx = \frac{C_1}{(C_2)^4} T^4 \int_0^\infty \frac{x^3}{\left(e^x - 1\right)} dx$$

(A.40)

By standard integral $\int_0^\infty \frac{x^3}{\left(e^x - 1\right)} dx = \frac{\pi^4}{15}$

$$\text{Hence, } H_L = \frac{C_1}{(C_2)^4} T^4 \frac{\pi^4}{15} = \frac{C_1 \pi^4}{C_2^{\,4} \times 15} T^4 = \sigma T^4 \qquad \text{(A.41)}$$

$$\sigma = \text{Stefans-Boltzman constant} = \frac{C_1 \pi^4}{C_2^{\,4} \times 15} = 5.6649 \times 10^{-8} \frac{W}{m^2 K^4}$$

The emissivity of air (ε_a), modify the long wave radiation. Hence, the expression for long wave radiation is:

$$H_L = \varepsilon_a \sigma (T_a + 273.16)^4 \qquad \text{(A.42)}$$

where

H_L = long wave radiation in W/m^2

T_a = Average daily air temperature in ^{0}C

The emissivity of the air depends on a number of factors, such as cloud height, vapor pressure and air temperature. A variety of expressions have been proposed for the emissivity. One of the most commonly used expressions was proposed by Swinbank (1961) and modified by Wunderlich (1968) as follows:

$$\varepsilon_a = \alpha_0 (1 + 0.17C)(T_a + 273.16)^2 \qquad \text{(A.43)}$$

where

α_0 = proportionality constant with a value of 0.937x10^{-5}

C = fraction of the sky covered by the cloud

Substituting (A.43) into (A.42),

$$H_L = \alpha_0 (1 + 0.17C_1)(T_a + 273.16)^2 \sigma (T_a + 273.16)^4$$

or

$$H_L = \alpha_0 (1 + 0.17C_1) \sigma (T_a + 273.16)^6 \qquad \text{(A.44)}$$

Table-A.1 Observed meteorological data

Day	T_a	RH	U_w	Day	T_a	RH	U_w
1	20.25	91.85	7	47	24.25	93.9	5
2	20.75	95.9	4	48	25.5	84.1	6
3	19.75	95.9	7	49	24.5	84.1	5
4	19.75	93.9	5	50	27.25	82.7	7
5	20	91.6	5	51	27.5	82.7	6
6	20.5	87.75	8	52	28.25	88.2	7
7	20	94	9	53	23.25	92.6	5
8	20	93.9	10	54	21.75	92.6	7
9	20	90	5	55	21.75	86.9	7
10	20.25	84.35	10	56	22	84.2	6
11	21.75	86.3	6	57	23	87.15	5
12	21.75	95.85	5	58	23.5	85.6	7
13	22.25	87.75	6	59	24	84.1	7
14	25.25	91.3	4	60	23	84.1	6
15	25.25	92.5	14	61	23.5	79.65	6
16	18	95.55	7	62	24.75	84.1	3
17	17.75	91.45	6	63	25.25	84.25	5
18	19.75	91.85	6	64	27.75	86.85	7
19	20.75	93.9	6	65	28.5	86.1	5
20	21.75	92.1	7	66	29.75	88.5	7
21	21.5	90.45	7	67	28.75	88.5	5
22	22.25	86.9	6	68	29	86.5	8
23	22	86.9	7	69	28.25	86.5	10
24	22.5	86.9	9	70	29	88.2	6
25	22	86.9	9	71	29.25	93.15	5
26	21.5	90.45	8	72	31	93.15	8
27	22.5	81.4	8	73	31	90.4	7
28	23.25	81.45	5	74	31.25	87.35	7
29	24	81.85	8	75	31.75	91.7	6
30	24.5	90.45	9	76	31	94.75	16
31	25.25	86.9	7	77	29.5	90.2	8
32	24.25	93.9	7	78	29.5	90.2	11
33	19.25	91.85	7	79	30.75	81.45	10
34	19.25	89.8	5	80	32.25	90.2	8
35	21.25	88.3	7	81	31.5	94.9	6
36	23.5	92.3	8	82	30.5	91.6	7
37	23.5	86.9	6	83	30	85.95	8
38	23.75	89.75	8	84	32.75	81.7	7
39	24	71.35	5	85	32.5	75.15	8
40	23	91.75	6	86	32	78.5	6
41	22	83.5	7	87	32.5	77.15	8
42	25.5	88.75	7	88	32	83.85	7
43	23	100	6	89	33.75	81.35	6
44	24.5	74.85	6	90	33.75	78.05	10
45	27.75	83.4	11	91	31.25	83.8	7
46	24.75	83.25	10	92	30	84.3	7

93	29.75	86	7	142	36	73.4	9
94	30.75	87.95	8	143	32	84.4	13
95	31.5	87.5	9	144	32.25	82.5	13
96	32	94.85	8	145	32.75	83.45	10
97	29	80.2	10	146	32.75	78.75	8
98	28	100	8	147	34	76.9	12
99	29	92.7	11	148	34.25	76.15	12
100	30	89.95	9	149	35.25	78.45	10
101	32.5	88.5	7	150	33.5	86.3	11
102	30.5	94.85	8	151	34	72	10
103	31.75	89.95	8	152	34.25	81.45	7
104	34	87.55	10	153	31	94.85	12
105	32.75	88.8	8	154	35.75	80.25	9
106	32.75	88.35	8	155	36	84	5
107	33.25	85.95	8	156	35.5	80.25	11
108	33.5	88.8	14	157	33	93.4	12
109	33.75	85.95	18	158	29.25	100	9
110	34	70.65	10	159	32.5	79.3	7
111	34.5	76.4	12	160	31.25	94.85	8
112	33	89.8	12	161	29	92.9	8
113	32.5	85.95	11	162	28.5	94.7	8
114	34.5	69.05	8	163	30.25	100	10
115	34.75	79.5	12	164	25.25	100	8
116	33.5	78	14	165	24.75	100	6
117	31.25	76.85	7	166	25	100	6
118	34	76.15	10	167	26.5	100	6
119	30	90	8	168	28.25	100	8
120	29.5	75.35	22	169	24.75	97.7	11
121	32.5	83.55	16	170	26.25	90.55	7
122	33.5	72.6	17	171	25.25	100	9
123	35	65.25	13	172	23.5	100	9
124	34.5	75.35	9	173	27.5	100	8
125	35.5	77.2	9	174	27.25	100	7
126	35.25	75.35	8	175	27.5	96.05	7
127	34.5	80.35	9	176	28	98.05	6
128	34.5	80.4	12	177	27.25	100	5
129	35.5	59.6	8	178	26	100	5
130	36.5	61.95	10	179	28.25	100	5
131	36.25	70.45	11	180	28.25	94.25	10
132	36.5	73.25	12	181	28	94.25	4
133	35.5	76	7	182	28.25	89.05	2
134	36.25	64.7	9	183	26.75	100	2
135	35.75	72.25	6	184	30.5	100	2
136	36.25	80.9	9	185	26.5	93.9	5
137	37.5	66.4	7	186	28	86.6	4
138	32.75	86.1	9	187	30.25	89.7	5
139	35.5	85.3	7	188	28.5	89.05	2
140	32.25	100	7	189	28	100	3
141	35.5	77.6	10	190	24	100	5

191	24.25	100	4	240	24	100	1
192	26.25	100	4	241	24.75	95.85	1
193	26.25	100	3	242	26	95.85	2
194	26.25	95.9	4	243	25.75	100	1
195	26.5	100	2	244	26.5	100	2
196	26.25	100	7	245	25.5	100	4
197	26.25	100	3	246	26.5	100	4
198	26.25	100	5	247	25.25	100	5
199	25.5	100	5	248	26.5	100	2
200	25.5	100	5	249	26.75	97.9	3
201	24.5	93.5	5	250	26	97.9	5
202	26.75	93.5	5	251	26.75	89.7	3
203	28.25	96.2	4	252	27	95.85	5.5
204	27.5	96.1	3	253	28.25	100	2.5
205	27.75	100	5	254	28.5	100	5
206	28.25	100	2	255	26.75	100	4
207	27.5	93.65	3	256	28	95.85	4
208	26.5	100	4	257	28	100	3
209	27.25	93.5	4	258	27	100	5
210	25.5	100	5	259	26.5	95.85	6
211	25.25	100	5	260	27.5	100	5
212	24.75	100	8	261	27.5	89.55	5
213	25.5	95.85	3	262	28	89.55	6
214	27	93.95	3	263	27	100	7
215	25	100	1	264	28	95.85	7
216	26.5	93.7	1	265	26.75	100	4
217	27.25	95.75	2	266	27.25	89.7	5
218	26.25	89.4	2	267	26.5	89.7	5
219	24.25	89.4	1	268	26	100	4
220	25	89.4	1	269	25	91.8	4
221	26.25	100	1	270	25	93.75	4
222	24.25	100	1	271	26.5	95.85	8
223	27	100	1	272	25.5	95.85	5
224	27.25	95.85	2	273	26.5	95.85	7
225	27.5	100	2	274	27.25	95.85	4
226	27.5	93.9	1	275	27	95.85	4
227	27	100	1	276	27	89.7	4
228	25.5	100	1	277	27	91.75	6
229	24	100	1	278	26.5	100	1
230	26.75	93.7	1	279	26	97.9	4
231	25.5	100	0	280	26	100	4
232	28.25	96.05	0	281	26.25	97.9	2
233	26.75	100	0	282	26.75	89.05	3
234	26.75	95.85	0	283	26.5	89.95	4
235	26.25	95.85	1	284	25.5	97.9	1
236	26.75	100	0	285	24.75	90.2	3
237	25.5	100	1	286	24.5	83.95	3
238	26	100	0	287	24.5	90.2	3
239	27	100	0	288	26	90.2	3

289	25.25	89.05	3	338	19.25	91.2	3
290	25.75	100	3	339	18.5	94.25	3
291	25.5	97.9	4	340	18.25	91.2	3
292	24.75	86	3	341	18.25	94.25	3
293	26	100	4	342	18.25	91.65	4
294	25.75	100	2	343	20	78.9	4
295	26.5	97.9	5	344	20	78.9	3
296	25.25	90.2	3	345	20	78.9	2
297	25	90.2	3	346	20	78.9	2
298	25	100	4	347	20.25	89.35	2
299	24.75	97.9	4	348	20.5	89.35	1
300	24.5	97.9	3	349	17.5	78.65	0
301	25	97.9	4	350	17.5	78.15	3
302	25	100	4	351	17.5	78.15	2
303	25	97.9	4	352	19	78.15	4
304	25	100	4	353	19.25	89.35	6
305	21.5	100	4	354	19.5	89.35	4
306	21.5	100	4	355	18.75	89.35	3
307	21.5	100	3	356	17.75	78.15	3
308	22.5	100	3	357	16.25	67.25	4
309	23	100	3	358	16	67.25	5
310	23.75	97.9	4	359	16.25	67.25	4
311	24	97.9	10	360	17.25	86.8	4
312	23.25	89.55	7	361	18.25	86.8	4
313	23	89.45	3	362	19.25	86.8	4
314	23	87.55	2	363	18.5	73.15	4
315	23.25	87.55	4	364	18.5	73.15	4
316	23	87.55	3	365	18.75	73.15	4
317	22.5	87.55	2				
318	22.25	87.55	3				
319	23	87.55	5				
320	23.5	89.45	3				
321	22.5	89.45	3				
322	21.5	89.45	4				
323	20	93.25	4				
324	20.75	93.25	4				
325	20.5	93.25	2				
326	21.25	93.25	2				
327	20.75	93.25	3				
328	20	93.25	3				
329	19.5	93.25	2				
330	19	91.65	2				
331	19	91.65	2				
332	21.25	91.2	3				
333	21.25	91.2	3				
334	20.5	91.65	3				
335	18.5	93.25	3				
336	19	93.25	3				
337	18	93.25	3				

B.1Computation of Storage Parameter S

The SCS method is used for estimation of direct runoff volume resulting from total rainfall occurring during a single storm or several storms in a calendar day. The time distribution, i.e., the rainfall intensity, is ignored. Soil properties, which influence the runoff volume, are considered indirectly. The soil is classified into A, B, C, and D groups based on the rate of infiltration through bared soil after prolonged wetting. The groups are:

A. (Low runoff potential) Soils having high infiltration rates even when thoroughly wetted and consisting chiefly of deep, well to excessively drained sands or gravels. These soils have a high rate of water transmission of order 5 to 11.5 cm/hr.

B. Soils having moderate infiltration rates when thoroughly wetted and consisting chiefly of moderate deep to deep, moderate well to well drained soils with moderate fine to moderately coarse textures. These soils have a moderate rate of water transmission of the order 4.7 to 5 cm/hr.

C. Soils having slow infiltration rates when thoroughly wetted and consisting chiefly of soils with a layer that impedes downward movement of water, or soils with moderately fine to fine textures. These soils have a slow rate of water transmission of the order 0.13 to 4 cm/hr.

D. (High runoff potential) Soils having very slow infiltration rates when thoroughly wetted and consisting chiefly of clay soils with a high swelling potential, soils with a permanent high water table, soils with a clay pan or clay layer at or near the surface, and shallow soils over nearly impervious material. These soils have slow rate of water transmission of the order 0 to 0.13 cm/hr.

Depending upon the soil group and land use, a runoff curve number is ascertained from the SCS Table. The relation between curve number (CN) and storage index (S) in SI unit is given by:

$$CN = \frac{25400}{S + 254} \tag{B.1}$$

or

$$S = \frac{25400}{CN} - 254 \tag{B.2}$$

S is the storage capacity that absorbs rainfall. Higher value of S means low runoff volume. The curve number CN is a dimensionless number and gives a convenient transformation of S to establish a 0 to 100 scale. For impervious and water surfaces CN=100.

The SCS rainfall runoff relationship is given by (SCS, 1972):

$$Q = \frac{(P - 0.2S)^2}{(P + 0.8S)}; \qquad P \geq 0.2S \tag{B.3}$$

where

P= total rainfall in a calendar day (mm)

Q = runoff volume (mm) corresponding to precipitation P (mm).

The storage index S is depleted as part of rainfall is infiltrated. Evaporation causes the storage index to increase. Therefore, the curve number needs to be updated considering the changes in storage index. Equation (B.3) can be simplified to (Hawkins, 1978):

$$Q = \frac{(P + 0.8S - S)^2}{(P + 0.8S)} = \frac{(P + 0.8S)^2 + S^2 - 2S * (P + 0.8S)}{(P + 0.8S)}$$

$$= P + 0.8S + \frac{S^2}{(P + 0.8S)} - 2S = P - 1.2S + \frac{S^2}{(P + 0.8S)}$$

$$= P - 1.2S + \frac{S^2}{(P + 0.8S)} = P - S\left[1.2 - \frac{S}{(P + 0.8S)}\right]$$

Hence, $Q = P - 1.2S$; *when* $P \to \infty$ (B.4)

It can be seen from (B.4) that as P becomes very large (i.e. $P \to \infty$) the possible difference between rainfall (P) and direct runoff (Q) is not S but 1.2S. Let V be equal to 1.2S. At time t, the storage available is

$$V(t) = 1.2S(t) = 1.2\left(\frac{25400}{CN(t)} - 254\right) \tag{B.5}$$

B.2 Computation of Soil Moisture Evaporation

Water in soil moves from high energy points to low energy points. If we consider the origin of z at the soil surface and positive in downward direction, then the hydraulic head H may be defined as:

$$H = h - z \tag{B.6}$$

where, h is the soil water pressure head (relative to the atmosphere) expressed in *cm* of water and z is the gravitational head (*cm*). In unsaturated soil, h is negative because work is needed to with draw water against the soil metric forces.

For one-dimensional vertical flow in the unsaturated soil, Darcy's law is given by:

$$v(z) = -k(\theta)\frac{\partial H}{\partial z} \tag{B.7}$$

where, $k(\theta)$ is the unsaturated hydraulic conductivity (*cm/h*) which depends on the soil moisture content θ. By substituting (B.6) into (B.7) yields:

$$v(z) = -k(\theta)\frac{\partial}{\partial z}(h - z)$$

or
$$v(z) = -k(\theta)\left(\frac{\partial h}{\partial z} - 1\right) \tag{B.8}$$

Applying the continuity principle (Law of conservation of mass) for a soil mass of unit area and height δz,

$$v(z)\delta t - \left(v(z) + \frac{v(z)}{\partial z}\delta z\right)\delta t = \theta_{t+\delta t}\delta z - \theta_t \delta z \tag{B.9}$$

or
$$\frac{\partial \theta}{\partial t} + \frac{\partial v(z)}{\partial z} = 0 \tag{B.10}$$

Substituting of (B.8) into (B.10) yields the partial differential equation to describe the flow of water in soil system as:

$$\frac{\partial\theta}{\partial t}+\frac{\partial}{\partial z}\left[-k(\theta)\left(\frac{\partial h}{\partial z}-1\right)\right]=0$$

or $$\frac{\partial\theta}{\partial t}=\frac{\partial}{\partial z}\left[k(\theta)\left(\frac{\partial h}{\partial z}-1\right)\right] \qquad \text{(B.11)}$$

Equation (B.11) is a second order, parabolic, nonlinear, partial differential equation, known as Richards' equation. It is better to consider h instead of θ as the independent variable (Philip, 1958). Using the specific water capacity, $C(h)$ in (B.11):

$$C(h)\frac{\partial h}{\partial t}=\frac{\partial}{\partial z}\left[k(h)\left(\frac{\partial h}{\partial z}-1\right)\right] \qquad \text{(B.12)}$$

Due to the strong nonlinearity of (B.11) and (B.12), there exists no general analytical solution. Hence, the discretization scheme i.e. explicit method has been used to solve the governing equation. Though there are different discretization schemes are available, explicit scheme has the advantage, it is simple and easy to program. However, for reason of stability the time step has been adjusted with (Haverkamp et al., 1977):

$$\Delta t<\frac{r(\Delta z)^2}{D_{\max}} \qquad \text{(B.13)}$$

where, Δt is the time step, Δz is the layer thickness, D_{max} is the maximum value of the soil water diffusivity $\left(D(\theta)=k(\theta)\frac{dh}{d\theta}\right)$ in the soil profile at time t and r is an arbitrary chosen coefficient equal to 0.5 for the sandy loam. The initial and boundary conditions which are to be satisfied for solving (B.12) are: at $t=0$, and $z>0$, $\theta(z,0)=\theta_i(z)$ = the initial soil moisture; and for $t\geq 0$, at $z=0$, $\theta(0,t)=\theta_u$. θ_u can be given by the following relationship (Mahfouf and Noilhan1991):

$$RH = 0.5\left[1-\cos\left(\frac{\theta_u}{\theta_{fc}}\pi\right)\right] \quad if \quad \theta_u < \theta_{fc} \qquad (B.14)$$
$$= 1 \qquad if \quad \theta_u \geq \theta_{fc}$$

where

RH= relative humidity (fraction)

θ_u = volumetric soil surface moisture content

θ_{fc} = volumetric soil moisture content at field capacity

Equation (B.14) is further simplified as:

$$\theta_u = \frac{\theta_{fc}}{\pi}\cos^{-1}(1-2RH) \qquad (B.15)$$

The rainfall events for which, runoff have been calculated by SCS-CN method and modified curve number method, is presented in the Figure B.1.

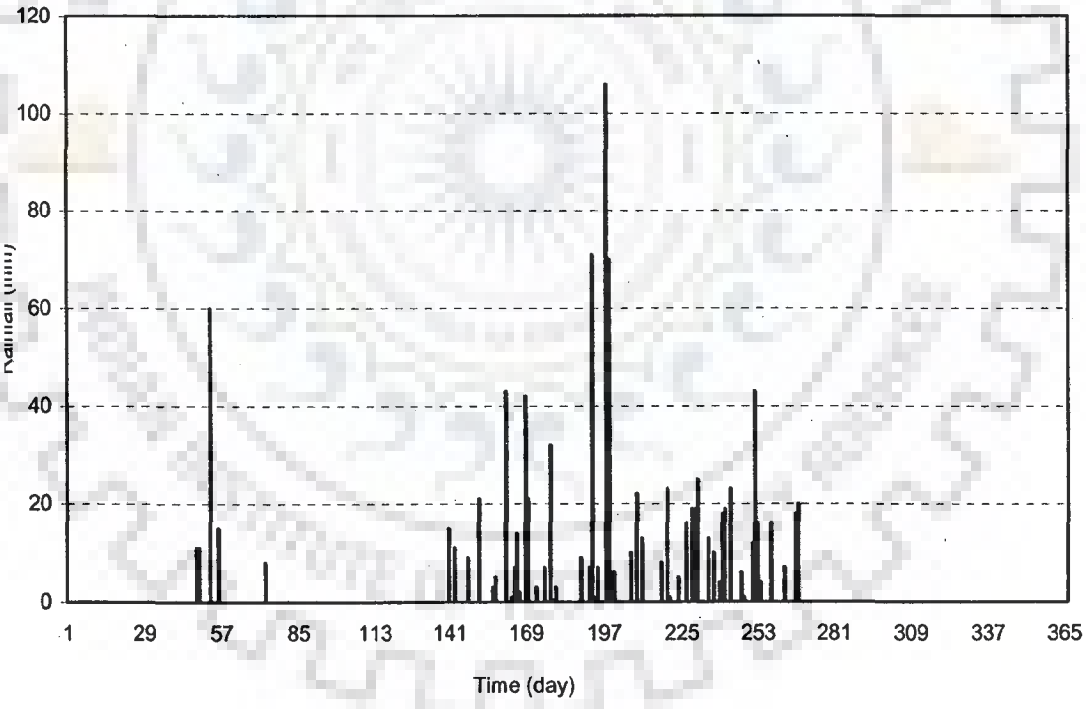

Fig.B.1 Rainfall during a year

The observed relative humidity for a normal year is shown in Figure B.2 (a) and B.2 (b) respectively. The change in volumetric soil moisture content in the top soil layer has been computed using soil moisture status at the ground surface. The variations in moisture content, at the ground surface during non rainy day are computed

corresponding to the relative humidity and during a rainy day the soil moisture at the ground surface is taken as saturated

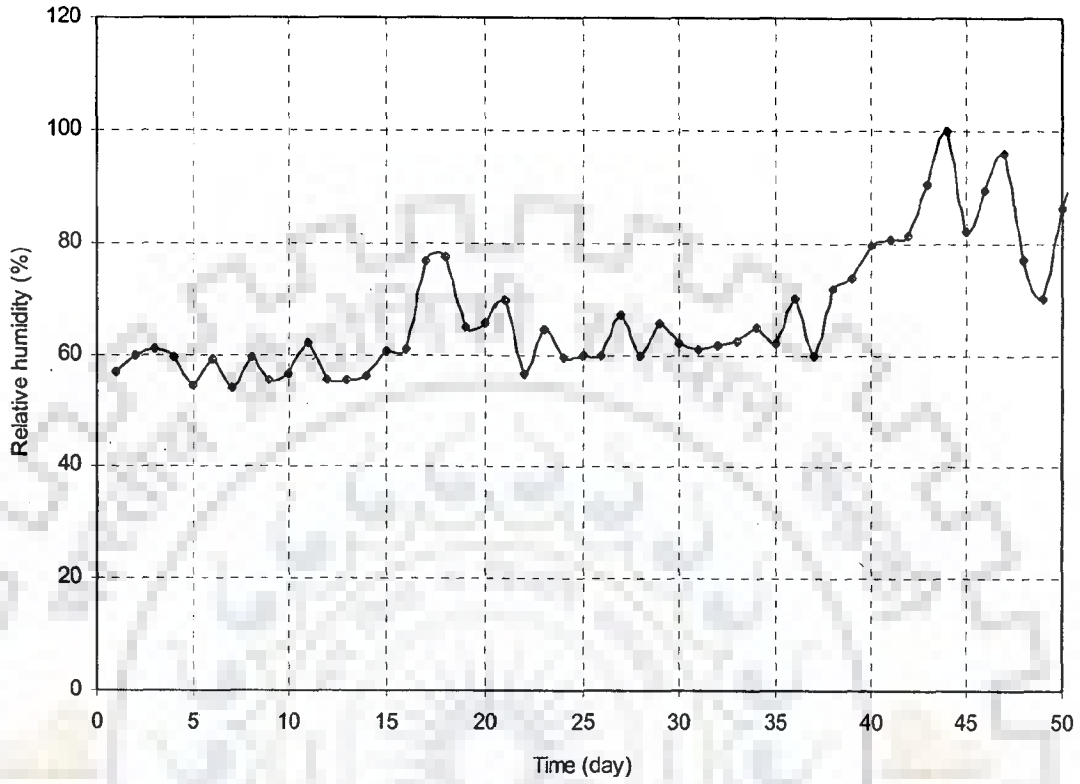

Fig.B.2 (a) Variation of relative humidity with time

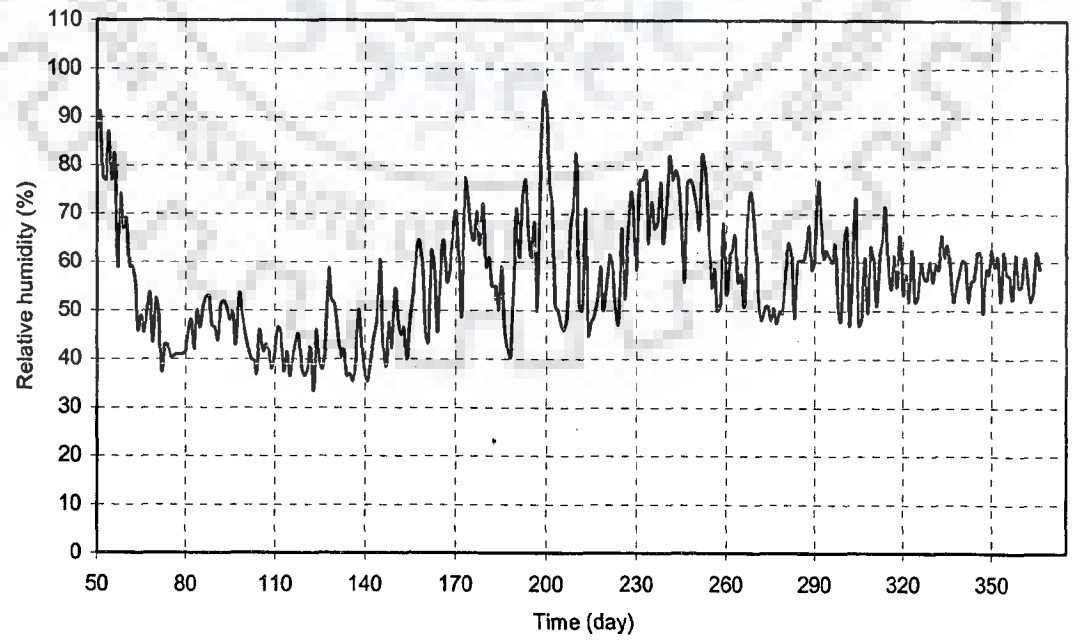

Fig. B. 2 (b) Variation of relative humidity with time

The variations of θ_u with time both for non rainy days and rainy days are shown in the Figure B.3 (a) and Figure B.3 (b) respectively. The movement of soil moisture profiles in the unsaturated zone (i.e. within 120 cm from ground surface) during pre-rainfall, rainfall and post rainfall day has been computed by applying Richard's equation based on above boundary conditions and presented in Figure B.4.

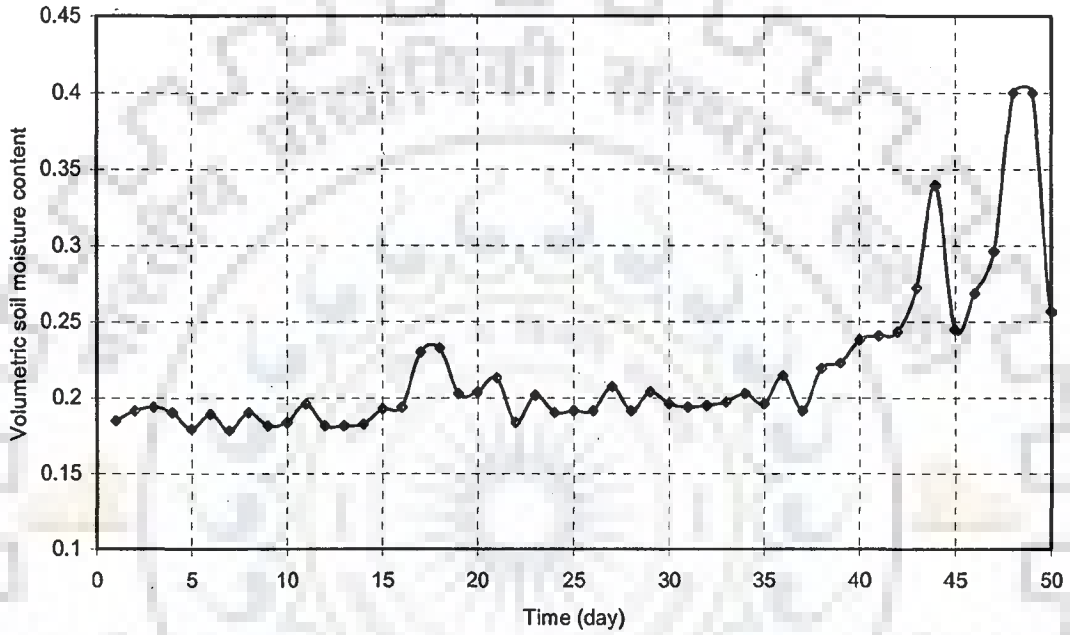

Fig. B. 3 (a) Variation of volumetric soil moisture with time

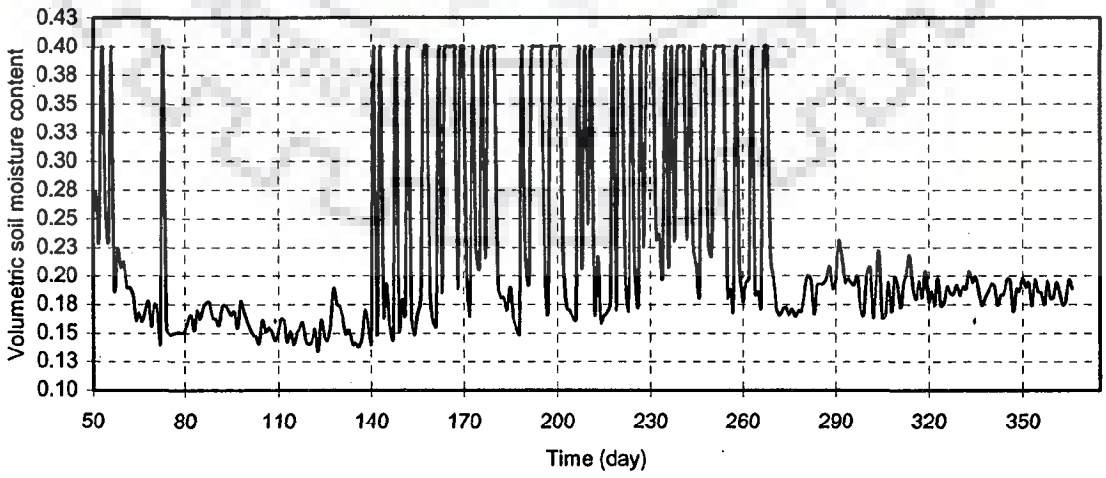

Fig.B.3 (b) Variation of volumetric soil moisture content with time, during pre-rainfall, rainfall and post-rainfall events

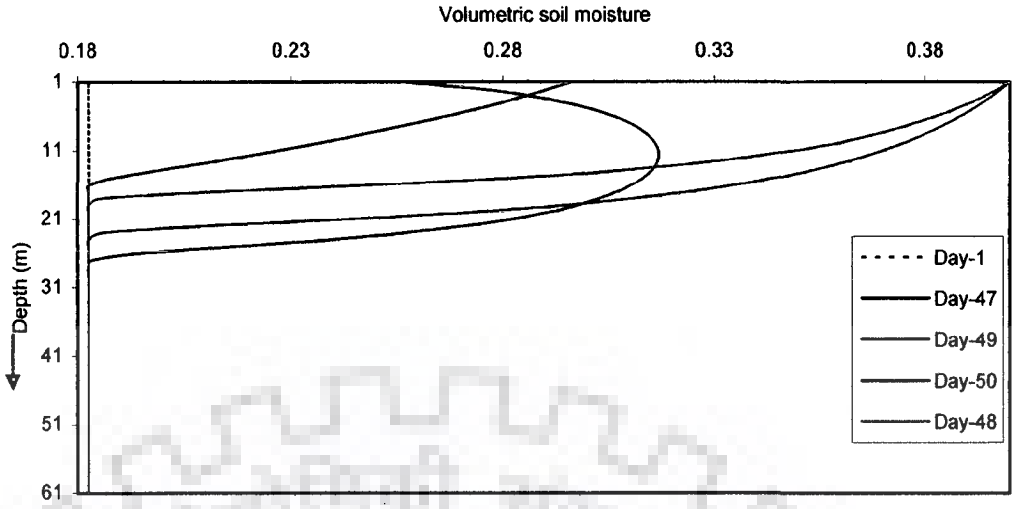

Fig.B.4 Variation of soil moisture content with depth during pre-rainfall day, rainfall day and post rainfall day

Table B.1 Runoff curve numbers for selected agricultural, suburban, and urban land uses (Antecedent Moisture Condition II, I_a =0.2S)

Land Use Description		Hydrological Soil Group			
		A	B	C	D
Cultivated land: without conservation treatment		72	81	88	91
with conservation treatment		62	71	78	81
Pasture or range land: poor condition		68	79	86	89
good condition		39	61	74	80
Meadow: good condition		30	58	71	78
Wood or forest land: thin stand, poor cover, no mulch		45	66	77	83
good cover		25	55	70	77
Open spaces, lawns, parks, golf courses, cemeteries, etc.					
good condition: grass cover on 75% or more of the area		39	61	74	80
fair condition: grass cover on 50% to 75% of the area		49	69	79	84
Commercial and business areas (85% impervious)		89	92	94	95
Industrial districts (72% impervious)		81	88	91	93
Residential:					
Average lot size	Average % impervious				
1/8 acre or less	65	77	85	90	92
1/4 acre	38	61	75	83	87
1/3 acre	30	57	72	81	86
1/2 acre	25	54	70	80	85
1 acre	20	51	68	79	84
Paved parking lots, roofs, driveways, etc.		98	98	98	98
Streets and roads:					
paved with curbs and storm sewers		98	98	98	98
gravel		76	85	89	91
dirt		72	82	87	89